Decoding Magma Plumbing and Geochemical Evolution of Active Volcanoes of the Central Andes (North Chile) with Petrological Methods

Von der Naturwissenschaftlichen Fakultät der

Gottfried Wilhelm Leibniz Universität Hannover

zur Erlangung des Grades

Doktor der Naturwissenschaften (Dr. rer. nat.)

genehmigte Dissertation

von

Dipl.-Geow. André Stechern

geboren am 08.01.1982 in Burgwedel

Je mannigfacher der Bau der Vulkane, d.h. der Erhebungen ist, welche den Kanal umschließen durch den die geschmolzenen Massen des inneren Erdkörpers an die Erdoberfläche gelangen, desto wichtiger ist es, diesen Bau mittels genauer Messung zu ergründen.

Alexander von Humboldt,
Über den Bau und die Wirkungsart der Vulkane,
Berlin, 1823

Acknowledgments

I would first like to acknowledge the Deutsche Forschungsgemeinschaft (DFG) for funding the project HO 1337/15-1.

Further thanks to my supervisors for their support: Prof. Dr. François Holtz and Dr. Roman Botcharnikov. I would also like to thank the reviewers of this dissertation: Prof. Dr. François Holtz, Prof. Dr. Gerhard Wörner, and PD Dr. Andreas Klügel.

.

This research was supported by the great effort of our workshop. I especially want to thank Otto Diedrich and Julian Feige and the whole workshop crew. Many thanks to: Paul Eric Wolff, Tim Müller, and Prof. Dr. Jürgen Koepke for all the help at the microprobe.

As the work with our IHPVs can at times be challenging, I greatly benefited from the knowledge and teamwork in the IHPV lab. Thank you: Sara Cichy, Adrian Fiege, and Alexander Bartels.

Thank you Magdalena Banaszak, Renat Almeev, Francesco Vetere, and Oliver Namur, who were always open for helpful discussions. Furthermore, I would like to thank the students who contributed to my work. In particular: Saskia Hövelmann, Tobias Just, and Carolin Klahn.

I would like to thank all participants of the 2010 Chile field trip, who made this a unique and unforgettable experience for me.

It was a pleasure to share everyday work with my friends and colleagues. Special thanks to: Paul Eric Wolff, Alexander Bartels, Tim Müller, Lennart Fischer, Sören Wilke, Svenja Erdmann, and Chao Zhang who were awesome office colleagues.

I also would like to thank all PhD-students at the Institut for Mineralogy for the great time!

A special thanks belongs to AMWK for all cakes and dinners!

Finally, I also had lots of personal support. In particular I would like to mention my parents Dina and Frank, who always supported me on the way to my Diploma and doctoral degree. Additionally I would like to thank my grandfather Opa Werner, even though he cannot read this anymore, who enthused me for geology and mineralogy from my earliest childhood on.

Abstract

Depth, size and shape of magma reservoirs under active stratovolcanoes are still largely unknown. On the basis of petrological, geochemical and geophysical data magma chambers were postulated at different depths from a few kilometers to the base of the crust. Topic of this thesis is the localization and characterization of magmatic reservoirs beneath active (Lascar), or potentially active (Lastarria), volcanoes in the Andean Central Volcanic Zone (CVZ) with different petrological approaches.

Lascar Volcano, located in Northern Chile, is the most active volcano of the CVZ. Its activity culminated in the last major explosive eruption in April 1993. Lascar andesites, erupted in April 1993, have a phase assemblage of plagioclase, clinopyroxene, orthopyroxene, Fe-Ti oxides, and rhyolitic glass. To better define constrains of storage conditions and mechanisms of magmatic differentiation for andesitic magmas in a thick continual crust, petrological experiments were performed in internally heated pressure vessels. To investigate the compositional evolution of residual liquids the crystallization sequence of an andesitic melt from Lascar Volcano was simulated experimentally at 300 and 500 MPa with various water activities (aH$_2$O). The experimental temperature (T) was between 900 and 1050°C, aH$_2$O varied between 0.1 and 1.0, and the log oxygen fugacity (fO$_2$) varied between QFM+1.5 and QFM+3.3 at aH$_2$O = 1. To estimate pre-eruptive magma storage conditions the comparison of experiments to natural phase assemblages, modal proportions, and mineral, glass and whole-rock compositions, was used. The phase equilibria constraints, in combination with geothermobarometric calculations, suggest that Lascar two-pyroxene andesitic magmas are stored at 975 ± 25°C, 300 MPa, log$f$O$_2$ of QFM+2.75 ± 0.25, under H$_2$O-undersaturated conditions with 3.0 to 4.5 wt.% H$_2$O in the melt. Thus, Lascar andesites and dacites can be produced in an upper-crustal magma chamber as a result of fractional crystallization of a parental basalt or basaltic andesite melt which might originate from the mantle wedge and fractionate from a high-Al low-Mg arc basalt. Additional geobarometric and geochemical results point out that shallow magma reservoirs are also a region where magma mixing between primitive and already evolved melts takes place.

The second volcano of this study is Lastarria, which is part of the Lazufre region. This volcanic region is one of the few places on earth where an ongoing uplift of the Earth's surface by a magmatic body can be observed with geophysical methods. The petrology of quaternary andesites and dacites from Lastarria volcano were investigated to reconstruct magma plumbing and storage beneath the volcano. The mineral phase compositions and whole-rock major and trace element compositions were used to constrain temperature, pressure and possible mechanisms for magma differentiation. The applied thermobarometric models include two-pyroxene thermobarometry, pyroxene-melt thermobarometry, plagioclase-melt thermometry, amphibole composition thermobarometry, and Fe-Ti oxide thermo- oxybarometry. The overall temperature range gained by several geo-thermometers is between 840 and 1060°C. Calculated oxygen fugacity for all samples corresponds to a range between NNO to NNO+1. Results of the geo-barometric calculations reveal multiple magma storage regions, with a distinct storage level in the uppermost crust (~6.5-8 km depth), a broad zone at shallow to mid-crustal levels (~11-15 km depth), and a potential deeper zone at intermediate to lower crustal levels (>20km depth), which is difficult to define from petrological information only. The highest temperatures are recorded in minerals stored in the mid-crustal levels. The whole-rock compositions clearly indicate that magma mixing is the main parameter controlling the general differentiation trends.

Zusammenfassung

Tiefenlage, Größe und Form von Magmakammern unter aktiven Stratovulkanen sind noch immer weitgehend unbekannt. Auf der Grundlage petrologischer, geochemischer und geophysikalischer Daten wurden Magmareservoire in unterschiedlichen Tiefen zwischen wenigen Kilometern bis zur Basis der Kruste postuliert. Thema dieser Doktorarbeit ist die petrologische Lokalisierung und Charakterisierung von Magmareservoiren unter aktiven (Lascar), oder potentiell aktiven (Lastarria), Vulkanen der zentralen Anden.

Der Lascar Vulkan befindet sich im Norden Chiles und ist der aktivste Vulkan der zentralen Anden. Seine rezente Aktivität gipfelte in der letzten großen explosiven Eruption im April 1993. Die geförderten Andesite der 1993 Eruption haben einen Phasenbestandbestand aus Plagioklas, Klinopyroxen, Orthopyroxen, Fe-Ti-Oxiden und rhyolithischem Glas. Hoch-Druck und hoch-Temperatur Experimente wurden in intern beheizten Gasdruckanlagen durchgeführt, um die präeruptiven Bedingungen und die Mechanismen der magmatischen Differenzierung in andesitischen und dazitischen Magmen des Lascar Vulkans zu untersuchen. Die Kristallisationssequenz einer primitiven Schmelze des Lascar Vulkans wurde experimentell bei 300 und 500 MPa und variierenden Wasseraktivitäten (aH$_2$O) simuliert, um die geochemische Entwicklung der entstehenden Restschmelzen zu untersuchen. Die Experimente wurden bei Temperaturen von 900-1050°C und Sauerstofffugazitäten (fO$_2$) zwischen QFM+1,5 und QFM+3,3 (bei aH$_2$O = 1) durchgeführt. Ein Vergleich der experimentellen Ergebnisse mit dem natürlichen Mineralbestand, den modalen Verhältnissen, und der Mineral-, Glas- und Gesamtgesteinszusammensetzungen wurde verwendet, um die präeruptiven Bedingungen der Eruptivgesteine zu bestimmen. Die experimentellen Ergebnisse, in Verbindung mit geothermobarometrischen Berechnungen, legen nahe, dass die zwei-Pyroxen Andesite des Lascar Vulkans bei 975 ±25°C unter H$_2$O-untersättigten Bedingungen von 3,0 bis 4,5 Gew.% Wasser gebildet wurden. Der präeruptive Druck lag bei ~300 MPa und die Sauerstofffugazität entsprach QFM+2,75 ±0,25. Somit können Andesite und Dazite des Lascar Vulkans in Magmakammern in der oberen kontinentalen Kruste infolge fraktionierter Kristallisation aus einer basaltischen oder basaltisch-andesitischen Schmelze entstehen. Zusätzliche geochemische und petrologische Befunde weisen darauf hin, dass in den flachen Magmareservoiren auch Magmamischung zwischen primitiven und bereits entwickelten Schmelzen stattfindet.

Der zweite untersuchte Vulkan ist Lastarria, der Teil der Lazufre-Region ist. Diese vulkanische Region ist einer der wenigen Orte auf der Erde, wo eine Hebung der Erdoberfläche durch einen magmatischen Körper mit geophysikalischen Methoden rezent beobachtet werden kann. Petrologische Untersuchungen an quartären Andesiten und Daziten des Lastarria Vulkans wurden durchgeführt, um das magmatische Fördersystem und potentielle Magmakammern zu rekonstruieren. Die Mineralzusammensetzungen, sowie Haupt- und Spurenelementanalysen der Gesamtgesteinszusammensetzungen wurden genutzt, um Druck- und Temperaturbedingungen, sowie mögliche Mechanismen der magmatischen Differenzierung zu bestimmen. Die angewandten thermobarometrischen Modelle sind: Zwei-Pyroxen Thermobarometrie, Pyroxen-Schmelz Thermobarometrie, Plagioklas-Schmelz Thermometrie, Amphibol Thermobarometrie und Fe-Ti-Oxid Thermo- Oxibarometrie. Der über die Geothermometer bestimmte Temperaturbereich liegt zwischen 840°C und 1060°C. Die berechnete Sauerstofffugazität entspricht für alle Proben einem Bereich von NNO bis NNO+1. Die Ergebnisse der Geobarometrie zeigen mehrere Tiefenlagen aus denen die Magmen stammen. Ein Reservoir liegt in der obersten Kruste in einer Tiefe von ~6,5-8 km und vermutliche mehrere Magmakammern liegen in einer Tiefen von ~11-15 km. Eine mögliche tiefere Magmazone in mittleren bis unteren Krustenniveaus (>20 km Tiefe) lässt sich anhand der petrologischen Ergebnisse vermuten, aber nicht mit Sicherheit bestimmen. Die Gesamtgesteinszusammensetzungen zeigen, dass Magmamischung der wichtigste Parameter in der Differenzierung der Lastarria Gesteine ist.

Table of Contents

DECODING MAGMA PLUMBING AND GEOCHEMICAL EVOLUTION BENEATH THE LASTARRIA VOLCANIC COMPLEX (NORTHERN CHILE) - EVIDENCE FOR MULTIPLE MAGMA STORAGE REGIONS

Objectives and Background

This thesis investigates mechanisms of andesitic magma evolution as well as the localization and characterization of magma storage regions with petrological methods within the continental crust. A special focus lies on andesites originating from active volcanoes of the Central Andes in northern Chile. The continental crust in the Central Andes reaches a thickness of up to 74 km (Beck *et al.*, 1996), which is two to three times the usual crustal thickness of a typical continental crust above a subduction zone. This requires large volumes of primitive magmas, which differentiate during their ascent through the crust. The presented data help to characterize the magma evolution and storage region(s) beneath active volcanoes in an exceptionally thick continental crust. At the same time it aims to contribute to the general understanding of the influence of physical and chemical parameters during the evolution of intermediate volcanic systems.

ANDESITES

Andesites belong to the most abundant volcanic rocks on earth and represent the dominant rock type in continental and island arcs. The name andesite is derived from the Andes mountain range in South America as it frequently occurs in this region. The average composition of the continental crust is andesitic (Wedepohl, 1995). Andesites are extrusive magmatic rocks of intermediate compositions of 57 to 63 wt.% SiO_2. The typical phenocryst assemblage is plagioclase plus pyroxene and/or amphibole. Magnetite, ilmenite, biotite, zircon, and apatite are common accessory minerals. Andesite is typically formed at convergent plate margins but may occur also in other tectonic settings. Intermediate volcanic rocks can be formed via several processes such as: (i) Fractional crystallization of a mafic parental magma. (ii) Partial melting of crustal material. (iii) Mixing processes between mafic and evolved magmas in a magma reservoir. (iv) Contamination of a primitive magma with more evolved country rock.

SUBDUCTION ZONE VOLCANISM

The dehydration of a submerging oceanic crust and the partial melting of the asthenosphere above the subduction slab generate primary magmas of continental arcs. Primary magmas have a tholeiitic composition. Because the larger thickness and lower density, the continental crust is likely to prevent the direct upwards migration of primary magmas (Herzberg *et al.*, 1983). Ascending primary magmas are likely to pond at the bottom of the continental crust, forming deep reservoirs. In these deep hot zones an underplating process takes place, where the primary magmas undergo magmatic differentiation through MASH (melting, assimilation, storage, and homogenization) processes. Fundamental to these MASH processes is that mafic magmas ascending from the mantle wedge are more dense than the crustal rocks and will therefore concentrate near the base of the crust, forming an underplated layer (Hildreth, 1981). The hydrous nature of primary arc magmas, with 1.2–2.5 wt.% H_2O in the melt (e.g. Sobolev and Chaussidon, 1996), results in the suppression of plagioclase formation and favors the crystallization of mafic minerals such as olivine, pyroxene, and spinel over an extended fractionation range (up to 50 vol.%; Müntener *et al.*, 2001) as the magma cools. Precipitation of these dense mafic minerals leads to the development of thick ultramafic cumulate layers at the base of the crust, which may define the seismic Moho in evolved continental arcs (Hildreth, 1981 and Herzberg *et al.*, 1983). The residual magmas are migrating upward in the crust towards the Earth's surface and form magma reservoirs at different crustal levels. Key parameters that will control ascent behavior include magma viscosity and host-rock properties: in ductile rocks, viscous magmas may rise buoyantly as diapirs, whereas in brittle rocks, even quite viscous magmas will advance by crack propagation (Shaw, 1980).

Identifying mechanisms which lead to the formation of more evolved andesitic to dacitic magma, within the thick continental crust beneath the Central Andes is the major objective of this thesis and is not reviewed here. However, the most obvious result of these processes is manifested in the appearance of volcanic activity on the Earth's surface.

VOLCANIC BACKGROUND

About 65 % of all subaerial volcanoes that have erupted during the past 10000 years are located along a belt of active volcanoes circling the Pacific (Schmincke, 2004). About 85 % of all historic volcanic eruptions have occurred from volcanoes above subduction zones. These include almost all well-known and all large explosive volcanic eruptions in the past 200 years, such as: Tambora (Sumbawa, Indonesia), 1815; Krakatau (Sunda Strait, Indonesia), 1883; Bezymianny (Kamchatka, Russia), 1956; Mount St. Helens (Washington, USA), 1980; Unzen (Japan), 1991; Pinatubo (Philippines), 1991; and Lascar (Chile), 1993. These volcanic eruptions are one of the most impressive manifestations of Earth inner dynamics. Stratovolcanoes (or composite volcanoes) are probably the most famous and recognized volcano type. They are steep cones built up of individual layers (strata) of lava and pyroclastic deposits. Typical for this volcanic geomorphological form are viscous intermediate to acidic magmas that erupt explosively and/or effusive. However, there are stratovolcanoes, which are not intermediate to acidic in their composition and still have a typical cone shape. Etna (Italy), Fuji (Japan), and Villa Rica (Chile) are basaltic examples.

Explosive eruptions of stratovolcanoes are classified as *plinian* if they are large (with eruption column heights in excess of 20-25 km and dense rock volumes >1 km^3), sustained, and produce widespread tephra deposits. This term derives from the 79 A.D. (Pompeii) eruption of Vesuvius (Italy). Eruptions with smaller volumes (0.1-1 km^3), lower eruption columns (<25 km), and more local tephra deposits are termed *subplinian*. Short-lived (typically tens of seconds) but intense explosions characterize so-called *vulcanian* eruptions, which are most common in volcanoes of intermediate (andesitic to dacitic) compositions (Schmincke, 2004).

Stratovolcanoes can collapse in the form of a caldera formation, as occurred at Pinatubo in 1991 (Newhall and Punongbayan, 1996) or by sector collapse, as illustrated by the 1980 eruption of Mount St. Helens (Lipman and Mullineaux, 1981).

Another end member for volcanic activity at stratovolcanoes is represented by effusive eruptions of very viscous silicic magma that create lava flows and/or domes. Although named effusive, these eruptions are especially hazardous due to pressurization and collapse of dense lava plugs. Recent well-observed dome eruptions of Mount St. Helens (e.g. 1980; Swanson and Holcomb, 1990) or Unzen (1991-1995; Nakada *et al.*, 1999) provided new insights into this eruption style.

Through intense observations of these and other volcanic eruptions and detailed examinations of the erupted rocks knowledge of magma storage systems prior to eruptions has improved enormously during the past 35 years.

CONSTRAINS ON MAGMA STORAGE BEANEATH ACTIVE VOLCANOES

Once a magma chamber has formed, the composition of magmas that potentially can erupt and the melt replenishment influence the physico-chemical properties of the reservoir. Processes in magma reservoirs, whether considered open or closed systems, can be complex and include crystallization, degassing, magma mingling and mixing, convection, compositional stratification, and assimilation of wall rock. Constraints on the temperature (T), pressure (P), volatile content (e.g. H_2O_{melt}), and oxidation state (fO_2) in magma reservoirs can be obtained by geothermometers, geobarometers (e.g. reviewed by Blundy & Cashman, 2008; and Putirka, 2008), melt inclusion studies, and comparison of natural phase assemblages (phases, phase proportions, and phase compositions) with those produced in experiments (e.g. Scaillet and Evans (1999); and Holtz *et al.*, 2005). Experimental studies of subduction zone volcanoes suggest that magma is commonly stored at relatively shallow depth, corresponding to pressures of 100–300 MPa, and mostly under volatile-saturated conditions (e.g. Muir *et al.*, 2014). Thus, the preserved phase assemblage provides tight constraints on storage conditions just prior to volcanic eruption. Information on pre-eruptive magma storage can also be derived from analysis of phenocryst-hosted melt inclusions. The preserved volatile concentration in the melt inclusions can potentially be used to constrain the pressure and

therefore also the depth of crystal formation. However an assumption, which has to be made, is that no change in volatile content in the melt inclusion has occurred.

Improvements in micro-analytical techniques are also providing new insight into the details of magma storage systems. Time scales of magmatic activity are constrained by isotopic (e.g. U-series isotopes) and diffusion studies. U-series studies are able to constrain phenocryst residence times within a magma storage reservoir (e.g. Bourdon *et al.*, 2000). Diffusion studies take advantage of chemical zoning profiles in phenocrysts (mostly plagioclase) caused by magma recharge or relocation within the crust (e.g. Costa and Morgan, 2010).

The combination of petrological constrains of magma storage with a geophysical localization of possible magma chambers is ideal for an integrated view on magmatic reservoirs within the Earth's crust. The depth, and partly also the three-dimensional propagation, of active magma intrusions can be identified with the help of geophysical data. A dramatic decrease in density and seismic velocity, and an increase in seismic attenuation and electrical conductivity can be observed at the transition between solid and partially molten crustal material. Typical geophysical techniques are based on detecting these differences in physical properties. A particularly important development in recent years is the increased use of interferometric synthetic aperture radar (InSAR) for identifying and monitoring active intrusions (e.g. Pritchard and Simons, 2004). In addition, improvements in data inversion techniques are increasingly detailed three-dimensional views of the active magmatic systems (e.g. Chaput *et al.*, 2012).

STUDY AREA

The Andes are the longest continental mountain range on Earth, continually stretching along the western coast of South America. This range is in total about 9000 km long extending from Colombia to the Chile triple junction around 46ºS, which defines the interaction point of the South American, Antarctic and Nazca plate. Along its length, the

Andes are split into several ranges, which are separated by intermediate depressions. The Andes are the result of the oceanic crust subduction under the South American plate. The main cause for the rise of the Andes is the compression of western South American Plate rim due to the subduction of the Nazca and the Antarctic Plate. The volcanic belt of the Andes is subdivided into four main volcanic zones that are separated from each other by regions without active volcanism. The four main areas of active volcanism in the Andean Volcanic Belt are: the Northern, Central, Southern and Austral Volcanic Zone, each of which can be seen as a separate continental volcanic arc. The volcanoes of the belt are diverse in terms of activity style, products and morphology (Schmincke, 2004).

The occurrence of volcanic activity along the subduction zone depends highly on variations of the subduction style. The primary factor controlling subduction style appears to be buoyancy, modified, for example, by anomalously thick (15-20km) oceanic crust (Gutscher, 2002). Within the regions of steep subduction (angles of ~30°) such as at the trench of the Central Volcanic Zone (CVZ), primary melts form as a result of the dehydration of the subducting oceanic plate. This process eventually leads to areas of intense volcanic activity.

A 5-10 times higher degree of upper plate seismicity is observed above flat-slab segments, compared to adjacent steep slab segments, implying a higher degree of interplate coupling (Gutscher, 2002). Segments of flat-slab subduction (angles of ~15°) change the thermal structure of the margin leading to a flat submergence of the oceanic plate beneath the continental plate. The hot asthenospheric wedge is displaced away from the trench. As a result the size of the forearc increases, with relatively low temperatures (~350-450°C; Gutscher, 2002). The formation of primary melts as a precursor for volcanism is inhibited with this subduction style.
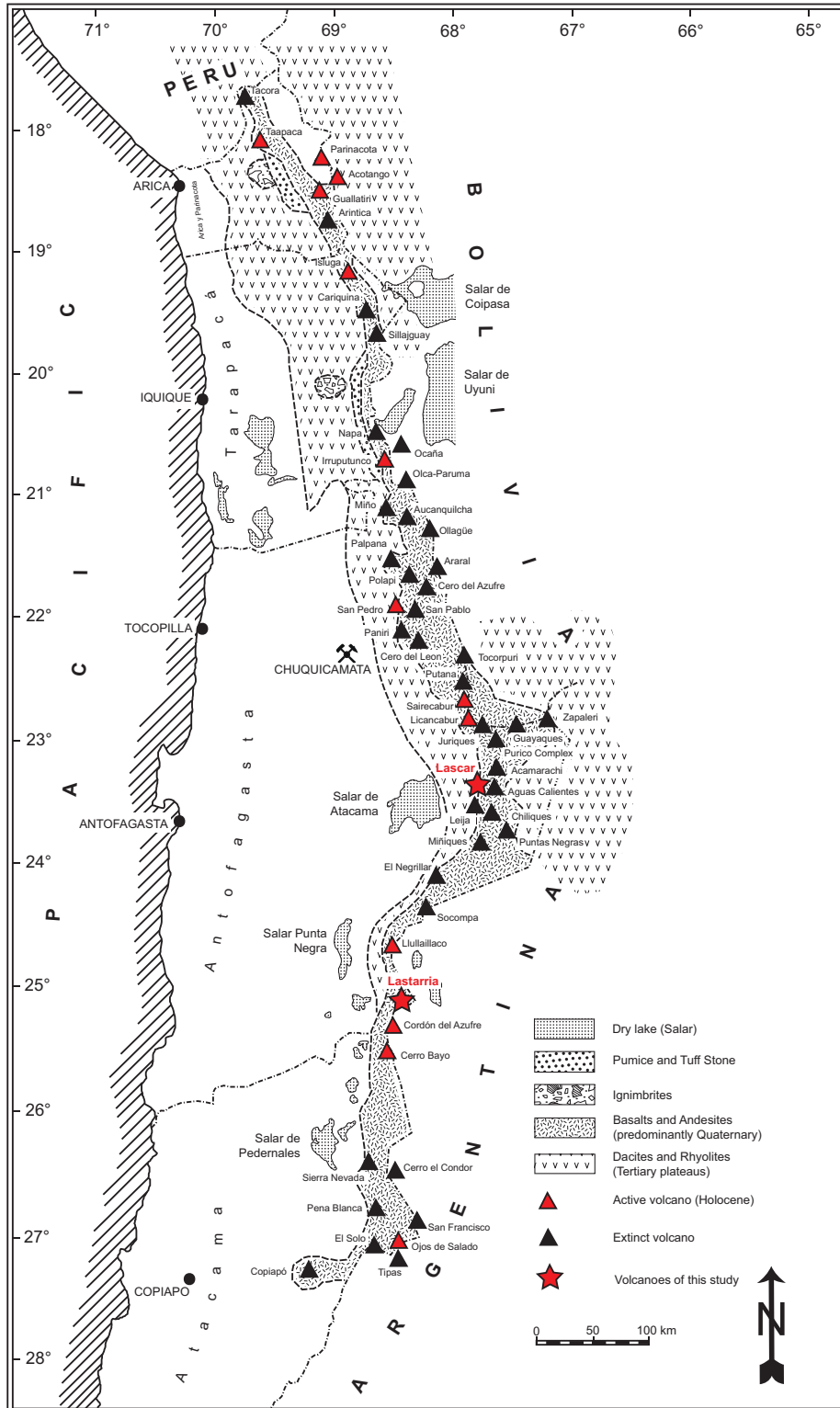
Figure 0.1: Simplified geological map of the Central Volcanic Zone in North Chile. Modified after Zeil (1964).

The study focus of this thesis is the Central Volcanic Zone. The CVZ extends from

Peru to Chile and forms the western boundary of the Altiplano-Puna plateau. A continental

crust that reaches a thickness of up to 74 km (Beck *et al.*, 1996) is characteristic for the CVZ. Within this zone there are 44 major and 18 minor volcanic centers that are considered to be active (de Silva & Francis, 1991). This volcanic zone also contains several potentially active large silicic volcanic systems, including the Lazufre area. Special focus lies on Lascar volcano, which is the most active volcano in the CVZ and Lastarria volcano, which is a potentially active volcano above a large silicic volcanic system (Lazufre area). Fig. 0.1 is a simplified geological map of the Chilean part of the Central Volcanic Zone with active and extinct volcanic centers.

OBJECTIVES

Major objectives of this thesis are defining mechanisms of andesitic magma evolution and the localization and characterization of magma storage regions through experiments and geothermobarometric approaches. Two volcanoes of the Central Andes were chosen as case studies for active and potentially active volcanism in this region. The thesis is composed of two main parts:

Part I focuses on crystallization experiments on andesitic compositions from Lascar volcano. These provide detailed information on the influence of pressure, temperature, volatile content of the melt, and oxygen fugacity on properties such as: the phase abundances, phase proportions, phase compositions and the liquid evolution. The experiments demonstrate that crystal fractionation is a major process for the magmatic evolution of Lascar eruptive rocks. Periods of magmatic mixing and crystal fractionation as the dominant process for magmatic differentiation can be distinguished during the evolution of Lascar volcano. The scientific outcomes contribute to the general understanding of calk-alkaline differentiation and can be also be applied on Lastarria volcano in order to understand the geochemical evolution presented in Part II.

Part II represents a combined petrological and geochemical study on Lastarria's andesites and dacites in order to reconstruct magma plumbing and storage beneath the volcano and the magmatic evolution of the eruptive rocks. The mineral phase compositions and whole-rock major and trace element compositions were used to constrain temperature, pressure, and possible mechanisms for magma differentiation. In particular the results of the geobarometric calculations can be directly compared with geophysical studies on the depth of possible magma reservoirs and the overall plumbing system.

Part I of this doctoral thesis is written to be a manuscript for *Journal of Petrology* as it combines natural observations with laboratory experiments to gain an overall view on the differentiation processes at Lascar. Part II has a clear focus on geothermobarometry to evaluate magma plumbing beneath Lastarria and to compare the results with geophysical observations. Part II is written as a manuscript to *Journal of Volcanology and Geothermal Research*.

REFERENCES

Beck, S. L., Zandt, G., Myers, S. C., Wallace, T. C., Silver, P. G., & Drake, L. (1996). Crustal-thickness variations in the central Andes. *Geology*, *24*(5), 407-410.

Blundy, J., & Cashman, K. (2008). Petrologic reconstruction of magmatic system variables and processes. *Reviews in Mineralogy and Geochemistry*, *69*(1), 179-239.

Bourdon, B., Wörner, G., & Zindler, A. (2000). U-series evidence for crustal involvement and magma residence times in the petrogenesis of Parinacota volcano, Chile. *Contributions to Mineralogy and Petrology*, *139*(4), 458-469.

Chaput, J. A., Zandomeneghi, D., Aster, R. C., Knox, H., & Kyle, P. R. (2012). Imaging of Erebus volcano using body wave seismic interferometry of Strombolian eruption coda. *Geophysical Research Letters*, *39*(7).

Costa, F., & Morgan, D. (2011). Time constraints from chemical equilibration in magmatic crystals. *Timescales of magmatic processes: from core to atmosphere. Wiley, Chichester*, 125-159.

de Silva S.L., & Francis P.W. (1991). Volcanoes of the Central Andes. Springer.

Gutscher, M. A. (2002). Andean subduction styles and their effect on thermal structure and interplate coupling. *Journal of South American Earth Sciences*, *15*(1), 3-10.

Herzberg, C. T., Fyfe, W. S., & Carr, M. J. (1983). Density constraints on the formation of the continental Moho and crust. *Contributions to Mineralogy and Petrology*, *84*(1), 1-5.

Hildreth, W. (1981). Gradients in silicic magma chambers: implications for lithospheric magmatism. *Journal of Geophysical Research: Solid Earth (1978–2012)*, *86*(B11), 10153-10192.

Holtz, F., Sato, H., Lewis, J., Behrens, H., & Nakada, S. (2005). Experimental petrology of the 1991–1995 Unzen dacite, Japan. Part I: phase relations, phase composition and pre-eruptive conditions. *Journal of Petrology*, *46*(2), 319-337.

Lipman, P. W., & Mullineaux, D. R. (Eds.). (1981). *The 1980 eruptions of Mount St. Helens, Washington*. US Dept. of the Interior, US Geological Survey.

Muir, D. D., Blundy, J. D., Rust, A. C., & Hickey, J. (2014). Experimental constraints on dacite pre-eruptive magma storage conditions beneath Uturuncu volcano. *Journal of Petrology*, *55*(4), 749-767.

Müntener, O., Kelemen, P. B., & Grove, T. L. (2001). The role of H_2O during crystallization of primitive arc magmas under uppermost mantle conditions and genesis of igneous pyroxenites: an experimental study. *Contributions to Mineralogy and Petrology*, *141*(6), 643-658.

Nakada, S., Shimizu, H., & Ohta, K. (1999). Overview of the 1990–1995 eruption at Unzen Volcano. *Journal of Volcanology and Geothermal Research*, *89*(1), 1-22.

Newhall, C. G., & Punongbayan, R. (Eds.). (1996). *Fire and mud: eruptions and lahars of Mount Pinatubo, Philippines*. Quezon City: Philippine Institute of Volcanology and Seismology.

Pritchard, M. E., & Simons, M. (2004). An InSAR-based survey of volcanic deformation in the central Andes. *Geochemistry, Geophysics, Geosystems*, *5*(2).

Putirka, K. D. (2008). Thermometers and barometers for volcanic systems. *Reviews in Mineralogy and Geochemistry*, *69*(1), 61-120.

Scaillet, B., & Evans, B. W. (1999). The 15 June 1991 eruption of Mount Pinatubo. I. Phase equilibria and pre-eruption P–T–fO_2–fH_2O conditions of the dacite magma. *Journal of Petrology*, *40*(3), 381-411.

Schmincke, H. U. (2004). *Volcanism*. Springer.

Shaw, H. R. (1980). The fracture mechanisms of magma transport from the mantle to the surface. *Physics of magmatic processes*, *64*, 201-264.

Sobolev, A. V., & Chaussidon, M. (1996). H_2O concentrations in primary melts from supra-subduction zones and mid-ocean ridges: Implications for H_2O storage and recycling in the mantle. *Earth and Planetary Science Letters*, *137*(1), 45-55.

Swanson, D. A., & Holcomb, R. T. (1990). Regularities in growth of the Mount St. Helens dacite dome, 1980–1986. In *Lava flows and domes* (pp. 3-24). Springer Berlin Heidelberg.

Wedepohl, H. K. (1995). The composition of the continental crust. *Geochimica et cosmochimica Acta*, *59*(7), 1217-1232.

Zeil, W. (1964). Die Verbreitung des jungen Vulkanismus in der Hochkordillere nordchiles. *Geologische Rundschau*, *53*(2), 731-757.

Dissertation of André Stechern

Petrological and Experimental Constrains on the Pre-eruptive Conditions of 1993 Lascar
Andesites and Insights Into the Evolution of Calc-alkaline Intermediate Lavas

Petrological and Experimental Constrains on the Pre-eruptive Conditions of 1993 Lascar Andesites and Insights Into the Evolution of Calc-alkaline Intermediate Lavas

1 ABSTRACT

Lascar Volcano, located in Northern Chile, is the most active volcano of the Andean Central Volcanic Zone (CVZ). Its activity culminated in the last major explosive eruption in April 1993. Lascar andesites, erupted in April 1993, have a phase assemblage of plagioclase, clinopyroxene, orthopyroxene, Fe-Ti oxides, and rhyolitic glass. To better define constrains of storage conditions and mechanisms of magmatic differentiation for andesitic magmas in a thick continual crust, petrological experiments were performed in internally heated pressure vessels (IHPV). To investigate the compositional evolution of residual liquids the crystallization sequence of an andesitic melt from Lascar Volcano was simulated experimentally at 300 and 500 MPa with various water activities (aH$_2$O). The experimental temperature (T) range was between 900 and 1050°C, aH$_2$O varied between 0.1 and 1.0, and the log oxygen fugacity (fO$_2$) varied between QFM+1.5 and QFM+3.3 at aH$_2$O = 1. To estimate pre-eruptive magma storage conditions, comparison of experiments to natural phase assemblages, modal proportions, and mineral, glass and whole-rock compositions, was used The phase equilibria constraints, in combination with geo-thermobarometric calculations, suggest that Lascar two-pyroxene andesitic magmas are stored at 975 ±25°C, 300 MPa, log$f$O$_2$ of QFM+2.75 ± .25, under H$_2$O-undersaturated conditions with 3.0 to 4.5 wt.% H$_2$O in the melt. Thus, Lascar andesites and dacites can be produced in an upper-crustal magma

Dissertation of André Stechern

Petrological and Experimental Constrains on the Pre-eruptive Conditions of 1993 Lascar
Andesites and Insights Into the Evolution of Calc-alkaline Intermediate Lavas

chamber as a result of fractional crystallization of a parental basalt or basaltic andesite melt which might originate from the mantle wedge and fractionate from a high-Al low-Mg arc basalt. This could be the initial composition for the shallow fractionation processes at Lascar. Additional geo-barometric and geochemical results point out that shallow magma reservoirs are also a region where magma mixing between primitive and already evolved melts takes place.

2 INTRODUCTION

To better understand storage and migration of magma in the continental crust major volcanic eruptions related to subduction zone settings were studied over the last 30 years. Main interest is directed towards clarifying numerous processes during magma emplacement and the further ascent towards the surface, like fractional crystallization, mixing with evolved magmas, crustal contamination, recharge, and convection in reservoirs caused by physical or chemical gradients in the system.

In continental arc settings, primary mafic magmas are generated in the mantle wedge (e.g. Davies and Stevenson, 1992). Well-studied volcanoes in this tectonic environment, like Mount St. Helens for example, indicate that the primitive magma is emplaced in a crustal reservoir at depths of 7-14 km, feeding in this case the eruption of May 18th, 1980. All subsequent dome-building eruptions at Mount St Helens from 1981 to 1986 tapped magma stored at a shallower depth of less than 4.5 km, suggesting a close relationship with the channel feeding magma from a deeper-seated reservoir (Blundy & Cashman, 2005; Cashman 1992).

However, this well studied example volcano and many more continental arc volcanoes are seated in a crust with a typical thickness of ~30 km. The continental crust in the Central Andes can reach more than twice the thicknesses of a "typical" continental crust. The main cause for the rise of the Andes is the compression of the western South American Plate due to the Nazca Plate subduction leading to maximum crustal thicknesses of 70-74 km under the

Dissertation of André Stechern

Petrological and Experimental Constrains on the Pre-eruptive Conditions of 1993 Lascar
Andesites and Insights Into the Evolution of Calc-alkaline Intermediate Lavas

Eastern and Western Cordillera (Beck *et al.*, 1996). Magmatism in the Central Andes is also caused by the subduction of the Nazca Oceanic Plate beneath the South American continent. The occurrence of volcanic activity along the subduction zone depends highly on variations of the subduction style. The primary factor controlling subduction style appears to be buoyancy of the submerging oceanic crust (Gutscher, 2002). Within the regions of steep subduction (angles of ~30°) such as at the trench of the Central Volcanic Zone (CVZ), primary melts form as a result of the dehydration of the subducting oceanic plate. This process eventually leads to areas of intense volcanic activity.

Lascar volcano is located at 23° 22′ S, 67° 41′ W in the Antofagasta Region of northern Chile, east of the Salar de Atacama and to the northeast of Laguna Lejía and lies directly between the Altinplano and Puna plateaus, which are commonly combined to the Altiplano-Puna plateau. Lascar is the most active volcano of the Andean Central Volcanic Zone. Its historic activity has been recorded since 1848, which is characterized by continuous fumarolic emissions and occasional sub-plinian eruptions, like the one in April 1993. Lascar volcano was in particular chosen for this study because of its location between the both plateaus (Altiplano and Puna), the broad intermediate composition, covering the range from basaltic andesites to dacites, and its specific geochemical signatures with the lowest Sm/Yb (~2) and Sr/Y (~25) ratios of the Quaternary eruptives from the CVZ (Mamani *et al.*, 2010). These particular geochemical signatures are crucial for understanding of arc magma geochemistry because they determine the pass way through the crust and the stagnation in different crustal reservoir levels, as these specific signatures are an indicator for the degree of crustal contamination undergone by magmas ascending from the mantle wedge.

A key phenomenon in a thickening continental crust is that its lower part is exposed to high lithostatic pressures, leading to the stabilization of garnet at the expense of plagioclase in the liquidus mineral assemblage of the magmas. (Hildreth and Moorbath, 1988; Müntener *et al.*, 2001; Lee *et al.*, 2006). The presence of garnet (together with amphibole and plagioclase) affects REE profiles of magmas interacting with, or generated in, the lower part

Dissertation of André Stechern

Petrological and Experimental Constrains on the Pre-eruptive Conditions of 1993 Lascar
Andesites and Insights Into the Evolution of Calc-alkaline Intermediate Lavas

of a thick continental crust (e.g. McMillan *et al.*, 1993). These processes are recorded by Sr/Y
and Sm/Yb ratios (e.g. Haschke *et al.*, 2002; Mamani *et al.*, 2010). Sr/Y and Sm/Yb ratios are
particularly sensitive to the presence of garnet versus plagioclase since Sr and Sm are
incorporated into plagioclase (Drake and Weill, 1975) and Y and Yb into garnet (Shimizu and
Kushiro, 1975; Green *et al.*, 1989). Thus, low Sr/Y and Sm/Yb ratios, as they can be observed
for Lascar rocks, are indicative for the presence of plagioclase and absence of garnet during
magma genesis and differentiation.

Lascars low Sr/Y and Sm/Yb ratios imply a shallow level of differentiation even
though the crust has a considerable thicknesses (~70 km), meaning that mafic melts from the
mantle wedge migrated through the thick crust without major stagnation periods in deep
crustal zones.

Geophysical investigations in the Central Andes have confirmed the existence of a
broad conductive zone (Brasse *et al.*, 2002) with a low seismic velocity at depths of ~20-40
km (Yuan *et al.*, 2000), interpreted as a region of partially molten material, located in the
center of the 70-74 km thick crust beneath the Eastern and Western Cordillera of the Central
Andes. This region in the thick continental crust is proposed to be the source for the
ignimbrites of the Altiplano-Puna volcanic complex (Lindsay *et al.*, 2001; Schmitt, 2001;
Muir *et al.*, 2014). However, recent magnetotelluric studies (Diaz *et al.*, 2012) show, that this
broad conductive zone does not expend towards the western border of the Altiplano-Puna
plateau at 23° S, where Lascar is located. Two-dimensional modeling has shown that this
broad anomaly in the crust is located at least 80 km East of Lascar at depth of 20-40 km.
Furthermore no magmatic reservoirs could be detected directly beneath Lascar using
magnetotellurics and three-dimensional modeling (Diaz *et al.*, 2012).

With all the previous work considered, structure, temporal and spatial evolution of
Lascars magmatic plumbing system and the geochemical evolution of magmas in the
extremely thick continental crust are still not well understood. The aim of this study is
therefore to constrain the current depth of magma storage region(s) beneath Lascar volcano

Dissertation of André Stechern

Petrological and Experimental Constrains on the Pre-eruptive Conditions of 1993 Lascar
Andesites and Insights Into the Evolution of Calc-alkaline Intermediate Lavas

and to identify pre-eruptive magmatic processes occurring within the magma plumbing system. In this way better understanding of the ongoing and past volcanism at Lascar can be obtained, as well as the potential for future activity.

Another important feature of Lascar eruptives is the presence of petrographic and geochemical mixing signatures between mafic and evolved components, indicating that a magmatic reservoir is periodically replenished with less evolved magma (Matthews *et al.* 1994). Two-pyroxene andesitic lavas from Lascar, mostly from the recent explosive activity (1986–1993), show little or no petrographic evidence for mixing with more evolved or primitive components (Matthews *et al.*, 1997). Therefore, crystal fractionation might be the controlling process for magmatic differentiation to evolved compositions.

This study aims to evaluate in detail possible mechanisms of magmatic differentiation and at which levels in a thick continental crust they take place. We present combined results of investigations on natural bulk rock samples, geothermo- and barometric calculations, the composition and volatile content of melt inclusions in plagioclase, orthopyroxene, and clinopyroxene, and the experimental determination of phase relations in Lascar andesites. Experimental temperature range was from 900 to 1050°C at pressures of 300 and 500 MPa. To investigate the influence of oxygen fugacity on the crystallization, experiments were conducted at moderately reducing conditions 1.5 log units above the quartz-fayalite-magnetite solid oxygen buffer (here after labeled as QFM+1.5) and at relatively oxidizing conditions of 3.3 log units above the quartz-fayalite-magnetite solid oxygen buffer (here after labeled as QFM+3.3). The comparison of the experimental products to natural samples is used to constrain the magmatic evolution of Lascar intermediate calc-alkaline rocks and the plumbing system beneath the volcano.

Dissertation of André Stechern

Petrological and Experimental Constrains on the Pre-eruptive Conditions of 1993 Lascar
Andesites and Insights Into the Evolution of Calc-alkaline Intermediate Lavas

3 EVOLUTION OF LASCAR VOLCANO

Lascar is currently the most active volcano of the CVZ. The volcanic body consists of two conjoined truncated cones with three ENE-WSW aligned summit craters and several minor craters. The active center has migrated westward from the eastern side, before switching back to the east side at ~7 kyr (Calder *et al.*, 2000). The evolution of the volcano can be sub-divided in four major stages as described in detail by Gardeweg *et al.* (1998). A brief summary of this evolution is given here as a background for the interpretation of the experimental and analytical results.

The volcanic activity started before the last glacial maximum but less than 50 kyr years ago. *Stage I* began less than 43 kyr ago with the eruption of blocky two-pyroxene andesitic lava and three, small volume, coarse-grained pyroclastic flow deposits building a stratocone at the eastern side of the present location. Ejecta from younger andesitic pyroclastic flow deposits of Stage I contain dacitic xenoliths.

Stage II (>26.5-22.3 kyr) activity is characterized by a migration of the active center to the west of the Stage I stratocone and the development of a silicic andesite dome complex, which has been widely destroyed. This unit, named Piedras Grandes, consists of large blocks of andesites with amphibole phenocrysts set in a welded ashy matrix. The Piedras Grandes unit is followed by the Soncor eruption (26.45 kyr ±0.5 kyr dated by radio carbon geochronology; Gardeweg *et al.*, 1998), the largest explosive eruption of the volcano, which produced 10-15 km^3 of amphibole-bearing andesitic to dacitic pyroclastic flow deposits and large Plinian fallout deposits.

Stage III (22.3-9.3 kyr) began with the formation of the andesitic and dacitic stratocone on the western side of the recent location overlaying the Soncor eruption vent. This western cone is build of thick porphyritic, amphibole free silicic andesite to dacite lavas and small andesite scoria flow deposits.

Dissertation of André Stechern

Petrological and Experimental Constrains on the Pre-eruptive Conditions of 1993 Lascar
Andesites and Insights Into the Evolution of Calc-alkaline Intermediate Lavas

The final *Stage IV* began 9.2 kyr ago with the Tumbre andesitic pumice fall and scoria flow eruption, shifting the active center again eastwards to the currently active part of the volcano. The deposits of this eruption consist of moderately vesicular basaltic andesite to andesitic scoria clasts and volcanic bombs, which are exposed on the northwest and west of the volcano. The most significant eruption from stage IV was the amphibole-bearing Tumbre-Talabre lava (7.1 kyr), which extends 8 km to the northwest of the volcano. This andesitic blocky lava flow was truncated by the formation of the first of three deep collapsed craters that document a progressive westward migration of the active volcanic center.

The historical behavior of Lascar has been recorded since the 1840's and can be characterized by continuous fumarolic activity in the form of a steam and SO_2 column, typically 1 km high, with intermitted short-lived volcanic explosions (Gardeweg *et al.*, 1998). Since 1984 the activity of the volcano is intensively monitored and described as a new eruptive phase with four recurring periodic cycles (3-4 years), summarized by Matthews *et al.* (1997). Cycles involve growth and subsidence of lava domes and the crater system, followed by explosive events, in September 1986, February 1990 and with the last major explosive eruption occurring on 18-20 April 1993, which generated an eruption column of 5-2 km height and pyroclastic flows reaching up to 9 km from the vent on the northwestern side of the volcano (Guarinos and Guarinos, 1993). The overall 1993 eruption produced more than 0.1 km³ of volcanic material (Matthews *et al.*, 1997). Subsequent, less intense, eruptions occurred in July 1994 and 1995, October 1996, July 2000, May 2005 and in April 2006 (Tassi *et al.*, 2009). Presently the activity of Lascar volcano is restricted to a permanent, sustained plume fed by the fumarolic field in the active crater (Tassi *et al.*, 2009). In January 2012 more than 300 volcanic tremors were reported over a period of 26 hours without leading to an eruption.

Matthews *et al.* (1999) studied the geochemical evolution of Lascar andesites and dacites in detail for the Piedras Grandes and Soncor eruptions. The erupted material commonly shows evidence of magma mixing, indicating that a fractionating magmatic system

Dissertation of André Stechern

Petrological and Experimental Constrains on the Pre-eruptive Conditions of 1993 Lascar
Andesites and Insights Into the Evolution of Calc-alkaline Intermediate Lavas

is periodically replenished with less evolved magma. However the geochemical data for all
four stages, we present here, does not indicate that magma mixing exclusively controls
magmatic differentiation at Lascar volcano and crystal fractionation may play a significant
role during the magmatic evolution.

4 NATURAL SAMPLES AND MELT INCLUSIONS

4.1 Major elements

25 rock samples from all four stages of Lascar eruptive history were collected during a
field campaign in 2007 (Fig. I.1).
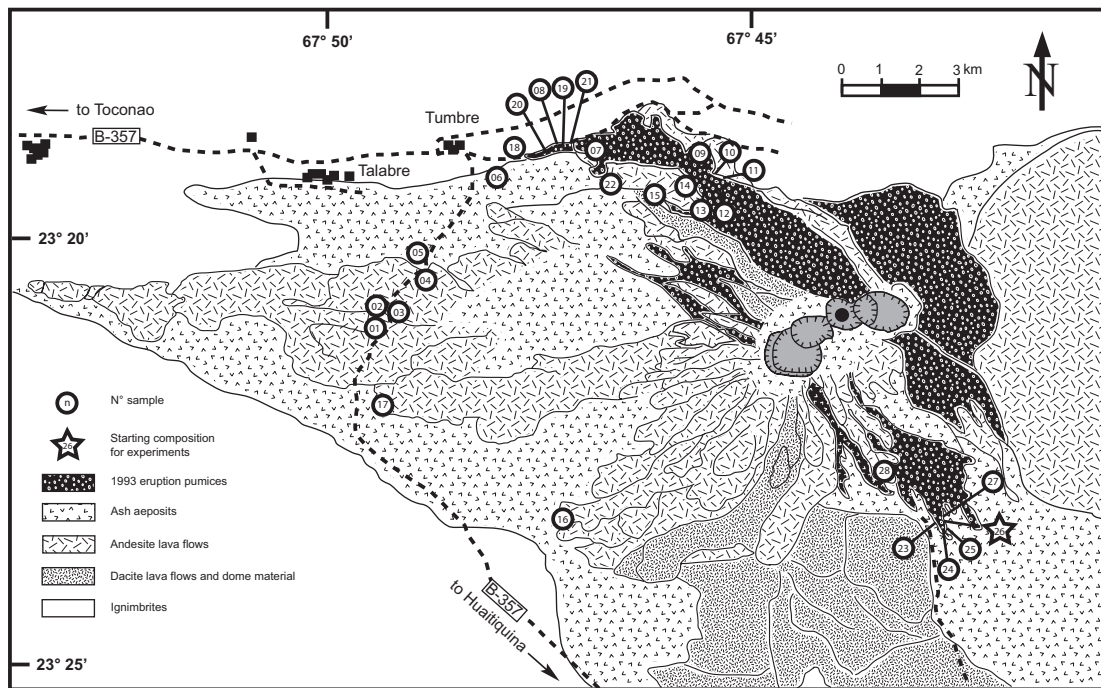
Figure I.1: Simplified geological map of Lascar volcano and sample sites.

Sampled material was from lava flows, as well as from different types of pyroclastic
rocks. Major element and trace element concentrations were determined by X-ray
Fluorescence (XRF) and Inductively Coupled Plasma-Mass Spectrometry (ICP-MS) analyses.
The major element compositions are listed in Tab. I.1. The trace element concentrations and

Petrological and Experimental Constrains on the Pre-eruptive Conditions of 1993 Lascar
Andesites and Insights Into the Evolution of Calc-alkaline Intermediate Lavas

details on analytical methods can be found in the supplementary material provided by

Mamani *et al.* (2010).

Table I.1: Whole rock major (determined by X-ray fluorescence, XRF) compositions of Lascar (Stage I to Stage IV) lavas. All iron is expressed as FeO_{total}

	Sample	SiO_2	TiO_2	Al_2O_3	FeO_{tot}	MnO	MgO	CaO	Na_2O	K_2O	P_2O_5	Total
Stage 1	LAS07-01	60.97	0.71	17.62	5.07	0.10	2.49	5.84	3.95	1.96	0.24	98.94
	LAS07-04	60.68	0.71	17.69	5.10	0.10	2.51	5.89	3.92	1.94	0.24	98.79
	LAS07-05	60.40	0.71	17.85	5.10	0.10	2.50	5.96	3.93	1.89	0.24	98.68
	LAS07-06	60.57	0.71	17.66	5.07	0.10	2.51	5.83	3.93	1.94	0.25	98.57
	LAS07-14	57.39	0.85	16.61	6.29	0.11	4.72	6.91	3.62	1.49	0.24	98.23
	LAS07-16	56.86	0.96	17.06	6.67	0.11	3.96	7.14	3.38	1.50	0.24	97.87
	LAS07-17	60.77	0.71	17.66	4.98	0.10	2.44	5.79	3.94	1.96	0.24	98.58
Stage 2	LAS07-02	61.50	0.66	16.34	5.01	0.10	2.84	5.24	3.59	2.26	0.21	97.75
	LAS07-03	61.65	0.69	16.16	5.27	0.10	2.95	5.25	3.58	2.26	0.21	98.12
	LAS07-18A	63.84	0.62	15.78	4.40	0.09	2.53	4.39	3.28	2.35	0.18	97.45
	LAS07-18B	60.96	0.73	16.15	5.25	0.10	3.42	5.06	3.03	2.01	0.21	96.91
Stage 3	LAS07-11	56.87	0.94	17.01	7.06	0.12	4.27	6.90	3.62	1.54	0.24	98.57
	LAS07-12	55.29	0.83	16.64	7.17	0.13	5.32	7.76	3.43	1.18	0.23	97.98
	LAS07-13	55.86	0.84	17.08	6.96	0.13	4.92	7.77	3.54	1.25	0.24	98.57
	LAS07-15	63.97	0.55	16.47	4.37	0.09	1.88	4.44	3.72	2.73	0.22	98.44
	LAS07-22	57.73	0.88	17.14	6.35	0.12	3.74	7.14	3.70	1.54	0.33	98.67
	LAS07-28	59.22	0.72	16.74	5.79	0.11	3.52	6.04	3.55	1.85	0.22	97.75
Stage 4	LAS07-07	58.02	0.85	17.22	6.19	0.12	3.68	7.17	3.73	1.55	0.32	98.85
	LAS07-08	57.39	0.86	17.18	6.21	0.12	3.67	7.09	3.64	1.54	0.33	98.03
	LAS07-20	59.35	0.72	16.70	5.93	0.11	3.83	6.37	3.47	1.87	0.19	98.54
	LAS07-21	58.07	0.76	16.42	6.46	0.12	4.88	7.28	3.39	1.57	0.19	99.14
	LAS07-23	58.43	0.75	16.33	6.34	0.12	4.65	7.04	3.38	1.66	0.19	98.90
	LAS07-24	58.41	0.76	16.42	6.45	0.12	4.79	7.20	3.39	1.61	0.19	99.34
	LAS07-25	59.71	0.73	16.42	5.73	0.11	3.50	5.97	3.48	1.99	0.20	97.83
	LAS07-26	58.46	0.75	16.01	6.51	0.12	4.70	6.91	3.29	1.68	0.19	98.61

The major element composition of the samples varies from medium-K andesites

(55.6 wt.% SiO_2, 5.4 wt.% MgO) to dacites (65.2 wt.% SiO_2, 2.6 wt.% MgO). As shown in

the binary diagrams in Fig. I.2, the evolution of Lascar bulk rock compositions does not

follow one single path. It seems that periods of magmatic mixing processes, leading to the

most evolved rock compositions at Lascar, are alternating with stages dominated by fractional

crystallization. However, none of the four eruptive stages covers the whole range of

compositions between the primitive and more evolved end-members mentioned above.

Stage I rocks seem to follow a trend resulting from crystal fractionation towards more

evolved compositions with SiO_2 contents between ~58 and 62 wt.% (Fig. I.2). Eruptive

material from Stage II collected during this field campaign as well as a large number of

Dissertation of André Stechern

Petrological and Experimental Constrains on the Pre-eruptive Conditions of 1993 Lascar
Andesites and Insights Into the Evolution of Calc-alkaline Intermediate Lavas

samples collected by Matthews *et al.* (1999) indicate that the compositional variation in this stage is dominated by mixing events (straight lines connecting the evolved and more primitive compositions in the binary diagrams in Fig. I.2). However, from the collected data it is not clearly discernible if there is only one mixing trend or there is also fractionation involved. The most primitive material collected from Lascar (lowest SiO_2 content) was erupted during Stage III. These samples are named *Manquez agglutinate* (Gardeweg et al, 1998) and are interpreted as the late phase of the Tumbres eruption or possibly associated with the late cone on the eastern margin of the Western Stratocone. The more evolved rocks from this stage follow a curved trend towards higher SiO_2 concentrations (Fig. I.2), which might be interpreted as an evolution resulting from crystal fractionation. Rocks from Stage IV have a relatively narrow range of compositions between ~58 and ~61 wt.% SiO_2 (3.5-5 wt.% MgO) and seem to follow a fractionation trend although it is not as clear as for Stage III.

Petrological and Experimental Constrains on the Pre-eruptive Conditions of 1993 Lascar Andesites and Insights Into the Evolution of Calc-alkaline Intermediate Lavas
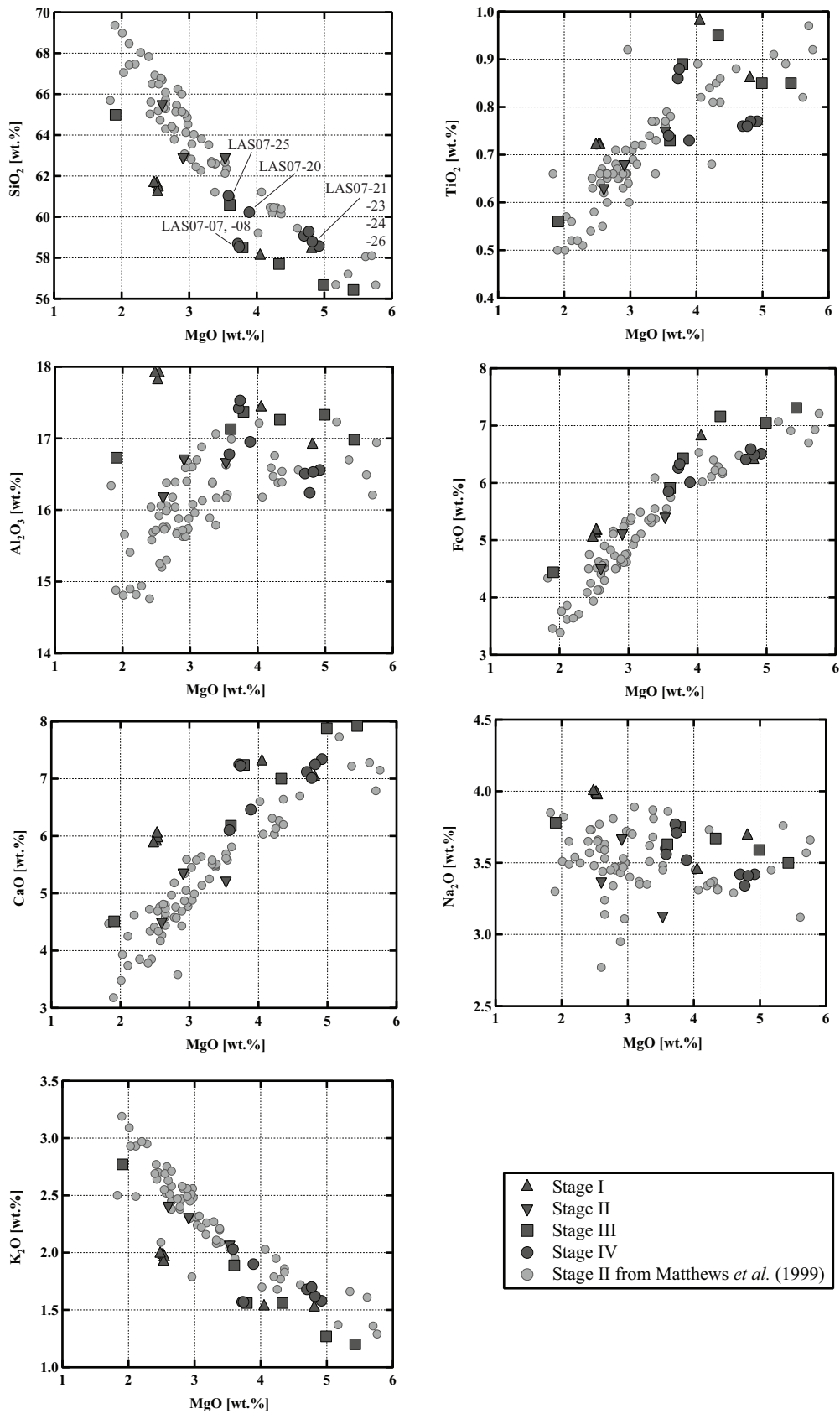
Figure I.2: Major element composition of Lascar volcanic rocks from all four stages plotted against MgO. Also shown are detailed bulk-rock data of Sage II from Matthews *et al.* (1999).

Dissertation of André Stechern
Petrological and Experimental Constrains on the Pre-eruptive Conditions of 1993 Lascar
Andesites and Insights Into the Evolution of Calc-alkaline Intermediate Lavas

4.2 Mineral abundances and compositions of Stage IV volcanic rocks

4.2.1 Modal proportions

A modal analysis of minerals in three samples from the recent 1993 eruptive material and in one older sample (Las07-07; 7.1 kyr) from Stage IV was carried out by point-counting on selected thin sections. The minerals were determined with a step size of either 300 or 350 µm (2 directions) resulting in a number of points ranging from ~6000 to ~9000. Results are given in Tab. I.2.

Table I.2: Modal phase proportions in Lascar's Stage IV rocks gained from point counting

Sample	LAS07-07	LAS07-23	LAS07-24	LAS07-26
Type	Stage IV andesitic lava flow	'93 eruption - grey andesitic bomb	'93 eruption - black pumice	'93 eruption - white pumice
Matrix	59,35	57.20	56.25	45.31
Plagioclase	28,68	27.68	26.29	27.02
Pyroxene	7,52	11.44	10.52	13.91
Oxides	2,91	2.48	6.94	13.76
Amphibole	1,55	0.00	0.00	0.00
Xenocryst cluts	0,00	1.19	0.00	0.00
Total	100	100	100	100
% Vesicularity	2,8	7.9	35.3	53.4

Plagioclase, clinopyroxene, and orthopyroxene are the major phenocrysts, which can be found in all of the samples. Approximately 40 area% of the thin section is composed of phenocrysts. Additional minerals present in the natural rocks are accessory apatite microphenocrysts, and very rare olivine (<0.1 area%) in only a few samples. Millimeter sized patches of xenocrysts can be found in some thin sections. The proportion of plagioclase phenocrysts is ~27-28% (surface area), pyroxenes form 7 to 14% of the rock. Amphibole is not present as major phenocrysts in 1993 rocks but can be found in various stages of breakdown in two older sample from Stage IV (LAS07-07, -08; Tumbre-Talabre lava, 7.1 kyr, Tab. I.2). Samples of older (Stage I-III) eruptive stages, in particular the Piedras Grandes and Soncor eruptions (21.0 kyr), contain amphibole and biotite in some dacitic eruptions.

Dissertation of André Stechern

Petrological and Experimental Constrains on the Pre-eruptive Conditions of 1993 Lascar
Andesites and Insights Into the Evolution of Calc-alkaline Intermediate Lavas

It is worth mentioning that the modal abundance of amphibole in Lascar rocks (if present) is usually very small (maximum 8 area% calculated on a vesicle-free basis in the Piedras Grandes unit). Amphibole phenocrysts are ragged and partially or wholly replaced by fine to coarse-grained plagioclase, pyroxene, and Fe-Ti oxides (Matthews *et al.*, 1994 and 1999).

4.2.2 Mineral compositions

Mineral compositions were determined by electron microprobe (EPMA) as described later in chapter 'Analytical methods'.

Plagioclases from 1993 eruptions have a wide range of anorthite contents between An_{37} and An_{80} but with a clear maximum between An_{50} and An_{65} (see AF1 and Tab. AT1 in the Appendix). Orthoclase components in the analyzed plagioclases range between $\sim Or_{0.5}$ and $\sim Or_{4.5}$ with most of the compositions having $\sim Or_{1.0}$.

Natural pyroxenes from Stage IV have a relatively narrow range of compositions. Orthopyroxenes are clinoenstatite with enstatite components between En_{62} to En_{83} and Wo <5 and with typical Mg numbers (Mg# = 100 · Mg/(Mg+Fe), in mol%) in the range 66-86. Clinopyroxenes are all high Ca-augites with Mg# in the range 71-89. The enstatite component ranges from En_{39} to En_{53} with wollastonite values from Wo_{38} to Wo_{45}. It can be observed that pyroxenes from the lava flow samples (Las07-07) have narrow compositional field with En and Wo values varying only little (±5 mol%), whereas samples from volcanic ejecta erupted 1993 reveal the largest variation in pyroxene end-member components (up to 20 mol%).

Rims of adjacent pyroxenes from different types of volcanic ejecta were analyzed to determine temperatures (and pressures) of last equilibration using the model of Andersen *et al.* (1993) for temperature (Fig. AF2 and Tab. AT2 in the Appendix) and the model of Putirka (2008) to estimate temperatures and pressures (Fig. I.3 and Tab. AT3). Temperatures calculated after Andersen *et al.* (1993) give average values between 980°C for a pumice (sample LAS07-26) and 1030°C for an andesitic lava flow (sample LAS07-07). Average

Dissertation of André Stechern

Petrological and Experimental Constrains on the Pre-eruptive Conditions of 1993 Lascar
Andesites and Insights Into the Evolution of Calc-alkaline Intermediate Lavas

temperatures calculated by the model of Putirka (2008) are between 940 and 1010°C with maximum values of 1050°C. Pressures gained by this model are in average between 250 to 500 MPa, with two frequency maxima around 300 and 500 MPa. Maximum determined pressures are up to 1 GPa. A clear correlation between *P-T* and a certain type and composition of ejecta cannot be concluded. However, it can be noted that the information on pressures obtained from the white pumice sample (*P* >550 MPa; LAS07-20) are higher in average when compared with pressures determined from the black pumice sample (mostly 200 to 400 MPa; LAS07-08). The bulk compositions of these two samples are not very different, but for a similar MgO concentration (3.7-3.8 wt.%) the SiO_2 content is ~2 wt.% higher in the white pumice when compared with the black pumice (Tab. I.1).
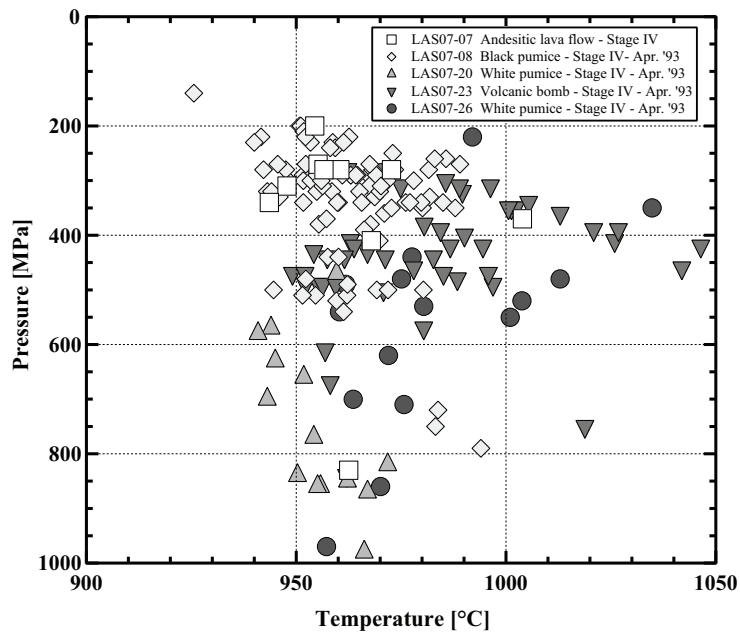
Figure I.3: Pressure-temperature (*P-T*) estimates for representative Stage IV lavas. P-T estimates are obtained using the Opx-Cpx geothermobarometer from Putirka (2008). Only results were shown which are in the K_d(Fe-Mg) confidence interval (1.09 ±0.14) recommended by Putirka (2008).

Magnetite and ilmenite are present in all Lascar rocks. Oxygen fugacities and temperatures were calculated according the method of Andersen and Lindsley (1985) applying the ILMAT scheme of Lepage (2003) and are shown in Fig. I.4 (see Tab. AT4 in the Appendix for details). Magnetite and ilmenite were checked for equilibrium using Mg-Mn

Dissertation of André Stechern

Petrological and Experimental Constrains on the Pre-eruptive Conditions of 1993 Lascar
Andesites and Insights Into the Evolution of Calc-alkaline Intermediate Lavas

partitioning criteria after Bacon & Hirschmann (1988), and only assemblages with
equilibrium compositions, low compositional variability and absence of exsolution lamellae
were used. Lascar eruptive material shows a relatively narrow field of log fO_2 ranging from
~QFM+1 to QFM+2 with temperatures between 880 and 940°C (QFM is quartz-fayalite-
magnetite oxygen buffer). Volcanic bombs (e.g. sample LAS07-23) show the most reducing
conditions at or even below QFM+1. All types of pumices (e.g. samples LAS07-08, -20, -26)
have intermediate log fO_2 between QFM+1 and QFM+2. The andesitic lava flow (sample
LAS07-07), which is older than the other studied samples, shows the highest oxygen
fugacities of QFM+2.
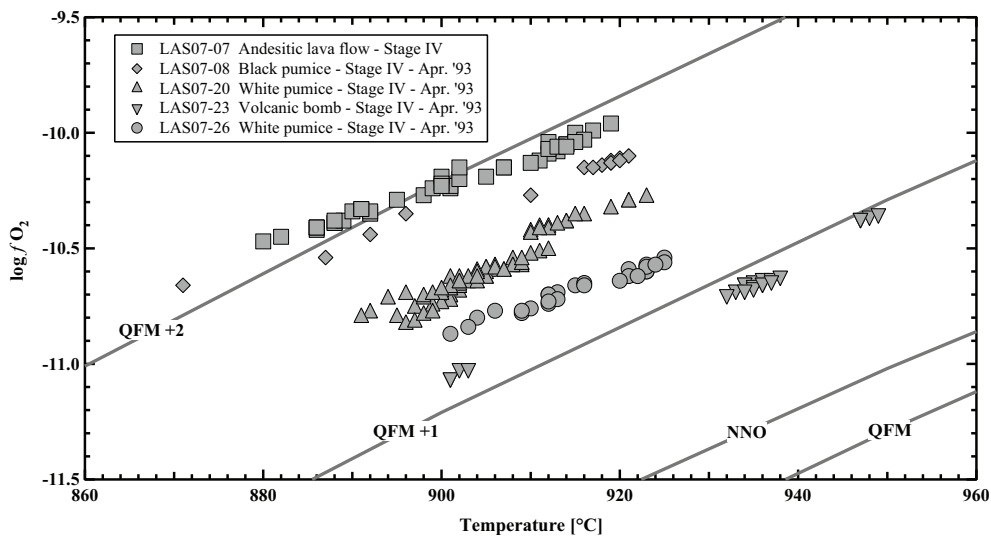
Figure I.4: Thermo-oxybarometry of Stage IV Lascar volcanic rocks: log oxygen fugacity (log fO_2) versus
temperature, calculated from Mt-Ilm equilibria (Stormer, 1983) using the ILMAT calculation sheet (LePage,
2003). Oxygen buffer curves (NNO: Ni-NiO, QFM: quartz-fayalite-magnetite) are taken from Frost (1991).

4.2.3 Melt inclusions

To better constrain the composition of melts from the andesitic magma, related to the
April 1993 eruption, we analyzed inclusions in phenocrysts of Lascar lavas and pyroclastics
of the 1993 eruption (sample LAS07-23 and LAS07-26). Phenocrysts of plagioclase, ortho-
and clinopyroxenes contain entrapped and well-preserved melt inclusions. Mineral separates
were extracted manually from the crushed bulk rock, mounted in an epoxy and polished on

Dissertation of André Stechern

Petrological and Experimental Constrains on the Pre-eruptive Conditions of 1993 Lascar
Andesites and Insights Into the Evolution of Calc-alkaline Intermediate Lavas

one side until the melt inclusion is exposed. The length of the host phenocrysts varies from ~500 to ~1000 μm and the width of the mineral grains is at least ~100 μm. The dimensions of inclusions vary from less than 10 to more than 100 μm, the largest ones being trapped in plagioclases. Only inclusions larger than 30 μm were selected for microprobe analysis. To check for possible crystallization of the inclusions after entrapment (e.g. Roedder, 1979), we analyzed and compared homogenized and non-homogenized melt inclusions from the same sample. Homogenization was performed at high pressure of 200 MPa using a drilled cylinder of the rock sample with a diameter of 4 mm and a length of about 15 mm. The rock cylinder was placed in an $Au_{80}Pd_{20}$ capsule and was heated in an internally heated pressure vessel (IHPV) pressurized with an Ar-H_2 gas mixture (see description of the apparatus below) at 1000°C and 200 MPa for 40 minutes. To minimize a possible reaction between the host mineral and the trapped melts a relatively low temperature of 1000°C and a short run duration were chosen. Reducing atmosphere in the IHPV was generated to prevent the loss of H_2 and therefore an oxidation of the trapped melts (e.g. Sobolev and Danyushevsky, 1994). The capsule was left open to prevent the formation of water inside the capsule at reducing conditions and to minimize physical stress on the sample. After the homogenization process, the experiment was rapidly quenched with a rate of approximately 150°C/s. The rock cylinder was cut along the center axis to access as many melt inclusions as possible.

4.2.4 Major Oxides

The composition of the glasses in the inclusions was analyzed by electron microprobe (analytical details are given in Appendix). Major element compositions and volatile contents are given in Tab. AT5 of the Appendix. The inclusions are generally more differentiated than the bulk rock (Fig. I.5). Melt inclusions are dacitic to rhyolitic in composition and show systematic trends for all major elements with a variation in SiO_2. Silica contents in Lascar melt inclusions range from 65 to 78 wt.% and the composition of the most evolved bulk rock sample is almost identical with the least evolved melt inclusion (~65 wt.% SiO_2 and ~1.9

Dissertation of André Stechern

Petrological and Experimental Constrains on the Pre-eruptive Conditions of 1993 Lascar
Andesites and Insights Into the Evolution of Calc-alkaline Intermediate Lavas

wt.% MgO). The data point out that the homogenized melt inclusions extend the differentiation trend shown by the bulk rock analyses towards more mafic compositions, whereas the non-heated inclusions have generally higher SiO_2 values (70-78 wt.% SiO_2) and are the most evolved compositions which were observed.

Melt inclusions (MI) in plagioclase phenocrysts are rhyolitic with no significant difference between heated and non-heated samples. The plagioclase composition in the vicinity of the MIs ranges from An_{55} to An_{74}. The MIs cover a relatively small compositional range with 70-75 wt.% SiO_2 and 0.2-0.7 wt.% MgO. In contrast, compositions of both types of pyroxene inclusions, heated and non-heated, cover the whole range from dacitic to rhyolitic glasses. MgO concentrations in all Lascar inclusions are typically low (0.1-2.0 wt.%) and correlate negatively with SiO_2. Al_2O_3, FeO_{tot}, and CaO also correlate negatively with SiO_2. K_2O is the only major oxide in the melt inclusions showing a positive correlation with SiO_2.

Petrological and Experimental Constrains on the Pre-eruptive Conditions of 1993 Lascar
Andesites and Insights Into the Evolution of Calc-alkaline Intermediate Lavas
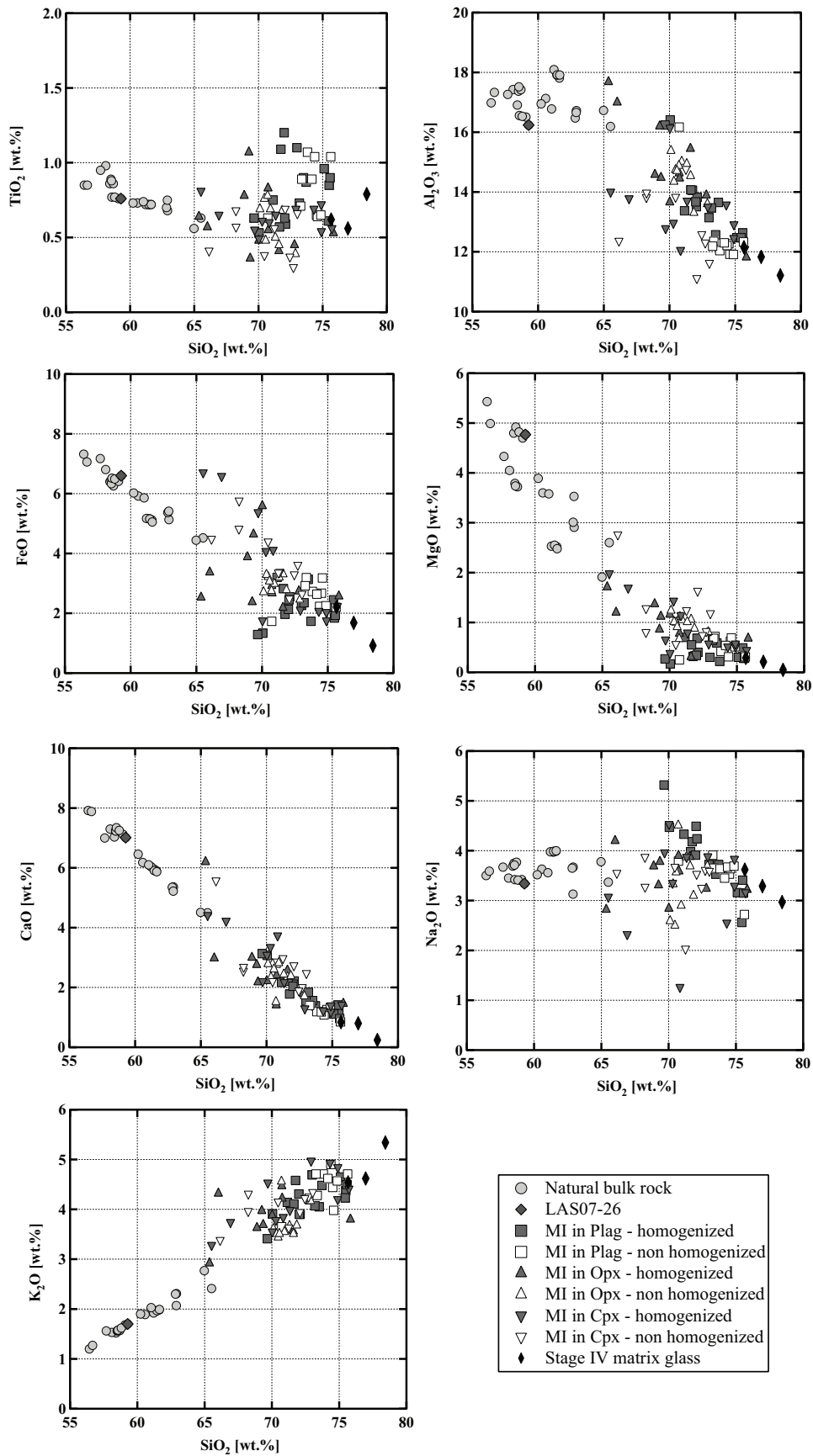
Figure I.5: Composition of melt inclusions in plagioclase, orthopyroxene, and clinopyroxene-heated and non-heated. Compositions of natural bulk-rock and residual matrix glass.

Dissertation of André Stechern

Petrological and Experimental Constrains on the Pre-eruptive Conditions of 1993 Lascar
Andesites and Insights Into the Evolution of Calc-alkaline Intermediate Lavas

4.2.5 Volatiles

H_2O concentrations in the MI were estimated from the microprobe analyzes reported in Tab. AT5 in the Appendix, using the "by difference" method (100% - microprobe analytical total). The estimated water concentrations in melt inclusions range from 0 to ~3 wt.% H_2O. No significant difference between MI from different host minerals, heated or not, can be observed. Nevertheless, these results should be interpreted with caution due to the high uncertainty of the method (see below). Sulfur concentrations in the melt inclusions from the 1993 eruptive material are low with a maximum of ~260 ppm, in good agreement with data reported by Wallace and Edmonds (2011) for evolved volcanic rocks from subduction zones. A decrease of sulfur concentration with increasing SiO_2 or K_2O of the inclusion can be observed but is not well pronounced (Fig. AF3 in the Appendix), suggesting that sulfur degassing or crystallization of S-bearing phases occurred in conjunction with crystal fractionation. Chlorine concentrations in the melt inclusions range from ~300 ppm up to ~1700 ppm and exhibit no systematic variation with incompatible element abundances (e.g. K_2O), indicating that no or only low Cl degassing occurred during differentiation (Fig. AF3 in the Appendix). The behavior of fluorine is very similar to chlorine with concentrations of 0 to ~1500 ppm for the majority of melt inclusions.

4.2.6 Interstitial glasses

Interstitial quenched glasses of Stage IV eruptive material (1993 eruption and older lavas) were analyzed to compare major oxide compositions with the results of the melt inclusions (Fig. I.5). Areas with large interstitial melt pools (>100 μm) were chosen and carefully checked for the absence of quench phases (e.g. plagioclase). However, many other melt pools in the same sample contained a high proportion of microlites, mainly composed of plagioclase. Glasses were measured several times to ensure the homogeneity of the matrix. Analyses of the natural glasses are given in Tab. I.3. The natural quenched glasses have

Dissertation of André Stechern

Petrological and Experimental Constrains on the Pre-eruptive Conditions of 1993 Lascar
Andesites and Insights Into the Evolution of Calc-alkaline Intermediate Lavas

higher SiO_2 compositions and represent the most evolved melts in this suite with ~75-77 wt.%

SiO_2 and 0.3-0.05 wt.% MgO. However, the compositions of the interstitial glasses need to be

interpreted with caution, considering the formation of microlites.

Table I.3: Composition of Stage IV natural matrix glass.

	Sample	n	SiO_2	TiO_2	Al_2O_3	FeO_{tot}	MnO	MgO	CaO	Na_2O	K_2O	Total
Stage 4	LAS07-07	16	76.74	0.78	10.97	0.90	0.03	0.05	0.24	2.91	5.22	97.84
			(0.53)	(0.08)	(0.26)	(0.17)	(0.05)	(0.05)	(0.09)	(0.42)	(0.11)	(0.57)
	LAS07-23	20	75.76	0.62	12.16	2.21	0.06	0.29	0.84	3.63	4.54	100.13
			(0.43)	(0.04)	(0.21)	(0.16)	(0.06)	(0.05)	(0.08)	(0.22)	(0.11)	(0.45)
	LAS07-26	17	76.87	0.56	11.81	1.67	0.04	0.21	0.80	3.28	4.61	99.87
			(0.45)	(0.04)	(0.21)	(0.13)	(0.04)	(0.06)	(0.11)	(0.25)	(0.15)	(0.65)

5 HIGH TEMPERATURE, HIGH PRESSURE PHASE EQULIBRIA EXPERIMENTS

5.1 Starting material

The natural andesite of sample LAS07-26 (Stage IV, April 1993 eruption) was chosen

as starting material for the phase equilibria experiments. This sample represents one of the

most primitive compositions found at Lascar volcano with 58.9 wt.% SiO_2 and 4.7 wt.%

MgO. Rock fragments were crushed and ground in a rotary swing mill. After 90 minutes of

melting in a Pt crucible at 1600°C and 1 atm. in a chamber furnace, the resulting melt was

quenched in a water bath and the obtained glass was ground in an agate mortar. The

homogeneity of the silicate glass was verified by electron microprobe (see analyses in Tab.

I.4). Two fractions with grain sizes of <100 μm and 100-200 μm were mixed together in a

ratio 1:1 to decrease the free volume between grains.

Table I.4: Experimental starting compositions of re-molten andesite in phase equilibria experiments (sample
LAS07-26).

SiO_2	TiO_2	Al_2O_3	FeO_{tot}	MnO	MgO	CaO	Na_2O	K_2O	P_2O_5	Total
58.41	0.75	15.80	6.63	0.13	4.81	6.82	3.44	1.67	0.19	98.63
(0.59)	(0.04)	(0.28)	(0.24)	(0.09)	(0.21)	(0.24)	(0.23)	(0.08)	(0.07)	(0.74)

Dissertation of André Stechern

Petrological and Experimental Constrains on the Pre-eruptive Conditions of 1993 Lascar
Andesites and Insights Into the Evolution of Calc-alkaline Intermediate Lavas

5.2 Experimental strategy

We conducted phase equilibrium experiments in which the andesite was equilibrated with H_2O-CO_2-bearing fluids at 300 MPa and at two oxygen fugacities corresponding to QFM+1.5 and QFM+3.3 at H_2O-saturated conditions; however, the redox conditions also depend on the activity of H_2O in the system (see below). In addition, experiments at 500 MPa and QFM+1.5 for H_2O-saturated samples were conducted to evaluate a possible pressure effect on the phase relations.

First order constraints for the experimental conditions were gained from natural pyroxene pairs (Fig. I.3 and Fig. AF2 in the Appendix). The temperature of the experimental runs was varied from 900 to 1050°C (either in 25°C or 50°C intervals), which is within the range of 940 - 1020 °C indicated by natural pyroxene pairs. All experiments were conducted at 300 or 500 MPa, which is in agreement with estimates of the prevailing pressure in the magma chamber prior to eruption estimated on two-pyroxene barometry using the model of Putirka (2008) as shown in Fig. I.3. The fO_2 conditions chosen for the high-pressure experiments were determined based on compositions of coexisting ilmenite-magnetite pairs from different types of eruptive material (Fig. I.4).

5.3 Experimental technique

The experiments were conducted in Au capsules, which were approximately 15 mm long (inner diameter of 2.6 mm). Different proportions of H_2O and CO_2 were added to 50 mg of glass powder to vary the composition of the fluid phase in our experiments. The total volatile content (CO_2 + H_2O) was kept at ~12 wt.% of the total charge. Silver oxalate ($Ag_2C_2O_4$) was used as a source of CO_2. The initial mole fraction of H_2O (X^{fl}_{H2Oini}) in the fluid phase was varied from $X^{fl}_{H2Oini} = 0.0$ (nominally dry, pure CO_2 in the fluid) to 1.0 (water-saturated), as listed in Tabs. I.5 to I.7. The amount of added volatiles was sufficient to

Dissertation of André Stechern

Petrological and Experimental Constrains on the Pre-eruptive Conditions of 1993 Lascar
Andesites and Insights Into the Evolution of Calc-alkaline Intermediate Lavas

produce a free fluid phase in all experimental runs at 300 and 500 MPa, verified using the
weight-loss method after opening the capsules.

The experiments were conducted in an IHPV. Total pressure (P) was measured and
recorded continuously with an uncertainty of about 1 MPa using a strain gauge manometer.
The variations of pressure during the experiments were ≤ 5 MPa. Temperature (T) was
measured with four unsheathed S-type (Pt–Pt$_{90}$Rh$_{10}$) thermocouples over a length of about 30
mm and temperature variations between the two sample thermocouples were below 5°C. The
IHPV was pressurized with an Ar–H$_2$ gas mixture for the experiments at reducing conditions
(QFM+1.5 at H$_2$O-saturated conditions). Hydrogen diffuses through gold into the capsules,
and at 700°C osmotic equilibrium is reached within ~2h (Schmidt et $al.$, 1995). To control the
fH$_2$ prevailing at high P and T, the IHPV is equipped with a Shaw-membrane made of Pt (a
detailed description of the apparatus is given by Berndt et $al.$, 2002). The fugacity of H$_2$ in the
experimental runs was chosen to ensure redox conditions close to QFM+1.5 in the capsules at
H$_2$O-saturated conditions. The calculation of fH$_2$ at certain P-T conditions is based on the
equations of Schwab & Küstner (1981) and applied to fill the vessel with the desired amount
of initial H$_2$. Since fH$_2$ and fO$_2$ are linked by the equilibrium reaction for water formation (H$_2$
+ ½O$_2$ ↔ H$_2$O), the prevailing oxygen fugacity in the individual capsules varied with aH$_2$O in
the melt. The calculated fO$_2$ for each experiment is reported in Tabs. 5-7.

The experiments at oxidizing conditions were performed in another IHPV pressurized
with pure Ar gas providing high intrinsic oxygen fugacity within the vessel (close to
QFM+3.3 at at H$_2$O-saturated conditions; Schuessler et $al.$, 2008). The fO$_2$ at H$_2$O-
undersaturated conditions can be estimated using the relation log fO$_2$^{capsule} = log fO$_2$ (at aH$_2$O
= 1) + 2 log aH$_2$O (e.g., Botcharnikov et $al.$, 2005), where aH$_2$O is determined from the water
concentration in the melt following the model of Burnham (1979). The overall error in the
determination of the fO$_2$ in each experiment is estimated to be ~0.2 log units (Botcharnikov et
$al.$, 2005).

Dissertation of André Stechern

Petrological and Experimental Constrains on the Pre-eruptive Conditions of 1993 Lascar
Andesites and Insights Into the Evolution of Calc-alkaline Intermediate Lavas

The duration of all experiments varied from 2 to 7 days with longer duration at lower temperatures. After the experiment, all capsules were rapidly quenched with a quench rate of about 150°C/s.

5.4 Analytical methods

Analyses of the experimental products were performed with a Cameca SX-100 electron microprobe at the Institute for Mineralogy, Leibniz University Hannover. Residual glasses were measured with a defocused beam of 5-10 μm, 4 nA beam current and counting times of 4 s for Na and K, 20 s for P and 8 s for the other elements. In samples with low melt fraction, the microprobe beam was defocused as much as possible. No significant alkali loss (within the uncertainty) was detected using these analytical conditions.

Minerals were analyzed with a focused beam at 15 kV, 15 nA beam current and counting times for major elements of 10 s. Na and K were analyzed first to minimize alkali loss. P was analyzed at last with counting times of 20 s. Multiple measurements were made for each phase within a sample to minimize possible analytical errors and check for homogeneity.

The 'by-difference' method was applied to determine the H_2O concentration in the quenched experimental glasses. To improve the quality of the 'by-difference' technique, hydrous standard basaltic and andesitic glasses with well-characterized water contents from 0.28 to 8.81 wt.% H_2O (after Botcharnikov *et al.*, 2006 and Shiskina *et al.*, 2010) were analyzed with the same EPMA setting. The results were used to establish a relation between the 'by-difference' value and the H_2O concentrations of the standard glasses determined by other techniques (Karl Fischer-Titration or infrared spectroscopy). As an example, a typical relationship obtained for an analytical session is $H_2O_{Melt}^{corrected} = 0.9984 \cdot H_2O^{by-difference} - 0.3024$. The typical error is usually ±0.5 wt.% H_2O. The possible effect of the redox state of the glass on H_2O determination was found to be within the error of the method (Botcharnikov

Dissertation of André Stechern

Petrological and Experimental Constrains on the Pre-eruptive Conditions of 1993 Lascar
Andesites and Insights Into the Evolution of Calc-alkaline Intermediate Lavas

et al., 2008). To further constrain the accurate determination of H_2O contents in the experimental glasses, samples above the liquidus were measured with Karl Fischer-Titration (KFT) [for a detailed description of the method see Behrens *et al.*, 1996]. H_2O concentrations measured with KFT are in a good agreement (±0.5 wt.% H_2O) with the corrected values gained by EPMA.

Dissertation of André Stechern

Petrological and Experimental Constrains on the Pre-eruptive Conditions of 1993 Lascar
Andesites and Insights Into the Evolution of Calc-alkaline Intermediate Lavas

6 EXPERIMENTAL RESULTS

6.1 Phase assemblages

The experimental conditions and the produced phase assemblages are given in Tabs.

I.5, I.6, and I.7. Detailed compositions of minerals and glasses analyzed by EPMA are listed

in the Appendix Tab. AT6.

Table I.5: Conditions of phase equilibria experiments at 300 MPa, QFM+1.5 and phase assemblage in experimental products.

Sample	aH$_2$O, ± 0.05	Log fO$_2$	ΔQFM calc	H$_2$O in glass wt% (1σ)	Phase assemblages (proportions)					ΣR^2
1040°C; 300 MPa; 72h										
Las-45	1.00	-8.47	+1.50	6.82 (0.53)	Gl (100.0)					-
Las-46	0.86	-8.77	+1.19	5.89 (0.56)	Gl (98.4)	Ol (1.6)				0.90
Las-47	0.55	-9.54	+0.43	4.46 (0.32)	Gl (93.2)	Cpx (2.7)	Opx (4.1)			0.78
Las-48	0.85	-8.78	+1.18	2.52 (0.18)	Gl (89.5)	Cpx (4.5)	Opx (6.0)	Ilm*		0.68
Las-49	0.09	-11.51	-1.54	1.00 (0.41)	Gl*	Cpx*	Opx*	Ilm*		-
1025°C; 300 MPa; 72h										
Las-17	1.00	-8.26	+2.07	7.91 (0.37)	Gl (95.2)	Ol (4.8)				1.09
Las-18	0.88	-8.37	+1.96	5.23 (0.39)	Gl (99.0)	Cpx (0.1)	Opx (0.9)			0.54
Las-16	0.63	-8.65	+1.67	4.47 (0.47)	Gl (96.1)	Cpx (0.6)	Opx (3.3)			0.39
Las-19	0.85	-8.40	+1.93	3.50 (0.64)	Gl	Cpx*	Opx	Ilm*		-
Las-20	0.11	-10.22	+0.11	2.02 (0.78)	Gl*	Cpx*	Opx*	Ilm*		-
1000°C; 300 MPa; 96h										
Las-30	1.00	-9.35	+1.35	7.71 (0.17)	Gl (97.0)	Ol (2.9)	Cpx (0.1)			0.82
Las-31	0.81	-9.54	+1.16	7.60 (0.40)	Gl (95.9)	Ol (2.6)	Cpx (1.5)			0.63
Las-32	0.79	-9.56	+1.14	7.51 (0.53)	Gl (95.5)	Ol (2.3)	Cpx (2.2)			0.64
Las-33	0.72	-9.64	+1.06	4.73 (0.52)	Gl (80.8)	Cpx (19.0)	Opx (0.2)			1.44
Las-34	0.13	-11.13	-0.42	0.73 (0.42)	Gl*	Cpx*	Opx*	Pl*	Ilm*	-
975°C; 300 MPa; 144h										
Las-55	1.00	-10.60	+0.49	8.10 (0.43)	Gl (91.9)	Ol (3.4)	Cpx (4.7)			0.60
Las-56	0.88	-10.71	+0.38	7.03 (0.23)	Gl (89.5)	Ol (4.5)	Cpx (5.9)	Opx (0.1)		0.95
Las-57	0.75	-10.85	+0.24	6.26 (0.20)	Gl (83.0)	Cpx (7.7)	Opx (9.2)			0.57
Las-58	0.74	-10.85	+0.23	3.83 (0.49)	Gl (58.3)	Cpx (8.5)	Opx (12.2)	Pl (20.9)		0.71
Las-59	0.08	-12.55	-1.46	-	Gl*	Cpx*	Opx*	Pl*	Ilm*	-
950°C; 300 MPa; 144h										
Las-35	1.00	-10.04	+1.46	7.46 (0.23)	Gl (87.3)	Cpx (5.3)	Opx (3.9)	Amp (3.1)	Mt (0.3)	0.66
Las-36	0.89	-10.14	+1.36	7.14 (0.32)	Gl (82.8)	Cpx (7.0)	Opx (4.8)	Amp (1.5)	Pl (3.7) Mt (0.2)	0.77
Las-37	0.74	-10.30	+1.20	6.19 (0.27)	Gl (74.4)	Cpx (9.2)	Opx (6.9)	Amp (2.8)	Pl (6.6) Mt (0.1)	0.16
Las-38	0.62	-10.45	+1.05	5.77 (0.07)	Gl (55.3)	Cpx (10.9)	Opx 10.9)	Pl (22.3)	Mt (0.6)	0.30
Las-39	0.11	-11.98	-0.48	-	Gl*	Cpx*	Opx*	Pl*	Mt*	-
925°C; 300 MPa; 168h										
Las-65	1.00	-10.47	+1.45	7.86 (0.41)	Gl (76.6)	Cpx (0.1)	Opx (0.7)	Amp (22.1)	Pl (0.3) Mt (0.3)	0.47
Las-66	0.87	-10.58	+1.34	6.18 (0.34)	Gl (63.7)	Cpx (4.9)	Opx(7.7)	Amp (10.7)	Pl (12.2) Mt (0.8)	0.45
Las-67	0.79	-10.67	+1.25	5.43 (0.26)	Gl (53.1)	Cpx (9.4)	Opx (12.5)	Amp (4.5)	Pl (22.0) Mt (0.6)	0.92
Las-68	0.65	-10.84	+1.08	4.40 (0.25)	Gl (46.0)	Cpx (10.0)	Opx (14.2)	Pl (29.0)	Mt (0.8)	0.61
Las-69	0.18	-11.94	-0.02	-	Close to solidus					-
900°C; 300 MPa; 240h										
Las-60	1.00	-12.11	+0.25	8.05 (0.28)	Gl (70.8)	Amp (26.6)	Pl (2.0)	Mt (0.6)		0.63
Las-61	0.90	-12.20	+0.16	7.20 (0.23)	Gl (64.7)	Amp (28.6)	Pl (6.3)	Mt (0.4)		0.55
Las-62	0.78	-12.33	+0.03	5.01 (0.26)	Gl (50.8)	Cpx (3.5)	Opx (4.5)	Amp (22.4)	Pl (18.6) Mt (0.1)	0.44
Las-63	0.60	-12.56	-0.20	4.19 (0.19)	Gl (35.5)	Cpx (11.8)	Opx (13.6)	Pl (38.2)	Mt(1.0)	0.65
Las-64	0.10	-14.16	-1.80	-	Close to solidus					-

* Phase composition is not determined

Petrological and Experimental Constrains on the Pre-eruptive Conditions of 1993 Lascar
Andesites and Insights Into the Evolution of Calc-alkaline Intermediate Lavas

The phase compositions (SiO_2, TiO_2, Al_2O_3, FeO_{tot}, MnO, MgO, CaO, Na_2O, K_2O, and P_2O_5) were used to calculate modal abundances (weight percentages of the minerals + residual glass which comprise the experimental products), using a least-squares fit of the starting composition, based on the mass balance program "PETMIX" published by Wright & Doherty (1970).

Table I.6: Conditions of phase equilibria experiments at 500 MPa, QFM+1.5 and phase assemblage in experimental products.

Sample	aH$_2$O, ± 0.05	Log fO$_2$	ΔQFM calc	H$_2$O in glass wt% (1σ)	Phase assemblages (proportions)					ΣR^2
1050°C; 500 MPa; 72h										
Las-5-6	1.00	-8.31	+1.52	9.40 (0.70)	Gl (100.0)					-
Las-5-7	0.81	-8.50	+1.33	7.86 (0.42)	Gl (100.0)					-
Las-5-8	0.27	-9.42	+0.40	4.79 (0.36)	Gl (93.2)	Cpx (3.9)	Opx (2.9)			0.38
Las-5-9	0.59	-8.77	+1.06	3.60 (0.77)	Gl (90.6)	Cpx (6.4)	Opx (3.0)	Ilm*		0.41
Las-5-10	0.31	-9.32	+0.51	2.14 (0.66)	Gl	Cpx	Opx*	Ilm*		-
1025°C; 500 MPa; 72h										
Las-5-32	1.00	-8.31	+1.88	7.64 (0.61)	Gl (100.0)					-
Las-5-31	0.83	-8.47	+1.71	6.77 (0.43)	Gl (93.6)	Cpx (4.4)	Opx (2.0)			0.75
Las-5-33	0.76	-8.54	+1.64	5.80 (0.58)	Gl (91.8)	Cpx (5.3)	Opx (2.9)			0.57
Las-5-34	0.74	-8.57	+1.61	4,60 (0.58)	Gl (86.8)	Cpx (8.2)	Opx (4.9)			0.37
Las-5-35	0.19	-9.74	+0.44	-	Gl*	Cpx*	Opx*	Pl*	Ilm*	-
1000°C; 500 MPa; 96h										
Las-5-1	1.00	-8.82	+1.74	9.14 (0.36)	Gl (100.0)					-
Las-5-2	0.88	-8.93	+1.62	7.93 (0.42)	Gl (94.0)	Cpx (4.8)	Opx (1.1)			0.61
Las-5-3	0.79	-9.02	+1.54	4.99 (0.27)	Gl (86.6)	Cpx (8.9)	Opx (4.5)			0.77
Las-5-4	-	-	-	2.91 (0.53)	Gl (71.6)	Cpx (25.4)	Opx (1.7)	Ilm (1.4)		1.77
Las-5-5	0.15	-10.44	+0.11	-	Gl*	Cpx*	Opx*	Pl*	Ilm*	-
975°C; 500 MPa; 120h										
Las-5-26	1.00	-9.01	+1.93	9.02 (0.37)	Gl (92.4)	Cpx (6.2)	Opx (0.1)	Mt (1.3)		0.65
Las-5-27	0.89	-9.11	+1.83	8.02 (0.55)	Gl (90.3)	Cpx (7.0)	Opx (1.3)	Mt (1.4)		0.76
Las-5-28	0.86	-9.14	+1.80	5.47 (0.33)	Gl (82.3)	Cpx (9.8)	Opx (7.5)	Mt (0.4)		0.24
Las-5-29	0.80	-9.19	+1.74	4.58 (0.34)	Gl (65.5)	Cpx (10.3)	Opx (8.6)	Pl (14.4)	Mt (1.2)	0.28
Las-5-30	0.20	-10.43	+0.51	-	Gl*	Cpx*	Opx*	Pl*	Ilm*	-
950°C; 500 MPa; 120h										
Las-5-12	1.00	-10.09	+1.26	6.96 (0.24)	Gl (81.5)	Cpx (0.3)	Amp (17.7)	Mt (0.5)		0.32
Las-5-13	0.88	-10.2	+1.14	4.36 (0.73)	Gl (76.0)	Cpx (5.1)	Amp (18.6)	Mt (0.3)		0.42
Las-5-11	0.78	-10.3	+1.04	3.06 (0.58)	Gl (66.0)	Cpx (6.0)	Opx (3.1)	Amp (16.3)	Pl (8.0) Mt (0.5)	0.34
Las-5-14	0.69	-10.4	+0.94	2.62 (0.42)	Gl (60,0)	Cpx (6.9)	Opx (6.9)	Amp (12.5)	Pl (14.1) Mt*	0.23
Las-5-15	0.18	-11.57	-0.22	-	Close to solidus					-
925°C; 500 MPa; 144h										
Las-5-21	1.00	-10.38	+1.38	8.61 (0.46)	Gl (77.3)	Amp (21.7)	Mt (1.1)			0.97
Las-5-22	0.94	-10.43	+1.33	6.26 (0.29)	Gl (75.6)	Amp (23.8)	Mt (0.6)			0.66
Las-5-23	0.90	-10.47	+1.29	4.60 (0.48)	Gl (63.9)	Amp (28.5)	Pl (7.2)	Mt (0.4)		0.46
Las-5-24	0.80	-10.57	+1.19	3.11 (0.50)	Gl (51.3)	Cpx (4.9)	Opx (5.3)	Amp (17.6)	Pl (20.2) Mt (0.7)	0.28
Las-5-25	0.26	-11.55	+0.21	-	Close to solidus					-
900°C; 500 MPa; 168h										
Las-5-16	1.00	-10.43	+1.77	8.68 (0.61)	Gl (73.1)	Amp (25.5)	Mt (1.4)			0.91
Las-5-17	0.94	-10.49	+1.71	6.22 (0.49)	Gl (73.2)	Amp (24.8)	Mt (2.0)			0.82
Las-5-18	0.90	-10.52	+1.68	4.42 (0.60)	Gl (58.5)	Amp (30.8)	Pl (10.0)	Mt (0.8)		0.49
Las-5-19	0.78	-10.64	+1.56	4.00 (0.57)	Gl (47.1)	Opx (2.3)	Amp (28.9)	Pl (20.9)	Mt (0.7)	0.47
Las-5-20	0.24	-11.68	+0.52	-	Close to solidus					-

* Phase composition is not determined

Petrological and Experimental Constrains on the Pre-eruptive Conditions of 1993 Lascar Andesites and Insights Into the Evolution of Calc-alkaline Intermediate Lavas

Calculated values (wt.%) are also given in Tabs. I.5, I.6 and I.7, together with the sum of the squares of the residuals of the fit (ΣR^2). Results of the most fits were satisfying with ΣR^2 values <0.5. However, some fits produced poor ΣR^2 (>0.5 to max. 1.77) for experimental products with high crystallinity or for experiments in which the compositions of the individual phases could not be analyzed correctly. In experiments where proportions are not given in the table, one or more phases were too small to be analyzed accurately with EPMA.

Table I.7: Conditions of phase equilibria experiments at 300 MPa, QFM+3.3 and phase assemblage in experimental products.

Sample	aH$_2$O, ± 0.05	Log fO$_2$[a]	ΔQFM calc	H$_2$O in glass wt% (1σ)	Phase assemblages (proportions)					ΣR^2
1040°C; 300 MPa; 48h										
Las-SH-18	1.00	-6.56	+3.55	6.92 (0.47)	Gl (98.0)	Opx (1.7)	Mt (0.3)			0.35
Las-SH-19	0.79	-6.89	+3.22	6.07 (0.33)	Gl (93.1)	Cpx (2.1)	Opx (4.6)	Mt (0.2)		0.29
Las-SH-17	-	-	-	4.69 (0.32)	Gl (90.8)	Cpx (4.8)	Opx (4.1)	Mt (0.3)		0.15
Las-SH-20	0.27	-6.95	+3.16	2.00 (0.54)	Gl	Cpx	Opx	Usp*		-
Las-SH-16	-	-	-	-	Gl*	Cpx*	Opx*	Pl*	Usp*	-
1000°C; 300 MPa; 72h										
Las-SH-12	0.90	-7.52	+3.17	5.49 (0.23)	Gl (80.8)	Cpx (13.6)	Opx (2.1)	Mt (3.6)		0.67
Las-SH-11	0.72	-7.68	+3.01	4.30 (0.51)	Gl (71.1)	Cpx (7.8)	Opx (5.8)	Pl (12.2)	Mt (3.1)	0.25
Las-SH-13	0.58	-7.86	+2.86	2.82 (0.42)	Gl (44.7)	Cpx (9.0)	Opx (9.3)	Pl (33.6)	Mt (3.4)	0.17
Las-SH-15	-	-	-	-	Gl*	Cpx*	Opx*	Pl*	Usp*	-
950°C; 300 MPa; 120h										
Las-SH-07	1.00	-7.90	+3.56	7.61 (0.55)	Gl (82.2)	Cpx (3.1)	Amp (12.1)	Mt (2.6)		0.46
Las-SH-06	0.79	-7.96	+3.50	7.42 (0.37)	Gl (80.3)	Cpx (4.5)	Amp (12.9)	Mt (2.3)		0.43
Las-SH-08	0.56	-8.67	+2.79	3.71 (0.64)	Gl (37.7)	Cpx (11.1)	Opx (10.7)	Pl (37.0)	Mt (3.5)	0.38
Las-SH-09	0.47	-8.81	+2.65	3.08 (0.37)	Gl (32.3)	Cpx (10.8)	Opx (12.0)	Pl (41.3)	Mt (3.5)	0.38
Las-SH-10	0.17	-	-	-	Close to solidus					-
900°C; 300 MPa; 168h										
Las-SH-02	1.00	-8.82	+3.48	7.23 (0.30)	Gl (65.6)	Amp (23.6)	Pl (8.0)	Ap (-0.3)	Mt (3.1)	0.37
Las-SH-01	0.84	-8.88	+3.42	6.65 (0.51)	Gl (54.5)	Amp (25.1)	Pl (17.2)	Ap (0.0)	Mt (3.1)	0.50
Las-SH-03	0.74	-8.94	+3.36	6.13 (031)	Gl (54.6)	Cpx (3.6)	Amp (23.0)	Pl (16.1)	Ap (-0.3) Mt (3.1)	0.33
Las-SH-04	0.61	-9.16	+3.14	4.92 (0.04)	Gl (41.2)	Cpx (7.3)	Opx (4.8)	Amp (10.8) Pl (32.2)	Ap* Mt (3.7)	0.39
Las-SH-05	0.39	-	-	-	Gl*	Cpx*	Opx*	Pl*	Ap* Mt*	-

* Phase composition is not determined

[a] fO$_2$ calculated using the model of Burnham (1979) for experiments with aH$_2$O < 1.00

Major crystalline phases identified in all three experimental series include plagioclase (Pl), clinopyroxene (Cpx), orthopyroxene (Opx), amphibole (Amp), and magnetite (Mt). The stability of minerals present in low proportions such as olivine (Ol), apatite (Ap), ilmenite (Ilm), and ulvöspinel (Usp) is either controlled by the oxygen fugacity of the specific experiment or by the amount of a certain element in the residual melt (e.g. P for apatite or Ti for ilmenite and ulvöspinel). Fig. I.6 displays representative back-scattered electron (BSE) images of a typical experimental series obtained at 1040°C and 300 MPa. Experiments conducted at high *T* and/or with high H$_2$O contents in the melt have low crystal contents and a homogeneous distribution of the minerals phases throughout the glass matrix. Crystals are

Dissertation of André Stechern

Petrological and Experimental Constrains on the Pre-eruptive Conditions of 1993 Lascar
Andesites and Insights Into the Evolution of Calc-alkaline Intermediate Lavas

generally euhedral in shape, and show no detectable compositional zoning. Some of the experimental products with high crystallinity have a heterogeneous crystal distribution (e.g. at 900°C), which is probably due to strong undercooling effects (Holtz *et al.*, 2005).

Experimental Set 3 (QFM+3.3), 300 MPa, 1040°C, 48 hours
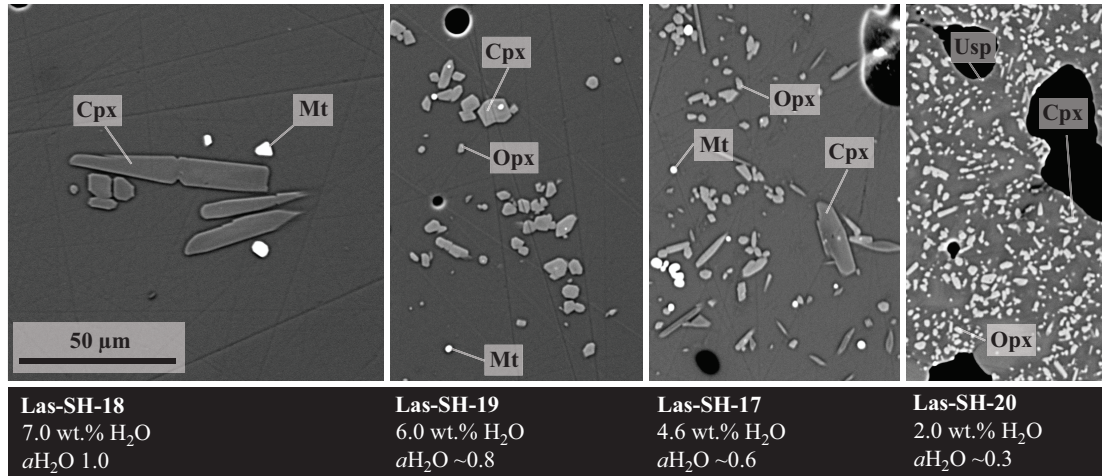
Figure I.6: Back-scattered electron images of run products obtained at 300 MPa and 1040°C after 48 hours with different water contents in the glass (7 wt.%, 6 wt.%, 4.5 wt.%, and 2.0 wt.% H_2O). Scale is in all pictures the same.

Isobaric (300 or 500 MPa) stability fields and phase relations as a function of *T* (in the range of 900-1050°C) and H_2O content of the melt (from ~0.5 to ~9 wt.% H_2O) are illustrated in Fig. I.7. As noted in several previous studies using the same experimental approach (e.g., Dall'Agnol *et al.*, 1999; Botcharnikov *et al.*, 2008), oxygen fugacity is not constant in the phase diagrams and that conditions are more reducing at lower water activities. Oxygen fugacities for given H_2O contents in the melt are listed in Tabs. I.5-I.7 and shown in Fig. I.7 with black arrows and dashed lines. Water-saturation curves have been drawn on the basis of the experimental results and data from Botcharnikov *et al.* (2006).

Dissertation of André Stechern

Petrological and Experimental Constrains on the Pre-eruptive Conditions of 1993 Lascar
Andesites and Insights Into the Evolution of Calc-alkaline Intermediate Lavas

6.1.1 Experimental Set 1 (300 MPa, reducing conditions)

At high temperatures and high water activities Ol is the first crystallizing phase (Fig. I.7A). Ol is only stable at high H_2O concentrations in the melt (~6-8 wt.% H_2O) and high T (975-1040°C). Cpx and Opx are crystallizing after Ol at lower T. For lower H_2O_{melt} (<5 wt.% H_2O) both types of pyroxenes are also observed at 1040 °C and below. The Ol-out and Opx-in curves in Fig. I.7A are almost overlapping, indicating that Ol stability field is limited by a peritectic reaction involving the formation of Opx. Cpx and Opx are not stable at low T (<950°C and 925 °C, respectively and H_2O_{melt} >6.0 wt.%). At water saturated conditions Pl starts to crystallize below 950°C. With decreasing H_2O content in the melt the crystallization of Pl is shifted to higher temperatures and is around 1040°C for nearly dry melts (<1 wt.% H_2O_{melt}). Ilm and Mt stability fields are controlled mainly by the prevailing redox conditions of the experiments and not by water activity (e.g. Snyder *et al.*, 1992; Toplis and Caroll, 1995; Botcharnikov *et al.*, 2008). In this case Mt is stable below 975°C independently on H_2O_{melt}. Ilm, however, is only stable at relatively low H_2O_{melt} (<3.5 wt.% H_2O) and T between 1025 and 975°C. Nevertheless, both Fe-phases, Mt and Ilm, were not coexisting together in a single experiment. Amp is only stable at low T (<975°C) and high H_2O_{melt} (>4.0 wt.% H_2O).

6.1.2 Experimental Set 2 (300 MPa, oxidizing conditions)

Compared to the phase diagram of *experimental set 1* at 300 MPa at reducing conditions phase stability fields for major minerals such as Opx, Cpx, Pl, and Amp do not change significantly at more oxidizing conditions (Fig. I.7A, B). However, Fe-bearing phases are strongly affected by the change in oxygen fugacity. At high fO_2, the crystallization of Ol is completely suppressed in favor of Mt, which is the liquidus phase in this experimental set. At low H_2O contents in the melt (<2.5 wt.% H_2O) and relatively high T (>1000°C) Usp is the Fe-Ti-phase, replacing Ilm at these redox conditions. Ap was detected in all experiments at

Dissertation of André Stechern

Petrological and Experimental Constrains on the Pre-eruptive Conditions of 1993 Lascar
Andesites and Insights Into the Evolution of Calc-alkaline Intermediate Lavas

900°C, which is contrasting the experimental results of 1 and 3 in where this mineral is absent at the same temperature.

6.1.3 Experimental Set 3 (500 MPa, reducing conditions)

At 500 MPa, the field above liquidus is enlarged compared to both experimental sets at 300 MPa (Fig. I.7C). Liquidus phases are Cpx and Opx, appearing nearly together below 1000°C at H_2O-saturated conditions (~9.0 wt.% H_2O). Stability fields for oxide phases are similar to the ones in *experimental set 1* (Fig. I.7A), with Mt crystallizing below 1000°C, independently on the H_2O content in the melt. Ilm crystallizes in a field at relatively low H_2O_{melt} (1.0-2.5 wt.% H_2O) at T above 1000 to 975°C. As for *Experimental Set 1*, Mt and Ilm were not co-existing in the same experiments. The Plag-in line is shifted towards lower H_2O_{melt} and lower temperature in the 500 MPa experimental set, beginning at ~6 wt.% H_2O_{melt} at 900°C and ~1 wt.% H_2O_{melt} at 1025°C. This is in agreement with general knowledge about the effect of pressure on plagioclase stability. Compared to the 300 MPa experiments, the stability field of Amp is enlarged to lower H_2O contents in the melt (2.5 wt.% H_2O) at 500 MPa. The crystallization temperature at high H_2O_{melt} is not dependent on pressure and is in the temperature range 950-975°C.

Petrological and Experimental Constrains on the Pre-eruptive Conditions of 1993 Lascar
Andesites and Insights Into the Evolution of Calc-alkaline Intermediate Lavas
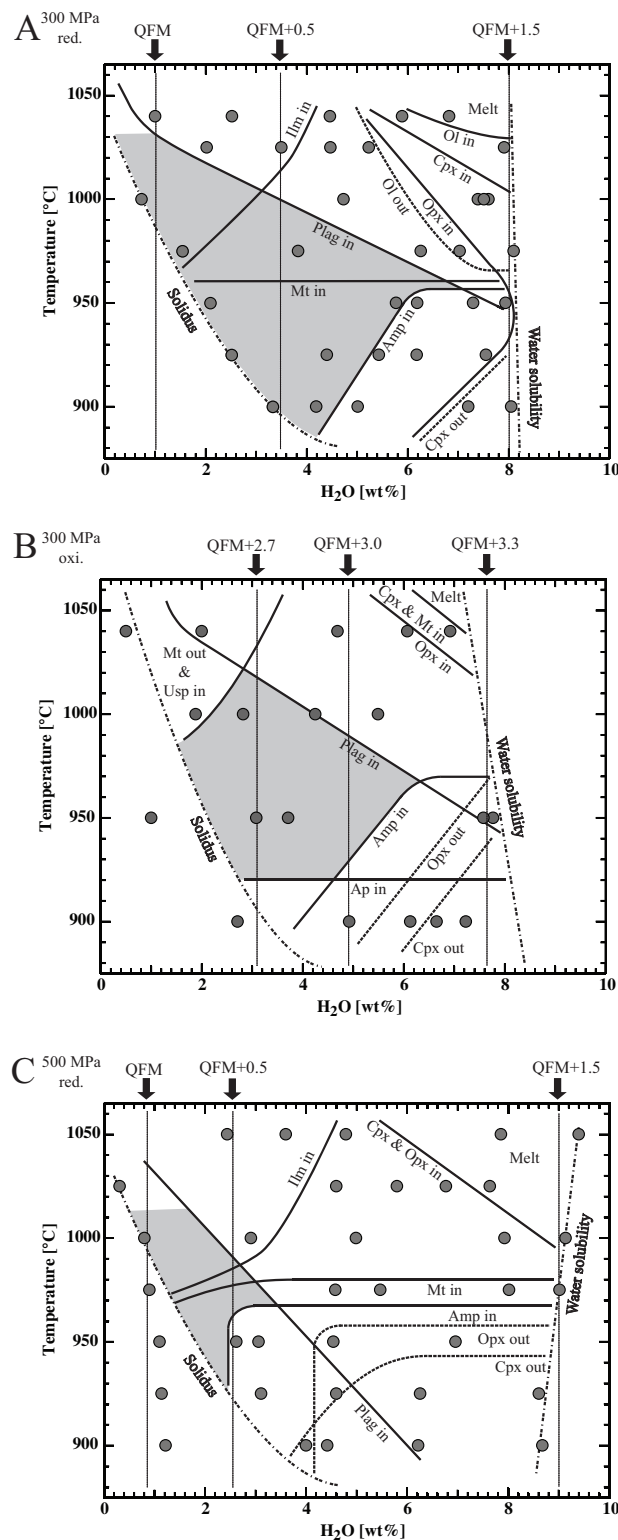
Figure I.7: Phase equilibria of Lascar andesite studied at 300 MPa (A and B) and 500 MPa (C) as a function of
water content in the melt and temperature. The nominal redox conditions are (A) and (C) QFM+1.5 and for (B)
QFM+3.3, with fixed hydrogen fugacities at $aH_2O=1$. Black arrows and vertical dotted lines represent estimated
redox conditions in the experiments (in ΔQFM notation). Ol: olivine; Plag: plagioclase; Cpx: clinopyroxene; Opx:
orthopyroxene; Amp: amphibole; Mt: magnetite; Ilm: ilmenite; Usp: ulvöspinel; Ap: aptite. Continuous lines
outline the stability fields of mineral phases. Dashed lines mark the disappearance of phases. The grey shaded area
represents the phase equilibrium assemblage of the natural two-pyroxene samples of Lascar (e.g. LAS07-26; 1993
eruption).

Petrological and Experimental Constrains on the Pre-eruptive Conditions of 1993 Lascar
Andesites and Insights Into the Evolution of Calc-alkaline Intermediate Lavas

6.2 Crystallinity

Calculated phase proportions are listed in Tabs. I.5-I.7. With decreasing X^{fl}_{H2Oini} and H_2O_{melt} the melt fraction decreases and the proportion of crystalline phases increases for all investigated experimental sets (Fig. I.8). As expected, the crystal fraction increases with decreasing T at a given H_2O_{melt}. In the high T range, the variation is ~10 wt.% for a T change of 50°C. At low experimental T (between 950 and 900°C) and low aH_2O the crystal fraction increase is more pronounced, especially at conditions at which Pl crystallizes.
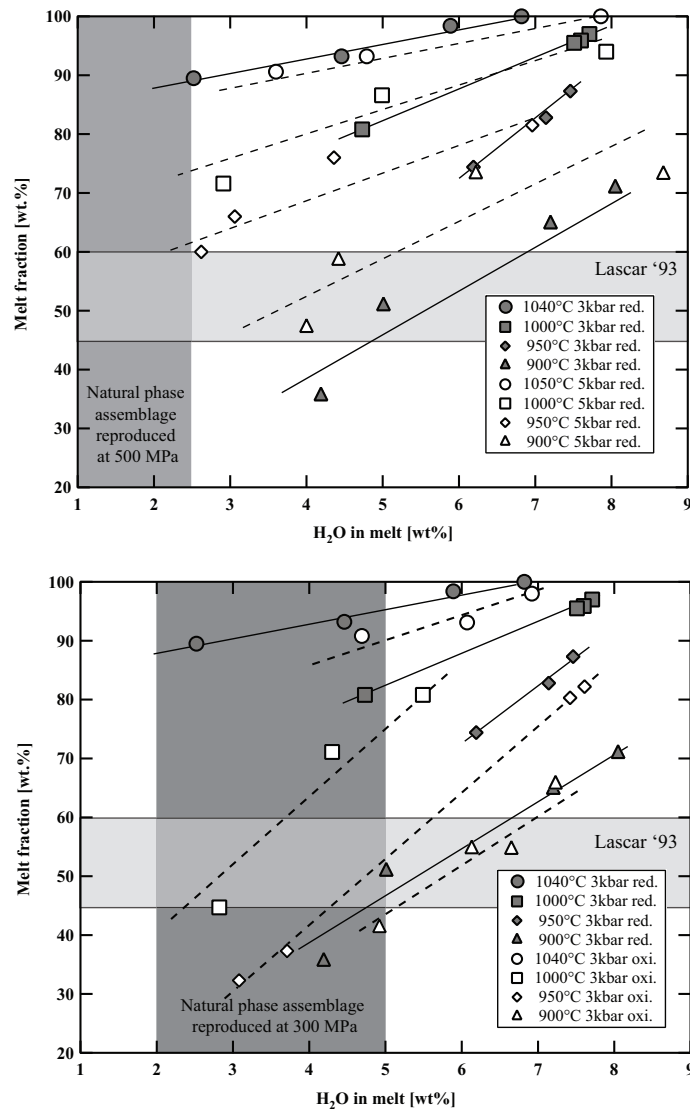
Figure I.8: Variation of melt fraction versus water content in the melt, temperature, and fO_2. Light grey shaded area represents the proportion of groundmass in natural Lascar andesites. Dark grey shaded field represents the experimental phase assemblage field of Plag, Cpx, Opx, and Fe-Ti oxides with respect to H_2O_{melt}.

Dissertation of André Stechern

Petrological and Experimental Constrains on the Pre-eruptive Conditions of 1993 Lascar
Andesites and Insights Into the Evolution of Calc-alkaline Intermediate Lavas

At 900°C the melt fraction decreases by ~35 wt.% (from 70 to 35 wt.%) with a
decrease of H_2O_{melt} from 8 to 4 wt.%. Comparing experiments at different oxygen fugacities
performed at 300 MPa it is noticeable that the experiments at more oxidizing conditions have
generally a slightly higher crystal fraction of about 5 wt.%. However, this variation remains
within the error of crystal fractions determination by mass balance and should be interpreted
with caution. In particular, there is no significant change of the Pl quantity when comparing
experiments at QFM+1.5 and QFM+3.3 at similar T and H_2O_{melt} (Fig. I.9).
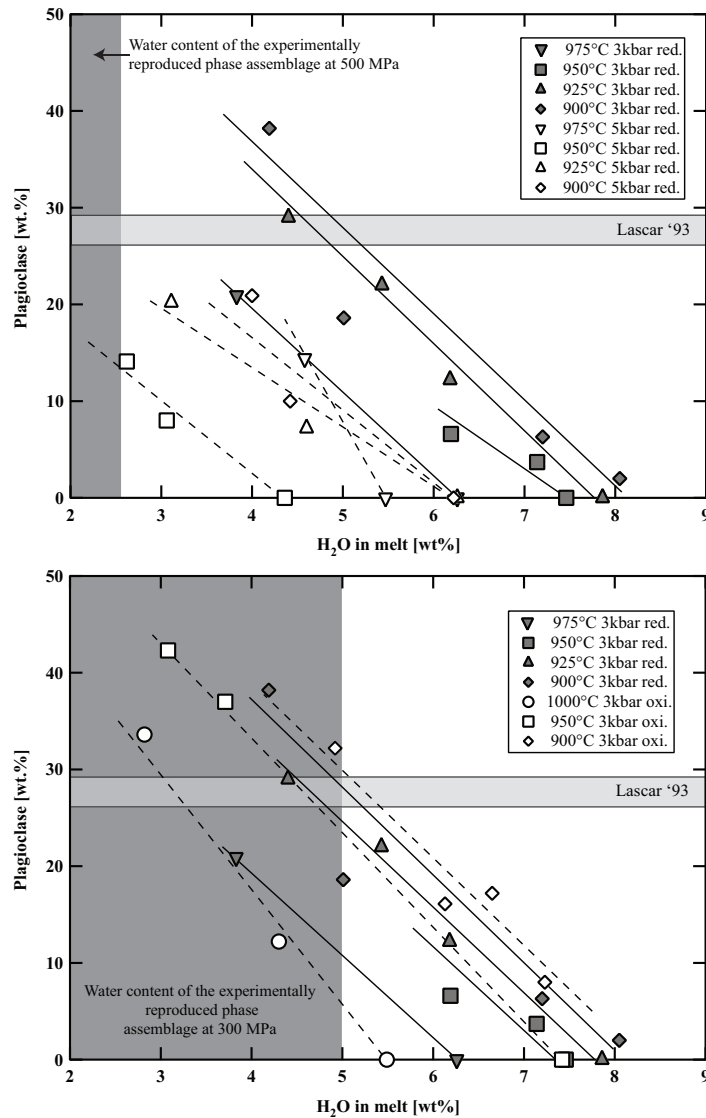
Figure I.9: Variation of plagioclase fraction (in wt.%) versus water content in the melt, temperature, and fO_2.
Light grey shaded area represents the proportion of plagioclase in natural Lascar andesites. Dark grey shaded field
represents the experimental phase assemblage field of Plag, Cpx, Opx, and Fe-Ti oxides with respect to H_2O_{melt}.

Dissertation of André Stechern

Petrological and Experimental Constrains on the Pre-eruptive Conditions of 1993 Lascar
Andesites and Insights Into the Evolution of Calc-alkaline Intermediate Lavas

These results are in agreement with a study of Botcharnikov *et al.* (2008) for ferrobasalts where no detectable or only little effect of fO_2 on the proportions of melt, Cpx, and Pl has been observed. At given H_2O_{melt} there is also no significant variation of the melt fraction when comparing experiments at 300 MPa and 500 MPa in the high *T* runs (1050-1000°C). At lower *T* (950-900°C) experiments at 500 MPa have a significantly higher melt fraction than at 300 MPa, which is most probably due to the depression of the Pl stability field with decreasing *P*. Fig. I.9 displays the amount of Pl in the run products (wt.% calculates by mass balance) as a function of H_2O_{melt}, *T*, *P*, and fO_2. An increase from 300 MPa to 500 MPa with similar H_2O_{melt} results in ~20 wt.% less Pl at 900°C.

6.3 Phase compositions

6.3.1 Olivine

Olivines are only present at *Experimental Set 1* (300 MPa; QFM+1.5). The forsterite content (Fo=Mg/[Mg+Fe], in mol%) of Ol varies only little from Fo_{79} to Fo_{84} (Tab. AT6 in the Appendix), which is due to the small stability field of Ol (Fig. I.8A). These results are in agreement with studies on basaltic andesites from Bezymianny volcano, Kamchatka (Almeev *et al.*, 2013). A slight decrease from Fo_{82} to Fo_{79} can be observed with decreasing water content in the melt at 1000°C. Almeev *et al.* (2013) also observed the replacement of Ol by Opx (and later Opx + Cpx) with increasing pressure (compare Fig. I.8A and I.7C).

6.3.2 Plagioclase

Plagioclase analyses were difficult due to their poor contrast with the residual glasses in back-scattered electron (BSE) images and small sizes of the crystals at low temperatures and low H_2O concentrations in the melt (<5 μm below 950°C and H_2O_{melt} <4 wt.%). Pl compositions are listed in Tab. AT6 in the Appendix and shown in Fig. I.10 as a function of *T*

Petrological and Experimental Constrains on the Pre-eruptive Conditions of 1993 Lascar
Andesites and Insights Into the Evolution of Calc-alkaline Intermediate Lavas

and H_2O_{melt} at different P and fO_2. As shown in previous experimental studies on andesites (e.g., Martel *et al.*, 1999; Botcharnikov *et al.*, 2008; Almeev *et al.*, 2013), the An content increases with increasing H_2O_{melt} (Fig. I.10; up to ~25 mol% variation in this study). In experiments at low T and H_2O-saturated conditions, maximum An contents of about 76 mol% were determined. In agreement with observations of Martel *et al.* (1999), no systematic effect of fO_2 on the compositions of plagioclase in andesitic systems is observed. The orthoclase component in the Pl varies from 0.4 to 5.1 mol%. Lower K_2O concentrations at similar temperatures are observed in plagioclases from experiments with high H_2O_{melt} (Tab. AT6).
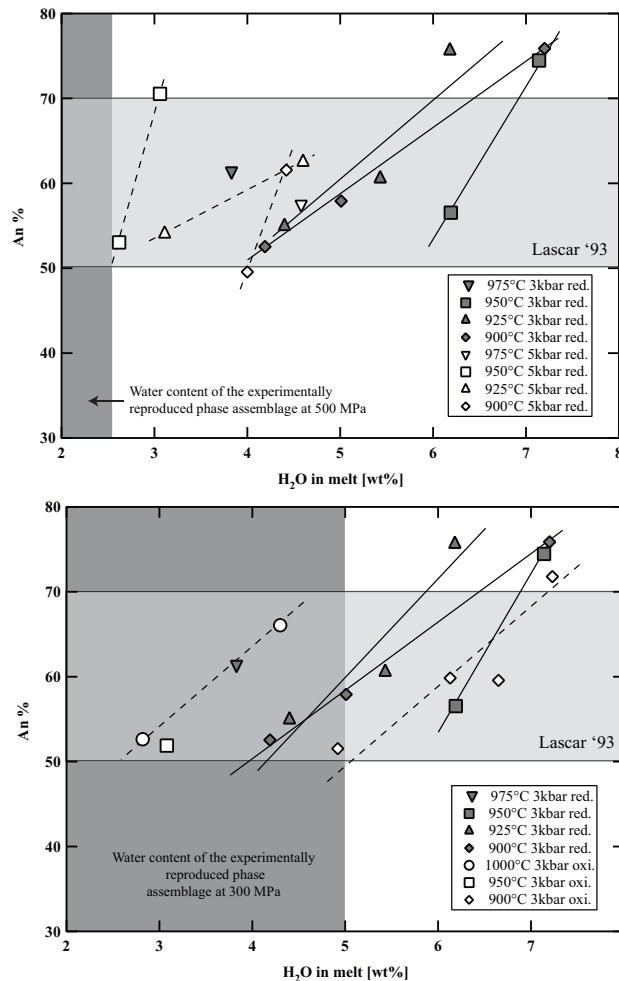
Figure I.10: Variation in anorthite content in experimental plagioclase versus water content in the melt, temperature and fO_2. Light grey shaded area represents the anorthite content of the natural Stage IV plagioclases of Lascar andesites. Dark grey shaded field represents the experimental phase assemblage field of Plag, Cpx, Opx, and Fe-Ti oxides with respect to H_2O_{melt}.

Dissertation of André Stechern

Petrological and Experimental Constrains on the Pre-eruptive Conditions of 1993 Lascar
Andesites and Insights Into the Evolution of Calc-alkaline Intermediate Lavas

The relatively high concentration of minor elements such as MgO and TiO_2 (below 1.0 wt.%) as well as FeO (0.7 to 1.9 wt.%) is difficult to interpret and is most probably due to the presence of small oxides in Pl or to contamination by the glass matrix.

6.3.3 Pyroxenes

The compositions of pyroxenes are given in the Appendix Tab. AT6. The change of pressure from 300 to 500 MPa does not influence the experimental pyroxene compositions significantly. Comparing both sets at 300 MPa at different fO_2 (Fig. I.7A, B), it can be noted that Opx compositions at oxidizing conditions (QFM+3.3) are clearly shifted towards higher enstatite components (En_{84} to En_{71}). Opx obtained at more reducing conditions contain less En components with En_{80} to En_{59} values. The wollastonite component in the Opx is not influenced by fO_2 and is between Wo_3 to Wo_5 in both sets (300 and 500 MPa). Experimental Cpx in both sets with reducing conditions have a relatively wide range of compositions with En_{40} to En_{50} and Wo_{35} to Wo_{44}. In contrast, Cpx crystallized at 300 MPa and oxidizing conditions have a narrow compositional field with En_{43} to En_{46} and Wo_{40} to Wo_{44} values. Finally, it is emphasized that the compositions of the experimental Opx and Cpx at high T are in an exactable agreement (±100 MPa at 300 MPa) with the thermobarometer of Putirka (2008), as shown in Fig. AF4 of the Appendix. Experiments at 500 MPa usually result in calculated P vales which somewhat lower using Eqn. 39 from Putirka (2008). For the low T experiments (900-975°C) the calculated T values are constantly too high and give values between 1000 and 1050°C. In addition the calculated pressures for the low T experiments (975-900°C) are highly underestimated using Eqn. 39 from Putirka (2008). Reasons for these problems are most likely the experimental calibration of the thermobarometer, which was done using data obtained at higher P-T conditions.

Dissertation of André Stechern

Petrological and Experimental Constrains on the Pre-eruptive Conditions of 1993 Lascar
Andesites and Insights Into the Evolution of Calc-alkaline Intermediate Lavas

6.3.4 Amphibole

Experimental amphiboles are euhedral, unzoned tschermakites (Tab. AT6 in the Appendix) according to the classification of Leake *et al.* (2004). At all temperatures, Amp compositions were found to be homogeneous among several grains in each run. The Mg# of the crystallized Amp (calculated with all iron as FeO_{tot}) increases with increasing H_2O_{melt}. In agreement with previous experimental studies (e.g. Sisson & Grove, 1993, for basalts and Martel *et al.*, 1999, for andesites) Al^{IV} increases with increasing *T*, whereas the number of Si atoms in the tetrahedral position of the amphibole formed at 975°C is lower than that of Amp obtained at lower *T*.

6.3.5 Fe-Ti oxides

Magnetite was stable in all three experimental sets (Fig. I.7). Due to the small size of the experimental oxide phases (Mt, Ilm, and Usp), analyses of these phases are difficult and often contaminated by the surrounding glass as illustrated by the high and changing SiO_2 contents (Tab. AT6 in the Appendix). Both experimental sets at reducing conditions show a systematic increase of X_{Ilm} content in Ilm (calculated after Anderson *et al.* 1993) at constant *T* with decreasing H_2O_{melt}. Ilm crystallized in runs with ~1-3 wt.% H_2O_{melt} at relatively high temperatures between 1025 and 975°C. In *Experimental Set 2* (300 MPa, oxidizing conditions) Usp crystallizes instead of Ilm at low H_2O contents and high *T* in the melt. Due to the very small size of the Usp crystals identification was only possible with EDX.

6.3.6 Glass

Residual experimental glasses have compositions ranging from andesitic through dacitic to rhyolitic, depending on the experimental conditions (Fig. I.11, Tab. AT6 in the Appendix). In all cases, compositions proved to be homogeneous within the analytical uncertainty, shown by the relatively small standard deviations of the measurements (Tab. AT6 in the Appendix).

Petrological and Experimental Constrains on the Pre-eruptive Conditions of 1993 Lascar
Andesites and Insights Into the Evolution of Calc-alkaline Intermediate Lavas

Figure I.11: Compositional evolution of experimental melts as a function of MgO (wt.%) content (all comparisons
are normalized to 100%).

Dissertation of André Stechern

Petrological and Experimental Constrains on the Pre-eruptive Conditions of 1993 Lascar
Andesites and Insights Into the Evolution of Calc-alkaline Intermediate Lavas

As expected, glass compositions show systematic compositional variations and are more evolved with increasing crystal fraction as a result of decreasing temperature and H_2O_{melt}. SiO_2 and K_2O increase with decreasing MgO, while Al_2O_3, CaO, and FeO_{tot} decrease. Na_2O shows neither systematic variation, nor a slight increase. Comparing *Experimental Sets 1* and *2*, both at reducing conditions but different pressures, no changes in general differentiation trends could be observed and the data at 500 MPa are omitted in Fig. I.11 for purpose of clarity. A detailed analysis of FeO_{tot} and TiO_2 concentrations shows that there are major differences depending on the prevailing oxygen fugacity (at constant *P* and *T*). At reducing conditions TiO_2 increases as a function of MgO in the MgO range from 5 to 1 wt.%, whereas at oxidizing conditions it decreases due to the crystallization of Ilm. FeO_{tot} decreases with decreasing MgO content in the melt at both investigated redox conditions. However, the decrease is more pronounced in the oxidizing experiments. At constant MgO content in the melt, the FeO_{tot} value can be up to ~2 wt.% higher at reducing conditions. The compositional differences as a function of fO_2 are also very clear in a FeO_{tot}/MgO vs. SiO_2 diagram (Fig. I.12).
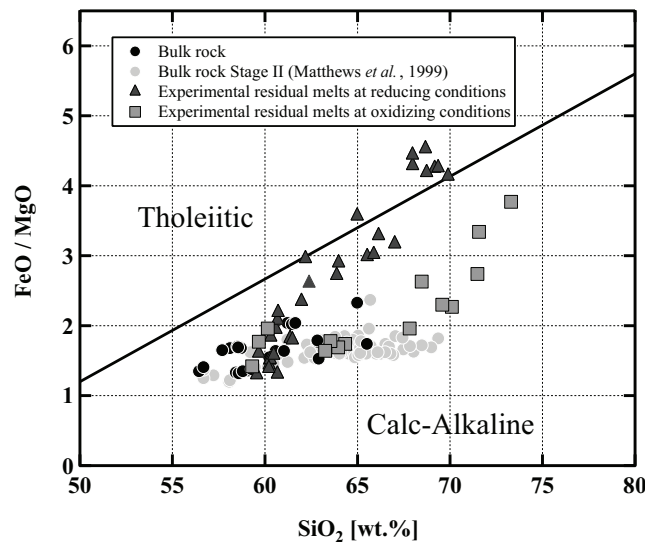
Figure I.12: SiO_2 versus FeO_{tot}/MgO ratio. Classification diagram for Lascar lavas and experimental residual glasses. Subdivison line after Miyashiro (1974).

Petrological and Experimental Constrains on the Pre-eruptive Conditions of 1993 Lascar
Andesites and Insights Into the Evolution of Calc-alkaline Intermediate Lavas
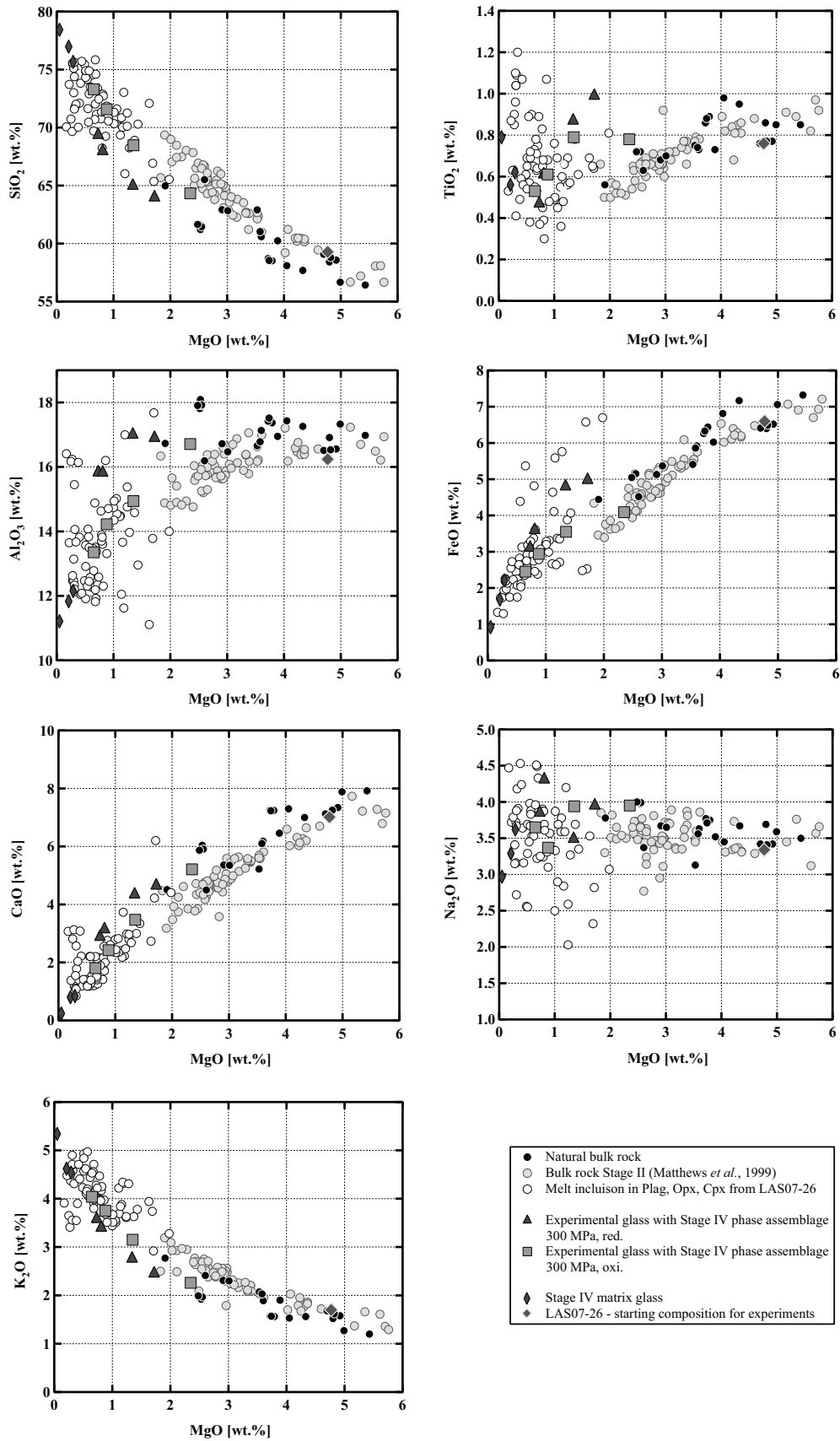
Figure I.13: Composition of natural bulk rocks, experimental melts in equilibrium with Stage IV mineral assemblage (Plag, Cpx, Opx), matrix glasses, and melt inclusions (heated and non heated) in Plag, Cpx, and Opx.

Dissertation of André Stechern

Petrological and Experimental Constrains on the Pre-eruptive Conditions of 1993 Lascar
Andesites and Insights Into the Evolution of Calc-alkaline Intermediate Lavas

The FeO_{tot}/MgO ratio increases more strongly with increasing SiO_2 in the reducing experiments when compared with the oxidizing experiments. In evolving residual melts, the FeO_{tot}/MgO values at reducing conditions are crossing the boundary from the calc-alkaline to the tholeiitic field (Miyashiro, 1974). Fig. I.13 combines the results of natural bulk rock compositions, experimental melt compositions, melt inclusion data, and ground mass glasses.

7 DISCUSSION

7.1 Comparison with previous work

The present work is in general agreement with previous phase equilibria studies on intermediate volcanic rocks (Martel *et al*., 1999; Scaillet and Evans, 1999; Costa *et al*., 2004; Botcharnikov *et al*., 2008; Parat *et al*., 2008, Almeev *et al*., 2013b). The main stable phases in andesitic magmas are Pl, Opx, Cpx, Amp, and Fe-Ti oxides. The change in liquidus phase from Pl at 1 atm total pressure (Eggler, 1972) to either Opx, Cpx, Amp (+ Pl), Mt, or Ol with increasing pressure in the same fO_2 range and for conditions close to H_2O_{melt} saturation is in agreement with studies from Sekine *et al.* (1979) and Maksimov *et al.* (1978). Ol has a restricted stability field in andesitic systems and this field is increasing with H_2O_{melt}. Ol was only found to be present at reducing conditions at 300 MPa, which is also shown by Botcharnikov *et al*. (2008) at 200 MPa, but is not stable at 500 MPa or at 300 MPa at higher fO_2. Opx and Cpx tend to be stable in the water-poor part of the phase diagrams with a maximum extension to high H_2O_{melt} between 850 to 950°C as shown in *Experimental Set 1* and *2*. This behavior is in very good agreement with studies from Scaillet and Evans (1999) and Costa *et al.* (2004). The compilation of all studies as well of additional data for more basaltic or dacitic compositions (Dall'Agnoll *et al.*, 1999, Freise *et al.*, 2009; Feig *et al.*, 2010) indicates that the stability fields of Cpx and Opx always reach a maximum in terms of H_2O_{melt} at intermediate T at around 850-1000°C. At lower T, Amp becomes the predominant Fe-Mg-bearing phase and reduces the stability field of the other mafic phases. Amp stability

Dissertation of André Stechern

Petrological and Experimental Constrains on the Pre-eruptive Conditions of 1993 Lascar
Andesites and Insights Into the Evolution of Calc-alkaline Intermediate Lavas

requires at least 4 wt.% of water in the melt at 300 MPa, which is in good agreement with all mentioned previous studies. Data at 200 MPa indicate that H_2O_{melt} above 5.5 wt.% H_2O may be necessary to stabilize Amp in andesitic systems (Martel *et. al.*, 1999). Considering our 300 and 500 MPa data, the Amp stability field seems to expend towards lower H_2O_{melt} at higher *P* (compare Figs. 7A and 7C). This observation, which needs to be confirmed, would imply that amphibole breakdown may not only occur in the low *P* range when the water solubility in the melt is below ~4 wt.% H_2O but also takes place during decompression in the range 500-200 MPa.

7.2 P-T-*f*O₂-H₂O constraints on magma storage

In the following section, experimental results, the chemical compositions of experimental products, natural bulk rocks, quenched glasses, minerals, and melt inclusions in minerals are used to determine the pre-eruptive conditions for Lascar's Holocene eruptive events, with particular attention to the 1993 eruption.

Crystallization experiments on andesitic bulk compositions performed under 300 and 500 MPa and varying *f*O₂ confirm that dissolved H_2O significantly influences the crystallization sequence, composition of minerals and their modal abundance, and consequently, the chemistry of the residual melts. Thus, the mineral assemblage existing in natural phases can be used as a proxy to constrain pre-eruptive melt water contents.

The phase diagrams for 300 MPa (Fig. I.7A, B) show that the natural phase assemblage can only be reproduced within a restricted field of H_2O_{melt} and *T* (grey field in Fig. I.7). The lack of Amp phenocrysts and the presence of Pl in the Lascar volcanic rocks from the recent 1993 eruption (samples LAS07-23, -26) and also eruptive rocks from previous stages with a very similar phase assemblage (e.g. sample LAS07-12 from Stage III) restricts conditions to the low H_2O_{melt} side of the phase diagrams, with *T* in the 950-1000°C range and with H_2O_{melt} contents <5 wt.%. One anhydrous mineral phase having a composition particularly sensitive to the H_2O content in the melt is Pl (e.g., Sisson and Grove, 1993; Almeev *et al.*, 2012).

Dissertation of André Stechern

Petrological and Experimental Constrains on the Pre-eruptive Conditions of 1993 Lascar
Andesites and Insights Into the Evolution of Calc-alkaline Intermediate Lavas

Accordingly, the pre-eruptive H_2O_{melt} and T can be more accurately bracketed by the comparison of the melt fraction, Pl composition, and Pl abundance between the experimental products and the eruptive material (Figs. I.9 and I.10). Within the field reproducing the natural phase assemblage, the compositions of natural Pl phenocrysts (An_{50} to An_{70}) were obtained under water-undersaturated conditions (aH_2O 0.75-0.56) with H_2O_{melt} of ~3-4.5 wt.% in the T range of 900-1000°C (300 MPa). The amount of melt, estimated from the proportion of groundmass and phenocrysts (Tab. I.2), was also reproduced for this range of water contents at 950 to 1000°C (Fig. I.8). The experiment at 300 MPa, 1000°C, and ~2.8 wt.% H_2O_{melt} (sample# Las-SH-13) led to the same crystal/melt ratio as one observed in the Lascar 1993 eruptive material, including all major phases of the natural rocks.

The pre-eruptive total pressure is more difficult to assess. Results of the two-pyroxene barometer suggest a minimum pressure of crystallization of 300 MPa. But pressures of 500 MPa or even higher may be realistic from the calculations (Fig. I.3) using the model of Putirka (2008). However, the experimental T-H_2O_{melt} field in which the natural phenocryst assemblage is reproduced shrinks significantly at 500 MPa (Fig. I.7) and is shifted towards very low H_2O_{melt} concentrations (<2.5 wt.%). In this field the natural Pl compositions and their abundance cannot be reproduced (Figs. I.9 and I.10). In addition, the field in which crystal/melt proportions observed in the natural lavas and ejecta are reproduced does not overlap with the field of the natural phase assemblage at 500 MPa (Fig. I.8), suggesting that crystallization pressure needs to be considerably lower than 500 MPa.

The prevailing oxygen fugacity is best constrained by pyroxene compositions. Pyroxene pairs from experiments at oxidizing conditions and relatively reducing conditions were compared to natural pairs (Fig. I.14) from the andesitic lava flow (sample LAS07-07, which contains also little amounts of Amp) and the white pumice (sample LAS07-26). The experimental set at 300 MPa and high log$f$O$_2$ (QFM+3.3 at aH_2O=1) produces pyroxene pairs of compositions in very good agreement with the natural pairs from the andesitic lava flow and white pumice. As a result, relatively high oxygen fugacity is necessary to obtain Fe/Mg

Dissertation of André Stechern

Petrological and Experimental Constrains on the Pre-eruptive Conditions of 1993 Lascar
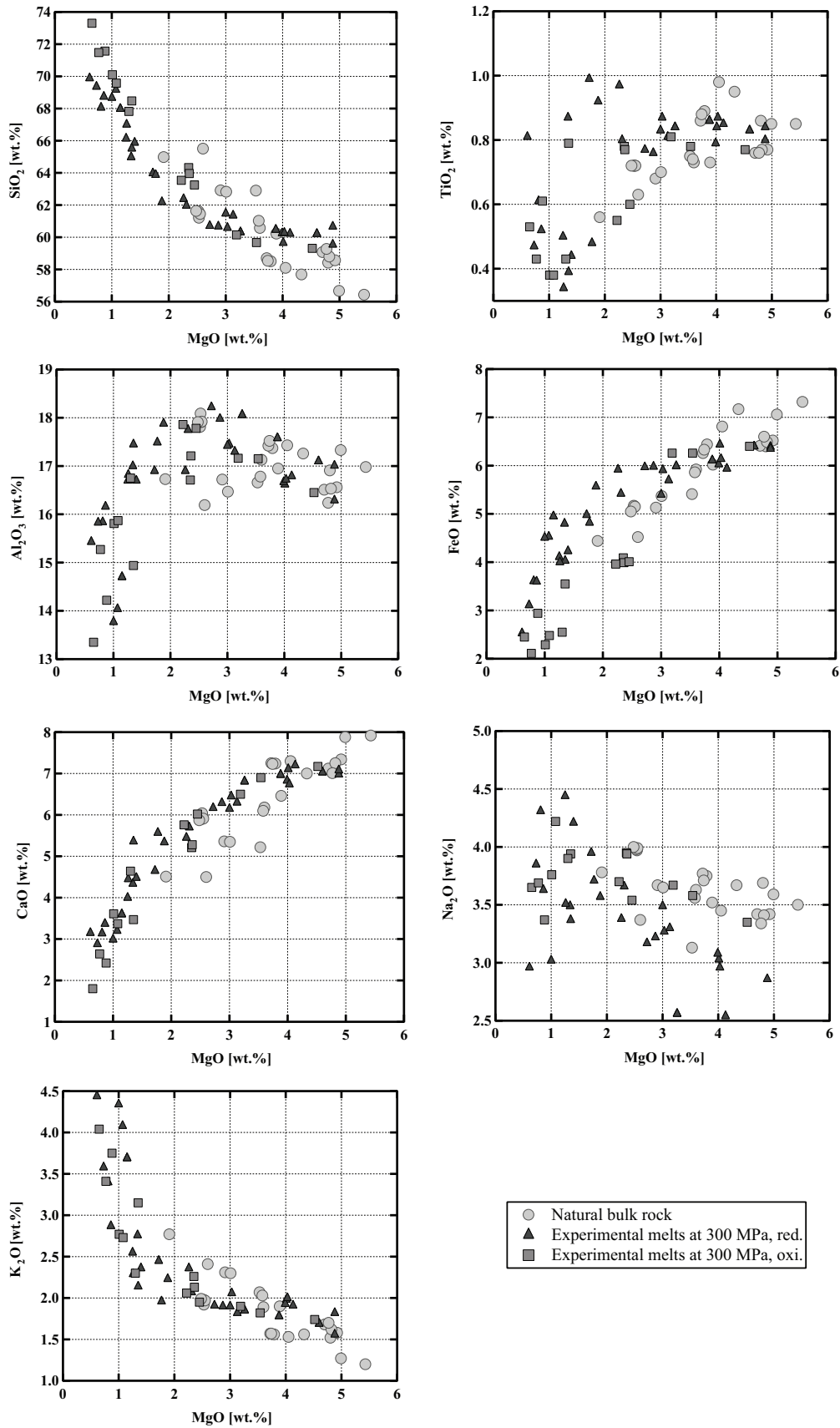Andesites and Insights Into the Evolution of Calc-alkaline Intermediate Lavas

ratios such as observed in natural pairs. On the contrary, Cpx and Opx from experiments at

lower $\log fO_2$ (QFM+1.5 at aH$_2$O=1) are clearly shifted towards higher hedenbergite and

ferrosilite components, indicating that experimental redox conditions were too reducing. The

calculated $\log fO_2$ values for the experiments reproducing the Opx-Cpx pairs at oxidizing

conditions are between QFM+2.7 and QFM+3.0 (Fig. I.7, Tab. I.7). These values are

approximately one log unit higher than those calculated from the natural Mt-Ilm pairs.

However, it is emphasized that no experiments in the T-H$_2$O$_{melt}$ field covering the natural

phase assemblage (grey fields in Fig. I.7) are available with $\log fO_2$ in the range predicted by

the Mt-Ilm pairs (QFM+1 to QFM+2.0).
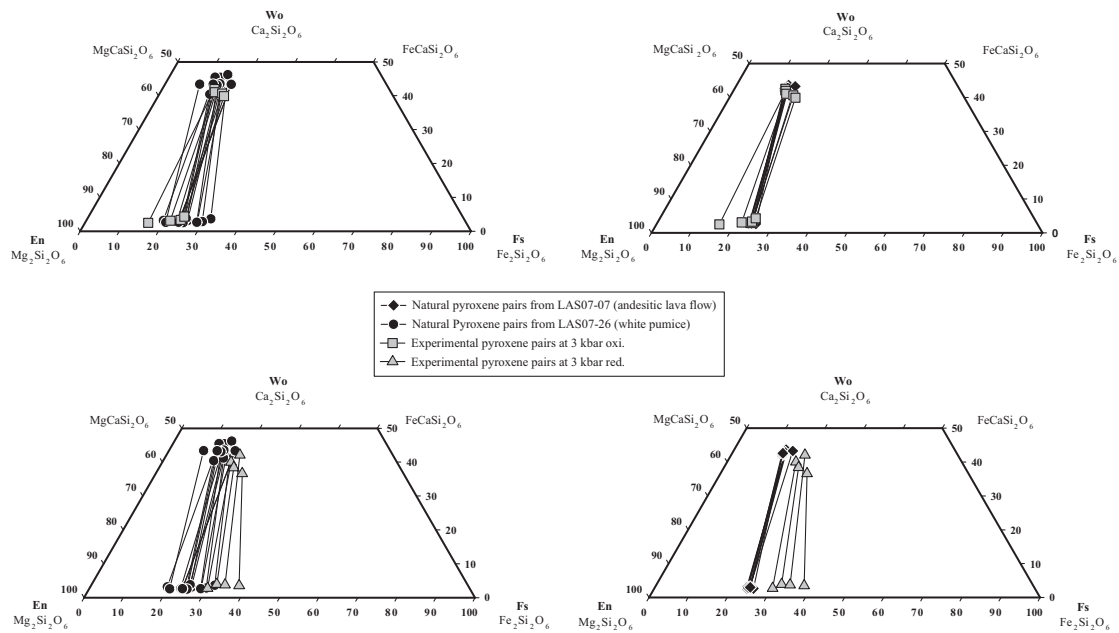
Figure I.14: Natural pyroxene pairs and experimental pyroxene pairs as a function of fO_2. Connecting lines between the markers represent corresponding pairs.

In summary, the combination of experimental results and mineral chemistry of natural

phases indicates that the pre-eruptive temperature of the Lascar 1993 andesites can be

constrained to 975 ±25°C (Figs. I.3 and I.7). The pressure cannot be much higher than 300

MPa as shown by the experimental results. The compositions of natural Opx-Cpx pairs can be

used to deduce that pressures of less than 200 MPa are not realistic (Fig. I.3). At a pressure of

Dissertation of André Stechern

Petrological and Experimental Constrains on the Pre-eruptive Conditions of 1993 Lascar
Andesites and Insights Into the Evolution of Calc-alkaline Intermediate Lavas

300 MPa, H_2O_{melt} of 2.0 to 4.5 wt.% is necessary to obtain the natural phase assemblage, but the crystal/melt ratio and the phase compositions are best reproduced for H_2O_{melt} of 2.5 ±0.5 wt.%. The conditions are relatively oxidizing as $logfO_2$ of QFM+2.75 ± 0.25 is predicted from the pyroxene compositions of our experiments between 950 and 1000°C. However, Ilm and Mt were never coexisting in our experiments, in contrast to the natural rocks. Thus, slightly more reducing conditions, at which Ilm and Mt should coexist, seem to be realistic and the estimated $logfO_2$ should be in the range QFM+2.0 ±0.5, which is in agreement with the $logfO_2$ range of QFM+1.5 ±0.5 calculated from the Mt-Ilm pairs. However, it should be noted that the corresponding temperature for natural Mt-Ilm pairs is 880-920°C, which is probably lower than T of the pre-eruptive conditions.

Additionally, pre-eruptive conditions for Amp-bearing samples can also be constrained on the base of the presented phase equlibria experiments. A somewhat higher H_2O_{melt} content (5-6.5 wt.% at 300 MPa) would favor the crystallization of Amp in a two-pyroxene andesite. In this case the pre-eruptive temperature can be bracketed even more precisely due to the upper thermal stability of Amp at around 960°C and the small stability field in which Plag, Cpx, Opx, Mt, and Amp are present (see Fig. I.7).

7.3 Lascar andesitic magmas: differentiation vs. magma mixing

The Lascar rocks have a wide range of bulk compositions (55.6-65.2 wt.% SiO_2) and the observed compositional variations, including all eruptive phases as well as melt inclusions and matrix glasses, cannot be interpreted by assuming only fractional crystallization or only magma mixing. Strong linear correlations for oxides pairs (e.g. SiO_2, TiO_2, FeO, CaO and K_2O vs. MgO) in variation diagrams can be found in particular for Stage II eruptions (Fig. I.13, grey dots), although those for the alkalis (in particular Na_2O) tend to be more scattered. These could be interpreted as evidence for magma mixing of two end-members at this particular Stage II. However, the role of magma mixing for the overall evolution of

Dissertation of André Stechern

Petrological and Experimental Constrains on the Pre-eruptive Conditions of 1993 Lascar
Andesites and Insights Into the Evolution of Calc-alkaline Intermediate Lavas

Lascar rocks (Stage I to Stage IV) might be overestimated due to the large amount of samples

collected from Stage II (database from Matthews *et al.*, 1999). Typical field observations for

magma mixing, like porphyritic or equigranular mafic inclusions in the andesitic and dacitic

ejecta as they can be found frequently at other CVZ volcanoes such as Taapaca (Banaszak,

2014) where only found in one sample of the 1993 eruption (LAS07-19) and are mostly found

in Stage II rocks as described by Matthews *et al.* (1999). Microscopic evidence for the

importance of an open-system magmatic behavior, such as disequilibrium phenocryst textures

(e.g. oscillatoryreverse zoning in plagioclase and/or sieve-textured plagioclase) is still present

in the Lascar rocks.

The bulk compositions of Lascar ejecta of Stage I and III, and some of Stage IV are not

plotting along a straight line in the binary variation diagrams (Figs. I.2 and I.13) and can be

interpreted as products of fractional crystallization. This is supported by the experimental data

showing the compositional evolution of the residual melts (Fig. I.13). The evolution of MI

compositions from Stage IV also points to a crystal fractionation trend (Fig. I.13). The

compositional variations of melts recorded by the MIs can be explained by fractionation of

plagioclase, ortho-, and clinopyroxene, and oxides in a shallow reservoir at a depth

corresponding to 300 MPa. The experiments confirm that residual melts after 40-55%

crystallization (with 25 to 30% plagioclase) match the composition of the silicic MIs

(compare grey squares and triangles to MI compositions marked by open circles in Fig. I.13).

The different crystal fractionation trends determined experimentally as shown in the binary

diagrams (compare grey squares and grey triangles in Fig. I.13) can be explained by the

changing redox conditions in magma reservoir. Experiments at reducing and oxidizing

conditions at the same *P* and *T* conditions show that the more reducing melts follow a more

bended trend in the variation diagrams. This is noticeable not only for redox sensitive oxides

such as FeO but can also be observed in diagrams with SiO_2, Al_2O_3, CaO, and K_2O vs. MgO.

The crystal fractionation trends obtained at different pressures (300 and 500 MPa) and at the

same oxygen fugacity do not show noticeable differences (within the error of the analytical

Dissertation of André Stechern

Petrological and Experimental Constrains on the Pre-eruptive Conditions of 1993 Lascar
Andesites and Insights Into the Evolution of Calc-alkaline Intermediate Lavas

technique). As a result, small variations in the major element plots of natural samples can be

explained by minor variations in the oxygen fugacity of the melt.

Our general observations deduced from major element variations are confirmed by the

trace element distribution in whole rock analyses. For example the Ni vs. Rb diagram

(Wörner, 1988) in Fig. I.15 underlines that magma mixing is a major factor controlling the

compositional variation of Stage II. However the majority of samples from Stage IV follow

also a typical mixing trend in the Ni vs. Rb diagram, even though no clear petrographic

evidences for mixing were found in these samples. Ni vs. Rb data show that crystal

fractionation processes may dominate in other Stages, such as Stage I and Stage III, but must

be a contributing factor to the geochemical evolution in all four stages in the eruptive history

of Lascar.
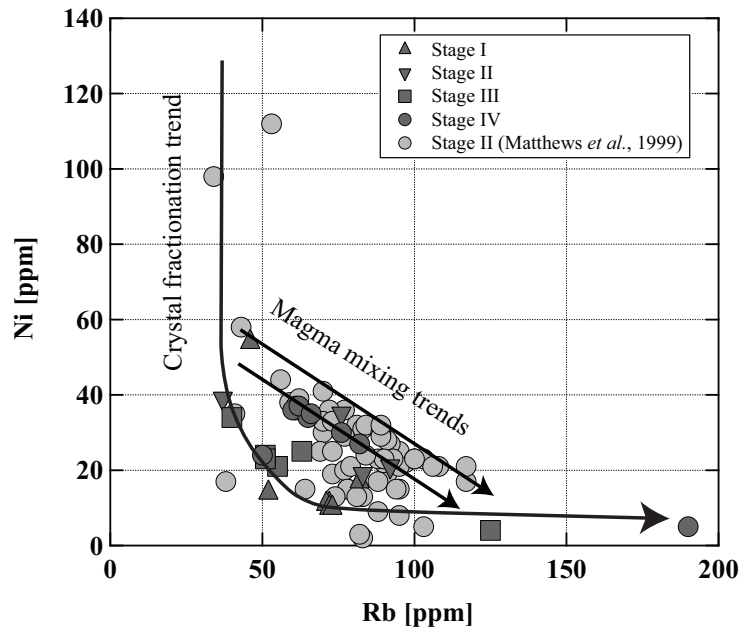
Figure I.15: Ni vs. Rb in Lascar rocks. Curved line is a fractional crystallization path; straight lines are mixing lines (both schematic).

A detailed investigation of the mineralogy of samples of the 1993 eruption may also

indicates that magmas erupted within one eruption event can record different differentiation

processes. As mentioned above, samples from Stage IV do not plot exclusively along a

Dissertation of André Stechern

Petrological and Experimental Constrains on the Pre-eruptive Conditions of 1993 Lascar
Andesites and Insights Into the Evolution of Calc-alkaline Intermediate Lavas

fractionation trend, even though this might be expected from petrographic criteria. Two

samples plotting along the fractionation trend are LAS07-07 and LAS07-26 (Fig. I.15). They

correspond to the andesitic lava flow (7.1 kyr) and white pumice samples (1993 eruption).

7.4 Andesitic magma genesis and a magma reservoir model
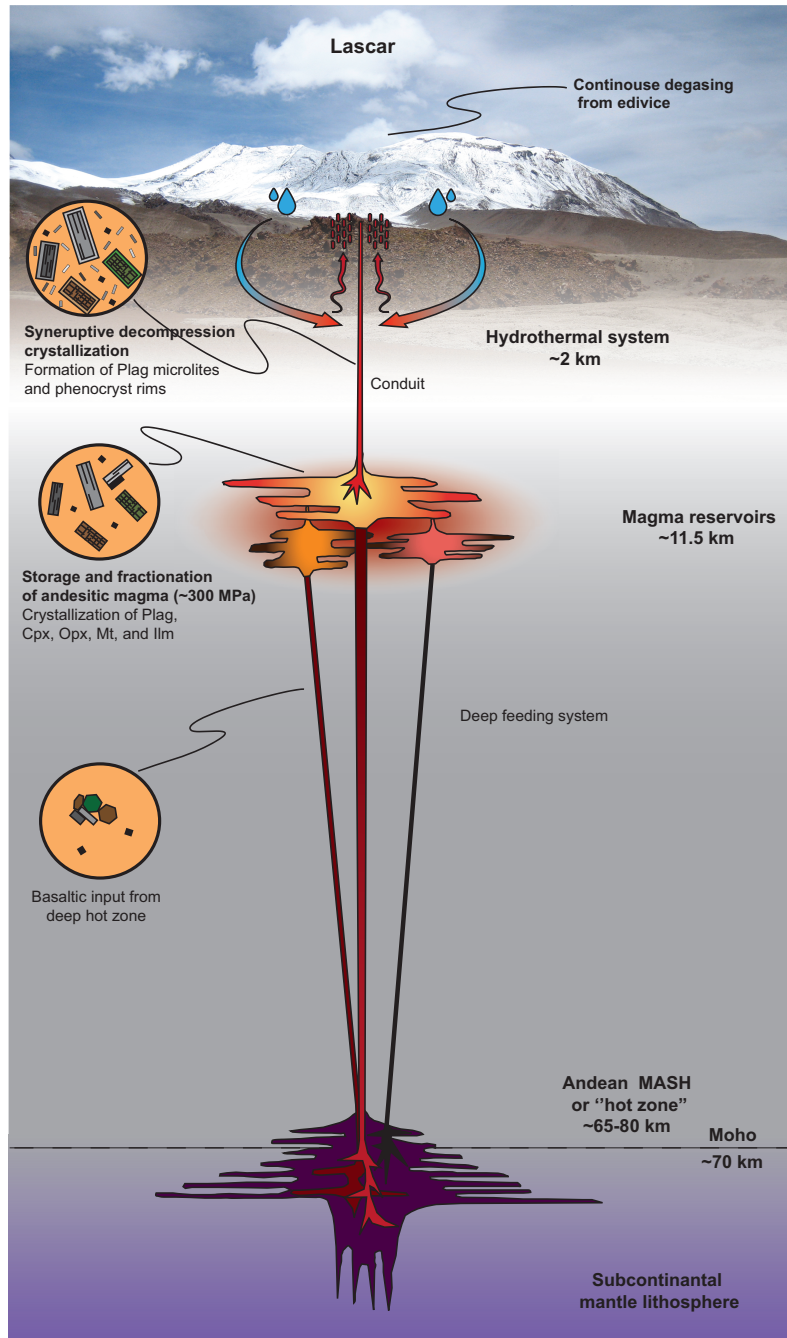
Figure I.16: Suggested model of the magma plumbing system beneath Lascar. Basaltic melt from the deep "hot zone" migrates into the shallow crust. Crystallization at ~300 MPa and ~975°C prior to eruption produces the observed phase assemblage of Plag, Opx, Cpx, and Fe-Ti-oxides. Magmatic heating and remobilization, by new batches of injected melt, may trigger eruptions.

Dissertation of André Stechern

Petrological and Experimental Constrains on the Pre-eruptive Conditions of 1993 Lascar
Andesites and Insights Into the Evolution of Calc-alkaline Intermediate Lavas

A variety of models for andesitic magma genesis were proposed and advanced based on various approaches including experimental work (e.g. Martel *et al.*, 1999; Sisson & Grove, 1993), melt inclusion studies (e.g. Reubi and Blundy, 2009), classic petrological studies (e.g. Almeev *et al.*, 2013b), and geochemical modeling (e.g. Annen *et al.*, 2006; Almeev *et al.*, 2013a). Based on the various models and hypotheses formulated in the literature as well as on experimental and analytical constraints gained by this study, a model for the magma plumbing system of Lascar, which may be characteristic for environments of thickened continental crust, is proposed in Fig. I.16.

(i) Primitive basaltic melts generated by partial melting of the mantle wedge (e.g. Davies and Stevenson, 1992) underplate the continental crust and may form deep magma reservoirs (Hildreth, 1981) at the base of the crust and close to the Moho (violet bottom part of Fig. I.16). However, the exact shape and extent of this structure is not known, and in particular the penetration of this zone into the crust is not clear. Therefore, the shape shown in Fig. I.16 does not accurately recreate the natural form and should be regarded only as a possibility.

(ii) The magma will remain in this reservoir until it fractionates enough (through MASH processes) that the remaining melt is less dense than the surrounding rock; the melt will then continue to migrate towards shallow crustal reservoirs, leaving behind the heavier mafic minerals which were crystallized during fractional crystallization. Very low Sr/Y (~25) and Sm/Yb (~2) ratios for Lascar eruptives suggest that these processes did not happen in the lower crust due to a lack of garnet signature, which would lead to higher Sr/Y and Sm/Yb ratios (Mamani *et al.*, 2010). The basaltic magmas originate from the mantle and migrate upwards into shallow magma reservoirs without major stagnation times in lower crustal reservoirs.

(iii) The ascending basaltic melts form magma reservoirs in the upper continental crust at pressures of around 300 MPa. This storage pressure corresponds to a depth of 11.5 km, assuming a density of the surrounding material of 2.8 g/cm^3 (Lucassen *et al.* (2001).

Dissertation of André Stechern

Petrological and Experimental Constrains on the Pre-eruptive Conditions of 1993 Lascar
Andesites and Insights Into the Evolution of Calc-alkaline Intermediate Lavas

Crystallization of the main andesitic phases (Plag, Cpx, Opx, Oxides, ±Amp) in this magma reservoir(s) produces a residual melt of dacitic to rhyolitic composition, traces of which are observed in melt inclusions from main phenocrysts. In this scenario, the least evolved andesites can be directly linked to the most evolved dacites along liquid lines of descent as demonstrated in the experiments. Small-scale variations in melt composition can be explained e.g. by variations of oxygen fugacity. During an eruptive event decompression driven crystallization in the dactic to rhyolitic melt of mainly plagioclase takes place (e.g. Cashman & Blundy, 2000) and this fractionation is reflected by the highly evolved matrix glasses observed in the volcanic rocks (~75-77 wt.% SiO_2).

The experimental results of this study in combination with the geo-barometric calculation using Putirka (2008) indicate that the shallow reservoirs beneath Lascar are located at depths with corresponding pressure of <500 MPa, most likely around 300 MPa. However, phenocrysts and in particular plagioclases in andesitic rocks commonly have complex zoning patterns indicating that the formation of these crystals involves additional complex processes such as: repeated recharge and mixing with less evolved melts, assimilation of crustal rocks, convection in the magma chamber, and degassing. Therefore fractional crystallization in a shallow magma reservoir is only one contribution to the evolution of intermediate magmas at Lascar.

(iv) In addition, our geochemical results of the 1993 eruption, in particular of samples LAS07-20, -23, -24, -25 point out that shallow reservoirs might not only be characterized by crystal fractionation, but also are regions where magma mixing between primitive and already evolved melts (due to crystal fractionation) takes place. These mixed magmas can be directly tapped during an eruption with no or only a short storage in crustal reservoirs <300 MPa. Several studies have suggested a shallow storage of silicic melts at pressures of about 150 ± 50 MPa, especially for ignimbritic eruptions in the Altiplano-Puna Volcanic Complex (APVC) in the Central Andes (Lindsay *et al.*, 2001; Schmitt, 2001; Muir *et al.*, 2014). Our phase equilibria experiments and geo-barometric calculations indicate that Lascar andesites

Dissertation of André Stechern

Petrological and Experimental Constrains on the Pre-eruptive Conditions of 1993 Lascar
Andesites and Insights Into the Evolution of Calc-alkaline Intermediate Lavas

are stored deeper (~300 MPa) at temperatures around 975°C in the thick continental crust prior to eruption. Recent magnetotelluric measurements in combination with 3D modeling do not indicate the existence of a shallow magmatic reservoir beneath Lascar (Diaz *et al.*, 2012). A shallow conductive layer observed directly beneath the volcanic edifice is interpreted to be caused by fluids from the hydrothermal system rather than by very shallow magma reservoirs. A large highly conductive anomaly was found beneath the Puna Plateau ~80 km to the East of Lascar, starting at ~20 km depth, and probably expending to greater depth (Diaz *et al.*, 2012). The presence of such an anomaly fits well with previous conductivity models obtained beneath the Altiplano to the North (Brasse et al., 2002; Brasse and Eydam, 2008). In addition, seismic data identifies a regional low-velocity zone, which is proposed as the magma source for many eruptions in the Altiplano region (Chmielowski *et al.*, 1999, Schmitz *et al.*, 1997). However, it is not clear from the recent magnetotelluric measurements whether this region has a direct connection to magmatic reservoir beneath Lascar. A less conductive structure which seems to escape from the highly conductive anomaly beneath the Puna, enhances the conductivity just below the volcanic arc at depths of ~ 40 km (Diaz *et al.*, 2012).

8 CONCLUSIONS

Phase equilibria experiments show that pre-eruptive andesite magma storage conditions for Holocene two-pyroxene magmas beneath Lascar volcano likely correspond to ~300 MPa (~11.5 km) at temperatures of 975°C, which is consistent with geo-thermobarometric calculations on natural samples. The starting material for experiments (LAS07-26) has plagioclase, clino-, and orthopyroxene as major phases. This mineral assemblage and its modal proportions are reproduced at 975 ±25°C, 300 MPa, log$f$O$_2$ of QFM+2.75 ±0.25, under H$_2$O-undersaturated conditions with 3.0 to 4.5 wt.% H$_2$O in the melt. Variations along the general differentiation trend can be explained by varying fO$_2$.

Dissertation of André Stechern

Petrological and Experimental Constrains on the Pre-eruptive Conditions of 1993 Lascar
Andesites and Insights Into the Evolution of Calc-alkaline Intermediate Lavas

Melt inclusion data and matrix glass compositions of Lascar rocks in combination with residual glasses from phase equilibria experiments give robust evidence for a magmatic evolution along liquid lines of decent as an addition to a magma-mixing model for Lascar's eruptive rocks.

Geochemical and experimental results of this study propose the production of a residual silicic melt by a partial crystallization of hydrous basalts originating from a lower crustal zone close to the Moho. Hydrous basaltic to basaltic andesite magma ascends buoyantly into the lower crust and forms magma reservoirs where magma undergoes extensive crystallization induced by conductive cooling leading to the phenocryst assemblage found in the eruptive rocks. During eruptive events decompression driven crystallization of the dacitic residual melt from the andesitic magmas takes place and this fractionation produces the most evolved matrix glass which can be found in all Lascar rocks.

Dissertation of André Stechern

Petrological and Experimental Constrains on the Pre-eruptive Conditions of 1993 Lascar
Andesites and Insights Into the Evolution of Calc-alkaline Intermediate Lavas

9 REFERENCES

Almeev, R. R., Holtz, F., Koepke, J., & Parat, F. (2012). Experimental calibration of the effect of H_2O on plagioclase crystallization in basaltic melt at 200 MPa. *American Mineralogist*, *97*(7), 1234-1240.

Almeev, R. R., Kimura, J. I., Ariskin, A. A., & Ozerov, A. Y. (2013a). Decoding crystal fractionation in calc-alkaline magmas from the Bezymianny Volcano (Kamchatka, Russia) using mineral and bulk rock compositions. *Journal of Volcanology and Geothermal Research*, *263*, 141-171.

Almeev, R. R., Holtz, F., Ariskin, A. A., & Kimura, J. I. (2013b). Storage conditions of Bezymianny Volcano parental magmas: results of phase equilibria experiments at 100 and 700 MPa. *Contributions to Mineralogy and Petrology*, *166*(5), 1389-1414.

Andersen, D. J., & Lindsley, D. H. (1985). New (and final!) models for the Ti-magnetite/ilmenite geothermometer and oxygen barometer. In *Abstract AGU 1985 Spring Meeting Eos Transactions. American Geophysical Union* (Vol. 66, No. 18, p. 416).

Andersen, D. J., & Lindsley, D. H. (1988). Internally consistent solution models for Fe-Mg-Mn-Ti oxides: Fe-Ti oxides. *The American Mineralogist*, *73*(7-8), 714-726.

Andersen, D. J., Lindsley, D. H., & Davidson, P. M. (1993). QUILF: A pascal program to assess equilibria among Fe-Mg-Mn-Ti oxides, pyroxenes, olivine, and quartz. *Computers & Geosciences*, *19*(9), 1333-1350.

Annen, C., Blundy, J. D., & Sparks, R. S. J. (2006). The genesis of intermediate and silicic magmas in deep crustal hot zones. *Journal of Petrology*, *47*(3), 505-539.

Banaszak, M. (2014). *Differentiation regimes in the Central Andean magma systems: case studies of Taapaca and Parinacota volcanoes, Northern Chile* (Doctoral dissertation, Göttingen, Georg-August Universität, Diss., 2014).

Bacon, C. R., & Hirschmann, M. M. (1988). Mg/Mn partitioning as a test for equilibrium between coexisting Fe-Ti oxides. *American Mineralogist*, *73*(1-2), 57-61.

Beck, S. L., Zandt, G., Myers, S. C., Wallace, T. C., Silver, P. G., & Drake, L. (1996). Crustal-thickness variations in the central Andes. *Geology*, *24*(5), 407-410.

Behrens, H., Romano, C., Nowak, M., Holtz, F., & Dingwell, D. B. (1996). Near-infrared spectroscopic determination of water species in glasses of the system $MAlSi_3O_8$ (M= Li, Na, K): an interlaboratory study. *Chemical Geology*, *128*(1), 41-63.

Berndt, J., Liebske, C., Holtz, F., Freise, M., Nowak, M., Ziegenbein, D., & Koepke, J. (2002). A combined rapid-quench and H_2-membrane setup for internally heated pressure vessels: description and application for water solubility in basaltic melts. *American Mineralogist*, *87*(11-12), 1717-1726.

Blundy, J., & Cashman, K. (2005). Rapid decompression-driven crystallization recorded by melt inclusions from Mount St. Helens volcano. *Geology*, *33*(10), 793-796.

Botcharnikov, R. E., Koepke, J., Holtz, F., McCammon, C., & Wilke, M. (2005). The effect of water activity on the oxidation and structural state of Fe in a ferro-basaltic melt. *Geochimica et Cosmochimica Acta*, *69*(21), 5071-5085.

Botcharnikov, R. E., Behrens, H., & Holtz, F. (2006). Solubility and speciation of C–O–H fluids in andesitic melt at *T* = 1100–1300° C and *P* = 200 and 500 MPa. *Chemical Geology*, *229*(1), 125-143.

Botcharnikov, R. E., Holtz, F., Almeev, R. R., Sato, H., & Behrens, H. (2008). Storage conditions and evolution of andesitic magma prior to the 1991–95 eruption of Unzen volcano: Constraints from natural samples and phase equilibria experiments. *Journal of Volcanology and Geothermal Research*, *175*(1), 168-180.

Brasse, H., Lezaeta, P., Rath, V., Schwalenberg, K., Soyer, W., & Haak, V. (2002). The Bolivian altiplano conductivity anomaly. *Journal of Geophysical Research: Solid Earth (1978–2012)*, *107*(B5), EPM-4.

Dissertation of André Stechern

Petrological and Experimental Constrains on the Pre-eruptive Conditions of 1993 Lascar
Andesites and Insights Into the Evolution of Calc-alkaline Intermediate Lavas

Brasse, H., & Eydam, D. (2008). Electrical conductivity beneath the Bolivian Orocline and its relation to subduction processes at the South American continental margin. *Journal of Geophysical Research: Solid Earth (1978–2012)*, *113*(B7).

Burnham, C. W. (1979). The importance of volatile constituents. *The evolution of the igneous rocks*, *439*, 82.

Calder, E. S., Sparks, R. S. J., & Gardeweg, M. C. (2000). Erosion, transport and segregation of pumice and lithic clasts in pyroclastic flows inferred from ignimbrite at Lascar Volcano, Chile. *Journal of Volcanology and Geothermal Research*, *104*(1), 201-235.

Cashman, K., & Blundy, J. (2000). Degassing and crystallization of ascending andesite and dacite. *Philosophical Transactions of the Royal Society of London. Series A: Mathematical, Physical and Engineering Sciences*, *358*(1770), 1487-1513.

Chmielowski, J., Zandt, G., & Haberland, C. (1999). The central Andean Altiplano-Puna magma body. *Geophysical Research Letters*, *26*(6), 783-786.

Costa, F., Scaillet, B., & Pichavant, M. (2004). Petrological and experimental constraints on the pre-eruption conditions of Holocene dacite from Volcán San Pedro (36 S, Chilean Andes) and the importance of sulphur in silicic subduction-related magmas. *Journal of Petrology*, *45*(4), 855-881.

Dall'Agnol, R., Scaillet, B., & Pichavant, M. (1999). An Experimental Study of a Lower Proterozoic A-type Granite from theEastern Amazonian Craton, Brazil. *Journal of Petrology*, *40*(11), 1673-1698.

Davies, J. H., & Stevenson, D. J. (1992). Physical model of source region of subduction zone volcanics. *Journal of Geophysical Research: Solid Earth (1978–2012)*, *97*(B2), 2037-2070.

Díaz, D., Brasse, H., & Ticona, F. (2012). Conductivity distribution beneath Lascar volcano (Northern Chile) and the Puna, inferred from magnetotelluric data. *Journal of Volcanology and Geothermal Research*, *217*, 21-29.

Drake, M. J., & Weill, D. F. (1975). Partition of Sr, Ba, Ca, Y, Eu^{2+}, Eu^{3+}, and other REE between plagioclase feldspar and magmatic liquid: an experimental study. *Geochimica et Cosmochimica Acta*, *39*(5), 689-712.

Eggler, D. H. (1972). Water-saturated and undersaturated melting relations in a Paricutin andesite and an estimate of water content in the natural magma. *Contributions to Mineralogy and Petrology*, *34*(4), 261-271.

Feig, S. T., Koepke, J., & Snow, J. E. (2010). Effect of oxygen fugacity and water on phase equilibria of a hydrous tholeiitic basalt. *Contributions to Mineralogy and Petrology*, *160*(4), 551-568.

Freise, M., Holtz, F., Nowak, M., Scoates, J. S., & Strauss, H. (2009). Differentiation and crystallization conditions of basalts from the Kerguelen large igneous province: an experimental study. *Contributions to Mineralogy and Petrology*, *158*(4), 505-527.

Frost, B. R. (1991). Introduction to oxygen fugacity and its petrologic importance. *Reviews in Mineralogy and Geochemistry*, *25*(1), 1-9.

Gardeweg, M. C., Sparks, R. S. J., & Matthews, S. J. (1998). Evolution of Lascar volcano, northern Chile. *Journal of the Geological Society*, *155*(1), 89-104.

Green, T. H., Sie, S. H., Ryan, C. G., & Cousens, D. R. (1989). Proton microprobe-determined partitioning of Nb, Ta, Zr, Sr and Y between garnet, clinopyroxene and basaltic magma at high pressure and temperature. *Chemical Geology*, *74*(3), 201-216.

Gutscher, M. A. (2002). Andean subduction styles and their effect on thermal structure and interplate coupling. *Journal of South American Earth Sciences*, *15*(1), 3-10.

Haschke, M. R., Scheuber, E., Günther, A., & Reutter, K. J. (2002). Evolutionary cycles during the Andean orogeny: repeated slab breakoff and flat subduction?. *Terra nova*, *14*(1), 49-55.

Hildreth, W., & Moorbath, S. (1988). Crustal contributions to arc magmatism in the Andes of central Chile. *Contributions to Mineralogy and Petrology*, *98*(4), 455-489.

Petrological and Experimental Constrains on the Pre-eruptive Conditions of 1993 Lascar
Andesites and Insights Into the Evolution of Calc-alkaline Intermediate Lavas

Holtz, F., Sato, H., Lewis, J., Behrens, H., & Nakada, S. (2005). Experimental petrology of the 1991–1995 Unzen dacite, Japan. Part I: phase relations, phase composition and pre-eruptive conditions. *Journal of Petrology*, *46*(2), 319-337.

Leake, B. E., Woolley, A. R., Birch, W. D., Burke, E. A., Ferraris, G., Grice, J. D., & Whittaker, E. J. (2004). Nomenclature of amphiboles: Additions and revisions to the International Mineralogical Association's amphibole nomenclature. *American Mineralogist*, *89*, 883-887.

Lee, C. T. A., Cheng, X., & Horodyskyj, U. (2006). The development and refinement of continental arcs by primary basaltic magmatism, garnet pyroxenite accumulation, basaltic recharge and delamination: insights from the Sierra Nevada, California. *Contributions to Mineralogy and Petrology*, *151*(2), 222-242.

Lepage, L. D. (2003). ILMAT: an Excel worksheet for ilmenite–magnetite geothermometry and geobarometry. *Computers & Geosciences*, *29*(5), 673-678.

Lindsay, J. M., Schmitt, A. K., Trumbull, R. B., De Silva, S. L., Siebel, W., & Emmermann, R. (2001). Magmatic evolution of the La Pacana caldera system, Central Andes, Chile: compositional variation of two cogenetic, large-volume felsic ignimbrites. *Journal of Petrology*, *42*(3), 459-486.

Lucassen, F., Becchio, R., Harmon, R., Kasemann, S., Franz, G., Trumbull, R., ... & Dulski, P. (2001). Composition and density model of the continental crust at an active continental margin - the Central Andes between 21 and 27 S. *Tectonophysics*, *341*(1), 195-223.

Maksimov, A. P., Kadik, A. A., Korovushkina, E. Y., & Ivanov, B. V. (1978). Crystallization of an andesite melt with a fixed water content at pressures up to 12 kbar. *Geochemistry International*, *15*, 20-29.

Mamani, M., Wörner, G., & Sempere, T. (2010). Geochemical variations in igneous rocks of the Central Andean orocline (13 S to 18 S): Tracing crustal thickening and magma generation through time and space. *Geological Society of America Bulletin*, *122*(1-2), 162-182.

Martel, C., Pichavant, M., Holtz, F., Scaillet, B., Bourdier, J. L., & Traineau, H. (1999). Effects of fO_2 and H_2O on andesite phase relations between 2 and 4 kbar. *Journal of Geophysical Research: Solid Earth (1978–2012)*, *104*(B12), 29453-29470.

Matthews, S. J., Jones, A. P., & Gardeweg, M. C. (1994). Lascar Volcano, Northern Chile; evidence for steady-state disequilibrium. *Journal of Petrology*, *35*(2), 401-432.

Matthews, S. J., Gardeweg, M. C., & Sparks, R. S. J. (1997). The 1984 to 1996 cyclic activity of Lascar Volcano, northern Chile: cycles of dome growth, dome subsidence, degassing and explosive eruptions. *Bulletin of Volcanology*, *59*(1), 72-82.

Matthews, S. J., Sparks, R. S. J., & Gardeweg, M. C. (1999). The Piedras Grandes–Soncor eruptions, Lascar volcano, Chile; evolution of a zoned magma chamber in the central Andean upper crust. *Journal of Petrology*, *40*(12), 1891-1919.

McMillan, N. J., Davidson, J. P., Wörner, G., Harmon, R. S., Moorbath, S., & Lopez-Escobar, L. (1993). Influence of crustal thickening on arc magmatism:, Nevados de Payachata volcanic region, northern Chile. *Geology*, *21*(5), 467-470.

Miyashiro, A., & Shido, F. (1975). Tholeiitic and calc-alkalic series in relation to the behaviors of titanium, vanadium, chromium, and nickel. *American Journal of Science*, *275*(3), 265-277.

Muir, D. D., Blundy, J. D., Hutchinson, M. C., & Rust, A. C. (2014). Petrological imaging of an active pluton beneath Cerro Uturuncu, Bolivia. *Contributions to Mineralogy and Petrology*, *167*(3), 1-25.

Müntener, O., Kelemen, P. B., & Grove, T. L. (2001). The role of H_2O during crystallization of primitive arc magmas under uppermost mantle conditions and genesis of igneous pyroxenites: an experimental study. *Contributions to Mineralogy and Petrology*, *141*(6), 643-658.

Parat, F., Holtz, F., & Feig, S. (2008). Pre-eruptive conditions of the Huerto andesite (Fish canyon system, San Juan volcanic field, Colorado): influence of volatiles (C–O–H–S) on phase equilibria and mineral composition. *Journal of Petrology*, *49*(5), 911-935.

Putirka, K. D. (2008). Thermometers and barometers for volcanic systems. *Reviews in Mineralogy and Geochemistry*, *69*(1), 61-120.

Dissertation of André Stechern

Petrological and Experimental Constrains on the Pre-eruptive Conditions of 1993 Lascar
Andesites and Insights Into the Evolution of Calc-alkaline Intermediate Lavas

Reubi, O., & Blundy, J. (2009). A dearth of intermediate melts at subduction zone volcanoes and the petrogenesis of arc andesites. *Nature*, *461*(7268), 1269-1273.

Roedder, E. (1992). Fluid inclusion evidence for immiscibility in magmatic differentiation. *Geochimica et Cosmochimica Acta*, *56*(1), 5-20.

Scaillet, B., & Evans, B. W. (1999). The 15 June 1991 eruption of Mount Pinatubo. I. Phase equilibria and pre-eruption P–T–fO2–fH2O conditions of the dacite magma. *Journal of Petrology*, *40*(3), 381-411.

1 Schmidt B. C., Scaillet, B., Holtz F. M. (1995). Accurate control of fH$_2$ in cold-seal pressure vessels with the Shaw membrane technique. *European Journal of Mineralogy*, 7 (1995), 893–903.

Schmitt, A., De Silva, S., Trumbull, R., & Emmermann, R. (2001). Magma evolution in the Purico ignimbrite complex, northern Chile: evidence for zoning of a dacitic magma by injection of rhyolitic melts following mafic recharge. *Contributions to Mineralogy and Petrology*, *140*(6), 680-700.

Schmitz, M., Heinsohn, W. D., & Schilling, F. R. (1997). Seismic, gravity and petrological evidence for partial melt beneath the thickened central Andean crust (21–23 S). *Tectonophysics*, *270*(3), 313-326.

Schuessler, J. A., Botcharnikov, R. E., Behrens, H., Misiti, V., & Freda, C. (2008). Amorphous Materials: Properties, structure, and Durability Oxidation state of iron in hydrous phono-tephritic melts. *American Mineralogist*, *93*(10), 1493-1504.

Schwab, R. G., & Küstner, D. (1981). Die Gleichgewichtsfugazitäten technologisch und petrologisch wichtiger Sauerstoffpuffer. *Neues Jahrb. Mineral. Abh.*, *140*, 111-142.

Sekine, T., Katsura, T., & Aramaki, S. (1979). Water saturated phase relations of some andesites with application to the estimation of the initial temperature and water pressure at the time of eruption. *Geochimica et Cosmochimica Acta*, *43*(8), 1367-1376.

Shimizu, N., & Kushiro, I. (1975). The partitioning of rare earth elements between garnet and liquid at high pressures: preliminary experiments. *Geophysical Research Letters*, *2*(10), 413-416.

Shishkina, T. A., Botcharnikov, R. E., Holtz, F., Almeev, R. R., & Portnyagin, M. V. (2010). Solubility of H$_2$O and CO$_2$-bearing fluids in tholeiitic basalts at pressures up to 500MPa. *Chemical Geology*, *277*(1), 115-125.

Sisson, T. W., & Grove, T. L. (1993). Experimental investigations of the role of H$_2$O in calc-alkaline differentiation and subduction zone magmatism. *Contributions to Mineralogy and Petrology*, *113*(2), 143-166.

Snyder, D. A., & Carmichael, I. S. (1992). Olivine-liquid equilibria and the chemical activities of FeO, NiO, Fe$_2$O$_3$, and MgO in natural basic melts. *Geochimica et Cosmochimica Acta*, *56*(1), 303-318.

Sobolev, A. V., & Danyushevsky, L. V. (1994). Petrology and geochemistry of boninites from the north termination of the Tonga Trench: constraints on the generation conditions of primary high-Ca boninite magmas. *Journal of Petrology*, *35*(5), 1183-1211.

Tassi, F., Aguilera, F., Vaselli, O., Medina, E., Tedesco, D., Huertas, A. D., ... & Kojima, S. (2009). The magmatic-and hydrothermal-dominated fumarolic system at the Active Crater of Lascar volcano, northern Chile. *Bulletin of volcanology*, *71*(2), 171-183.

Toplis, M. J., & Carroll, M. R. (1995). An experimental study of the influence of oxygen fugacity on Fe-Ti oxide stability, phase relations, and mineral-Melt equilibria in ferro-basaltic systems. *Journal of Petrology*, *36*(5), 1137-1170.

Wallace, P. J., & Edmonds, M. (2011). The sulfur budget in magmas: evidence from melt inclusions, submarine glasses, and volcanic gas emissions. *Reviews in Mineralogy and Geochemistry*, *73*(1), 215-246.

Wörner, G., Harmon, R. S., Davidson, J., Moorbath, S., Turner, D. L., McMillan, N., & Moreno, H. (1988). The Nevados de Payachata volcanic region (18 S/69 W, N. Chile). *Bulletin of Volcanology*, *50*(5), 287-303.

Wright, T. L., & Doherty, P. C. (1970). A linear programming and least squares computer method for solving petrologic mixing problems. *Geological Society of America Bulletin*, *81*(7), 1995-2008.

Dissertation of André Stechern

Petrological and Experimental Constrains on the Pre-eruptive Conditions of 1993 Lascar
Andesites and Insights Into the Evolution of Calc-alkaline Intermediate Lavas

Yuan, X., Sobolev, S. V., Kind, R., Oncken, O., Bock, G., Asch, G., ... & Comte, D. (2000). Subduction
and collision processes in the Central Andes constrained by converted seismic phases. *Nature*, *408*(6815), 958-
961.

Dissertation of André Stechern

Decoding Magma Plumbing and Geochemical Evolution Beneath the Lastarria Volcanic
Complex (Northern Chile) - Evidence for Multiple Magma Storage Regions

Decoding Magma Plumbing and Geochemical Evolution Beneath the Lastarria Volcanic Complex (Northern Chile) - Evidence for Multiple Magma Storage Regions

1 ABSTRACT

The petrology of quaternary andesites and dacites from Lastarria volcano is investigated to reconstruct magma plumbing and storage beneath the volcano. The mineral phase compositions and whole-rock major and trace element compositions were used to constrain temperature, pressure and possible mechanisms for magma differentiation. The applied thermobarometric models include two-pyroxene thermobarometry, pyroxene-melt thermobarometry, plagioclase-melt thermometry, amphibole composition thermobarometry, and Fe-Ti oxide thermo- oxybarometry. The overall temperature range gained by several geo-thermometers is between 840 and 1060°C. Calculated oxygen fugacity for all samples corresponds to a range between NNO to NNO+1. Results of the geo-barometric calculations reveal multiple magma storage regions, with a distinct storage level in the uppermost crust (~6.5-8 km depth), a broad zone at mid-crustal levels (~10-18 km depth), and a potential deeper zone at intermediate to lower crustal levels (>20km depth), which is difficult to define from petrological information only. The highest temperatures are recorded in minerals stored in the mid-crustal levels (~10-18 km depth). The whole-rock compositions clearly indicate that magma mixing is the main parameter controlling the general differentiation trends. Complex zoning patterns and textures in the plagioclase phenocrysts is interpreted as a

Dissertation of André Stechern

Decoding Magma Plumbing and Geochemical Evolution Beneath the Lastarria Volcanic
Complex (Northern Chile) - Evidence for Multiple Magma Storage Regions

reheating and remobilization remnant of the resident magma by an intrusion of hotter more mafic magma rising from depth into shallow reservoirs.

2 INTRODUCTION

The Lastarria volcanic complex is part of the Central Volcanic Zone (CVZ) of the Andes, which includes ~50 active or potentially active volcanoes distributed along a 1500 km arc between South Peru and Chile. Most of these volcanoes, including Lastarria, are located in remote areas difficult to access and, as a consequence, their petrological and geochemical features are not well known. Among these volcanoes Lastarria is particularly interesting. Lastarria is a part of the Lazufre (an acronym of Lastarria and Azufre) Volcanic Complex, a ~30 km long chain of overlapping Quaternary volcanic centers, aligned in a NE-SW direction between Lastarria and Cerro Bayo volcanoes, located on the border between Chile and Argentina. This volcanic complex is one of the few places on Earth where, due to processes in the volcanic plumbing system, an ongoing crustal deformation has been observed and monitored with geophysical methods over a period of several years, starting from 1995 (Pritchard and Simons, 2002; 2004). Recent observations have shown that this volcanic area is one of the largest volcano systems on earth, comparable in size with Yellowstone or Long Valley (both USA), and which is recently undergoing an active deformation (Froger *et al.*, 2007; Remy *et al.*, 2014). Proposed mechanisms causing the ground deformation include (i) an injection of magma in a crustal reservoir, (ii) migration of hydrothermal fluids towards the surface, and (iii) a rock volume variation caused by phase changes related to the evolution of a pre-caldera volcanic system (Pritchard and Simons, 2002; 2004; Froger *et al.* 2007; Ruch *et al.*, 2008). Pritchard and Simons (2004) assume that the deformation has started sometimes between 1996 and 1998 and the depth of the source for the uplift has been estimated between 9 and 17 km. Later studies have shown a deformation rate up to 3 cm/yr affecting an area of ~50 by ~38 km over 5 years (Anderssohn *et al.*, 2009) at the Lazufre Volcanic Complex. A locally restricted deformation, directly around Lastarria's edifice, over a 50 km^2 area was

Dissertation of André Stechern

Decoding Magma Plumbing and Geochemical Evolution Beneath the Lastarria Volcanic Complex (Northern Chile) - Evidence for Multiple Magma Storage Regions

detected with deformation rates up to 1.5 cm/yr (Froger *et al.*, 2007; Ruch *et al.*, 2009). Even though no historic eruption is documented, the present status of Lascar has been characterized by a strong continuous fumarolic activity from several vents, which generate plumes of volcanic gases on the northern summit and the northwestern flank. These observations of volcanic activity were already made before the beginning of the uplift (e.g. Naranjo, 1985). Ground deformations of the Earth's surface around volcanoes are a direct consequence of magmatic processes in the plumbing system (e.g. Remy *et al.*, 2014). Consideration of intermediate magma systems temporal changes (e.g. composition, structure, and volume) in addition to the geophysical observations are important for understanding of the dynamics before and during explosive eruptions. Furthermore, they are yielding information about the evolution of the Earth's crust in general. In addition to the surface processes characterization, pre-eruptive magma storage parameters like pressure (P), temperature (T), water content of the melt (H_2O_{melt}), and oxygen fugacity (fO_2) are crucial for defining the magma chamber processes and physical properties of magmas during volcanic eruptions (e.g. Holtz *et al.*, 2005; and Dahren *et al.*, 2012). Estimates of the storage depth as well as thermal information are in particularly critical for the interpretation of geophysical observations and the resulting models, i.e. the depth and the temperature of a magma reservoir affecting density, seismic velocity, and conductivity in the crust (e.g. Iyer, 1984). Moreover, temperatures strongly control the viscosity of melts, which is one of the key parameters influencing the migration of partially molten material towards the Earth's surface.

In this paper, we present whole-rock major and trace element analyses and mineral compositions, as well as thermobarometric calculations from Lastarria's eruptive products in order to characterize the petrology and possible mechanisms for the magmatic evolution of Lastarria rocks.

Dissertation of André Stechern

Decoding Magma Plumbing and Geochemical Evolution Beneath the Lastarria Volcanic
Complex (Northern Chile) - Evidence for Multiple Magma Storage Regions

3 GEOLOGICAL SETTING

The Lastarria volcanic complex is located in the southern part of the CVZ of the Andes on the Chilean-Argentinean border about 300 km east of the subduction trench (25.168° S 68.507° W). Other volcanoes belonging to the Lazufre Volcanic Complex are the Cordon del Azufre and the Cerro Bayo to the SW. Both volcanoes are Quaternary and form a series of craters and associated lava flows (de Silva and Francis, 1991) but show no fumarolic activity. The Lazufre Volcanic Complex is part of the Puna Plateau, which had started to form during the Eocene as a result of the Nazca Plate subduction beneath the South American Plate. The compressive regime at this convergent plate boundary caused rising of the plateau up to 4000 m. During the mid-Miocene to Pliocene the magmatic activity in this area reached its maximum through a period of rapid subduction, steepening of the subduction angle, and crustal shortening and thickening (e.g. Gregory-Wodzicki, 2000). The continental crust in this area reaches a thickness of about 60-65 km (Wölbern *et al.*, 2009). The Puna Plateau is dominated by several distinct volcanic centers (de Silva and Francis, 1991). One of these centers is the Lastarria volcano (Summit ~5706 m). Lastarria is characterized by a strong and persistent fumarolic activity localized on the SW and E side of the recent crater and on a fracture system along the NW flank of the volcanic edifice (700 m below the crater rim). The area around the volcano is composed of Tertiary and Quaternary ignimbrites, lava flows, and salars. Compositions of the surrounding volcanic rocks are mainly intermediate to felsic, with ages ranging from 17.14 myr (^{40}Ar/^{39}Ar ages, Richards *et al.*, 2013) to recent. No historic eruption of Lastarria has been reported (Naranjo and Francis, 1987). Lastarria volcano is andesitic to dacitic in composition. The volcanic activity shows a northward migration along a 10 km-long ridge and Naranjo (1992) groups three distinct structures that form the volcanic complex: (i) The *Southern Spur* with a N-S orientation is the oldest. (ii) The presently active Lastarria volcano to the North, joining the *Southern Spur* at ~5500m, is the main structure of the system and formed by five NW-SE aligned nested craters. (iii) The *Negriales lava field* is

Decoding Magma Plumbing and Geochemical Evolution Beneath the Lastarria Volcanic Complex (Northern Chile) - Evidence for Multiple Magma Storage Regions

a geographically associated andesitic to dacitic lava field, situated SW of the main volcanic

structure, and formed by several up to 10 km long lava flows erupted from a single fissure.
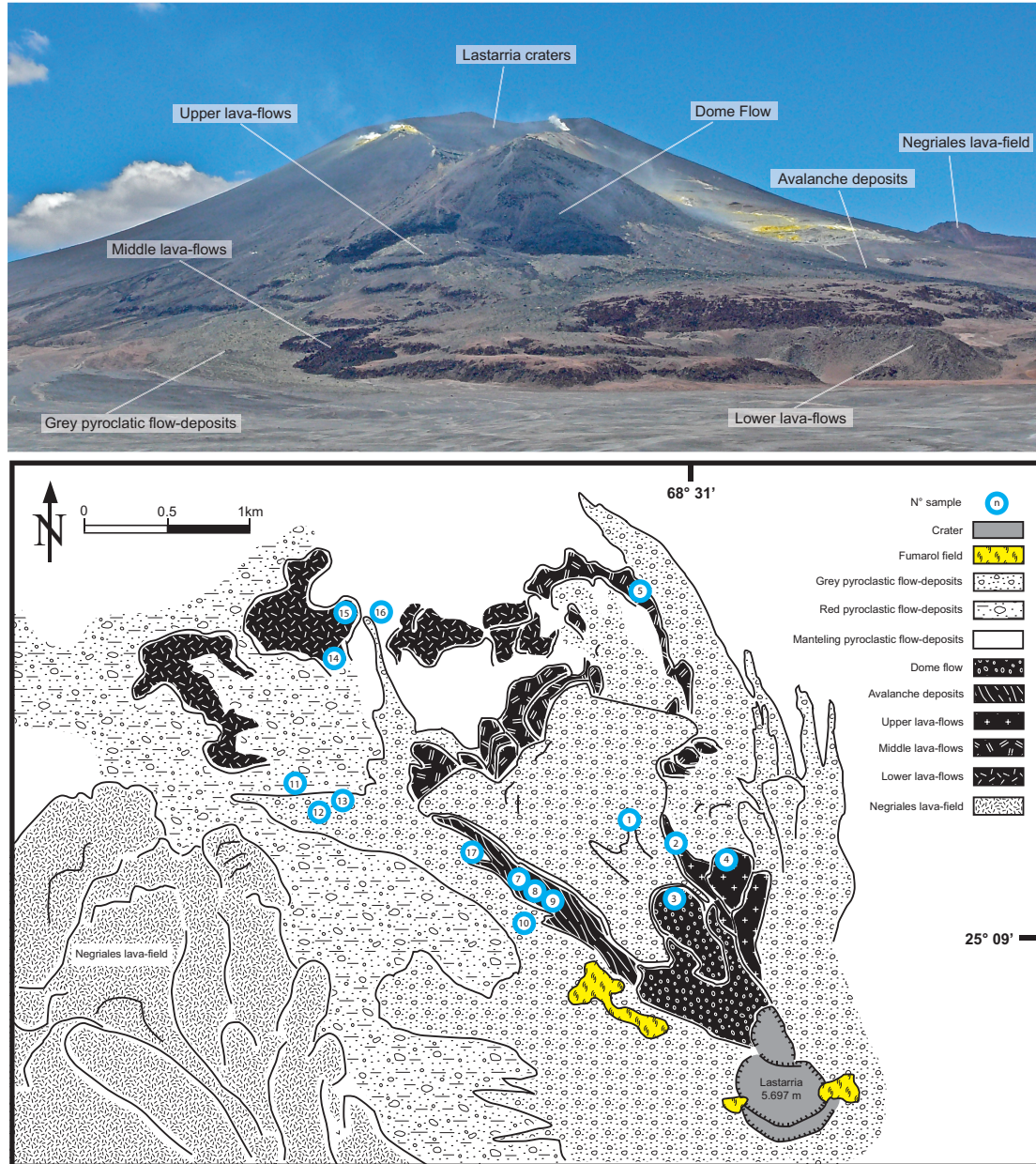
Figure II.1: Photograph of Lastarria summit taken towards SE labeled with the main volcanic features and a simplified geological map with the sampling locations.

On the NW flank of Lastarria edifice several lava flows, avalanche deposits, pyroclastic-flow

deposits, and a dome collapse can be identified. At least three different generations of lava

flows (upper, middle, and lower) can be distinguished even though no absolute age data exist.

Dissertation of André Stechern

Decoding Magma Plumbing and Geochemical Evolution Beneath the Lastarria Volcanic
Complex (Northern Chile) - Evidence for Multiple Magma Storage Regions

All other flanks of the volcano are mainly covered with mantling pyroclastic deposits and are of difficult access due to land-mine fields close to the Chilean-Argentinian border. Fig. II.1 shows a photograph of Lastarria taken towards SE and a simplified geological map with the main volcanic and petrographic features.

4 PETROGRAPHY, MINERAL CHEMISTRY AND GEOCHEMISTRY OF LASTARRIA ERUPTIVE PRODUCTS

4.1 Sampling and analytical techniques

Fieldwork was carried out in 2010 with the aim of sampling representative specimen, free of any visible alteration, from all types of eruptive material mentioned in the above paragraph (juvenile blocks and bombs from the pyroclastic flow deposits, the lava flows, avalanche deposits, and volcanic ash). Sample locations are displayed in Fig. II.1.

Eighteen rock and ash samples (labeled LAST-10-01 to LAST-10-17D) were washed in distilled water, cut (in case of rocks), and afterwards crushed using a steel mortar. Rock chips were milled in a tungsten carbide ring grinder. Whole-rock major and trace elements (Ba, Ce, Co, Cr, Cu, Ga, Hf, La, Mo, Nb, Nd, Ni, Pb, Rb, S, Sc, Sm ,Sr, Th, U, V ,Y, Yb, Zn, Rz) have been analyzed at the Geowissenschaftliches Zentrum, Universität Göttingen, using a *PANalytical Axios Advanced* Wavelength-Dispersive X-ray fluorescence (XRF) spectrometer. Analyses were carried out on fused glass discs, prepared using 2.8000 g of rock powder mixed with 5.6000 g of Spectromelt A12 (66% lithium tetraborate and 34% Lithium metaborate) and 0.6400 g LiF. In general, the precision for each major and most minor elements is better than 1% relative to the reported value, monitored using an andesitic in-house rock standard. Fe was measured as total Fe_2O_3 and analyses were recalculated to 100% volatile free and total FeO. Major and trace element analyses are reported in Tab. II.1.

Decoding Magma Plumbing and Geochemical Evolution Beneath the Lastarria Volcanic Complex (Northern Chile) - Evidence for Multiple Magma Storage Regions

Table II.1: Whole rock major and trace element (determined by X-ray fluorescence, XRF) compositions of Lastarria eruptives. All iron is expressed as FeO$_{total}$.

Sample	LAST-10-01	LAST-10-02	LAST-10-03	LAST-10-04	LAST-10-05	LAST-10-07	LAST-10-08	LAST-10-09	LAST-10-10	LAST-10-12	LAST-10-13	LAST-10-14	LAST-10-15	LAST-10-16	LAST-10-17A	LAST-10-17B	LAST-10-17C	LAST-10-17D
Type	compact, dark lava flow	light gray pumice	compact, dark lava flow	compact, dark dome material	compact, dark lava flow	gray pumice	compact, dark lava	compact, dark lava	gray pyroclastic ash	dark pumice	gray pyroclastic ash	compact, light gray lava flow	compact, light gray lava flow	compact, dark gray lava	gray lapilli tephra	gray lapilli tephra	gray pyroclastic ash	gray pyroclastic ash
Major elements determined by XRF (wt.%)																		
SiO$_2$	59.34	59.39	60.72	59.54	60.54	62.55	60.74	60.91	60.91	59.51	60.52	60.98	60.99	60.77	60.61	61.46	62.46	59.57
TiO$_2$	1.03	1.01	0.98	0.99	0.96	0.87	0.86	0.95	0.95	1.01	0.88	0.87	0.91	0.85	1.02	0.87	0.89	1.00
Al$_2$O$_3$	16.18	15.84	15.83	15.90	16.22	15.88	16.32	15.89	15.89	16.27	14.50	16.03	16.39	16.36	15.08	15.15	15.25	15.54
FeO$_{tot}$	6.11	5.99	5.72	5.86	5.59	5.12	0.00	5.59	5.59	6.03	5.12	5.05	5.21	5.23	6.01	5.47	5.02	6.07
MnO	0.10	0.09	0.09	0.09	0.09	0.08	0.09	0.09	0.09	0.09	0.09	0.08	0.08	0.08	0.07	0.09	0.07	0.07
MgO	4.04	3.84	3.85	3.71	3.46	2.84	2.70	3.59	3.59	4.02	3.10	2.75	2.78	2.68	3.26	3.40	2.46	3.59
CaO	6.21	6.00	5.81	5.99	5.83	4.99	5.52	5.79	5.79	6.15	5.37	5.46	5.16	5.37	4.88	5.01	4.50	5.23
Na$_2$O	3.50	3.46	3.51	3.51	3.54	3.49	3.40	3.51	3.51	3.50	2.82	3.41	3.41	3.35	3.33	3.14	3.08	3.37
K$_2$O	2.32	2.37	2.50	2.56	2.60	2.91	2.80	2.56	2.56	2.35	2.41	2.78	2.71	2.83	2.73	2.50	2.60	2.53
P$_2$O$_5$	0.26	0.24	0.25	0.27	0.26	0.21	0.24	0.24	0.24	0.25	0.20	0.22	0.22	0.22	0.27	0.19	0.17	0.28
Total	99.07	98.23	99.25	98.43	99.09	98.94	92.67	99.12	99.12	99.19	95.00	97.62	97.86	97.74	97.26	97.27	96.50	97.25
Trace elements determined by XRF (ppm)																		
Ba	473	480	517	503	518	520	590	509	509	480	450	506	503	613	526	478	499	498
Ce	67	65	70	71	73	71	61	71	71	62	67	68	77	63	67	65	71	70
Co	22	21	21	20	19	16	19	19	19	22	17	16	17	18	19	18	15	19
Cr	90	85	102	81	69	49	32	84	84	87	51	34	34	30	83	64	51	84
Cu	45	46	54	38	31	32	27	36	36	39	37	23	32	25	40	34	41	33
Ga	21	21	21	21	21	20	21	21	21	21	19	20	20	21	21	20	20	20
Hf	5.2	4.9	4.7	5.3	4.8	5.4	5	5.3	5.3	5.3	4.9	5	5.5	5.2	5.1	4.8	5.4	5.2
La	32	34	36	38	39	35	36	36	36	36	33	37	42	37	38	36	37	36
Mo	1.5	1.5	1.6	1.7	1.7	2.1	1	1.7	1.7	1.5	1.9	1.9	1.9	1.1	2.1	1.9	2.2	2
Nb	12.6	12.6	12.6	13.1	12.9	13.2	12	12.8	12.8	12.2	12.5	12.6	13.7	11.4	14	12	12.9	13.3
Nd	32.4	30.2	34.4	32.7	34.7	32.3	33	32.4	32.4	31.8	30.4	32.4	35.6	33.7	29.3	29.9	31.9	31.8
Ni	44	41	50	42	37	28	21	46	46	41	28	25	26	19	41	33	26	44
Pb	13.3	13.8	13.5	13.1	13.4	16	15	13.7	13.7	12	14.5	16.1	15.5	15.4	16.7	16.4	18.1	11.5
Rb	98	101	110	115	119	143	109	115	115	101	122	133	131	103	124	118	125	113
S	81	2413	1381	2337	33	113	220	549	549	17	14206	2162	15	135	3656	4957	6902	1711
Sc	15	15	16	15	14	13	14	15	15	16	14	11	12	13	16	13	12	17
Sm	6.4	6.4	5.9	6.3	7	6.1	7	7	7	6.5	6.4	6.7	6.9	6.6	5.7	5.4	5.7	6.6
Sr	526	507	515	542	567	462	499	509	509	521	465	480	471	507	505	507	514	512
Th	17.1	17.7	19	21	22.1	27.3	15	20.5	20.5	18	23.2	24.6	26.3	13.5	23.1	22.3	24.1	21.8
U	4.2	4.4	4.7	5.1	5.4	6.6	4	5	5	4.4	5.7	6	6.4	3.4	5.6	5.4	5.8	5.3
V	156	155	143	152	144	127	133	140	140	156	127	127	131	129	156	128	126	155
Y	18.6	18.4	18.2	19	19.3	18.1	20	18.7	18.7	18.6	17.2	18.7	22.9	21	16.1	16.3	14.8	16.6
Yb	2.3	2.2	2.7	1.8	3	2.5	2	2.3	2.3	2.6	2.8	2.6	2.7	2.4	2.2	2.7	2.7	2.5
Zn	90	89	88	87	85	83	83	87	87	89	79	80	87	84	74	81	72	78
Zr	189	188	195	196	200	203	205	204	204	188	183	193	207	207	200	176	219	194

Dissertation of André Stechern

Decoding Magma Plumbing and Geochemical Evolution Beneath the Lastarria Volcanic
Complex (Northern Chile) - Evidence for Multiple Magma Storage Regions

The major element compositions of minerals and melt inclusions of 13 representative samples of the eruptive products were determined at the Institut for Mineralogy, Leibniz University Hannover, using a CAMECA SX-100 microprobe. The beam conditions for analyses of silicate minerals were 15 kV accelerating voltage, 10 nA beam current, and 10 s counting time. For oxides a beam current of 40 nA was applied. Melt inclusions were measured with a defocused beam of 5-10 µm and 15 kV accelerating voltage, 4 nA beam current with counting times of 4 s for Na and K to minimize alkali loss, and 8 s for the other elements.

4.2 Petrography and mineral chemistry

Blocks from the pyroclastic flow deposits are dark grey to brown in appearance, in part vesicular, and porphyritic (~20 vol.% phenocrysts). Lava- and dome flow samples, and the avalanche deposits are more dense, light to dark grey and have a higher amount of phenocrysts (up to ~35 vol.%). All samples have a porphyritic texture with plagioclase, clinopyroxene, orthopyroxene phenocrysts, and accessory Fe-Ti oxides as the main mineral phases. Some samples contain amphibole (sample# LAST-10-: 02, 03, 04, 11, 12, 16) and/or biotite (sample# LAST-10-: 01, 02, 03, 05, 07, 08, 09, 12, 14, 15, 16), which are smaller in size and less frequent. Other accessory minerals are apatite and zircon. Tab. II.2 gives an overview on the phases of each sample used for petrologic studies.

These phenocryst phases are described below and typical compositions of all major phases are reported in Tab. II.3. Representative microphotographs of mineral grains and rock textures from Lastarria are displayed in Fig. II.2 and analyses of all measured phases can be found in the Appendix.

Decoding Magma Plumbing and Geochemical Evolution Beneath the Lastarria Volcanic
Complex (Northern Chile) - Evidence for Multiple Magma Storage Regions

Table II.2: Mineral content in the samples used for thermobarometric analyzes.

Sample	Plag	Cpx	Opx	Amp	Bt	Mt	Ilm	MI in Plag
LAST-10-01	X	X	X	-	X	X	X	X
LAST-10-02	X	X	X	X	X	X	X	X
LAST-10-03	X	X	X	X	X	X	X	X
LAST-10-04	X	X	X	X	-	X	X	X
LAST-10-05	X	X	X	-	X	X	X	X
LAST-10-07	X	X	X	-	X	X	X	X
LAST-10-08	X	X	X	-	X	X	X	X
LAST-10-09	X	X	X	-	X	X	X	X
LAST-10-11	X	X	X	X	-	X	X	X
LAST-10-12	X	X	X	X	X	X	X	X
LAST-10-14	X	X	X	-	X	X	X	X
LAST-10-15	X	X	X	-	X	X	X	X
LAST-10-16	X	X	X	X	X	-	X	X
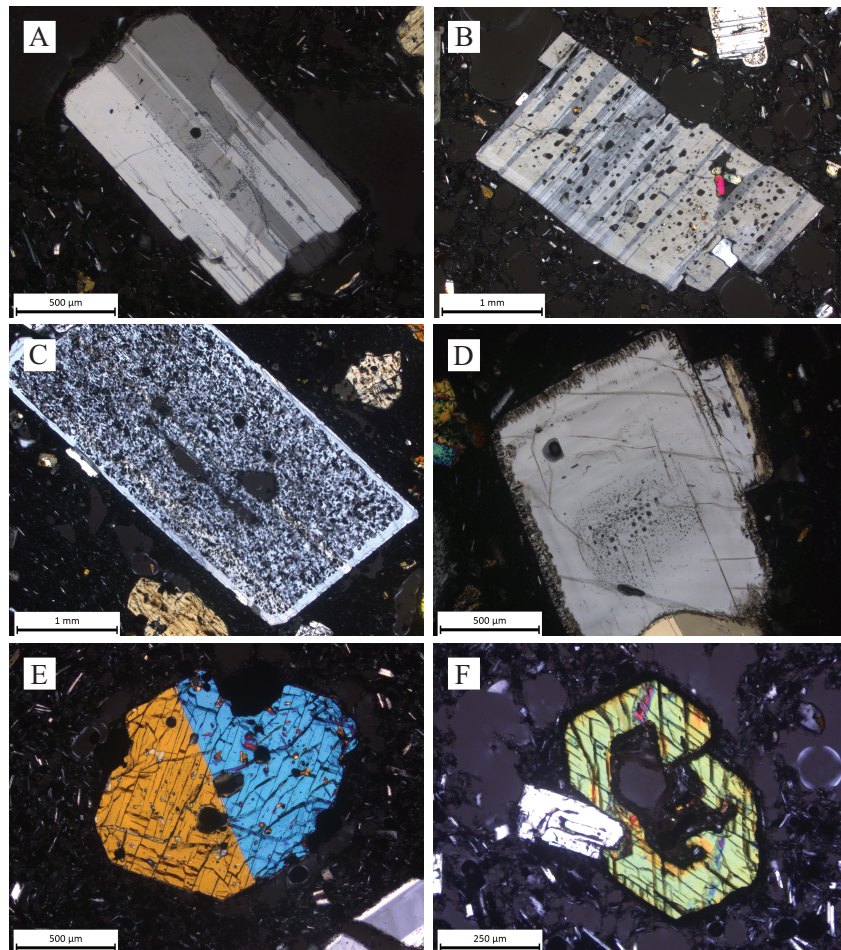
Figure II.2: Representative microphotographs under crossed polarized light of **A** euhedral plagioclase crystal with no signs of alteration. **B** Euhedral plagioclase with numerous melt inclusions and a Cpx inclusion. **C** Euhedral plagioclase crystal with a highly sieve-textured core and an overgrowth rim. **D** Subhedral plagioclase crystal with resorbed rim and a melt inclusion-rich core. **E** Euhedral, twinned, clinopyroxene crystal. **F** Euhedral amphibole crystal with a resorbed core and a dark overgrowth rim.

Dissertation of André Stechern

Decoding Magma Plumbing and Geochemical Evolution Beneath the Lastarria Volcanic
Complex (Northern Chile) - Evidence for Multiple Magma Storage Regions

The groundmass is microcrystalline and dominated by plagioclase microlites but contains also high proportions of tiny crystals of pyroxenes and Fe–Ti oxides. Micrometer-sized pools of quenched interstitial glass can be identified in the groundmass with the microprobe for some samples. Millimeter-sized clots of minerals occur in all thin sections.

Table II.3: Representative mineral compositions from Lastarria eruptives.

Mineral	Plag	Plag	Cpx	Cpx	Opx	Opx	Mt	Mt	Ilm	Ilm	Amp	Amp	Bio
Sample	LAST-10-16	LAST-10-08	LAST-10-14	LAST-10-02	LAST-10-14	LAST-10-12	LAST-10-11	LAST-10-09	LAST-10-11	LAST-10-09	LAST-10-02	LAST-10-16	LAST-10-14
Analysis #	Plag 4	Plag 6	Cpx 10	Cpx 8	Opx 6	Opx 4	Mt 10	Mt 2	Ilm 7	Ilm 6	Amph 5	Amph 2	Bio 5
Notes	Core, An$_{36}$	Core, An$_{53}$	Mg# 0.77	Mg# 0,83	Mg# 0.68	Mg# 0.80							
SiO$_2$	59.51	55.20	53.49	51.01	54.50	55.12	0.08	0.11	0.01	0.05	42.04	44.22	38.16
TiO$_2$	0.00	0.04	0.22	0.87	0.12	0.25	7.61	17.64	38.02	48.48	2.88	3.12	5.39
Al$_2$O$_3$	25.33	28.57	1.03	4.57	0.50	2.01	1.79	1.52	0.39	0.16	12.64	9.65	13.46
Fe$_2$O$_3$*	-	-	-	-	-	-	52.95	32.94	30.91	11.83	-	-	-
FeO*	-	-	-	-	-	-	36.18	45.08	29.47	38.18	-	-	-
FeO$_{tot}$	0.23	0.39	8.84	7.61	20.47	13.25	-	-	-	-	13.23	11.33	13.32
MnO	0.00	0.01	0.29	0.15	0.70	0.25	0.31	0.40	0.26	0.41	0.15	0.19	0.07
MgO	0.02	0.05	14.73	14.93	23.99	28.67	1.70	1.57	2.51	2.83	13.60	15.32	16.15
CaO	7.65	11.04	22.03	21.56	1.01	1.42	0.00	0.02	0.01	0.02	10.98	11.16	0.05
Na$_2$O	7.08	5.15	0.31	0.38	0.03	0.05	0.00	0.00	0.00	0.00	2.35	2.28	0.76
K$_2$O	0.80	0.47	0.00	0.00	0.00	0.00	0.23	0.00	0.00	0.00	0.72	0.66	8.93
Total	100.62	100.94	100.95	101.10	101.33	101.02	100.66	99.31	101.57	101.78	98.62	97.97	96.30

* Recalculation of Fe$_{tot}$ using the method of Charmichael (1967)

Dissertation of André Stechern

Decoding Magma Plumbing and Geochemical Evolution Beneath the Lastarria Volcanic Complex (Northern Chile) - Evidence for Multiple Magma Storage Regions

4.2.1 Plagioclase

Plagioclase (Plag) minerals are mainly euhedral to subhedral in shape, occasionally broken, and are the most common phenocrysts with ~12-18 vol.% in all samples. Sizes of the phenocrysts are typically 2.5 mm and can reach 6 mm. The compositional range of the plagioclase phenocrysts is small with anorthite (An) values between An_{38} to An_{53}. Mineral grains have only little zoning in the cores but reveal several different zonation patterns over the whole size of a plagioclase: normally zoned, reverse zoned, strongly oscillatory zoned, and combinations of all patterns. Four major types of plagioclase can be found and distinguished by their textures in all Lastarria rocks (see Fig. II.2A-D).

Type A plagioclases (Fig. II.2A) are usually euhedral and show little internal zoning. Parallel layers of small melt inclusions sometimes indicate the zoning. No signs of alteration are found in these plagioclases. Type B plagioclases (Fig. II.2B) are comparable to Type A but carry numerous large melt inclusions (up to 100 μm) which show no predominant orientation or alignment. Small pyroxene grains are enclosed in Type B. Type C plagioclases have cores with highly pronounced sieve-textures and rim-overgrowth with no signs of alteration (Fig. II.2C). Type D plagioclases have a Type A like center and are surrounded by highly resorbed outer rims (Fig. II.2D). The compositions of all plagioclases analyzed in this study can be found in the supplementary files and are illustrated in Fig. II.3A.

4.2.2 Pyroxenes

Both clino- and orthopyroxene (Cpx and Opx) can be found in all Lastarria samples even though Cpx is more frequent (2–5 vol.%). Occasionally overgrowth rims and partly resorbed interiors have been observed for pyroxene crystals. Melt inclusions in pyroxenes are less frequent compared to plagioclase.

Decoding Magma Plumbing and Geochemical Evolution Beneath the Lastarria Volcanic
Complex (Northern Chile) - Evidence for Multiple Magma Storage Regions
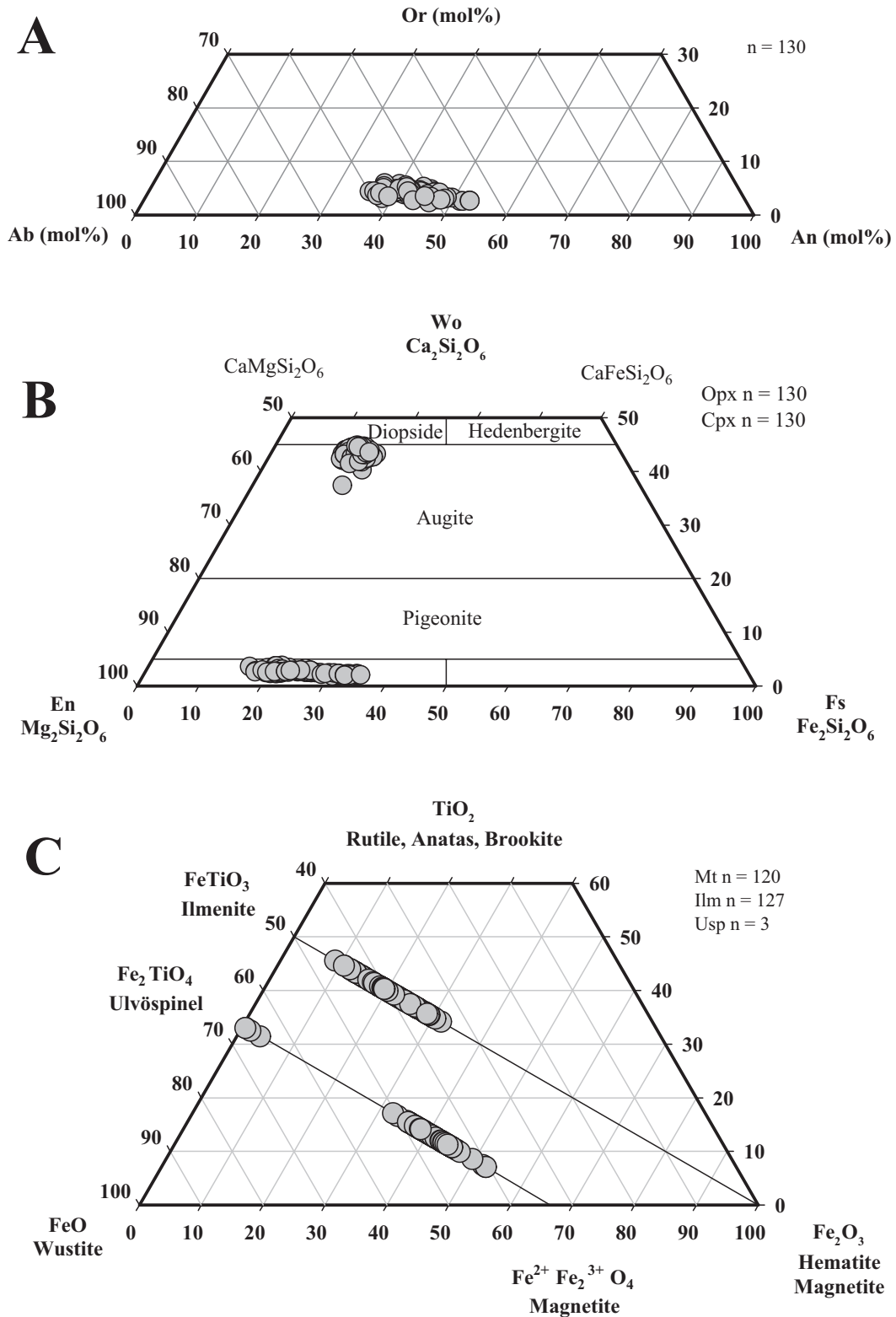
Figure II.3: A Composition of all analyzed plagioclase data points (n = 130). Plagioclase composition varies between An_{38} to An_{53}. **B** Composition of clinopyroxene (n = 130) and orthopyroxene crystals (n = 130). All clinopyroxene analyzes are in a narrow region in the augite fild. Orthopyroxenes are all ednstatites in compositions and are more heterogeneous. **C** Composition of magnetite (n = 120), ilmenite (n = 130) and Ulvöspilnel crystals (n = 3).

Dissertation of André Stechern

Decoding Magma Plumbing and Geochemical Evolution Beneath the Lastarria Volcanic
Complex (Northern Chile) - Evidence for Multiple Magma Storage Regions

Compositions of all analyzed pyroxenes in this study can be found in the supplementary files and are illustrated in Fig. II.3B.

Cpx phenocrysts are augites and show a narrow compositional range (En_{40-48}, Wo_{37-45}). Their Mg# ($100 \cdot Mg/(Mg+Fe)$ in mol%) is between 73 and 85. Mineral grains exhibit mostly euhedral shapes in all samples (see Fig. II.2E for a Cpx). Modest normal and reverse zoning in the Cpx can be observed in most analyzed samples. Two types of Cpx populations can be clearly distinguished in the eruptive rocks by their Al_2O_3 and TiO_2 contents (see Fig. II.4A). Type 1 Cpx phenocrysts contain ~1.0-1.5 wt.% Al_2O_3 and 0.2-0.4 wt.% TiO_2. Type 2 Cpx have higher Al_2O_3 concentrations (2.5-5.5 wt.%) and also TiO_2 values are higher, ranging from 0.6 to 1.2 wt.%. Some thin sections contain both Cpx types, some thin sections contain only Type 1 (Fig. II.4).

Opx are euhedral phenocrysts and are less common compared to Cpx (1-3 vol.%). Opx crystals have a wider range of compositions (En_{63-78}) with Mg# from 65 to 83, either without zoning or with normal or reverse zonation. As for Cpx, the Al_2O_3 content can be used to distinguish Lastarria's Opx into two groups. Type 1 Opx has ~0.5-1.5 wt.% Al_2O_3 at MgO values of ~22-26 wt.%. Type 2 Opx have higher concentrations of Al_2O_3 (1.5-4.1 wt.%) and higher MgO concentrations of 25-30 wt.% (see Fig. II.4B). The concentrations in total iron also differ between the two Opx groups (see Fig. II.4C). Type 1 Opx has high FeO^{tot} concentrations between 19 and 22 wt.%, whereas Type 2 Opx have considerably lower FeO^{tot} values of 11-18 wt.%. A significant difference in TiO_2 is not observable in Lastarria's Opx.

Naranjo (1992) already reported the two Opx and Cpx populations stating that the high and low Al_2O_3 Cpx and Opx can be found in all of his samples. However, our set of samples includes some specimen (mostly from the lower most lava-flows) where only Type 1 pyroxenes (low Al_2O_3) are present (samples# LAST-10-07, -14, -15). In all other samples low-Al pyroxenes are by fare less frequent compared to high-Al pyroxenes or were not even found.

Decoding Magma Plumbing and Geochemical Evolution Beneath the Lastarria Volcanic
Complex (Northern Chile) - Evidence for Multiple Magma Storage Regions
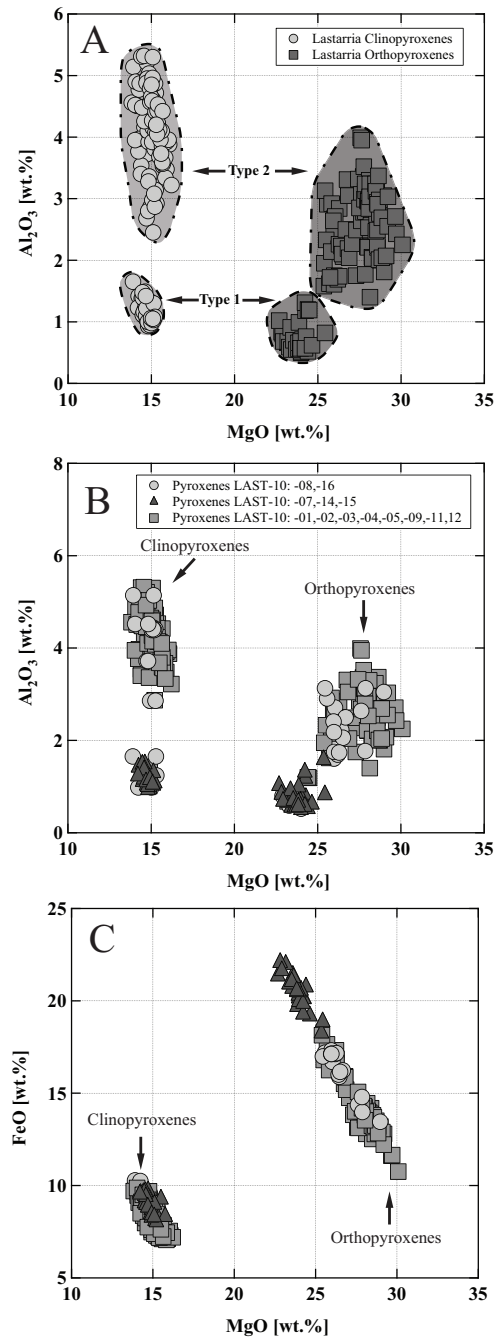
Figure II.4: A & B Al₂O₃ vs. MgO diagram to illustrate pyroxene populations and their compositional differences. **C** FeO vs. MgO diagram to illustrate variety of orthopyroxene compositions.

4.2.3 Amphibole

Amphibole (Amp) occurs, if present in the samples, as euhedral, tabular phenocrysts and micro-phenocrysts always surrounded by microcrystalline opacitic rims, with varying widths (Fig. II.3F). Some crystals are partly resorbed in the center. The majority of

Decoding Magma Plumbing and Geochemical Evolution Beneath the Lastarria Volcanic
Complex (Northern Chile) - Evidence for Multiple Magma Storage Regions

amphiboles are tschermakites or pargasites, after the nomenclature of Leake *et al.* (2004).

Only amphiboles from sample LAST-10-16 have more Si per formula unit and less Al_2O_3

(see Figs. II.5A and II.5C) and are therefore either tschermakitic hornblende or pargasitic

hornblende. To visualize differences in the amphibole compositions variations in cation site

occupation as well as the Al_2O_3 content are shown in Fig. II.5. Typical compositions are

given in Tab. II.3 and all analyzes of amphiboles from this study can be found in the

supplementary files.
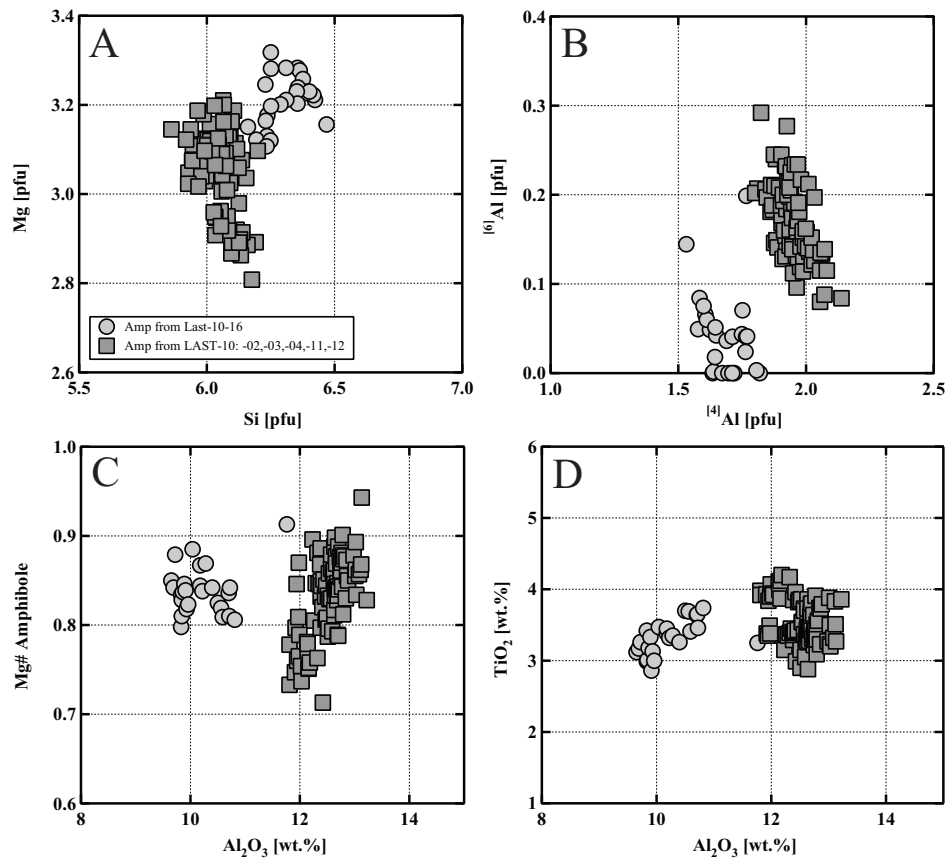
Figure II.5: A & B Variations in cation site occupation in Lastarria amphiboles reveals two distinct groups of amphibole compositions. **C & D** Variations in Al_2O_3 content between the two amphibole compositions.

4.2.4 Biotite

Biotite (Bt) is more frequent than amphibole in Lastarria rocks but is not found in all

samples. Biotite phenocrysts are tabular euhedral to subhedral, almost always rounded and

Dissertation of André Stechern

Decoding Magma Plumbing and Geochemical Evolution Beneath the Lastarria Volcanic
Complex (Northern Chile) - Evidence for Multiple Magma Storage Regions

have mostly reaction rims. Common inclusions in biotite are apatite and zircon. Biotite
phenocrysts have a uniform composition in all samples and have high TiO_2 concentrations of
4.9-5.9 wt.% and Mg# of 52-58 (see Appendix for analyses).

4.2.5 Fe-Ti Oxides

Fe-Ti Oxides are present in all Lascar rocks as micro-phenocrysts. Only sample LAST-
10-16 does not contain magnetite crystals. No exsolution lamellae were found in both types of
oxides and therefore are suitable for thermo- oxybarometry. Compositions of magnetites,
ilmenites, and also very rarely found ulvöspinel are displayed in a ternary diagram
(Fig. II.3C) and the full set of analyzes is provided in the Appendix.

4.3 Major and trace element geochemistry of whole-rock samples

4.3.1 Major elements

The new whole-rock analyses presented in this study extend the dataset of Lastarria
volcanic rocks published by Naranjo (1992). Lastarria eruptive rocks are classified as high-K
calc-alkaline, andesites and dacites (Fig. II.6) after the classification of Le Maitre (2002),
displaying typical compositions of volcanic arc samples from the Andean Central Volcanic
Zone (e.g. Mamani *et al.*, 2010). The compositions are in the same range than the previous
ones published by Naranjo (1992).

Decoding Magma Plumbing and Geochemical Evolution Beneath the Lastarria Volcanic
Complex (Northern Chile) - Evidence for Multiple Magma Storage Regions
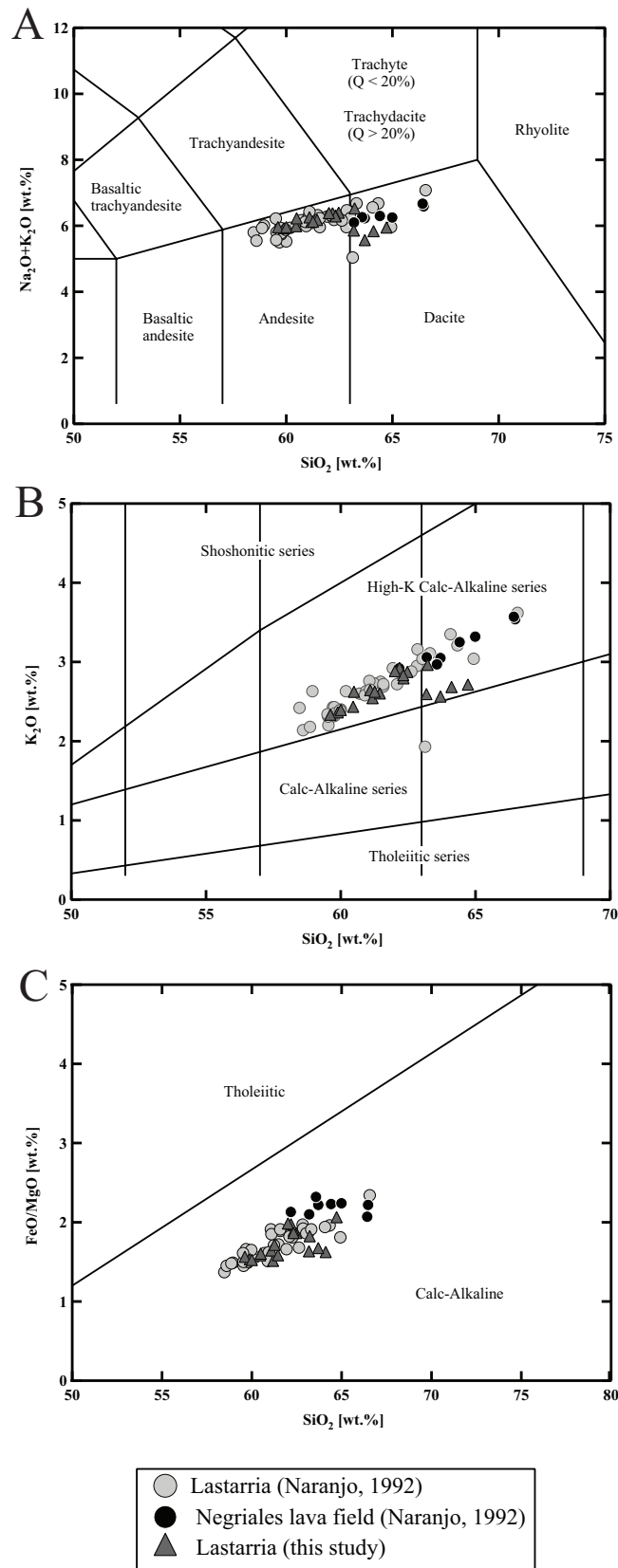
Figure II.6: Classification diagrams for eruptives from Lastarria and the associated Negriales lava field. **A** Total alkali versus silica (TAS) diagram (Le Bas *et al.*, 1986). **B** K_2O vs. SiO_2, showing that lavas belong to the high-K calc-alkaline type (Le Maitre *et al.*, 2002). **C** Plot of SiO_2 against FeO/MgO ratio. Subdivision lines are after Miyashiro (1974) and Arculus (2003).

Decoding Magma Plumbing and Geochemical Evolution Beneath the Lastarria Volcanic Complex (Northern Chile) - Evidence for Multiple Magma Storage Regions

Lastarria eruptive rocks span a relatively small continuous compositional trend between 58 wt.% and 67 wt.% SiO_2, 4.8 to 1.2 wt.% MgO, and 2.1 to 3.6 wt.% K_2O (normalized to an anhydrous basis) compared with other major volcanic centers in the CVZ like Lascar (Matthews *et al*., 1999) or Parinacota (Wörner *et al.*, 1988). However, in the MgO vs. SiO_2 and MgO vs. CaO variation diagrams, four ash samples (sample# LAST-10-10, -13, -17b, -17c) have slightly higher SiO_2 concentrations and lower CaO concentrations than the other rock samples, probably due to a decrease in the crystal content with distance from the vent during the deposition. Results of a series of ash-analyses (sample# Last-10-17A-D, Tab. II.1) from the same sample site, with different particle sizes, support this assumption. Analyses from fine grained material (<0.25 mm) show an increase of SiO_2 concentration of ~3 wt.% compared to analyses of particles <4mm.

In general, the observed major element trends as a function of MgO (Fig. II.7) are linear and show no change of slope or an inflection point. With a decrease in MgO there is a systematic increase in SiO_2 and K_2O coupled with a decrease in CaO, FeO, and TiO_2 (Fig. II.7). The trends for Na_2O and P_2O_5 vs. MgO show only a little decrease with decreasing MgO, whereas Al_2O_3 remains almost constant over the whole range of Lastarria compositions (except of the fine grained ash samples).

Decoding Magma Plumbing and Geochemical Evolution Beneath the Lastarria Volcanic
Complex (Northern Chile) - Evidence for Multiple Magma Storage Regions
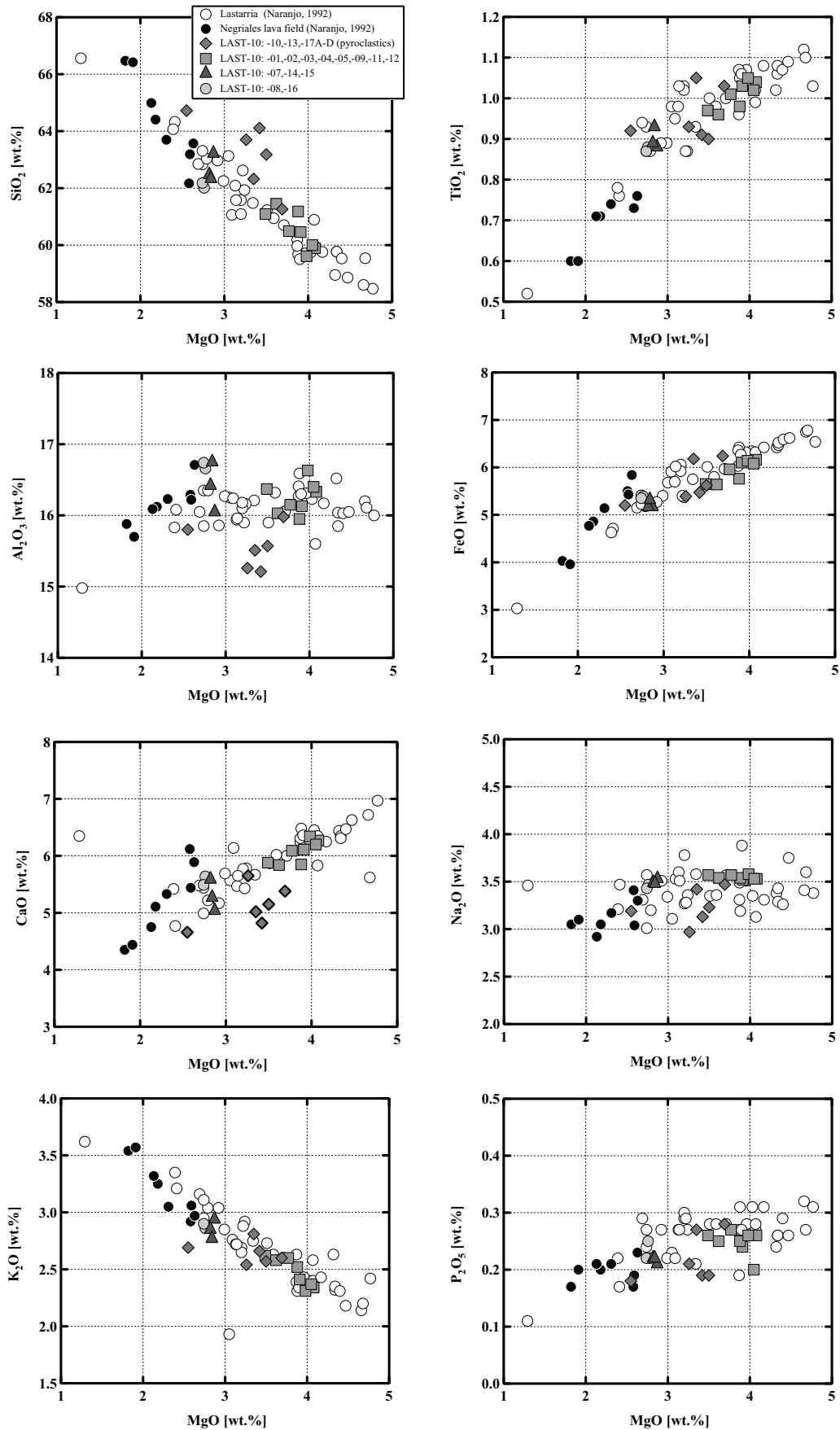
Figure II.7: Major element compositions of Lastarria and the associated Negriales lava field plotted against MgO.

Dissertation of André Stechern

Decoding Magma Plumbing and Geochemical Evolution Beneath the Lastarria Volcanic
Complex (Northern Chile) - Evidence for Multiple Magma Storage Regions

4.3.2 Trace elements

Trace element X-ray fluorescence (XRF) analyses for Lastarria samples are given in Tab. II.1 and are plotted against MgO as differentiation index for compatible and incompatible trace elements, respectively (Figs. II.8 and II.9). Compatible trace elements (Cr, Ni, Sr, V) display a negative, linear variation with decreasing MgO concentration. Analyzes from Negriales lavas (Naranjo, 1992) exhibit usually the lowest concentrations in compatible trace elements. Y exhibits no negative correlation with decreasing MgO and remains almost constant over the whole compositional range. Y concentrations in Negriales lavas are somewhat slightly higher compared with the Lastarria samples (Fig. II.8).

In the Lastarria rocks, Ni and Cr behavior is most likely controlled by magnetite and clinopyroxene crystallization, respectively (Nielsen *et al.*, 1994; Righter *et al.*, 2006). A strong V decrease in the samples denotes the permanent crystallization of magnetite (Luhr and Carmichael, 1980). The decrease of Sr is slightly less pronounced and usually explained by plagioclase fractionation since Sr is particularly compatible with plagioclases (e.g. Bédard, 2006).

In contrast, incompatible trace elements usually exhibit positive correlations with the index of differentiation. Concentrations of Rb, Th, and Pb increase by at least a factor of two (Tab. II.1, Fig. II.9), whereas the increase in Ba-content is less pronounced. Samples from the Negriales Lava Field have considerably lower Ba concentrations compared to Lastarria rocks. Nb shows no clear variation with MgO decrease. In general, andesite-dacite samples from Lastarria appear to inherit their geochemical characteristics with respect to many trace elements.

Decoding Magma Plumbing and Geochemical Evolution Beneath the Lastarria Volcanic
Complex (Northern Chile) - Evidence for Multiple Magma Storage Regions

Figure II.8: Compatible trace element compositions of Lastarria volcanic rocks and the associated Negriales lava field.

Decoding Magma Plumbing and Geochemical Evolution Beneath the Lastarria Volcanic
Complex (Northern Chile) - Evidence for Multiple Magma Storage Regions
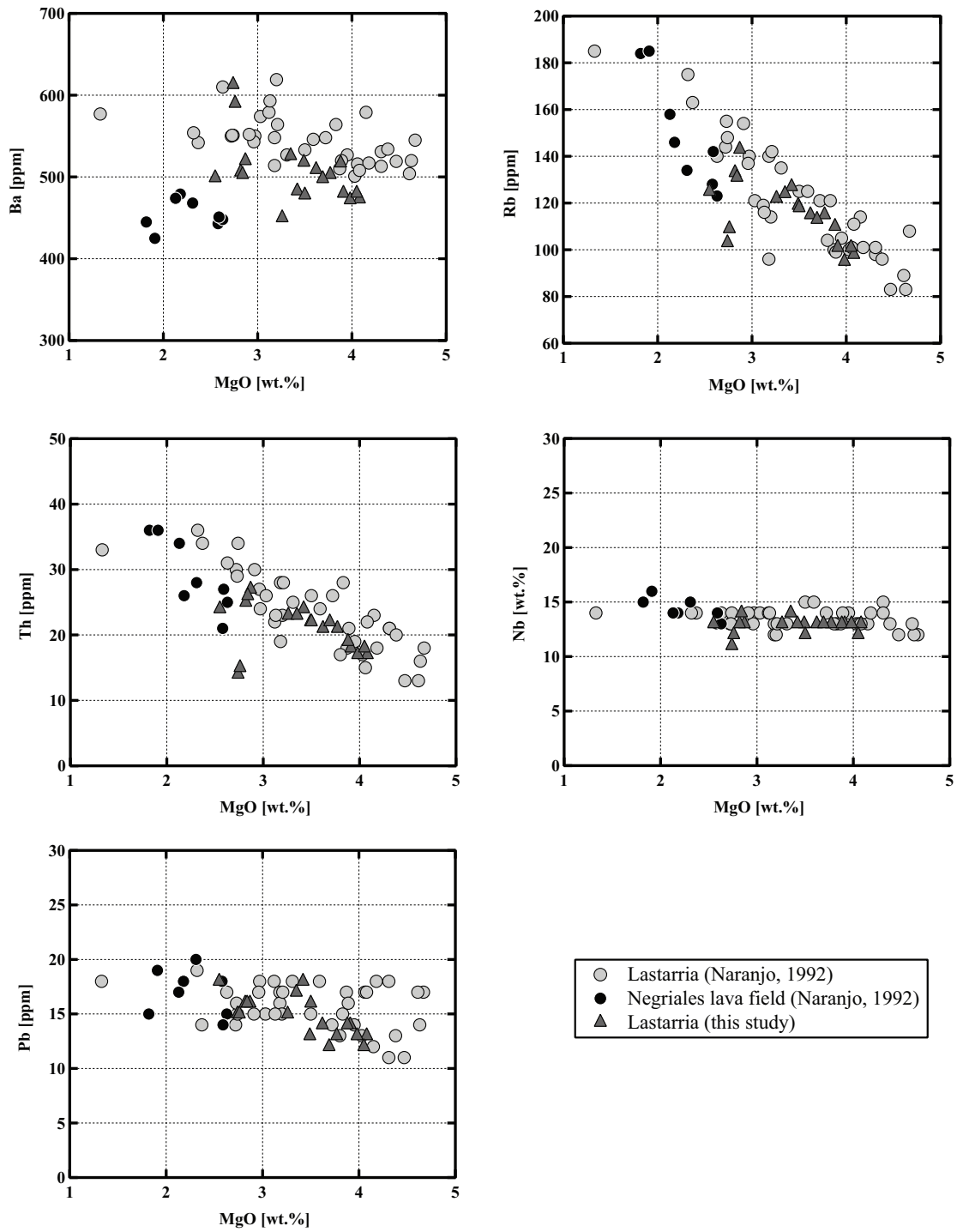
Figure II.9: Incompatible trace element compositions of Lastarria volcanic rocks and the associated Negriales lava field.

Dissertation of André Stechern

Decoding Magma Plumbing and Geochemical Evolution Beneath the Lastarria Volcanic
Complex (Northern Chile) - Evidence for Multiple Magma Storage Regions

5 MAGMA STORAGE CONDITIONS

The mineral assemblage of clino- and orthopyroxene, plagioclase, Fe-Ti oxides, and amphibole in Lastarria volcanic rocks permits calculations and detailed comparisons magma storage conditions (pressure, temperature, volatile concentration, and oxygen fugacity) using multiple mineral-mineral-pair and melt-mineral-pair equilibria. The dataset comprises 13 thin sections including 780 analyses of pyroxenes, 130 Plag-melt pairs, 120 Mt-Ilm pairs, and 115 single Amp analyses. The complete data set is provided in the Appendix. Average values for each geothermobarometer are given for each sample in Tabs. II.3-II.6. Fig. II.10 shows backscattered electron (BSE) images of typical mineral-mineral and melt-mineral pairs used in this study.
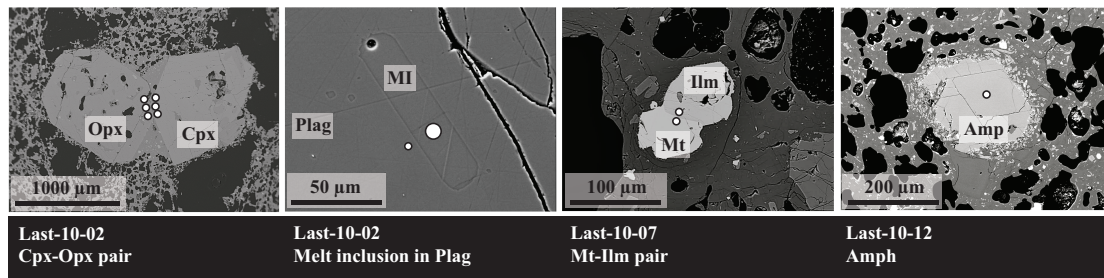
Figure II.10: Representative BSE images of mineral-mineral pairs (Cpx-Opx, Mt-Ilm), mineral-melt pairs (Plag-melt), and single amphiboles used for thermobarometry. White dots indicate EPMA spot analyses.

5.1 Determination of pre-eruptive pressures and depths of storage

We have determined the pressures of coexisting pairs of Cpx and Opx using the thermodynamic model described by Putirka (2008). Equations (38) and (39) were used to calculate P (Tab. II.4) either independently on temperature or including a T value, respectively. In the latter case, the applied temperatures for the calculations of P were obtained from the Mt-Ilm thermometer and the Plag-melt thermometer (see below). The pressure calculation is mainly based on [6]Al in Opx and the En, Fs, and Wo components in the pyroxenes. Only crystals free from overgrowth rims and resorbed interiors that were

Dissertation of André Stechern

Decoding Magma Plumbing and Geochemical Evolution Beneath the Lastarria Volcanic
Complex (Northern Chile) - Evidence for Multiple Magma Storage Regions

directly in contact with each other were taken into account for the calculations (see Fig. II.10 for an example). Single spot analyzes were performed as close as possible at the contact border between the two pyroxenes. The average of three single measurements on each pyroxene was combined to obtain one Cpx-Opx pair. We obtained in total 130 pairs (780 single measurements before calculating average values).

The compositions of co-existing Cpx and Opx phenocryst pairs from Lastarria samples reveal three groups of concordant pressures (see Fig. II.11).
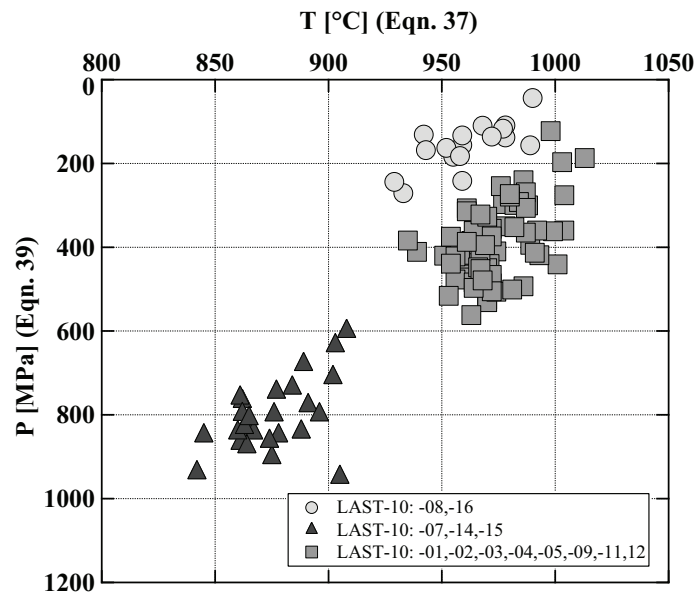
Figure II.11: Results of the two-pyroxene themobarometric calculations using Putirka (2008).

Group 1 includes the samples LAST-10-07, -14, -15 with calculated pressures ranging from 600 to 950 MPa. Pyroxenes from these three samples are exclusively Type 1 pyroxenes (see Fig. II.4). Low-Al concentrations have been observed for both Cpx and Opx.

Group 2 includes majority of samples (LAST-10-01, -02, -03, -04, -05, -09, -11, -12) and calculations imply intermediate pressures with the greater part of equilibrium pairs falling between 250 and 550 MPa. Mineral pairs in this group include both, high- and low-Al pyroxenes, which can be found together within the same sample (see Appendix tables for details). However, Type 1 pyroxenes (low-Al) are by far less frequent (<10% of all pyroxenes

Dissertation of André Stechern

Decoding Magma Plumbing and Geochemical Evolution Beneath the Lastarria Volcanic
Complex (Northern Chile) - Evidence for Multiple Magma Storage Regions

have low Al values). Pressure calculations of pairs including exclusively low-Al pyroxenes
were discarded from this group and are not displayed in the diagrams. However, calculated
pressures (and temperatures) are in the exact same range (600 to 950 MPa) as the observed
values from *Group 1*. The results for *P-T* calculation with respect to high and low-Al
pyroxene groups are displayed in the Appendix Fig. AF.II.1. Mixed pyroxene pairs with low
and high Al contents were not found.

Pressures calculated for the Last-10-08 and Last-10-16 samples are between 50 and
300 MPa, with the most values ranging between 100 and 200 MPa, and are considered as an
independent low pressure *Group 3*. These two samples also contain very few pairs of low-Al
pyroxenes giving again high *P-T* values as for *Group 1*. Average pressures for each sample
are given in Tab. II.4.

Table II.4: Results of the clinopyroxene-orthopyroxene thermobarometry after Putirka (2008) for Lastarria
eruptives. Calculated *P* and *T* values are given as average and standard deviation.

	Two pyroxene thermo- barometer, Putirka (2008)								Equilibrium (K$_D$ 1.09±0.14)
Sample	Eqn. 36		Eqn. 37		Eqn. 38		Eqn. 39		
	T [°C]	Stdev. [°C]	T [°C]	Stdev. [°C]	P [MPa]	Stdev. [MPa]	P [MPa]	Stdev. [MPa]	K$_D$(Fe-Mg)
LAST-10-01	996	±12	975	±15	368	62	427	44	0.99
LAST-10-02	992	±8	965	±12	318	44	421	30	1.03
LAST-10-03	993	±16	972	±15	376	86	336	59	1.07
LAST-10-04	1019	±47	1000	±54	498	138	294	116	1.07
LAST-10-05	999	±18	972	±14	488	163	395	105	1.13
LAST-10-07	892	±16	863	±14	1028	91	861	042	0.68
LAST-10-08	986	±7	971	±13	496	114	158	45	1.00
LAST-10-09	997	±9	978	±13	376	58	284	44	1.05
LAST-10-11	1002	±9	979	±12	375	48	476	64	1.02
LAST-10-12	996	±10	971	±13	339	58	398	43	1.02
LAST-10-14	903	±17	879	±19	1149	136	752	82	0.73
LAST-10-15	908	±16	882	±17	1238	261	807	86	0.70
LAST-10-16	976	±11	955	±19	519	63	159	65	0.96

Of crucial importance for obtaining accurate results from the applied Cpx-Opx
barometer is to test whether minerals represent coexisting equilibrium pairs. Mineral-mineral
equilibrium was examined by comparing Mg-Fe exchange between Cpx and Opx. The
exchange coefficient of Fe-Mg between Cpx-Opx [K$_D$ (Fe-Mg)$^{\text{Cpx-Opx}}$ = (X_{Fe}^{Cpx} / X_{Mg}^{Cpx}) / (X_{Fe}^{Opx}
/ X_{Mg}^{Opx})] is recommended by Putirka (2008) to test for equilibrium between pyroxene crystals.

Decoding Magma Plumbing and Geochemical Evolution Beneath the Lastarria Volcanic
Complex (Northern Chile) - Evidence for Multiple Magma Storage Regions

The author gives a value of 1.09 ±0.14 for K_D (Fe-Mg)$^{Cpx-Opx}$ for pyroxenes to be in equilibrium.

Majority of *Group 2 & 3* pyroxene pairs fulfill these equilibrium criteria recommended by Putirka (2008) while 15 pairs do not. However, the average K_D is 1.01 for *Group 2 & 3* pyroxene pairs.
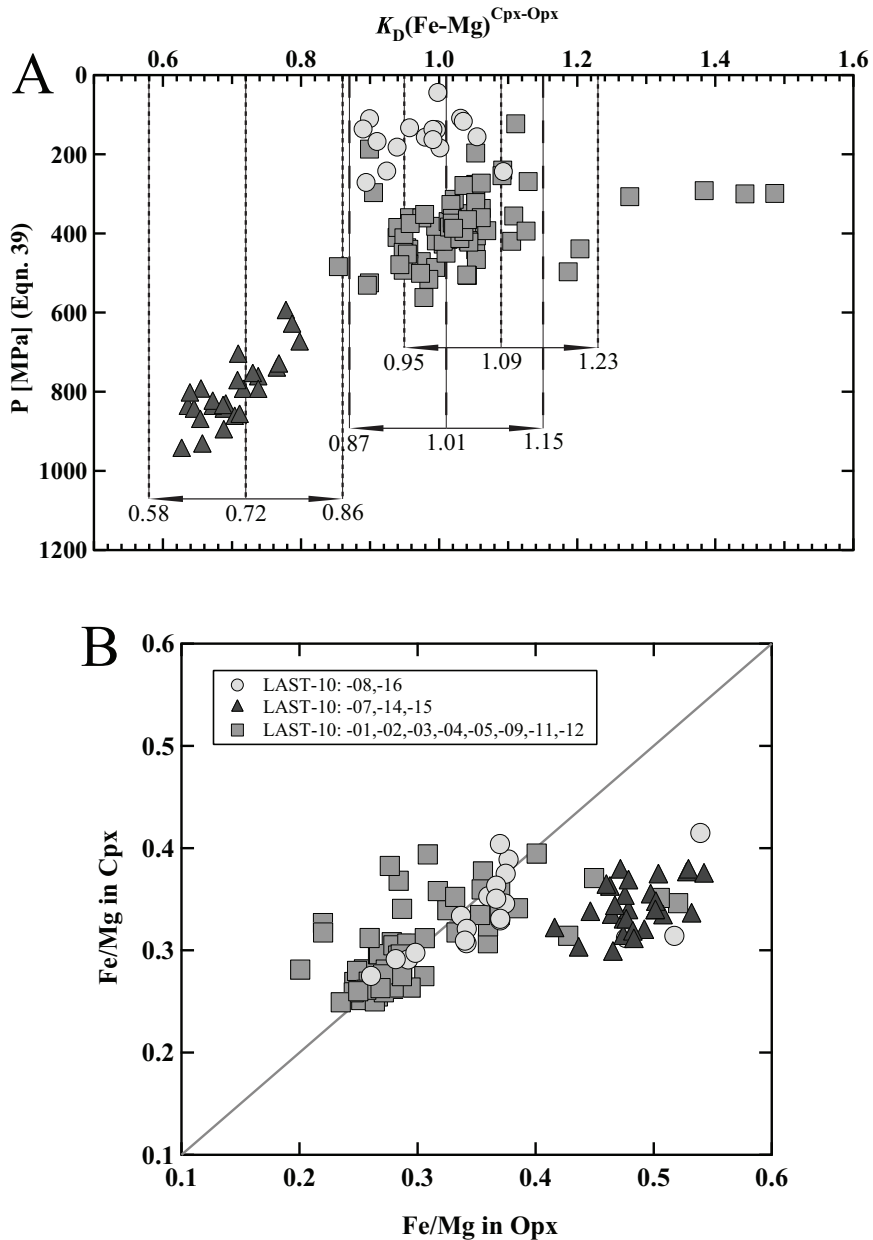
Figure II.12: A K_D(Fe-Mg) values between Cpx-Opx pairs from Lastarria eruptivs and from these pairs pressures. Pairs show an offset to lower K_D values observed in Lastarria calc-alkaline lavas relatively to the K_D range (1.09±0.14) given by Putirka (2008). Average K_D values for the three samples groups are added. **B** Fe/Mg Cpx vs. Fe/Mg Opx reveals higher Fe concentrations in Opx from samples LAST-10: -08, -14, -15.

If the proposed 1σ confidence interval (±0.14) is assumed for this value, all pyroxene pairs except seven fall within this range. Even though a few pyroxene pairs do not match the K_D criteria, the corresponding calculated pressure (and temperature) values do not differ from the mean values of these two groups. K_D values for the high pressure *Group 1* pyroxene pairs (and low-Al pyroxene pairs in general), however, differ significantly from the proposed equilibrium value (see Fig. II.12A) with an average value of 0.72.

In particular the Fe/Mg ratio for Opx is shifted towards higher Fe concentrations (see Fig. II.9B). The question whether the calculated pressure and temperature values for *Group 1* pyroxenes (and low-Al pyroxenes in general) are still realistic and applicable is discussed later. Average K_D values for each sample from the pyroxene pairs are given in Tab. II.4.

The variety of minerals found in Lastarria samples allows the application of different barometric methods. For comparison of the results from the Cpx-Opx barometer, amphibole (if present) was used to calculate pressures of crystallization by applying the models proposed by Ridolfi *et al.* (2010), hereafter called R2010, and Ridolfi and Renzulli (2012) hereafter called RR2012. The R2010 thermobarometer is well calibrated for magnesio- hornblende and tschermakites from calc-alkaline products of subduction-related systems and is, therefore best suited for Lastarria compositions. The pressure calculation is based on an empirical equation using the Al_T ($^{[4]}Al$ + $^{[6]}Al$; atoms per formula unit) in the amphiboles. The later extension RR2012 includes a wider range of whole-rock compositions and can be also applied on kaersutites and pargasites from alkaline rocks. Barometric equations in RR2012 were derived by multivariate least squares regressions of experimental amphiboles and the corresponding melt compositions from which they crystallized. The advantage of both models is that they do not require other minerals to be in equilibrium. Both barometers are later compared to prove their applicability on intermediate calc-alkaline rocks. Single point measurements for Amp analyses were taken in the unaltered centers of the crystals to avoid effects of re-equilibration of temperature-sensitive major and minor elements by diffusion.

105

Decoding Magma Plumbing and Geochemical Evolution Beneath the Lastarria Volcanic
Complex (Northern Chile) - Evidence for Multiple Magma Storage Regions
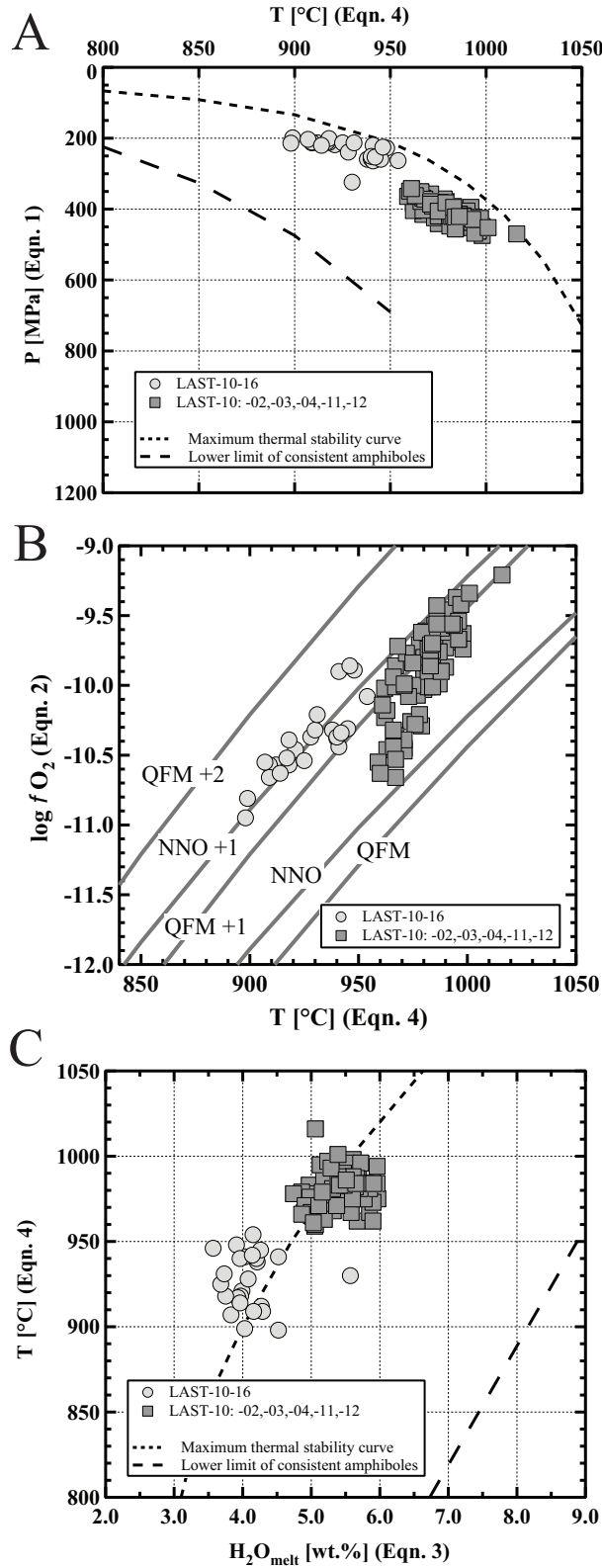
Figure II.13: Results of the single amphibole thermobarometry after Ridolfi *et al.* (2010). **A** Calculated pressure vs. temperature. **B** log oxygen fugacity vs. temperature (fO$_2$ buffer curves are drawn after Frost, 1991). **C** Temperature vs. water content in the melt.

Decoding Magma Plumbing and Geochemical Evolution Beneath the Lastarria Volcanic
Complex (Northern Chile) - Evidence for Multiple Magma Storage Regions

Table II.5: Results of the single amphibole thermobarometry after Ridolfi *et al.* (2010) for Lastarria eruptives. Calculated P, T, fO_2, and H_2O_{melt} values are given as average and standard deviation.

Sample	Single amphibole thermo- barometer, Ridolfi *et al.* (2010)							
	Eqn. 1		Eqn. 4		Eqn. 2		Eqn. 3	
	T [°C]	Stdev. [°C]	P [MPa]	Stdev. [MPa]	$fO2$ [bar]	Stdev. [bar]	H_2O_{melt} [wt.%]	Stdev. [wt.%]
LAST-10-01	*		*		*		*	
LAST-10-02	983	12	416	18	-9.8	0.2	5.5	0.2
LAST-10-03	978	7	392	25	-9.8	0.1	5.2	0.2
LAST-10-04	966	9	368	30	-10.5	0.3	5.1	0.4
LAST-10-05	*		*		*		*	
LAST-10-07	*		*		*		*	
LAST-10-08	*		*		*		*	
LAST-10-09	*		*		*		*	
LAST-10-11	983	7	419	21	-9.7	0.1	5.5	0.2
LAST-10-12	985	11	420	31	-9.7	0.2	5.5	0.3
LAST-10-14	*		*		*		*	
LAST-10-15	*		*		*		*	
LAST-10-16	924	16	230	29	-10.5	0.3	4.1	0.4

* No Amp present in sample

Pressure and temperature results of the two models are shown in Figs. II.13 and II.14 and average values for each Amp-bearing sample are given in Tabs II.5 and II.6, respectively. Pressure-temperature values gained from R2010 show that all measured amphiboles are in the expected thermal stability field of Amp (Fig. II.14). As for the Cpx-Opx barometer, two pressure populations from the Amp compositions can be clearly distinguished. *Group 2* samples, which show intermediate pressures from the Cpx-Opx pairs, give values in the range between 350 and 450 MPa if calculated with the R2010 formulation for pressure calculation. A low pressure *Group 3* is also confirmed from Amp compositions. Values gained from the Amp phenocrysts in sample LAST-10-16 are in a very narrow range of 200 to 250 MPa and overlap therefore directly with the results from the two pyroxene barometer. If the RR2012 model is applied on the same Amp compositions, comparable observations in terms of pressure can be made (see Fig. II.14).

Decoding Magma Plumbing and Geochemical Evolution Beneath the Lastarria Volcanic
Complex (Northern Chile) - Evidence for Multiple Magma Storage Regions
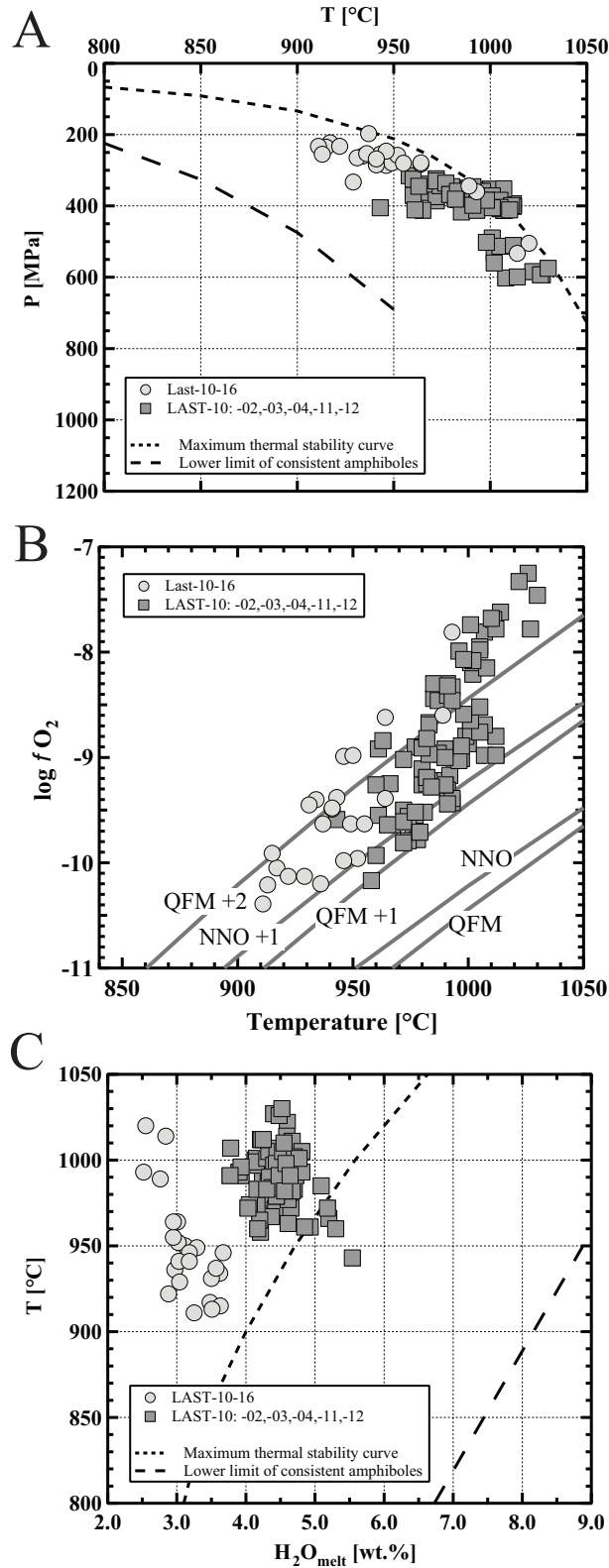
Figure II.14: Results of the single amphibole thermobarometry after Ridolfi & Renzulli (2012). **A** Calculated pressure vs. temperature. **B** log oxygen fugacity vs. temperature (fO_2 buffer curves are drawn after Frost, 1991). **C** Temperature vs. water content in the melt.

Decoding Magma Plumbing and Geochemical Evolution Beneath the Lastarria Volcanic
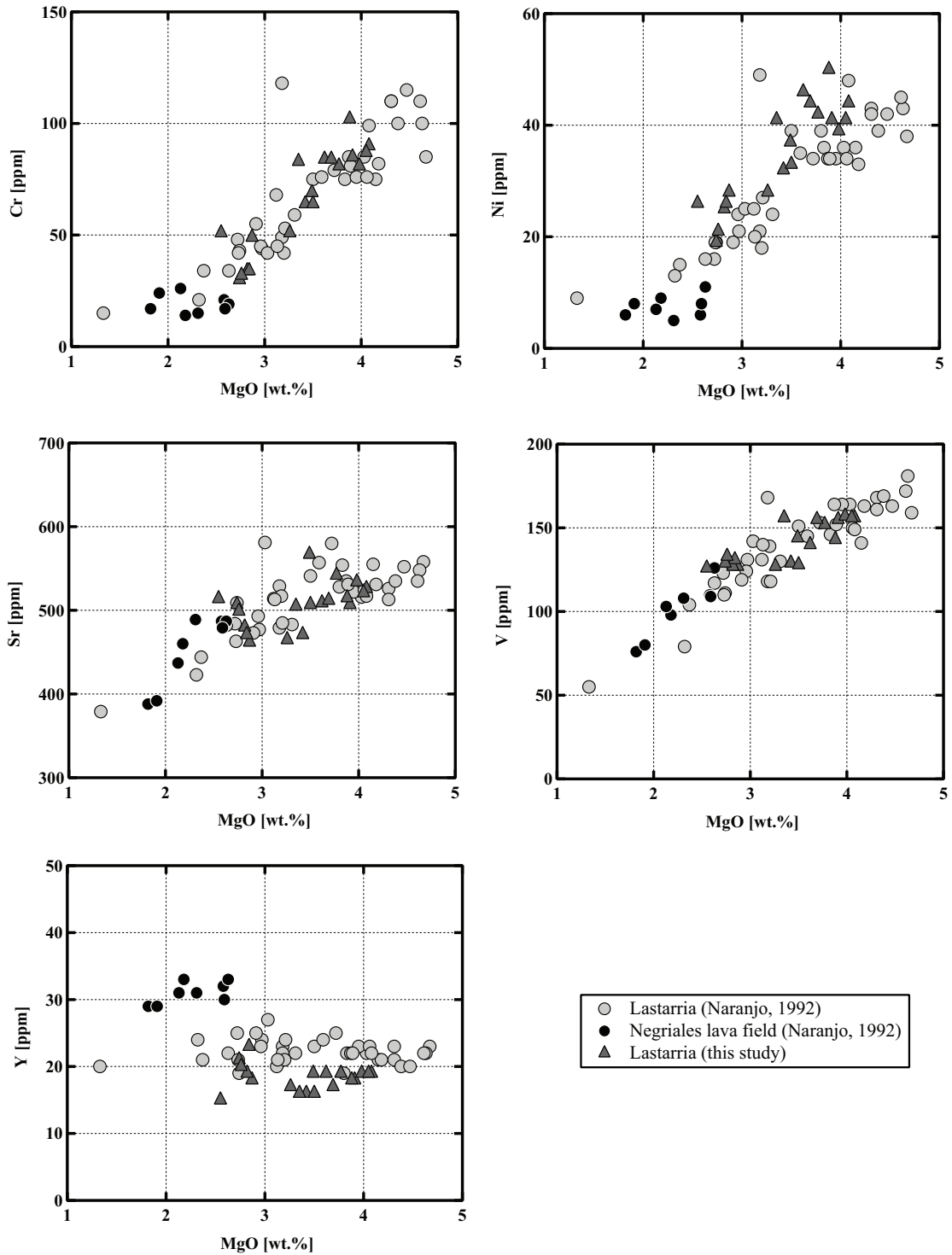Complex (Northern Chile) - Evidence for Multiple Magma Storage Regions

Table II.6: Results of the single amphibole thermobarometry after Ridolfi & Renzulli (2012) for Lastarria eruptives. Calculated P, T, fO_2, and H_2O_{melt} values are given as average and standard deviation.

Sample	Single amphibole thermo- barometer, Ridolfi & Renzulli (2012)							
	T [°C]	Stdev. [°C]	P [MPa]	Stdev. [MPa]	$fO2$ [bar]	Stdev. [bar]	H_2O_{melt} [wt.%]	Stdev. [wt.%]
LAST-10-01	*		*		*		*	
LAST-10-02	984	15	363	17	-9.3	0.3	4.5	0.3
LAST-10-03	992	9	399	62	-8.4	0.3	4.5	0.2
LAST-10-04	981	26	363	26	-9.3	0.4	4.3	0.4
LAST-10-05	*		*		*		*	
LAST-10-07	*		*		*		*	
LAST-10-08	*		*		*		*	
LAST-10-09	*		*		*		*	
LAST-10-11	991	12	394	67	-9.0	0.4	4.5	0.1
LAST-10-12	998	18	434	83	-8.3	0.6	4.6	0.2
LAST-10-14	*		*		*		*	
LAST-10-15	*		*		*		*	
LAST-10-16	948	29	289	78	-9.3	1.0	3.1	0.3

* No Amph present in sample

Group 2 samples do not significantly differ in terms of pressure comparing the R2010 and RR2012 models. Calculated pressures by RR2012 are slightly lower with values between 300 and 400 MPa. Within the error of the method, no deviation of pressure estimates can be observed for *Group 3* Amp compositions comparing R2010 and RR2012. However, a few Amp composition from both groups lead to pressure values between 500 and 600 MPa using the RR2012 model, which was not observed with the earlier version of the barometer (see Figs. II.13 and II.14 for comparison).

An additional geobarometer (and geothermometer) that could theoretically be used is the Amp-Plag equilibria model of Holland and Blundy (1994). To determine the pressures and also temperatures using this geothermobarometer, it is necessary to have Plag crystals in equilibrium with Amp. This is difficult to evaluate from petrographic criteria, since no unaltered Amp crystals are in direct contact to Plag. Also no inclusions of Amp in Plag or vise versa were found in this set of samples. Due to these petrographic reasons the Holland and Blundy (1994) model was discarded.

After calculating pressures with the individual geobarometers, the gained P values can be translated into depths, using a density model of the crust in northern Chile. Lucassen *et al.* (2001) give rock densities for the Central Andes between 21° and 27° S of 2.68 and

Dissertation of André Stechern

Decoding Magma Plumbing and Geochemical Evolution Beneath the Lastarria Volcanic
Complex (Northern Chile) - Evidence for Multiple Magma Storage Regions

2.89 g/cm^3 beneath the volcanic arc. Given the uncertainties, we use a mean density of 2.8 g/cm^3 for the conversion of pressure estimates to depths.

Group 1 samples correspond to a depth of ~20-30 km in the continental crust. The intermediate *Group 2* samples correlate to depths between 10 to 18 km. *Group 3* samples with the lowest calculated pressures have a pre-eruptive depth of storage between 6.5 and 8 km.

5.2 Magma Temperatures

All applied mineral-mineral or mineral-melt equilibrium models and also the empirical calibration of the amphibole compositions of R2010 and RR2012 are geothermometers and were applied to gain information about crystallization temperatures of Lastarria rocks. In total five different thermometers were tested and compared for samples containing all major phases (including Amp). Therefore values for the pre-eruptive temperatures of Lastarria samples can be bracketed accurately.

The same Cpx-Opx pairs as mentioned in the paragraph above were used to calculate pre-eruptive temperatures using Eqs. (36) and (37) described by Putirka (2008). The thermometer is based on the partitioning of enstatite and ferrosilite between Cpx and Opx. Equation (37) is expected to provide better precision, since the calibration data base is restricted to include only Mg-rich systems, in this case defined as those experimental Cpx-Opx pairs with Mg# Cpx >75. Mg# from Lastarria Cpx are between 73 and 85 and therefore Eq. (37) was considered as the better suited for calculating temperatures from pyroxene compositions.

In addition, the proposed Plag-melt thermometer by Putirka (2005 and 2008) was also used to evaluate pre-eruptive T in all selected thin sections from Lastarria products since Plag is by far the most abundant mineral. The proposed temperature equation (Eqn. (23) in Putirka, 2008) is based on regression analysis of partial melting experiments where Plag formed at fixed P-T conditions from varying melt compositions. Pressure values obtained from the two-

Dissertation of André Stechern

Decoding Magma Plumbing and Geochemical Evolution Beneath the Lastarria Volcanic
Complex (Northern Chile) - Evidence for Multiple Magma Storage Regions

pyroxene barometer were taken as input parameters for the calculations. Equilibrium was tested by comparing Ab-An exchange (see Putirka, 2008). However, the equilibrium constant is not precisely constant, but sensitive to T. At T <1050°C, the value should be about 0.1 ±0.05 (Putrika (2008). Only Type A and B Plag crystals (see Fig. II.2) were chosen for analyses. On each Plag crystal several mineral-melt pairs were analyzed (if possible) to check for compositional zoning of the crystal and a change in melt compositions in the inclusions. Spot-analyzes on Plag crystals were taken as close as possible to the corresponding melt inclusions. Melt analyzes were taken at the center of a melt inclusion. All analyzed melt inclusions were at least ~30 μm in size and always free of secondary crystals. Fig. II.10 shows a typical inclusion in Plag.

The empirical calibration of the Amp compositions of R2010 and RR2012 were both applied to calculate T from Amp-bearing samples in this study. The equation in R2010 for calc-alkaline systems is based on a dependence of Si and [4]Al in Amp with T. In addition, other major cations in Amp are also included in the equation leading to R^2 vales of 0.84. Errors of the method are given by the authors to be in the rage of ±22 to ±57°C. The calibration of RR212 is based on regression analysis of temperature vs. amphibole compositions including the experimental pressure as an independent variable leading to R^2 values of 0.92. The authors argue that temperature mainly rules the variation of Si, Ti, Al, Fe and Mg in Amp, rather than Ca, Na, K, or the pressure at which the crystallization takes place.

The last geothermometer used in this study is the magnetite-ilmenite geothermometer/oxygen barometer by Andersen and Lindsley (1985 and 1988), which has been translated into the ILMAT worksheet provided by Lepage (2003). The temperature (and oxygen-fugacity) sensitive exchange reactions of $Fe^{2+}+Ti \rightarrow 2Fe^{3+}$ between magnetite and ilmenite are commonly used for geothermometer formulations and the determination of equilibrium temperature. Equilibrium between coexisting magnetite and ilmenite crystals was tested using partitioning of Mg and Mn between the oxide pairs, following the method of

Dissertation of André Stechern

Decoding Magma Plumbing and Geochemical Evolution Beneath the Lastarria Volcanic
Complex (Northern Chile) - Evidence for Multiple Magma Storage Regions

Bacon and Hirschmann (1988). As for the Cpx-Opx pairs, only crystals directly in contact

with each other were taken into account for the calculations. Also BSE images of the oxide

phases were carefully checked for the absence of exsolution lamellae. A typical oxide pair is

shown in Fig. II.10.

Average values for each sample and all geothermometers are listed in in Tabs. II.4-II.8.

Results are displayed in Fig. II.15 and grouped together following the pressure calculations

results.

Table II.7: Results of the plagioclase-melt thermometer and hygrometer after Putirka (2008) for Lastarria
eruptives. Calculated T and H_2O_{melt} values are given as average and standard deviation.

	Plagioclase-melt thermometer, Putirka (2005, 2008)				
Sample	Eqn. 23		Eqn. 25b		Equilibrium (K$_D$ 0.10±0.05)
	T [°C]	Stdev. [°C]	H$_2$O$_{melt}$ [wt.%]	Stdev. [wt.%]	K$_D$(Ab-An)
LAST-10-01	990	±10	1.9	±0.4	0.05
LAST-10-02	990	±16	2.2	±0.6	0.05
LAST-10-03	978	±8	1.7	±0.6	0.04
LAST-10-04	958	±4	1.3	±0.4	0.03
LAST-10-05	992	±15	2.1	±1.2	0.07
LAST-10-07	951	±6	1.9	±0.5	0.03
LAST-10-08	927	±18	1.0	±0.3	0.02
LAST-10-09	971	±16	1.2	±0.3	0.05
LAST-10-11	1006	±3	2.4	±0.4	0.06
LAST-10-12	984	±18	1.6	±0.7	0.05
LAST-10-14	931	±7	1.2	±1.0	0.02
LAST-10-15	930	±7	1.2	±0.7	0.03
LAST-10-16	925	±11	2.4	±0.4	0.02

The gained temperature intervals for each sample correlate directly with observations

made by the barometric calculations independent of the applied thermometer. The three

groups with individual pressure regimes (*Group 1* - high *P*, *Group 2* - intermediate *P*, and

Group 3 - low *P*) reveal also separation of the calculated temperatures.

Group 1 samples (high *P*) determine the lowest temperature intervals in this data set,

ranging from 840 to 960°C. Only Plag-melt, Mt-Ilm, and two-pyroxene thermometry (with

and without a value for *P*) were applied on these samples since no amphibole is present in this

Dissertation of André Stechern

Decoding Magma Plumbing and Geochemical Evolution Beneath the Lastarria Volcanic
Complex (Northern Chile) - Evidence for Multiple Magma Storage Regions

particular group. In two of the three samples belonging to this group the calculated

temperature intervals overlap fairly well (see Fig. II.15 samples LAST-10-14 and -15) with a

temperature median of ~910°C.
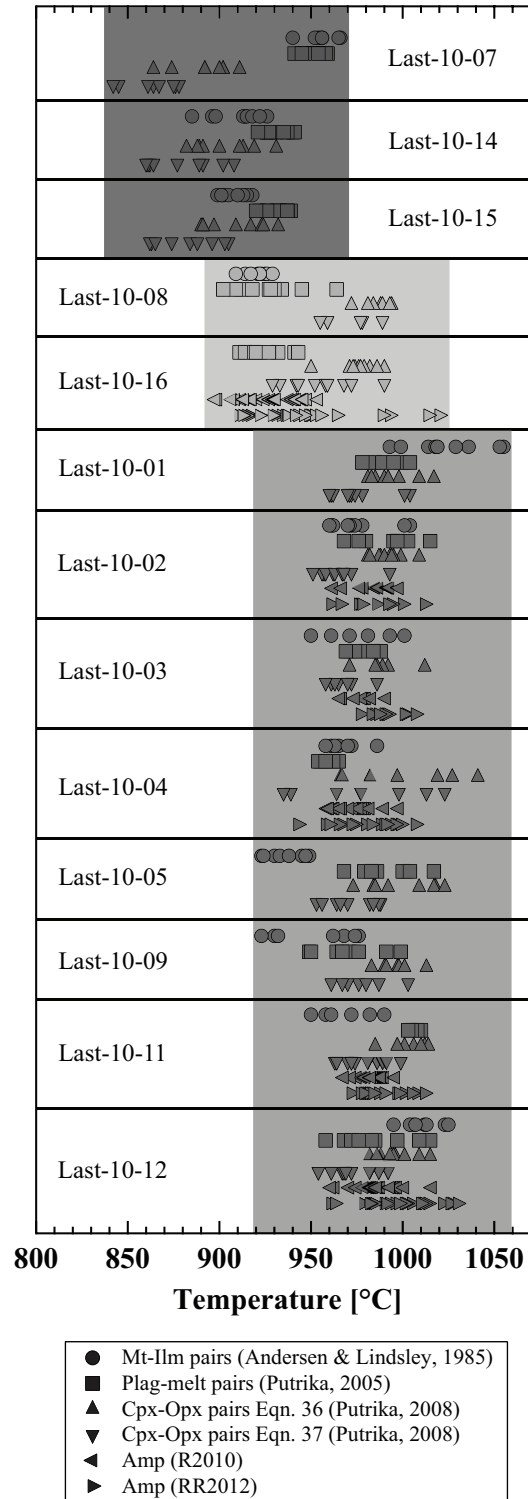
Figure II.15: Combined results of all applied geothermometers. Boxes are drawn to visualize distinct groups of samples. Grey-scales are the same as used for the results in the other barometric diagrams.

Dissertation of André Stechern

Decoding Magma Plumbing and Geochemical Evolution Beneath the Lastarria Volcanic
Complex (Northern Chile) - Evidence for Multiple Magma Storage Regions

However, for sample LAST-10-07 the temperature calculation of the two-pyroxene thermometers give ~50°C lower values. The fact that the samples with the highest calculated pressures reveal the lowest temperatures is discussed later on.

Calculations of temperatures for the *Group 2* samples (intermediate *P*) result in the highest temperature interval for all Lastarria rocks with values between 920 and 1050°C. In most of the samples all six geothermometers were applied and compared (see Fig. II.15). Average temperature in this group is ~990°C. All applied geothermometers give overlapping values for the eight individual samples of this group.

Group 3 samples (low *P*) have intermediate temperatures. The range in this group (samples LAST-10-08 and -16) is between 900 and 1020°C. Average temperature in this group is ~950°C.

5.3 Oxygen fugacity

Pre-eruptive oxygen fugacity was determined using the Andersen & Lindsley (1985, 1988) magnetite-ilmenite oxygen barometer in the same way as mentioned above for the temperature determination. Redox equilibrium defined by the reaction $4Fe_3O_4 + O_2 = 6Fe_2O_3$ (Andersen & Lindsley, 1988) is used for the oxygen barometer formulations and estimation of log fO$_2$. Oxide formulas were calculated after Stormer (1983). Magnetite-ilmenite pairs were tested for chemical equilibrium using Mg-Mn atomic ratios in both oxide phases (Bacon & Hirshmann, 1988). The same Mt-Ilm pairs as mentioned in the paragraph above were used to calculate pre-eruptive log fO$_2$.

Oxygen fugacities were also calculated following the equations of R2010 and RR2012 using the Amp compositions. The empirical formulation for log fO$_2$ calculation by R2010 is mainly based on a correlation of Mg concentration in Amp plus contributions of other major cations with oxygen fugacity. The derived Eqn. (3) from RR2012 depends also only on the amphibole composition and shows high R^2 values of 0.96.

Decoding Magma Plumbing and Geochemical Evolution Beneath the Lastarria Volcanic Complex (Northern Chile) - Evidence for Multiple Magma Storage Regions

Results from the Fe-Ti oxybarometer are shown in Fig. II.16. The majority of Mt-Ilm pairs from Lastarria samples record log redox conditions between the nickel-nickel oxide oxygen buffer (NNO) and NNO+1 in temperature range between 890 and 1040°C.
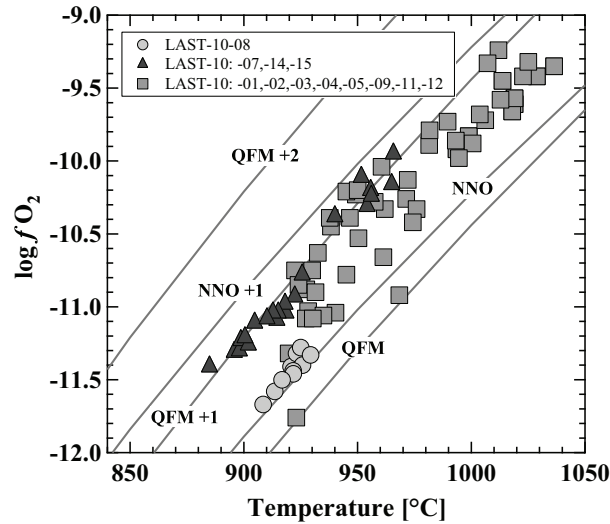
Figure II.16: Results of the magnetite-ilmenite oxygen barometry and thermometry after Andersen and Lindsley (1985, 1988). fO_2 buffer curves are drawn after Frost (1991).

Group 1 samples (high *P*) reveal a constant log fO_2 of NNO+0.7, which is equal to QFM+1 (QFM corresponds to the quartz-fayalite-magnetite buffer) in this temperature range. *Group 2* samples (intermediate *P*) exhibit the highest variability in terms of log fO_2 (and *T*) between NNO and NNO+1. Correlation of certain samples with a specific fO_2 range was not observed. Even in one sample results from Mt-Ilm pairs vary by the given log fO_2 range. In contrast Mt-Ilm pairs from *Group 3* (low *P*) give a very narrow range of log fO_2 and also *T*. However, only one sample Last-10-08 belongs to this group. Results from the Mt-Ilm oxythermobarometer are in a reliable range of log fO_2. Several studies have shown that the accuracy of log fO_2 estimated by application of current formulations starts to decreases above NNO+1 (Rutherford and Devine, 1996; Evans and Scaillet, 1997; Scaillet and Evans, 1999). However, Amp compositions additionally give the possibility to calculate log fO_2 by applying the formulations of R2010 and RR2012. Results can be directly compared to the ones from Mt-Ilm pairs. Amp compositions from *Group 2* samples (intermediate *P*) give almost the

Dissertation of André Stechern

Decoding Magma Plumbing and Geochemical Evolution Beneath the Lastarria Volcanic
Complex (Northern Chile) - Evidence for Multiple Magma Storage Regions

same log fO_2 and T values of NNO to NNO+1 between 960 and 1020°C as the Fe-Ti oxides
(compare Figs. II.13B and II.16). Results from Amp compositions of *Group 3* (low P) give
log fO_2 values, which are one log unit higher as the ones for the same group gained by the Fe-
Ti oxides (compare Figs. II.13B and II.16). However, considering the error of the calculations
overall results are still in the NNO to NNO+1 range.

Results from RR2012 calculation on Amp compositions reveal slightly different
results. All gained oxygen fugacity values are one log unit higher compared to both previous
calculation schemes. Results for both Amp bearing groups are between NNO+1 and NNO+2.
Differences in T between the two groups remain constant (compare Figs. II.14A, II.14B, and
II.16).

5.4 Water content in the melt

Pre-eruptive water contents for Lastarria andesitic magmas were estimated using the
Plag-melt hygrometer of Putirka (2008) where the author argues that the plagioclase-liquid
equilibrium has the potential to be useful as a hygrometer. However the formulation of the
water content in the melt (H_2O_{melt}) is a rearrangement of the equation for the temperature
estimation and therefore leaves the calculated water contents highly sensitive to T. A change
of ±38°C can cause an error of ±1.0 wt.% H_2O_{melt}. Therefore, results should be interpreted
with caution.

Also the R2010 and RR2012 models provide formulations to estimate the water
contents of calc-alkaline magmas that contain Amp. The empirical formulation in R2010 is
based mainly on [6]Al in Amp from experiments on hydrous melts. The error given by the
authors is ~0.41wt.% H_2O_{melt}, which in the range of the "by difference" method commonly
used to determine hydrous glasses in experiential studies. The RR2012 H_2O_{melt} equation is
again derived by multivariate least-squares regressions of experimental Amp. Equation (4)
from RR2012 shows that the volatile content in alkaline and calc-alkaline magmas can be

Dissertation of André Stechern

Decoding Magma Plumbing and Geochemical Evolution Beneath the Lastarria Volcanic
Complex (Northern Chile) - Evidence for Multiple Magma Storage Regions

related to the Amp compositions crystallized in these magmas. The uncertainty of the method

given by the authors is ±0.78 wt.% H_2O_{melt}

H$_2$O$_{melt}$ concentrations calculated by the Plag-melt hygrometer are between 1.0 and

2.4 wt.% (see Tab. II.7). No correlation between the H_2O_{melt} and certain group of samples or a

specific mineralogical, or chemical composition was observed. H_2O_{melt} values from Amp

compositions give generally higher results compared with the Plag-melt hygrometer. Values

are between ~3.5 and 6.0 wt.% H_2O_{melt} using Eqn. (3) from R2010 for the calculations. Most

of the amphiboles are in the thermal stability field given by R2010 regarding H_2O_{melt} and T

(see Fig. II.13C). However, analyses from tschermakitic hornblende and pargasitic

hornblende of sample LAST-10-16 (low T) are outside the thermal stability field, but still

close to the stability curve. If the error of the method is taken into account, all gained H_2O_{melt}

values after R2010 fall within a reasonable range of ~4.0 to ~6.0 wt.% H_2O_{melt}. If water

contents in the melt are calculated using the later RR2012 model for Amp H_2O_{melt}

concentrations are somewhat lower with values between ~2.5 and 5.5 wt.%. Due to a shift

towards higher temperatures and also lower H_2O_{melt} values obtained using this model, almost

none of the amphiboles fall into the stability field, with respect to H_2O_{melt} and T

(see Fig. II.14C). The general differences between *Group 2* and *Group 3* samples as

mentioned above for the R2010 method are still evident. It has to be emphasized that H_2O_{melt}

calculations using RR2012 require an input parameter for P. Depending on the equation

applied for P determination (Eqns. (1a)-(1e) in RR2012) the corresponding obtained P value

was used for calculation H_2O_{melt}. This procedure did not necessarily lead to the highest

H_2O_{melt} values. If values for P from another equation (Eqns. (1a)-(1e) in RR2012) was used

the calculated values can lie in the stability field for H_2O_{melt} and T.

Dissertation of André Stechern

Decoding Magma Plumbing and Geochemical Evolution Beneath the Lastarria Volcanic
Complex (Northern Chile) - Evidence for Multiple Magma Storage Regions

6 DISCUSSION

6.1 Magma storage conditions

Our two-pyroxene, single amphibole composition, Fe-Ti oxides, and plagioclase-melt thermobarometry produces three distinct and separate groups of P–T estimates. This strongly indicates three separate levels of crystallization and thus possibly three different levels of magma storage.

In particular, the two groups of samples with low to medium pressures (named above as *Group 2* and *Group 3*) give matching results for pressure and temperature estimates using different barometric approaches. In this case, very similar results for P and T are obtained with the respectively different thermobarometers. The determined K_D $(Fe-Mg)^{Cpx-Opx}$ values of the two pyroxenes are in a range described by Putirka (2008) as equilibrium conditions during crystallization. In particular, the estimation of the pressure, and along with this the depth of magma storage, is in very good agreement with the P results from the Amp compositions. These matching results of different barometers and thermometers for the respective samples suggest that it is possible to distinguish two different crystallization levels.

Somewhat more difficult to interpret are the results from the few low-Al pyroxene pairs in *Group 2* and *3* and all pairs of *Group 1* (LAST-10-07, -14, -15), since they are exclusively low-Al pyroxene pairs. Due to the absence of Amp only the results of the two-pyroxene barometer can be used to determine the absolute pressure for *Group 1*.

There are several possible explanations for the chemistry of *Group 1*. One explanation is that the pyroxene pairs from *Group 1* are actually in a chemical disequilibrium and therefore the P-T calculations give incorrect results. Another possibility is that although the recommended equilibrium criteria are not matched, it could be possible that P-T conditions still remain in a realistic range due to a limited calibration database of the pyroxene barometer. Arguments for and against formation in equilibrium are discussed in the next paragraph.

Dissertation of André Stechern

Decoding Magma Plumbing and Geochemical Evolution Beneath the Lastarria Volcanic
Complex (Northern Chile) - Evidence for Multiple Magma Storage Regions

6.2 Validity of *P-T* determination for *Group 1*

The calculated K_D $(Fe-Mg)^{Cpx-Opx}$ between the two pyroxenes, indicates that the low-Al Opx and low-Al Cpx are not in equilibrium following Putirka (see Fig. II.12A). A closer analysis shows that the Opx from *Group 1* are significantly different in their Fe-content and therefore also the enstatite and ferrosilite components, which are critical for the *P-T* calculations according to the formulations given by Putirka (2008). Additionally, the geological interpretation of the results obtained for the temperatures is difficult. The temperatures for *Group 1* represent the lowest of all the samples. Typically, it could be expected that these temperatures may be assigned to a rather shallow storage level.

The fact that samples LAST-07, -14, -15 (high *P*) do not differ petrographically in appearance (besides the lack of Amp) from the other Lastarria samples, but differ significantly from the proposed equilibrium K_D values recommended by Putirka (2008), raises a question whether the equilibrium criteria for the two-pyroxene thermobarometer are feasible at all.

The suggested range of K_D values that reflects equilibrium conditions is 1.09 ±0.14. Almost all samples from the low and intermediate pressure range match these criteria. The Fe/Mg ratio in Cpx and Opx is nearly identical in these samples (see Fig. II.12B). The high-*P* samples (LAST-07, -14, -15) show somewhat higher Fe concentrations in Opx and Fe/Mg ratios between Cpx and Opx are not the same. The equilibrium criteria of Putirka (2008) have not been achieved between these pairs. The *P-T* calculations, however, lead to results, which fall in reasonable geological range. Several reasons suggest that the proposed equilibrium interval is too small and might extend in particular towards lower K_D values. The experiments on Lascar samples (Part I of the thesis) show that pyroxene populations, which obviously originated in a chemical equilibrium, do not match the equilibrium criteria given by Putirka (2008). The reason for this might lie in the experimental set, which was utilized for the calibration of the geothermobarometer. These experiments were conducted at much higher

Dissertation of André Stechern

Decoding Magma Plumbing and Geochemical Evolution Beneath the Lastarria Volcanic
Complex (Northern Chile) - Evidence for Multiple Magma Storage Regions

pressures (>1 GPa) and high temperatures (>1000°C), which are far from reasonable upper

crustal *P-T* conditions. This limited experimental data-background might exclude certain

pyroxene compositions to be in equilibrium, in spite of the strong indications they actually

are. For example, pyroxene compositions, as shown in Lascar experiments, are also sensitive

to the redox state of the melt from which they originate (Fig. I.14; Part I of the thesis). This

aspect for example is not taken into account in the formulations of Putirka (2008). Therefore,

two chemically different Opx compositions (varying in Fe/Mg ratios) can crystallize at

constant *P-T* conditions only by changing the redox state of the system.

As a consequence, pyroxene pairs with systemically lower K_D values may reflect

equilibrium conditions even though they are excluded by the criteria given by Putirka (2008)

and calculated absolute *P* values might not be accurate. Additionally natural pyroxene pairs

from Parinacota volcano (Banaszak, 2014) show a systematical shift towards lower K_D

compared to the ones recommended by Putirka (2008) to be in equilibrium. Average K_D

values for Parinacota pyroxenes are between 0.80 and 1.07. Parinacota samples give no

petrographic evidence for disequilibrium of the pyroxenes.

6.2.1 Theoretical re-calculation of pyroxene pairs from Group 1

To test whether the obtained temperature (and pressure) results are in a feasible range a

number of new *P-T* calculations were made. For this, the average Opx compositions from

Group 2 and *3* were used respectively for re-calculations of *P-T* values in reference to Putirka

(2008). In this test, it was found that the obtained K_D (Fe-Mg)$^{Cpx-Opx}$ between the Cpx from

Group 1 and average Opx from *Group 2* and *3* respectively are higher in both cases and fit

mostly to the recommended K_D interval of equilibrium given by Putirka (2008). The results of

the new calculations are shown in Fig. II.17A-D.

Decoding Magma Plumbing and Geochemical Evolution Beneath the Lastarria Volcanic
Complex (Northern Chile) - Evidence for Multiple Magma Storage Regions
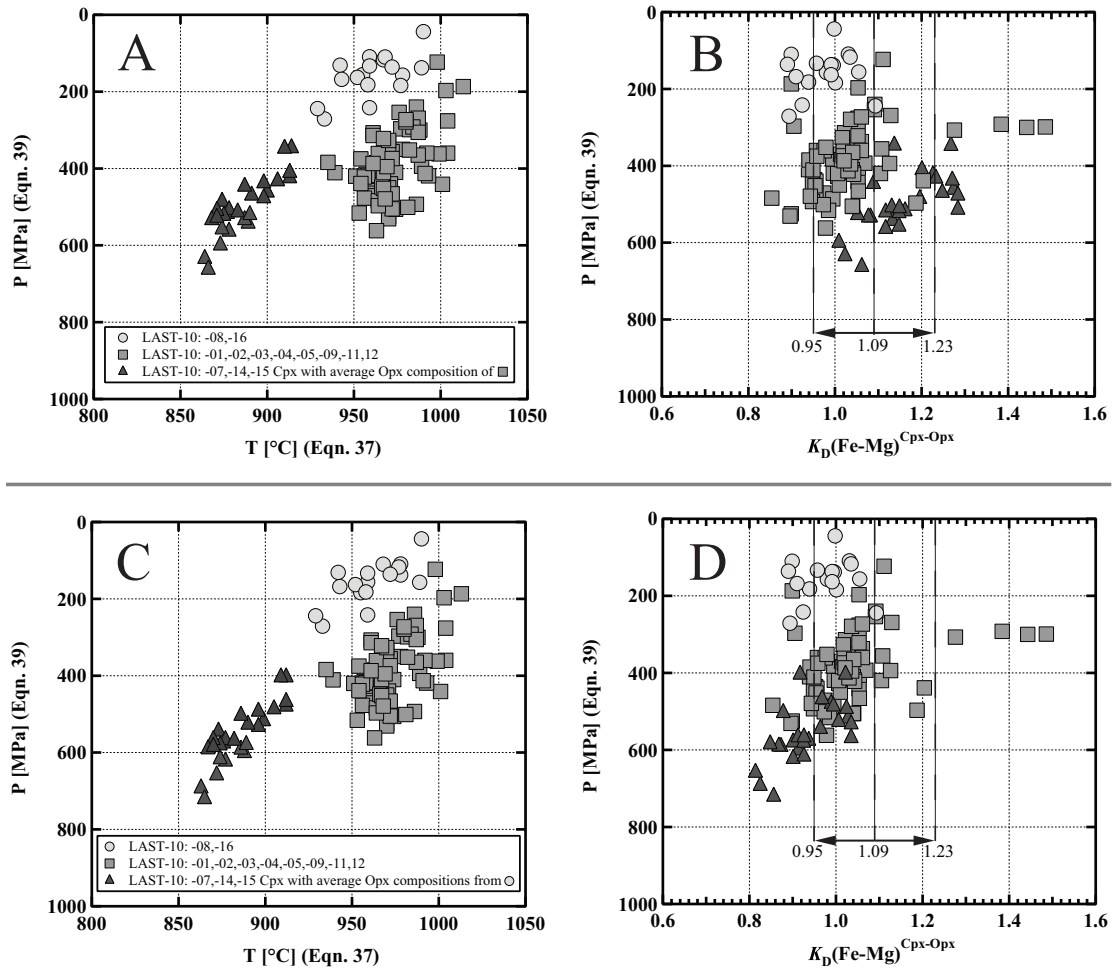
Figure II.17: A & C Thermobarometric re-calculation of the pyroxene pairs from samples LAST-10-: -07, -14, -15. For a detailed description see text. **B & D** Resulting K_D(Fe-Mg) values between Cpx-Opx pairs after re-calculations.

In particular, the calculations of the *Group 1* Cpx with the average *Group 2* Opx give K_D (Fe-Mg)$^{Cpx-Opx}$ which would represent an equilibrium (see Fig. II.17B). It is shown that in both theoretical equilibrium calculations, the temperature interval obtained does not differ strongly from the one calculated from the original Opx (compare Figs. II.12 and Fig. II.17A and C). The temperatures obtained are still in a rather low range between 860 and 910°C, and consistent with the results of the other applied thermometers. It was also found that the *P* values of ~600-900 MPa (see Fig. II.11) calculated from the original approach appear to be too high. Pressures were determined using the theoretical approach with the Opx from *Group*

Dissertation of André Stechern

Decoding Magma Plumbing and Geochemical Evolution Beneath the Lastarria Volcanic
Complex (Northern Chile) - Evidence for Multiple Magma Storage Regions

2 and *3* respectively are in the range of ~400-500 MPa. This pressure range corresponds to the highest pressures identified for *Group 2* pyroxenes.

6.2.2 Pyroxene-melt thermobarometry

Additionally, the pyroxene-melt (Opx-melt and Cpx-melt) thermobarometers of Putirka (2008) were tested on the critical samples (*Group 1*) to check whether these would provide similar *P-T* values or give new information on the disequilibrium process. For this purpose, melt inclusions (results are given in the Appendix) were measured in pyroxenes. The calculated temperature values are nearly identical to the results from the two-pyroxene thermometer. Unfortunately no reasonable results for the pressure could be determined. The calculation of the pressure depends largely on the water content in the melt (see Eqns. (29a)-(31) in Putirka, 2008). However, this is difficult to accurately determine in this sample set since (i) the glassy matrix is largely degassed and includes many microlites and (ii) the melt inclusions in the pyroxenes are less frequent and are often an order of magnitude smaller (max. 5-10 μm) than the ones in plagioclase. The EMPA results do not yield a consistent picture of the water content in the melt and therefore, the pyroxene-melt barometer in particular cannot be applied in this case.

These facts considered, it can be assumed that the samples from *Group 1* (LAST-10: -07, -14, -15) give realistic values for the temperature. However, a clear distinction with respect to the pressures calculated for *Group 2* cannot be made. Calculated theoretical pressures of ~400-500 MPa are nevertheless still among the highest values obtained from all samples.

Dissertation of André Stechern

Decoding Magma Plumbing and Geochemical Evolution Beneath the Lastarria Volcanic Complex (Northern Chile) - Evidence for Multiple Magma Storage Regions

6.2.3 Origin of disequilibrium between Opx-Cpx in Group 1

The fact that in most of the samples of *Group 2* and *Group 3* low-Al pyroxene pairs were found, even though very few, might suggest that these particularly low-Al pyroxenes have another origin in terms of *P* and *T* conditions.

Using two individual barometers, two groups of samples can be distinguished relative to *P* (*Group 2* with *P* of ~ 300-500 MPa and *Group 3* with *P* of ~ 200±50 MPa). Pressures from the *Group 1* samples cannot be reliably determined. However, there are indications that these samples are crystallized at relatively high pressures of >400 MPa (see above). The absence of amphibole in this sample group might suggest that the crystalizing magma had low H_2O concentration (most likely <2.5 wt.% H_2O_{melt}) and therefore the formation of amphibole was suppressed.

One possible scenario is, that samples from *Group 1* (LAST-10-07, -14, -15) did not form in an equilibrium mixture of crystals and melt, but rather display a re-mobilized crystal mush consisting of Plag, Cpx, and Opx plus a secondary melt. Crystal mushes are remnants in magma chambers after a large part of the melt was extracted and ascended towards the Earth's surface. The remaining liquid fraction is only <40% and the temperature is lower than in a typical magma (e.g. Bachmann and Bergantz, 2003; Burgisser and Bergantz, 2011). Such a crystal mush cannot erupt due to its high viscosity. The injection of a new primitive melt into a crystal mush can cause a re-mobilization and the minerals of the mush can be transported upwards with the new melt. If this process is fast, the minerals of the crystal mush have no sufficient time to re-equilibrate with the newly injected melts and the low temperatures values gained by the geothermometers remain low. For the pyroxene thermobarometer in particular, slowly diffusing elements such as Fe and Mg are crucial for the calculation of the temperature. The sample LAST-10-07, which may be derived from such a crystal mush, shows slightly elevated temperatures for the Fe-Ti oxides (see Fig. II.15). The Fe-Ti equilibrium is particularly sensitive to rapid temperature changes (Venezky and

Dissertation of André Stechern

Decoding Magma Plumbing and Geochemical Evolution Beneath the Lastarria Volcanic
Complex (Northern Chile) - Evidence for Multiple Magma Storage Regions

Rutherord, 1999). Therefore, slightly elevated temperatures of Fe-Ti oxides, in particular for samples LAST-10-07 could be an indication of a remobilization of a crystal mush by a juvenile, hot melt.

This would also explain the occasional occurrence of low-Al pyroxenes in all other samples. With the ascending primitive magmas remnants of the crystal mush were transported in small quantities into shallower magma chambers. The absence of amphibole in the high-pressure samples (*Group 1*) can be explained by low amounts of H_2O_{melt} (<2.5 wt.% H_2O) in the system. The magma from which the potential crystal mush originated would have had low water contents and therefore no amphiboles could form. The later injected mafic magmas were water-rich, re-mobilized the mush, and ascended further upwards towards shallow crustal levels.

In the shallow magma chambers of the upper crust magmas stagnated for a longer period and the observed phenocrystal assemblage, including amphiboles and biotite crystals, has formed.

6.3 Oxygen Fugacity and Water Content of the Melt

Values for oxygen fugacity in all the samples are similar when comparing the results of the Fe-Ti oxides and the amphibole calculations. A consistent $\log fO_2$ was calculated for all samples in the range between NNO and NNO+1. Only the results of RR2012 exhibit higher values. The results for the pre-eruptive water content from Lastarria samples show significant differences between the two hygrometers used in this study. In particular water contents, as determined with the Plag-melt pairs, are much too low for the Amp containing samples. Additionally the H_2O_{melt} calculations using the Plag-melt hygrometer are highly dependent on the *T*-input parameter and already small changes in *T* can largely affect the calculated H_2O_{melt} values. Therefore, the water contents of the Amp calculations are assumed to give a more accurate estimation of the pre-eruptive water content in the melt. Additionally, this shows that

Dissertation of André Stechern

Decoding Magma Plumbing and Geochemical Evolution Beneath the Lastarria Volcanic
Complex (Northern Chile) - Evidence for Multiple Magma Storage Regions

the later Amp model of RR2012 gives rather unsatisfactory results for the Amp-bearing samples. For calc-alkaline, intermediate rocks the proposed model of R2010 is preferable. A reason for this is in particular the limited, but therefore specific range of calibration, primarily based on calc-alkaline samples ranging between basalts and rhyolites. However, estimations of H_2O_{melt} derived only from Amp compositions should be handled with caution. To more precisely determine the water content of the melt additional spectroscopic measurements (Infrared and/or Raman Spectroscopy) on melt inclusions from plagioclases and pyroxenes would be needed.

6.4 Sample locality

Some correlations between the sample locations and the determined pre-eruptive depths can be found. The (oldest) lower lava flows (sample Last 10-14 and -15) of the volcano are free of amphiboles and contain pyroxenes, which might have originated in a chemical disequilibrium but pressure estimates are still in a realistic range. This would mean that the oldest Lascar rocks are derived from relatively deep reservoirs and might be a re-mobilized crystal mush.

Samples of the avalanche deposit, in particular, show a variety of different rock types and appear to be a blend of various rock fragments. Light and dark samples can be found directly side-by-side but not as one single piece of rock. This indicates the probability that these fragments originated in different reservoirs. It is either volcanic material, seemingly from different magma chambers and ejected together, or rock fragments of previous eruptive stages were dragged along during the eruption and were deposited together. The other samples exhibit no apparent relationship between sample locality, chemistry, or *P-T* values.

Dissertation of André Stechern

Decoding Magma Plumbing and Geochemical Evolution Beneath the Lastarria Volcanic
Complex (Northern Chile) - Evidence for Multiple Magma Storage Regions

6.5 Magmatic differentiation

In order to obtain a comprehensive view on the magmatic plumbing system it is not sufficient to detect distinct reservoirs and determine the respective pressure and temperature ranges. It is also important to understand which magmatic processes take place in the individual reservoirs. Conclusions about the evolution of the eruptive rocks can be accordingly made. Several mechanisms of magmatic differentiation are generally recognized for subduction zone settings: (i) the chemical evolution of a melt through fractional crystallization along liquid lines of descent, whereby a primitive melt develops through continuous crystallization of individual mineral phases and residual melt and, therefore the whole-rock compositions are always more differentiated; (ii) Mixing of a differentiated magma with a primitive magma, where the composition of the newly formed intermediate magma depends on the volumetric ratio between the two end members (e.g. Clynne, 1999); (iii) Contamination of a basaltic magma with an evolved country rock also leads to rocks with intermediate compositions.

The results of the Lastarria whole-rock analyses show linear relationships of the main elements with an index of differentiation, such as MgO or SiO_2, between the primitive and the most differentiated samples (see Figs. II.7 and II.18). Experimental studies of andesitic systems have clearly shown that whole-rock development by crystallization follows a non-linear trend of the main oxides vs. incompatible oxides (e.g. Botcharnikov *et al.*, 2008; Almeev *et al.*, 2013). Individual oxides may first be enriched and with ongoing differentiation then depleted; depending on the volumetric proportion of the phase they get incorporated into. Lastarria whole-rock analyses are shown in Fig. II.18 and additionally the experimental results of the crystallization experiments from Lascar andesites (Part I of this thesis). The black lines correspond to experiments performed at 300 MPa, 900-1050°C, and oxidizing conditions of NNO+3.3 at $X_{H2O} = 1$. The most primitive composition of Lascar corresponds in many oxides (see Fig. II.18) with the ones from Lastarria. The evolution of the melt

Dissertation of André Stechern

Decoding Magma Plumbing and Geochemical Evolution Beneath the Lastarria Volcanic
Complex (Northern Chile) - Evidence for Multiple Magma Storage Regions

composition by crystallization in the experiments is displayed in Fig. II.18 with arrows, labeled with 'CF'.

Comparison between the natural Lastarria samples and experiments on Lascar samples clearly shows that differentiation by crystallization can be excluded or that it plays only a marginal roll. A large-scale contamination of primitive melt with the surrounding country rock is also rather unlikely. Additionally, very large amounts of country rock would be needed to drive the primitive magmas towards more differentiated compositions.

Decoding Magma Plumbing and Geochemical Evolution Beneath the Lastarria Volcanic
Complex (Northern Chile) - Evidence for Multiple Magma Storage Regions
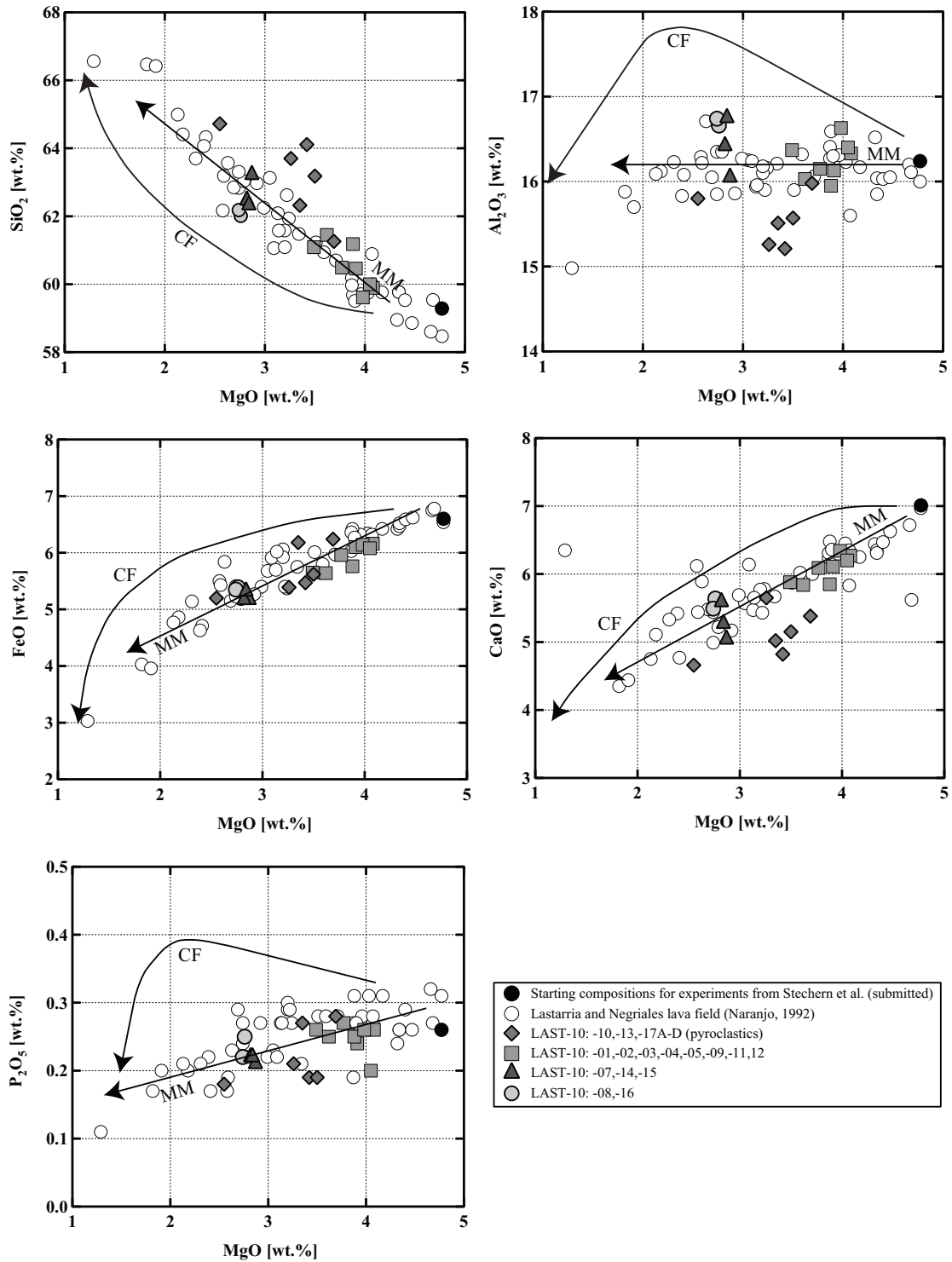
Figure II.18: Selected variation diagrams of Lastarria and Negriales rocks. Arrows labeled with 'MM' represent magma mixing trends. Arrows labeled with 'CF' are derived from crystallizations experiments on Lascar lavas (Part I of this thesis) and represent liquid lines of descent (LLDs). Starting compositions of the experiments is given as a black dot.

Decoding Magma Plumbing and Geochemical Evolution Beneath the Lastarria Volcanic
Complex (Northern Chile) - Evidence for Multiple Magma Storage Regions

Our observations deduced from major element variations are furthermore confirmed by

the trace element distribution in whole rock analyses. The Ni vs. Rb diagram in Fig. II.19

underlines that magma mixing is the major factor controlling the compositional variation of

Lastarria samples. To better compare the mixing signature with a typical crystal fractionation

signature, data from Lascar volcano (Matthews *et al.*, 1999 and Mamani *et al.*, 2010) are

additionally represented in Fig. II.19. Trends for crystal fractionation and magma mixing are

derived from Wörner *et al.* (1988).
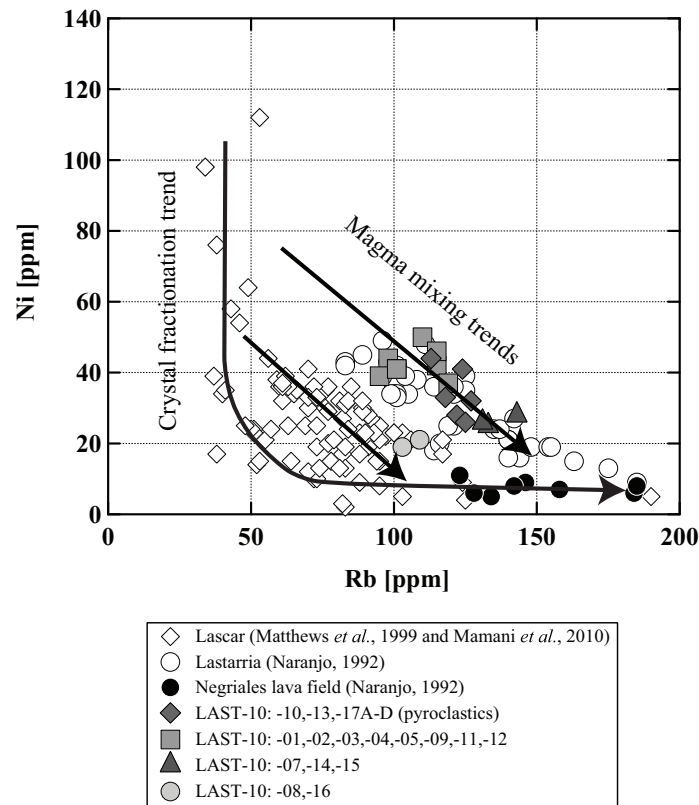
Figure II.19: Ni vs. Rb in samples from Lastarria and Lascar volcanoes and Negriales lava filed. Curved line is a
fractional crystallization path; straight lines are mixing lines (both schematic).

The curved line is characteristic of fractional crystallization or combined assimilation-

fractional crystallization. Lascar eruptive rocks reveal stages where either mixing or fractional

crystallization is the main process for magmatic differentiation (Part I of this thesis). By

contrast, Lastarria andesites and dacites plot above this trend, along a straight line suggestive

for magma mixing. Eruptive rocks from the Negriales Lava Filed (Naranjo, 1992) follow

Dissertation of André Stechern

Decoding Magma Plumbing and Geochemical Evolution Beneath the Lastarria Volcanic Complex (Northern Chile) - Evidence for Multiple Magma Storage Regions

clearly the crystal fractionation signature. This signature indicates that the lava field, although geographically associated to Lastarria, strongly differs in the magmatic processes leading to the evolved dacitic compositions. It is likely that the Negriales Lava Field was not fed from the same magma reservoirs as Lastarria or the differentiation processes changed significantly in the magma chamber(s) after the eruption of the lava field.

The uniform macroscopic appearance (no mafic enclaves or schlieren) of the Lascar samples supports the assumption that efficient magma mixing processes occurred before eruption. Although the compositions of the individual mineral phases are in a comparably small range (e.g. Plag with An_{38} to An_{53}; Fig. II.3A), textural features can be observed, which usually reflect a highly dynamic magmatic system. Sieve textures in combination with overgrowth rims and complex zonation patterns can be found, occurring frequently in subduction zone related, intermediate volcanic rocks (e.g. Nelson and Montana, 1992). Sieve textures can be a result of a crystallographically preferential orientation of crystal dissolution due to an influx of a high temperature melt. In such a system plagioclase would in particular become unstable. Possible processes, which can cause such dissolution, are partial melting (e.g. Johannes *et al.*, 1994) or the mixture of a felsic magma, containing Ab-rich plagioclase, with a hotter, mafic melt (e.g. Tsuchiyama, 1985; Andersson and Eklund, 1994). Another explanation for the origin of the sieve-like textures is the formation of very rapid skeletal growth at conditions of supersaturation due to rapid undercooling and/or mixing of two magmas to an intermediate composition (e.g. Landi *et al.*, 2004).

The fact that the mixing process in Lastarria magmas was very efficient can be explained by the absence of any macroscopic patches of mafic material in the erupted rocks. Volcanoes with signs for incongruent mixing usually exhibit mingling structures between the evolved rock and mafic enclaves (e.g. Perugini and Poli 2004). Chemical patterns reveal a bimodal distribution of the main and trace elements. A typical example for this is Taapaca in the CVZ (Banaszak, 2014). In Lastarria samples only microscopic schlieren structures can be

Dissertation of André Stechern

Decoding Magma Plumbing and Geochemical Evolution Beneath the Lastarria Volcanic
Complex (Northern Chile) - Evidence for Multiple Magma Storage Regions

found. These very fine flow structures are most likely a result of the effective mechanical mixing of the end members. As a result also an efficient chemical homogenization took place. A possible mixing process could occur with the following scenario: The initial phase of magma mixing can be better described as a mechanical mingling progresses in which a primitive juvenile basaltic magma encounters an existing magma chamber. Since the thermal diffusion is several orders of magnitude higher than the chemical diffusion, chemical homogenization of the newly formed hybrid magma occurs after a thermal equilibrium was reached. Existing crystals in the magma may be acting as stirring rods and enhance mixing. These mixing processes can be very efficient depending on the reservoir volumes and the timespan prior to an eruption and, therefore, can only be detected as micro-textures in rocks and geochemical patterns. The occurrence of low-Al pyroxenes in all low-*P* and intermediate-*P* samples, even though only very few, could mean that the low-Al pyroxenes have their origin in deeper crustal zones (>20 km), probably from a crystal mush, and were transported into the upper crust by ascending melts or magmas. In the shallow to intermediate magma chambers the low-Al pyroxenes are preserved as relicts from deeper reservoirs.

6.6 Magma plumbing system

The combination of different geophysical methods, results of the petrological analyses, and *P-T* calculations allow a more detailed picture of the magmatic plumbing system beneath Lastarria volcano. GPS measurements of the ground deformation and the evaluation of InSAR data sets make it possible to determine the minimum depth or the roof of a possible magma reservoir. In addition, the volume and lateral extent of the uppermost magma reservoir can be estimated. Megnetotelluric studies of the continental crust beneath a volcano, however, reveal information about the depth of the entire plumbing system and the origin of magmas. The results of the thermobarometric calculations on minerals found in the erupted rocks allow the determination of different storage levels. Furthermore, physical and chemical

Dissertation of André Stechern

Decoding Magma Plumbing and Geochemical Evolution Beneath the Lastarria Volcanic
Complex (Northern Chile) - Evidence for Multiple Magma Storage Regions

parameters of (former) magma reservoirs can be determined exactly. In the following, a

model of the magmatic plumbing system under Lastarria Volcano (see Fig. II.20).
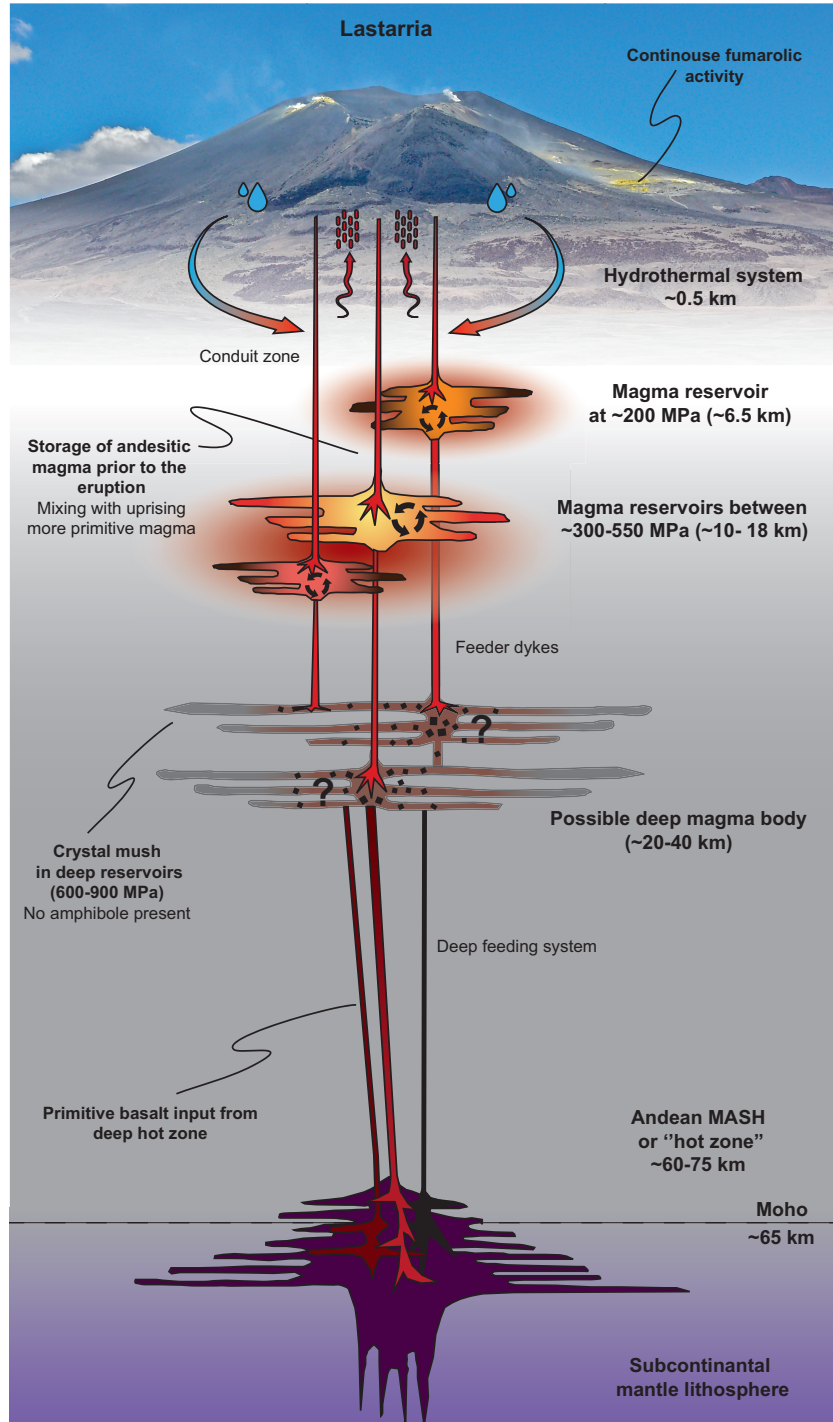
Figure II.20: Suggested model of the magma plumbing system beneath Lastarria. Depth of the possible deep crystal mush reservoir is constrained from magnetotelluric data (Budach *et al.*, 2013) and barometric calculations on samples LAST-10-: -07. -14, -15. Intermediate magma reservoirs at ~300-550 MPa and the shallow storage zone at ~200 MPa were detected by the geobarometric calculations. Samples from all storage levels show signs of effective magmatic mixing prior to the eruptions.

Decoding Magma Plumbing and Geochemical Evolution Beneath the Lastarria Volcanic
Complex (Northern Chile) - Evidence for Multiple Magma Storage Regions

The uppermost part of the plumbing system is the near-surface hydrothermal system. Aguilera *et al.* (2008) have shown that two types of fumaroles are currently active on the edifice of the volcano. High and low temperature fumaroles are present, which differ in the concentrations of the ejected gases and have potentially different sources. The authors argue that the presence of highly acidic compounds clearly indicates Lastarria's fumarolic fluids and gasses are affected by conspicuous contribution from a high-temperature source.

The geobarometric results show that the upper most magma reservoir is located at a depth corresponding to approximately 150-250 MPa. If the density of the country rock is taken into account these pressure values correspond to a depth of ~5-8 km below the earth's surface. This result agrees very closely with the latest results of the InSAR analysis. Remy *et al.* (2014) have modeled several two- and three-dimensional bodies able to explain the elevation of the entire Lazufre area. Here, the shape of a truncated elliptical cone provided the best results. The minimum depth for the location of the reservoir roof is highly dependent on the three-dimensional shape of the modeled body in these calculations. The best models give values of ~5.3 km for the magma chamber roof. The results of our geobarometric calculations suggest that this is only the upper most magma reservoir of a more complex system of multiple magma storage levels. The lateral extent of the detected body under the whole Lazufre Volcanic Complex is given with 27 km and 15 km for the major and minor axes, respectively. The volume estimate for the truncated elliptical cone model lying at shallow depth seems to be large with a volume greater than 400 km^3 given by Remy *et al.* (2014). However, ignimbrites erupted in the vicinity of the Lazufre area are comparable in volumes. The Cerro Galan caldera, for instance, is the source of a ~1000 km^3 ignimbrite (Francis *et al.*, 1983) and La Pacana caldera is the source of at least two major ignimbrite eruptions with a combined estimated volume of ~2700 km^3 (Lindsay *et al.*, 2001).

The results of a magnetotelluric study beneath Lastarria (Budach *et al.*, 2013) show no conductive body at shallow depths of about 5-8 km directly beneath the volcanic edifice. However, 2-D and 3-D modeling shows consistently a wide conductive body that begins at a

Dissertation of André Stechern

Decoding Magma Plumbing and Geochemical Evolution Beneath the Lastarria Volcanic
Complex (Northern Chile) - Evidence for Multiple Magma Storage Regions

depth of about 15 km and is detectable down to the Moho. This may call for a deep leveling

plumbing system having multiple storage levels, which are connected to each other via feeder

dikes, transporting partially molten material from the Moho into the individual reservoirs.

Based on the geobarometric calculations it can be assumed that several reservoirs at deeper

levels beneath Lastarria volcano exist or were at least present at earlier times. The calculated

pressures of most samples of this study are between 300-550 MPa, corresponding to depths of

approximately 10 to 18 km. This area conforms to the top of the deep-reaching conductive

zone described by Budach *et al.* (2013). This conductive zone extends at least 45 km down to

the Moho in the suggested 2-D and 3-D models. This is an indication of the deep magmatic

plumbing system beneath the volcano. Whether this is a network of feeder channels, or even

individual storage reservoirs of crystal mushes, cannot be resolved accurately based on the

existing magnetotelluric data set. The authors, however, suggest a melt fraction of at least 5-

8 % in the partially molten system under the assumption of specific conductivity values for

liquid media. This melt proportion might be an indicator for crystal mushes even though melt

proportions might be to low for a typical mush (e.g. Huber et al. 2010).

Assuming the results from *Group 1* pyroxene pairs are in a feasible range, it provides a

consistent picture of the magma storage system, whereby amphibole-bearing (volatile-rich)

magma bodies are present in the upper and middle crust, somewhat obstructing the eruption

of low-Al pyroxene-bearing magmas or crystal mushes. The upper and middle crustal

andesites and dacites provide evidence, due to the occurring low-Al pyroxenes, that melt

batches from depth were able, at least intermittently, to penetrate shallow storage zones. This

probably occurred in a melt-rich regime, where ascending melts are more likely to be

intercepted and subsequent mixing will lead to the mineralogical features of magmas from

Group 2 and *3*, with a majority of pyroxenes as real phenocrysts (high-Al) and a few

remaining low-Al pyroxenes as a remnant of the crystal mush.

The whole plumbing system is fed by primitive basaltic melts generated by partial

melting of the mantle wedge, which underplate the continental crust and form magma

Dissertation of André Stechern

Decoding Magma Plumbing and Geochemical Evolution Beneath the Lastarria Volcanic
Complex (Northern Chile) - Evidence for Multiple Magma Storage Regions

reservoirs at the base of the crust and close to the Moho (violet bottom part of Fig. II.20). The exact shape and extend of this structure is not known, and in particular the scenario of penetration of this zone into the crust is not clarified. Therefore, the shape shown in Fig. II.20 does not accurately depict the actual case and should be regarded only as a possibility.

As for the Lascar model (Part I of the thesis) magma will remain in this deep reservoir until it fractionates enough (through MASH processes) that the remaining melt is less dense than the surrounding rock; the melt will then continue to migrate towards shallow crustal reservoirs. Low Sr/Y (~27) and Sm/Yb (~3) ratios for Lastarria eruptives (comparable to Lascar) suggest that stagnation and MASH processes did not happen in the lower crust due to a lack of garnet signature, which would lead to higher Sr/Y and Sm/Yb ratios (Mamani *et al.*, 2010). The basaltic magmas originate from the mantle and migrated upwards into shallow magma reservoirs without major stagnation times in lower crustal reservoirs.

7 CONCLUSION

The results presented here of the petrological examination of Lastarrias historical rocks can provide a new understanding to the pre-eruptive magmatic processes and of the plumbing system beneath the potentially active volcano. Lastarria samples provide evidence for a complex magma system that comprises a shallow storage region, a mid-crustal storage zone, likely made up of multiple magma storage reservoirs, and a diffuse, deep crustal zone potentially/possibly characterized by crystal mushes.

Matching results from pyroxene and amphibole barometry, indicate at least two different crystallization depths. A relatively shallow crystallization level at a depth of ~5-8 km and an intermediate level at depths of ~10-18 km. The upper most storage level was detected in a similar depth by the evaluation of InSAR data sets (Remy *et al.*, 2014). The deeper system of possible magma reservoirs, from which the majority of Lastarria samples originates, is at intermediate crustal depths. Magnetotelluric measurements

Dissertation of André Stechern

Decoding Magma Plumbing and Geochemical Evolution Beneath the Lastarria Volcanic
Complex (Northern Chile) - Evidence for Multiple Magma Storage Regions

(Budach *et al.*, 2013) have determined a broad conductive zone, which is consistent in depth with those identified on the base of the here presented geobarometric calculations. A possible, deep magma reservoir level, which might consist of crystal mushes, cannot be proven with absolute certainty, since the two pyroxene populations in the corresponding samples show signs of a disequilibrium. Calculated oxygen fugacity for all samples corresponds to a range between NNO to NNO+1, which was calculated either from Fe-Ti oxide pairs or single amphibole compositions using R2010.

The results of the major and trace element analyses clearly illustrate that there has been mixing events, leading to the intermediate rock compositions found at Lastarria. Complex zonation, disequilibrium textures and Fe-rich crystal zones, observed in all sample sets, indicate an interaction of cooler magmas with hotter magmas ascending from depth. Recharge magmas may contain (resorbed) crystal cargoes from a mush, indicating a crystal recycling and decompression-induced resorption. In this way they contribute to the overall textural diversity of the Lastarria eruptive products. Multiple disequilibrium textures preserved within single samples might indicate multiple magma mixing events.

Dissertation of André Stechern

Decoding Magma Plumbing and Geochemical Evolution Beneath the Lastarria Volcanic
Complex (Northern Chile) - Evidence for Multiple Magma Storage Regions

8 REFERENCES

Aguilera, F., Tassi, F., Darrah, T., Moune, S., & Vaselli, O. (2012). Geochemical model of a magmatic–hydrothermal system at the Lastarria volcano, northern Chile. *Bulletin of volcanology*, *74*(1), 119-134.

Almeev, R. R., Holtz, F., Ariskin, A. A., & Kimura, J. I. (2013). Storage conditions of Bezymianny Volcano parental magmas: results of phase equilibria experiments at 100 and 700 MPa. *Contributions to Mineralogy and Petrology*, *166*(5), 1389-1414.

Andersen, D. J., & Lindsley, D. H. (1985). New (and final!) models for the Ti-magnetite/ilmenite geothermometer and oxygen barometer. In *Abstract AGU 1985 Spring Meeting Eos Transactions. American Geophysical Union* (Vol. 66, No. 18, p. 416).

Andersen, D. J., & Lindsley, D. H. (1988). Internally consistent solution models for Fe-Mg-Mn-Ti oxides: Fe-Ti oxides. *The American Mineralogist*, *73*(7-8), 714-726.

Anderssohn, J., Motagh, M., Walter, T. R., Rosenau, M., Kaufmann, H., & Oncken, O. (2009). Surface deformation time series and source modeling for a volcanic complex system based on satellite wide swath and image mode interferometry: The Lazufre system, central Andes. *Remote Sensing of Environment*, *113*(10), 2062-2075.

Andersson, U. B., & Eklund, O. (1994). Cellular plagioclase intergrowths as a result of crystal-magma mixing in the Proterozoic Åland rapakivi batholith, SW Finland. *Contributions to Mineralogy and Petrology*, *117*(2), 124-136.

ARCULUS, R. J. (2003). Use and abuse of the terms calcalkaline and calcalkalic. *Journal of Petrology*, *44*(5), 929-935.

Bachmann, O., & Bergantz, G. W. (2003). Rejuvenation of the Fish Canyon magma body: a window into the evolution of large-volume silicic magma systems. *Geology*, *31*(9), 789-792.

Bacon, C. R., & Hirschmann, M. M. (1988). Mg/Mn partitioning as a test for equilibrium between coexisting Fe-Ti oxides. *American Mineralogist*, *73*(1-2), 57-61.

Banaszak, M. (2014). *Differentiation regimes in the Central Andean magma systems: case studies of Taapaca and Parinacota volcanoes, Northern Chile* (Doctoral dissertation, Niedersächsische Staats-und Universitätsbibliothek Göttingen).

Bédard, J. H. (2006). Trace element partitioning in plagioclase feldspar. *Geochimica et Cosmochimica Acta*, *70*(14), 3717-3742.

Botcharnikov, R. E., Holtz, F., Almeev, R. R., Sato, H., & Behrens, H. (2008). Storage conditions and evolution of andesitic magma prior to the 1991–95 eruption of Unzen volcano: Constraints from natural samples and phase equilibria experiments. *Journal of Volcanology and Geothermal Research*, *175*(1), 168-180.

Budach, I., Brasse, H., & Díaz, D. (2013). Crustal-scale electrical conductivity anomaly beneath inflating Lazufre volcanic complex, Central Andes. *Journal of South American Earth Sciences*, *42*, 144-149.

Burgisser, A., & Bergantz, G. W. (2011). A rapid mechanism to remobilize and homogenize highly crystalline magma bodies. *Nature*, *471*(7337), 212-215.

Carmichael, I. S. E., & Nicholls, J. (1967). Iron‐titanium oxides and oxygen fugacities in volcanic rocks. *Journal of Geophysical Research*, *72*(18), 4665-4687.

Clynne, M. A. (1999). A complex magma mixing origin for rocks erupted in 1915, Lassen Peak, California. *Journal of Petrology*, *40*(1), 105-132.

Dahren, B., Troll, V. R., Andersson, U. B., Chadwick, J. P., Gardner, M. F., Jaxybulatov, K., & Koulakov, I. (2012). Magma plumbing beneath Anak Krakatau volcano, Indonesia: evidence for multiple magma storage regions. *Contributions to Mineralogy and Petrology*, *163*(4), 631-651.

de Silva S.L., & Francis P.W. (1991). Volcanoes of the Central Andes. Springer.

Dissertation of André Stechern

Decoding Magma Plumbing and Geochemical Evolution Beneath the Lastarria Volcanic Complex (Northern Chile) - Evidence for Multiple Magma Storage Regions

Evans, B. W., & Scaillet, B. (1997). The redox state of Pinatubo dacite and the ilmenite-hematite solvus. *American Mineralogist*, *82*(5), 625-629.

Francis, P. W., O'Callaghan, L., Kretzschmar, G. A., Thorpe, R. S., Sparks, R. S. J., Page, R. N., & Gonzalez, O. E. (1983). The Cerro Galan ignimbrite. *Nature*, 301 (1983), pp. 51-53.

Froger, J. L., Rémy, D., Bonvalot, S., & Legrand, D. (2007). Two scales of inflation at Lastarria-Cordon del Azufre volcanic complex, central Andes, revealed from ASAR-ENVISAT interferometric data. *Earth and Planetary Science Letters*, *255*(1), 148-163.

Frost, B. R. (1991). Introduction to oxygen fugacity and its petrologic importance. *Reviews in Mineralogy and Geochemistry*, *25*(1), 1-9.

Gregory-Wodzicki, K. M. (2000). Uplift history of the Central and Northern Andes: a review. *Geological Society of America Bulletin*, *112*(7), 1091-1105.

Holland, T., & Blundy, J. (1994). Non-ideal interactions in calcic amphiboles and their bearing on amphibole-plagioclase thermometry. *Contributions to Mineralogy and Petrology*, *116*(4), 433-447.

Holtz, F., Sato, H., Lewis, J., Behrens, H., & Nakada, S. (2005). Experimental petrology of the 1991–1995 Unzen dacite, Japan. Part I: phase relations, phase composition and pre-eruptive conditions. *Journal of Petrology*, *46*(2), 319-337.

Huber, C., Bachmann, O., & Dufek, J. (2010). The limitations of melting on the reactivation of silicic mushes. *Journal of Volcanology and Geothermal Research*, *195*(2), 97-105.

Iyer, H. M. (1984). Geophysical evidence for the locations, shapes and sizes, and internal structures of magma chambers beneath regions of Quaternary volcanism. *Philosophical Transactions of the Royal Society of London. Series A, Mathematical and Physical Sciences*, *310*(1514), 473-510.

Johannes, W., Koepke, J., & Behrens, H. (1994). Partial melting reactions of plagioclases and plagioclase-bearing systems. In *Feldspars and their Reactions* (pp. 161-194). Springer Netherlands.

Landi, P., Métrich, N., Bertagnini, A., & Rosi, M. (2004). Dynamics of magma mixing and degassing recorded in plagioclase at Stromboli (Aeolian Archipelago, Italy). *Contributions to Mineralogy and Petrology*, *147*(2), 213-227.

Leake, B. E., Woolley, A. R., Birch, W. D., Burke, E. A., Ferraris, G., Grice, J. D., & Whittaker, E. J. (2004). Nomenclature of amphiboles: Additions and revisions to the International Mineralogical Association's amphibole nomenclature. *American Mineralogist*, *89*, 883-887.

Le Bas, M. J., Le Maitre, R. W., Streckeisen, A., & Zanettin, B. (1986). A chemical classification of volcanic rocks based on the total alkali-silica diagram. *Journal of petrology*, *27*(3), 745-750.

Le Maitre, R. W., Streckeisen, A., Zanettin, B., Le Bas, M. J., Bonin, B., & Bateman, P. (Eds.). (2002). *Igneous rocks: a classification and glossary of terms: recommendations of the International Union of Geological Sciences Subcommission on the Systematics of Igneous Rocks*. Cambridge University Press.

Lepage, L. D. (2003). ILMAT: an Excel worksheet for ilmenite–magnetite geothermometry and geobarometry. *Computers & Geosciences*, *29*(5), 673-678.

Lindsay, J. M., Schmitt, A. K., Trumbull, R. B., De Silva, S. L., Siebel, W., & Emmermann, R. (2001). Magmatic evolution of the La Pacana caldera system, Central Andes, Chile: compositional variation of two cogenetic, large-volume felsic ignimbrites. *Journal of Petrology*, *42*(3), 459-486.

Lucassen, F., Becchio, R., Harmon, R., Kasemann, S., Franz, G., Trumbull, R., ... & Dulski, P. (2001). Composition and density model of the continental crust at an active continental margin—the Central Andes between 21 and 27 S. *Tectonophysics*, *341*(1), 195-223.

Luhr, J. F., & Carmichael, I. S. (1980). The colima volcanic complex, Mexico. *Contributions to Mineralogy and Petrology*, *71*(4), 343-372.

Mamani, M., Wörner, G., & Sempere, T. (2010). Geochemical variations in igneous rocks of the Central Andean orocline (13 S to 18 S): Tracing crustal thickening and magma generation through time and space. *Geological Society of America Bulletin*, *122*(1-2), 162-182.

Dissertation of André Stechern

Decoding Magma Plumbing and Geochemical Evolution Beneath the Lastarria Volcanic
Complex (Northern Chile) - Evidence for Multiple Magma Storage Regions

Matthews, S. J., Sparks, R. S. J., & Gardeweg, M. C. (1999). The Piedras Grandes–Soncor eruptions, Lascar volcano, Chile; evolution of a zoned magma chamber in the central Andean upper crust. *Journal of Petrology*, *40*(12), 1891-1919.

Miyashiro, A. (1974). Volcanic rock series in island arcs and active continental margins. *American Journal of Science*, *274*(4), 321-355.

Naranjo, J. A. (1985). Sulphur flows at Lastarria volcano in the North Chilean Andes. Nature, 313, 778-780.

Naranjo, J. A., & Francis, P. (1987). High velocity debris avalanche at Lastarria volcano in the north Chilean Andes. *Bulletin of Volcanology*, *49*(2), 509-514.

Naranjo, J. A. (1992). Chemistry and petrological evolution of the Lastarria volcanic complex in the north Chilean Andes. *Geological Magazine*, *129*(06), 723-740.
Nelson, S. T., & Montana, A. M. (1992). Sieve-textured plagioclase in volcanic rocks produced by rapid decompression. *American Mineralogist*, *77*, 1242-1249.

Nielsen, R. L., Forsythe, L. M., Gallahan, W. E., & Fisk, M. R. (1994). Major-and trace-element magnetite-melt equilibria. *Chemical Geology*, *117*(1), 167-191.

Perugini, D., & Poli, G. (2004). Analysis and numerical simulation of chaotic advection and chemical diffusion during magma mixing: petrological implications. *Lithos*, *78*(1), 43-66.

Pritchard, M. E., & Simons, M. (2002). A satellite geodetic survey of large-scale deformation of volcanic centres in the central Andes. *Nature*, *418*(6894), 167-171.

Pritchard, M. E., & Simons, M. (2004). An InSAR-based survey of volcanic deformation in the central Andes. *Geochemistry, Geophysics, Geosystems*, *5*(2).

Putirka, K. D. (2005). Igneous thermometers and barometers based on plagioclase+ liquid equilibria: tests of some existing models and new calibrations. *American Mineralogist*, *90*(2-3), 336-346.

Putirka, K. D. (2008). Thermometers and barometers for volcanic systems. *Reviews in Mineralogy and Geochemistry*, *69*(1), 61-120.

Remy, D., Froger, J. L., Perfettini, H., Bonvalot, S., Gabalda, G., Albino, F., ... & De, M. (2014). Persistent uplift of the Lazufre volcanic complex (Central Andes): New insights from PCAIM inversion of InSAR time series and GPS data. *Geochemistry, Geophysics, Geosystems*, *15*(9), 3591-3611.

Richards, J. P., Jourdan, F., Creaser, R. A., Maldonado, G., & DuFrane, S. A. (2013). Geology, geochemistry, geochronology, and economic potential of Neogene volcanic rocks in the Laguna Pedernal and Salar de Aguas Calientes segments of the Archibarca lineament, northwest Argentina. *Journal of Volcanology and Geothermal Research*, *258*, 47-73.

Ridolfi, F., Renzulli, A., & Puerini, M. (2010). Stability and chemical equilibrium of amphibole in calc-alkaline magmas: an overview, new thermobarometric formulations and application to subduction-related volcanoes. *Contributions to Mineralogy and Petrology*, *160*(1), 45-66.

Ridolfi, F., & Renzulli, A. (2012). Calcic amphiboles in calc-alkaline and alkaline magmas: thermobarometric and chemometric empirical equations valid up to 1,130° C and 2.2 GPa. *Contributions to Mineralogy and Petrology*, *163*(5), 877-895.

Righter, K., Leeman, W. P., & Hervig, R. L. (2006). Partitioning of Ni, Co and V between spinel-structured oxides and silicate melts: Importance of spinel composition. *Chemical Geology*, *227*(1), 1-25.

Ruch, J., Anderssohn, J., Walter, T. R., & Motagh, M. (2008). Caldera-scale inflation of the Lazufre volcanic area, South America: Evidence from InSAR. *Journal of Volcanology and Geothermal Research*, *174*(4), 337-344.

Rutherford, M. J., & Devine, J. D. (1996). Preeruption pressure-temperature conditions and volatiles in the 1991 dacitic magma of Mount Pinatubo. *Fire and mud: eruptions and lahars of Mount Pinatubo, Philippines*, 751-766.

Decoding Magma Plumbing and Geochemical Evolution Beneath the Lastarria Volcanic
Complex (Northern Chile) - Evidence for Multiple Magma Storage Regions

Scaillet, B., & Evans, B. W. (1999). The 15 June 1991 eruption of Mount Pinatubo. I. Phase equilibria and pre-eruption P–T–fO2–fH2O conditions of the dacite magma. *Journal of Petrology*, *40*(3), 381-411.

Stormer, J. C. (1983). The effects of recalculation on estimates of temperature and oxygen fugacity from analyses of multicomponent iron-titanium oxides. *American Mineralogist*, *68*(5-6), 586-594.

Tsuchiyama, A. (1985). Dissolution kinetics of plagioclase in the melt of the system diopside-albite-anorthite, and origin of dusty plagioclase in andesites. *Contributions to Mineralogy and Petrology*, *89*(1), 1-16.

Venezky, D. Y., & Rutherford, M. J. (1999). Petrology and Fe–Ti oxide reequilibration of the 1991 Mount Unzen mixed magma. *Journal of Volcanology and Geothermal Research*, *89*(1), 213-230.

Wölbern, I., Heit, B., Yuan, X., Asch, G., Kind, R., Viramonte, J., & Wilke, H. (2009). Receiver function images from the Moho and the slab beneath the Altiplano and Puna plateaus in the Central Andes. *Geophysical Journal International*, *177*(1), 296-308.

Wörner, G., Harmon, R. S., Davidson, J., Moorbath, S., Turner, D. L., McMillan, N., & Moreno, H. (1988). The Nevados de Payachata volcanic region (18 S/69 W, N. Chile). *Bulletin of Volcanology*, *50*(5), 287-303.

Appendix

1 PART I

The data presented in Part I contain electron microprobe analysis of experimental and natural samples. Natural samples from Lascar were collected by M. Banaszka, F. Holtz and G. Wörner during a field campaign in 2007. The data was obtained using a Cameca SX-100 microprobe at the Leibniz University of Hannover.

Microprobe analyses (and *P-T* calculation) presented in Tabs. AT1, AT3 and AT4 (digital Appendix) were done by M. Banaszak at Geowissenschaftliches Zentrum Universität Göttingen, Abteilung Geochemie.
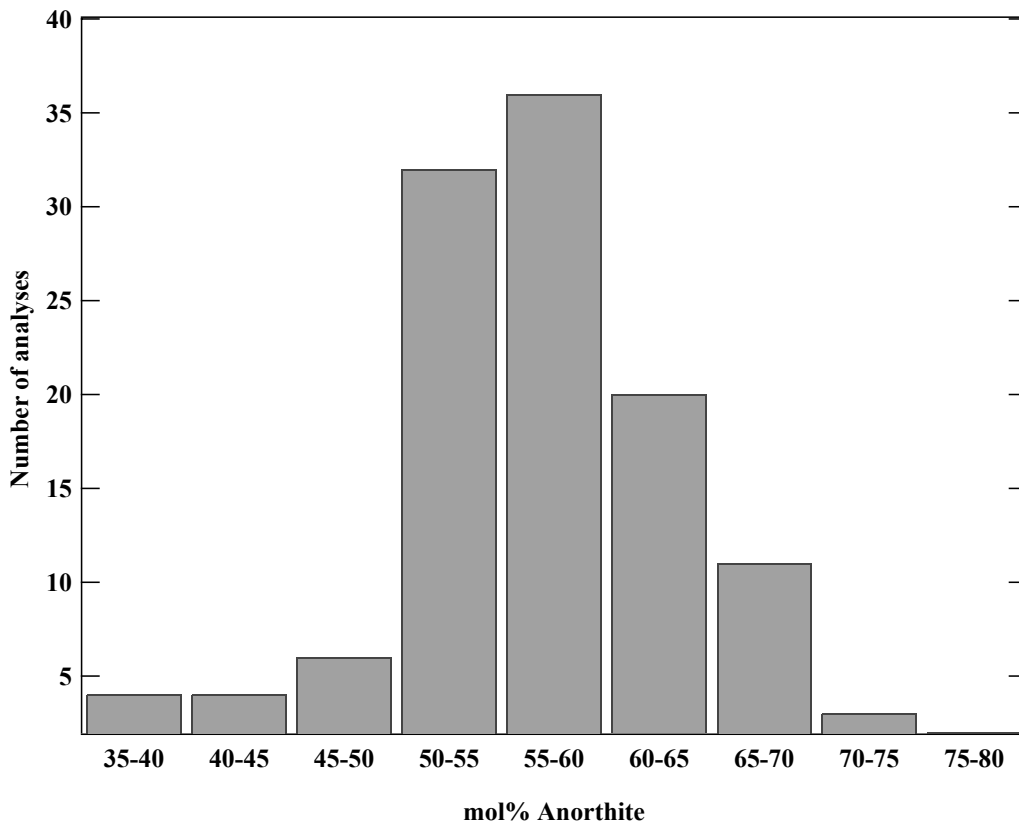
Figure AF1: Histogram of anorthite contents in natural Stage IV plagioclases.
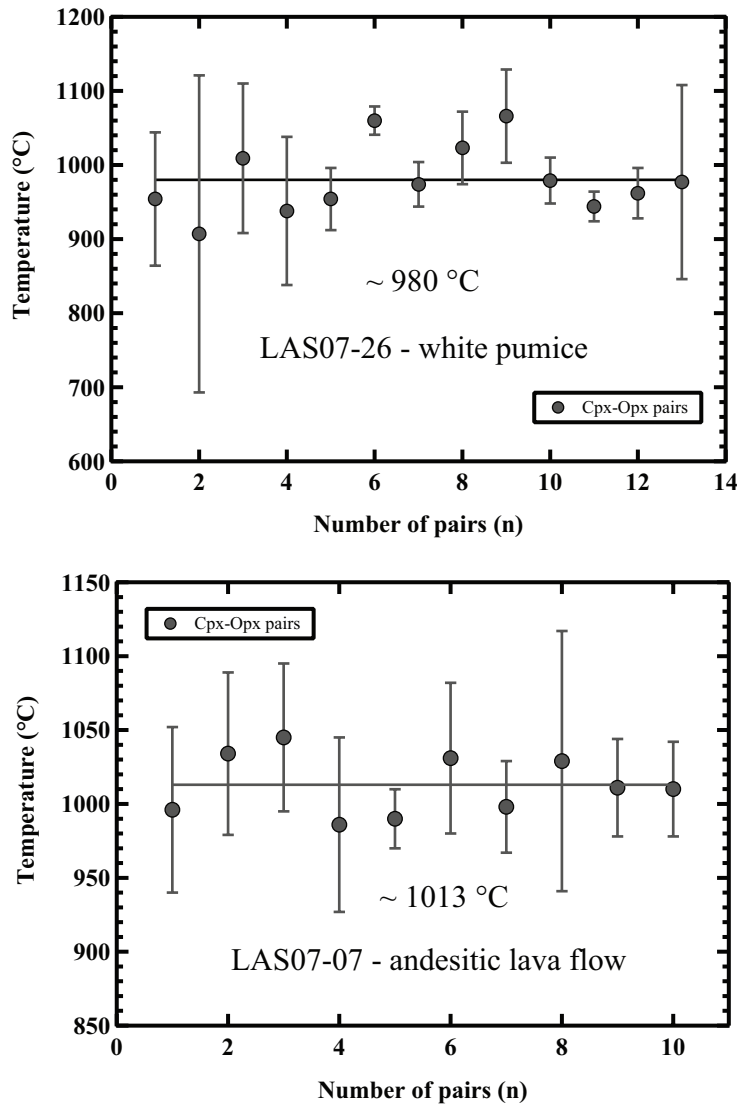
Figure AF2: Temperature estimates for representative Stage IV eruptives using the Opx-Cpx geothermobarometer from Andersen *et al.* (1993).
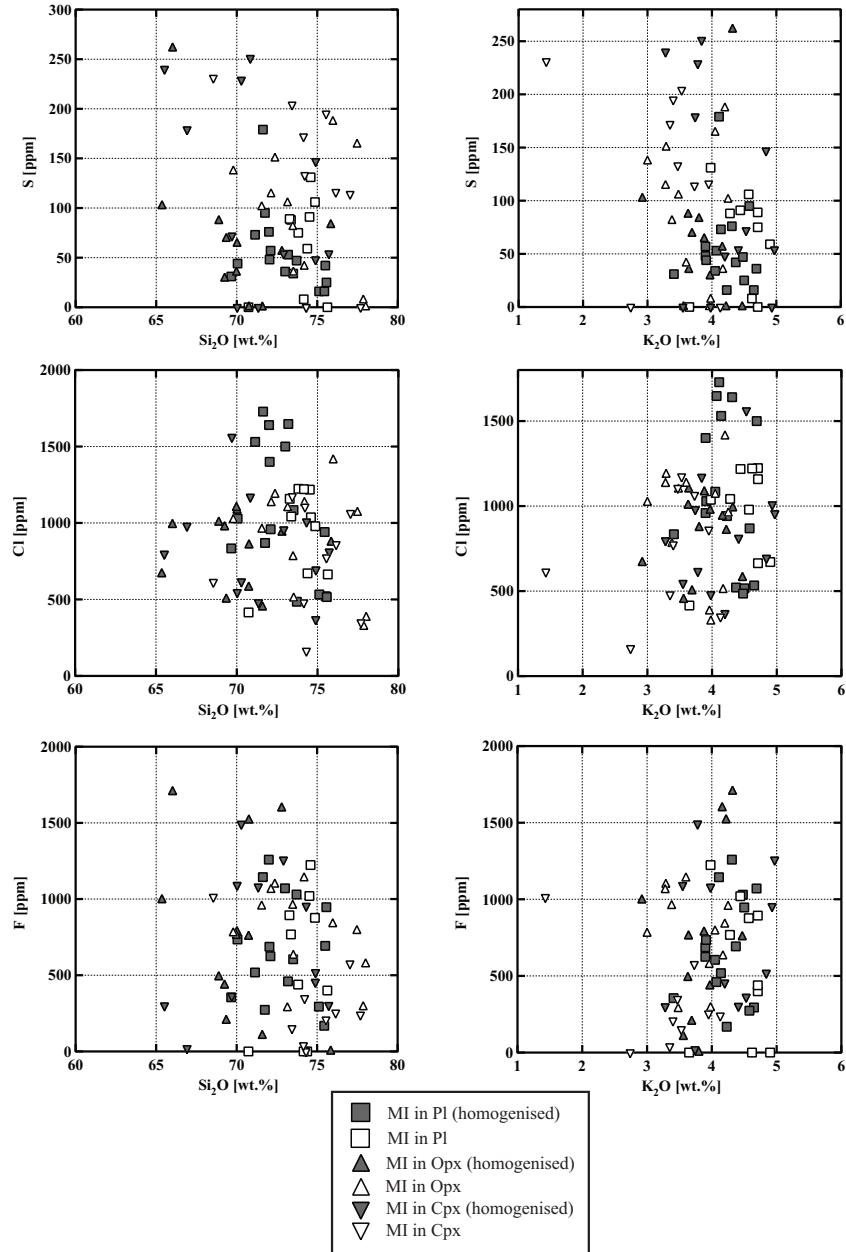
Figure AF3: Concentrations of S, F and Cl in melt inclusions from sample LAS07-26.

Melt inclusions were analyzed with a Cameca SX-100 electron microprobe at the Institute for Mineralogy, LUH. The analyses of the glasses were conducted using a 15 kV acceleration voltage, 4 nA beam current, and a 5-10μm defocused electron beam. Peak counting times for major elements were 5-10 s. Sulfur, chlorine, and fluorine were measured as the last elements with 30 nA beam current and the counting times for S, Cl, and F were 30, 30 and 60 s, respectively. BaSO$_4$, ZnS, NaCl, and SrF$_2$ were used as standard materials for S, Cl, and F analyzes.
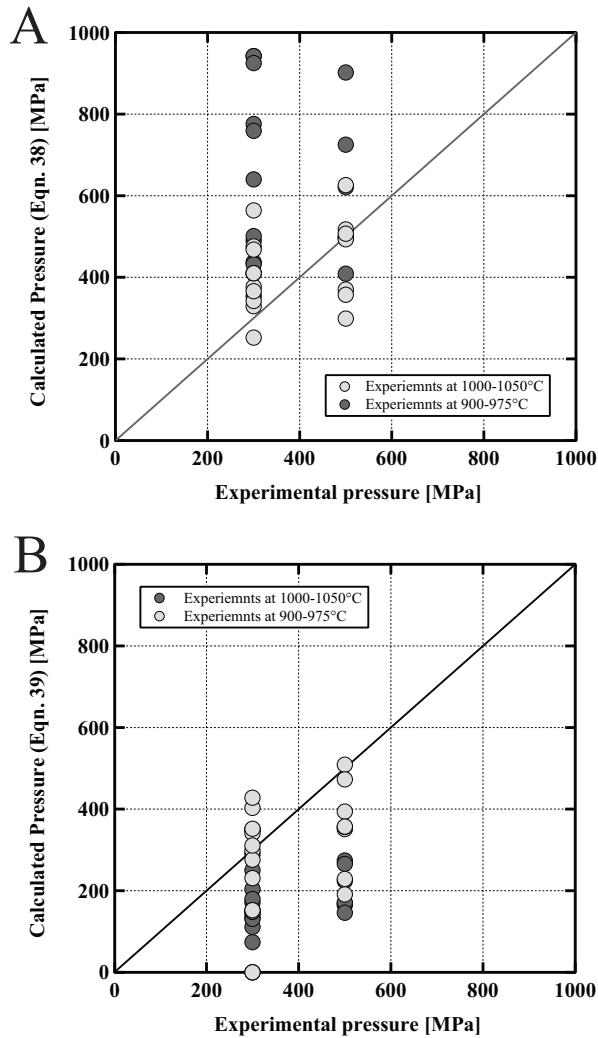
Figure AF4: A Experimental pressures vs. calculated pressures from experimental pyroxene pairs using Eqn. 38 from Putirka (2008). Calculation is independent of a *T* input-parameter. **B** Experimental pressures vs. calculated pressures from experimental pyroxene pairs using Eqn. 39 from Putirka (2008). Experimental *T* is included in the calculation.

Table AT2: Clinopyroxene and Orthopyroxene compositions used for temperature calculations using Quilf95 after Andersen *et al.* (1993).

Sample	Clinopyroxene composition										Orthopyroxene composition										Quilf95 (1993)	
	SiO$_2$	TiO$_2$	Al$_2$O$_3$	FeO$_{tot}$	MnO	MgO	CaO	Na$_2$O	K$_2$O	Total	SiO$_2$	TiO$_2$	Al$_2$O$_3$	FeO$_{tot}$	MnO	MgO	CaO	Na$_2$O	K$_2$O	Total	T [°C]	Error [°C]
LAS07-07 Px-pair_1	51.08	0.58	2.30	8.01	0.28	15.18	21.54	0.43	0.02	99.49	54.20	0.21	0.85	15.52	0.49	26.74	1.45	0.03	0.00	99.51	996	56
LAS07-07 Px-pair_2	51.21	0.52	2.18	8.12	0.29	15.36	21.11	0.41	0.01	99.25	54.22	0.24	0.84	14.87	0.55	27.05	1.61	0.03	0.01	99.4	1034	55
LAS07-07 Px-pair_3	51.45	0.58	2.32	8.26	0.36	15.46	21.24	0.38	0.01	100.07	53.47	0.39	1.52	15.50	0.53	26.75	1.80	0.02	0.00	100.04	1045	50
LAS07-07 Px-pair_4	50.76	0.68	2.58	7.96	0.38	15.19	21.38	0.34	0.00	99.29	54.03	0.22	0.79	15.07	0.53	27.12	1.37	0.01	0.01	99.17	986	59
LAS07-07 Px-pair_5	51.72	0.47	1.72	7.98	0.34	16.04	20.86	0.34	0.01	99.47	52.78	0.34	1.61	15.74	0.62	26.05	1.34	0.00	0.01	98.53	990	20
LAS07-07 Px-pair_6	51.54	0.53	2.11	8.16	0.37	15.57	21.18	0.38	0.01	99.89	54.31	0.21	0.73	14.87	0.54	26.85	1.60	0.02	0.01	99.17	1031	51
LAS07-07 Px-pair_7	51.73	0.42	1.75	7.74	0.34	15.85	21.03	0.35	0.01	99.31	53.26	0.32	1.59	15.12	0.60	26.54	1.41	0.04	0.01	98.95	998	31
LAS07-07 Px-pair_8	49.23	1.13	3.85	9.07	0.28	14.39	20.85	0.45	0.01	99.27	52.88	0.47	1.95	15.32	0.49	26.55	1.63	0.00	0.00	99.36	1029	88
LAS07-07 Px-pair_9	51.81	0.43	1.68	8.04	0.33	16.08	21.18	0.31	0.00	99.9	54.30	0.21	0.75	15.33	0.49	27.18	1.51	0.02	0.00	99.88	1011	33
LAS07-07 Px-pair_10	52.28	0.50	1.83	7.88	0.37	15.93	21.23	0.31	0.01	100.34	53.30	0.29	1.75	15.43	0.52	26.64	1.54	0.01	0.00	99.51	1010	32
LAS07-26 Px-pair_1	50.34	0.58	3.54	8.16	0.09	14.58	22.28	0.40	0.01	99.99	53.74	0.19	2.38	14.90	0.33	26.99	1.37	0.07	0.00	99.98	954	90
LAS07-26 Px-pair_2	51.35	0.64	4.02	7.71	0.15	15.48	21.59	0.37	0.02	101.32	54.40	0.21	1.51	16.13	0.38	25.83	1.62	0.04	0.00	100.12	907	214
LAS07-26 Px-pair_3	49.64	0.43	2.76	7.53	0.20	15.75	23.31	0.34	0.01	99.97	52.94	0.17	2.68	12.95	0.35	29.19	1.67	0.03	0.02	100.00	1009	101
LAS07-26 Px-pair_4	46.72	0.42	1.56	9.76	0.48	15.35	25.24	0.37	0.01	99.91	47.90	0.34	2.26	21.38	0.68	25.34	1.99	0.05	0.01	99.96	938	100
LAS07-26 Px-pair_5	52.18	0.58	1.94	9.21	0.32	14.87	20.77	0.35	0.01	100.21	54.19	0.26	1.06	18.55	0.53	25.71	1.36	0.02	0.00	101.67	954	42
LAS07-26 Px-pair_6	53.40	0.40	2.38	7.98	0.21	16.53	19.95	0.32	0.00	101.17	54.39	0.38	1.80	16.00	0.30	26.81	1.79	0.05	0.00	101.52	1060	19
LAS07-26 Px-pair_7	51.93	0.47	1.89	8.79	0.30	15.08	21.18	0.39	0.01	100.03	53.52	0.20	1.22	18.98	0.62	24.78	1.45	0.03	0.01	100.80	974	30
LAS07-26 Px-pair_8	52.68	0.59	2.05	9.31	0.29	15.62	20.48	0.41	0.01	101.43	53.79	0.33	1.83	16.60	0.42	26.14	1.59	0.03	0.01	100.74	1023	49
LAS07-26 Px-pair_9	52.46	0.45	1.71	8.48	0.40	15.08	21.54	0.36	0.01	100.49	54.25	0.39	1.52	16.07	0.48	26.12	1.96	0.04	0.01	100.83	1066	63
LAS07-26 Px-pair_10	52.81	0.38	2.96	5.42	0.15	16.82	21.28	0.30	0.01	100.14	55.17	0.20	1.66	13.70	0.31	29.25	1.37	0.01	0.00	101.67	979	31
LAS07-26 Px-pair_11	52.52	0.53	1.78	8.16	0.31	15.33	21.17	0.30	0.01	100.11	54.15	0.29	1.28	17.98	0.66	25.26	1.35	0.01	0.02	101.01	944	20
LAS07-26 Px-pair_12	51.36	0.56	3.68	7.52	0.20	15.52	21.16	0.29	0.01	100.30	54.90	0.22	1.04	16.20	0.44	26.95	1.30	0.02	0.01	101.08	962	34
LAS07-26 Px-pair_13	51.22	0.64	3.05	10.31	0.17	13.75	20.91	0.49	0.01	100.57	54.27	0.22	2.16	15.41	0.31	27.16	1.35	0.04	0.02	100.93	977	131

Table AT5: Representative composition of homogenized and non-homogenized melt inclusions of host Plag, Cpx, and Opx phenocrysts from sample LAS07-26 (white Pumice).

Sample	Pl	Opx	Cpx	homogenized	SiO_2	TiO_2	Al_2O_3	FeO_{tot}	MnO	MgO	CaO	Na_2O	K_2O	P_2O_5	S	Cl	F	Total	$H2O^a$
MI 1	X			X	74.59	0.84	12.32	1.81	0.00	0.28	1.17	3.36	4.32	0.10	0.004	0.052	0.069	98.92	1.08
MI 2	X			X	73.54	0.94	12.21	2.14	0.00	0.30	1.08	3.10	4.55	0.05	0.002	0.053	0.029	97.99	2.01
MI 3	X			X	73.35	0.88	12.26	1.87	0.00	0.27	0.94	3.06	4.36	0.08	0.002	0.052	0.095	97.21	2.79
MI 4	X			X	72.93	0.59	12.06	2.37	0.19	0.47	1.37	2.48	4.09	0.13	0.002	0.094	0.017	96.78	3.22
MI 5	X			X	71.08	1.08	13.93	1.96	0.04	0.32	1.76	4.14	4.54	0.22	0.009	0.087	0.027	99.19	0.81
MI 6	X			X	73.19	0.86	13.55	1.72	0.12	0.22	1.37	3.69	4.44	0.11	0.005	0.049	0.103	99.43	0.57
MI 7	X			X	72.77	0.89	12.44	3.10	0.03	0.59	1.55	3.49	4.01	0.13	0.003	0.108	0.061	99.18	0.82
MI 8	X			X	71.19	0.58	13.64	2.52	0.10	0.40	2.19	4.18	3.85	0.08	0.006	0.096	0.063	98.91	1.09
MI 9	X			X	71.17	0.75	13.38	3.21	0.07	0.70	2.18	4.33	4.14	0.12	0.007	0.153	0.052	100.26	-0.26
MI 10	X			X	71.00	0.63	13.32	2.41	0.12	0.67	2.07	4.42	3.84	0.08	0.005	0.140	0.069	98.77	1.23
MI 11	X			X	71.44	0.57	14.04	2.81	0.00	0.55	2.20	3.97	4.10	0.06	0.018	0.173	0.114	100.04	-0.04
MI 12	X			X	71.78	1.20	13.63	2.12	0.10	0.34	2.04	3.90	4.30	0.28	0.008	0.164	0.126	99.99	0.01
MI 13	X			X	69.88	0.53	16.37	1.32	0.00	0.17	3.06	4.46	3.90	0.06	0.004	0.103	0.074	99.93	0.07
MI 14	X			X	72.87	1.10	13.12	2.26	0.00	0.30	1.55	3.71	4.68	0.24	0.004	0.150	0.107	100.08	-0.08
MI 15	X			X	72.03	0.72	13.26	2.31	0.00	0.63	1.81	3.58	4.00	0.07	0.005	0.165	0.046	98.63	1.37
MI 16	X			X	69.42	0.63	16.19	1.28	0.02	0.27	3.11	5.30	3.39	0.06	0.003	0.083	0.036	99.79	0.21
MI 17	X				74.64	1.03	12.17	2.17	0.00	0.30	0.84	2.68	4.65	0.21	0.000	0.066	0.040	98.79	1.21
MI 18	X				74.06	0.64	12.19	2.65	0.03	0.61	1.19	3.51	4.42	0.09	0.009	0.122	0.102	99.62	0.38
MI 19	X				73.68	0.89	12.41	3.20	0.00	0.72	1.42	3.67	4.30	0.13	0.009	0.104	0.077	100.61	-0.61
MI 20	X				72.80	1.06	11.87	2.70	0.13	0.41	1.18	3.59	4.64	0.23	0.007	0.122	0.044	98.79	1.21
MI 21	X				74.06	0.64	11.83	3.16	0.00	0.69	1.25	3.61	3.95	0.09	0.013	0.104	0.122	99.52	0.48
MI 22	X				73.74	1.03	12.10	2.21	0.00	0.31	1.07	3.64	4.86	0.17	0.006	0.067	0.000	99.22	0.78
MI 23	X				72.25	0.70	12.02	2.88	0.12	0.67	1.38	3.85	4.65	0.09	0.009	0.116	0.089	98.81	1.19
MI 24	X				73.87	0.64	11.75	2.23	0.13	0.50	1.31	3.64	4.51	0.09	0.011	0.098	0.088	98.88	1.12
MI 25	X				69.96	0.63	16.00	1.71	0.12	0.25	2.78	3.75	3.61	0.11	0.000	0.041	0.000	98.94	1.06
MI 26	X				73.15	0.87	12.13	2.61	0.07	0.54	1.16	3.40	4.56	0.14	0.001	0.122	0.000	98.75	1.25
MI 27		X		X	70.89	0.49	13.83	5.66	0.04	1.17	2.24	2.88	3.93	0.10	0.006	0.108	0.078	101.44	-1.44
MI 28		X		X	70.39	0.37	14.70	4.71	0.18	1.14	2.22	3.84	3.74	0.21	0.007	0.050	0.020	101.58	-1.58
MI 29		X		X	70.85	0.83	14.66	2.92	0.16	0.78	1.42	3.91	4.47	0.15	0.000	0.058	0.075	100.29	-0.29
MI 30		X		X	75.82	0.53	11.82	2.57	0.02	0.68	1.46	3.22	3.80	0.06	0.008	0.087	0.000	100.07	-0.07
MI 31		X		X	73.03	0.45	13.93	2.74	0.07	0.79	1.78	3.25	4.18	0.10	0.006	0.094	0.160	100.57	-0.57
MI 32		X		X	70.00	0.79	14.82	3.94	0.04	1.39	3.04	3.75	3.68	0.16	0.009	0.100	0.049	101.78	-1.78
MI 33		X		X	69.90	1.08	16.35	2.40	0.10	0.87	2.78	3.34	4.00	0.10	0.003	0.097	0.043	101.08	-1.08
MI 34		X		X	65.43	0.64	17.70	2.54	0.10	1.71	6.20	2.82	2.92	0.05	0.010	0.067	0.099	100.28	-0.28
MI 35		X		X	66.33	0.57	17.08	3.38	0.09	1.21	3.00	4.22	4.34	0.25	0.026	0.099	0.170	100.77	-0.77
MI 36		X		X	72.29	0.41	15.60	2.22	0.00	0.31	2.59	3.92	3.59	0.04	0.000	0.045	0.010	101.03	-1.03
MI 37		X		X	70.80	0.55	14.46	2.67	0.13	1.11	2.41	3.59	4.22	0.10	0.000	0.086	0.152	100.29	-0.29
MI 38		X			71.60	0.45	14.54	3.31	0.12	1.06	2.35	3.69	3.51	0.07	0.004	0.113	0.114	100.93	-0.93
MI 39		X			71.85	0.68	13.31	2.78	0.12	0.88	2.39	3.10	3.68	0.18	0.015	0.118	0.110	99.21	0.78
MI 40		X			70.46	0.76	14.74	3.22	0.12	1.00	2.79	2.50	3.44	0.24	0.019	0.141	0.084	99.51	0.48
MI 41		X			70.11	0.69	15.38	2.71	0.00	1.24	2.79	2.59	3.61	0.21	0.004	0.051	0.063	99.44	0.55
MI 42		X			70.93	0.69	15.02	2.99	0.12	1.05	2.82	2.90	3.55	0.10	0.010	0.096	0.095	100.37	-0.37
MI 43		X			70.71	0.78	14.88	2.75	0.17	0.67	1.52	4.51	4.56	0.17	0.014	0.102	0.078	100.91	-0.91
MI 44		X			72.88	0.39	13.60	2.46	0.14	0.81	1.71	3.69	4.17	0.09	0.008	0.078	0.096	100.12	-0.12
MI 45		X			70.33	0.49	14.35	3.29	0.02	1.01	2.34	3.33	3.51	0.04	0.011	0.113	0.106	98.90	1.1
MI 46		X			71.31	0.50	14.94	3.20	0.11	1.01	2.44	3.87	3.67	0.04	0.010	0.110	0.029	101.23	-1.23
MI 47		X			70.56	0.48	14.71	3.07	0.05	0.91	2.61	3.57	3.51	0.04	0.016	0.107	0.079	99.71	0.288
MI 50			X	X	66.84	0.65	13.77	6.57	0.00	1.69	4.22	2.31	3.73	0.13	0.018	0.098	0.002	99.99	0.01
MI 51			X	X	64.84	0.80	13.85	6.63	0.13	1.96	4.37	3.04	3.25	0.10	0.024	0.080	0.030	99.10	0.90
MI 52			X	X	76.32	0.57	12.18	2.25	0.00	0.45	1.42	3.18	4.45	0.03	0.005	0.081	0.030	100.92	-0.92
MI 53			X	X	71.95	0.66	13.82	3.40	0.06	0.80	2.19	3.90	4.02	0.06	0.000	0.048	0.108	101.01	-1.01
MI 54			X	X	73.72	0.68	13.46	2.06	0.12	0.50	1.21	2.53	4.89	0.02	0.000	0.101	0.095	99.39	0.61
MI 55			X	X	71.27	0.60	12.12	4.13	0.10	1.14	3.76	1.27	3.86	2.35	0.025	0.117	0.444	101.20	-1.20
MI 56			X	X	71.61	0.68	13.25	2.07	0.00	0.56	1.27	3.81	4.89	0.14	0.005	0.096	0.126	98.44	1.56
MI 57			X	X	69.29	0.48	15.97	1.73	0.02	0.37	3.05	4.49	3.52	0.04	0.000	0.055	0.109	99.11	0.89
MI 58			X	X	73.46	0.53	12.66	1.72	0.04	0.50	1.16	3.23	4.75	0.08	0.015	0.069	0.052	98.21	1.79
MI 59			X	X	69.19	0.60	12.76	4.00	0.06	1.41	3.28	3.30	3.72	0.11	0.023	0.062	0.149	98.66	1.34
MI 60			X	X	75.65	0.73	12.58	2.06	0.00	0.58	1.41	3.87	4.24	0.05	0.005	0.037	0.046	101.10	-1.10
MI 61			X	X	70.03	0.55	12.85	5.40	0.06	0.65	2.21	3.98	4.56	0.19	0.007	0.156	0.036	100.68	-0.68
MI 62			X		72.72	0.30	12.30	3.61	0.21	0.82	2.00	3.61	4.25	0.00	0.012	0.086	0.025	99.94	0.05
MI 63			X		72.45	0.37	12.58	3.29	0.14	0.74	1.89	3.25	4.22	0.08	0.019	0.077	0.021	99.12	0.87
MI 64			X		68.24	0.68	13.82	4.82	0.00	0.80	2.55	3.87	3.96	0.24	0.011	0.106	0.058	99.15	0.84
MI 65			X		71.25	0.56	14.76	3.35	0.12	1.24	2.97	2.03	3.63	0.06	0.000	0.035	0.024	100.02	-0.02
MI 66			X		70.46	0.38	13.83	4.39	0.05	0.56	2.20	3.67	4.15	0.10	0.017	0.048	0.004	99.85	0.14
MI 67			X		72.08	0.69	11.11	2.48	0.00	1.63	2.73	3.53	3.94	0.11	0.013	0.111	0.035	98.45	1.54
MI 68			X		73.03	0.66	11.62	2.64	0.02	1.18	2.47	3.59	4.34	0.12	0.020	0.117	0.015	99.82	0.17
MI 69			X		68.25	0.57	13.97	5.76	0.23	1.28	2.68	3.27	4.31	0.12	0.012	0.095	0.013	100.56	-0.56
MI 70			X		66.15	0.41	12.36	4.48	0.17	2.76	5.57	3.55	3.38	0.00	0.016	0.088	0.020	98.95	1.04

^{a} H_2O = 100% - microprobe analytical total

Table AT6.1: Composition of experimental phases (300 MPa; NNO+1.5).

Sample	T°C	Phase	n	SiO$_2$	TiO$_2$	Al2O3	FeO[a]	MnO	MgO	CaO	Na$_2$O	K$_2$O	P$_2$O$_5$	Total	#Mg[b]	#Ca[c]
Las-45	1040	Gl	8	53.35 (0.63)	0.78 (0.03)	15.80 (0.17)	5.93 (0.14)	0.11 (0.03)	4.53 (0.14)	6.48 (0.11)	1.25 (0.29)	1.45 (0.21)	0.19 (0.01)	92.88 (0.53)	0.58	0.85
Las-46	1040	Gl	5	56.47 (0.31)	0.78 (0.03)	16.04 (0.05)	6.00 (0.17)	0.14 (0.04)	4.32 (0.08)	6.59(0.08)	1.70 (0.14)	1.59 (0.02)	0.17 (0.01)	93.81 (0.56)	0.56	0.81
		Ol	8	40.02 (0.20)	0.02 (0.01)	0.03 (0.02)	16.52 (0.23)	0.26 (0.06)	44.62 (0.23)	0.19 (0.04)	0.01 (0.01)	0.01)0.01)	0.07 (0.02)	101.75 (0.33)	0.83	0.95
Las-47	1040	Gl	5	57.59 (0.24)	0.82 (0.02)	16.74 (0.07)	5.82 (0.16)	b.d.	3,69 (0.11)	6.64 (0.09)	1.94 (0.19)	1.69 (0.06)	0.18 (0.01)	95.24 (0.32)	0.53	0.79
		Cpx	7	52.13 (1.04)	0.45 (0.12)	3.25 (0.88)	7.27 (0.41)	0.19 (0.06)	17.13 (0.5&)	19.51 (0.53)	0.34 (0.08)	0.08 (0.06)	0.03 (0.03)	100.39 (0.39)	0.81	0.98
		Opx	9	54.99 (0.24)	0.20 (0.01)	1.73 (0.26)	12.17 (0.41)	0.26 (0.06)	30.14 (0.37)	1.78 (0.15)	0.04 (0.01)	0.02 (0.01)	0.02 (0.03)	101.33 (0.43)	0.82	0.98
Las-48	1040	Gl	5	58.60 (0.13)	0.82 (0.02)	17.55 (0.19)	5.82 (0.11)	0.09 (0.02)	3.17 (0.08)	6.62 (0.16)	2.49 (0.07)	1.80 (0.04)	0.21 (0.01)	97.18 (0.18)	0.49	0.75
		Cpx	8	50.83 (1.17)	0.56 (0.11)	4.49 (0.71)	8.20 (0.58)	0.20 (0.04)	15.59 (0.41)	19.48 (0.46)	0.38 (0.06)	0.07 (0.05)	0.09 (0.02)	99.89 (0.48)	0.77	0.98
		Opx	5	50.55 (0.52)	0.42 (0.04)	1.41 (0.32)	27.95 (1.28)	0.47 (0.06)	14.75 (0.81)	4.67 (0.24)	0.10 (0.07)	0.02 (0.01)	0.05 (0.03)	100.37 (0.29)	0.48	0.98
Las-49	1040	Gl	5	67.10 (0.76)	1.49 (0.05)	14.51 (0.05)	4.89 (0.29)	b.d.	1.14 (0.03)	3.55 (0.05)	1,92 (0.76)	3.64 (0.13)	0.40 (0.04)	98.73 (0.41)	0.29	0.67
Las-16	1025	Gl	3	57.70 (0.63)	0.83 (0.05)	16.61 (0.26)	5.63 (0.34)	0.15 (0.11)	2.89 (0.17)	6.14 (0.17)	3.12 (0.19)	1.96 (0.03)	0.19 (0.02)	95.33 (0.47)	0.48	0.69
		Ol	7	40.01 (0.41)	0.01 (0.01)	0.03 (0.01)	15.29 (0.39)	0.26 (0.06)	45.71 (0.42)	0.13 (0.03)	0.01 (0.01)	0.01 (0.01)	0.07 (0.03)	101.53 (0.53)	0.84	0.93
Las-17	1025	Gl	3	54.65 (0.61)	0.74 (0.01)	14.95 (0.06)	5.83 (0.16)	0.12 (0.09)	4.48 (0.30)	6.50 (0.14)	2.62 (0.21)	1.67 (0.06)	0.21 (0.02)	91.94 (1.03)	0.58	0.73
		Cpx	8	52.03 (0.51)	0.45 (0.05)	3.06 (0.42)	7.42 (0.51)	0.20 (0.06)	16.96 (0.33)	19.84 (0.53)	0.27 (0.03)	0.03 (0.01)	0.03 (0.03)	100.28 (0.46)	0.80	0.99
		Opx	9	54.84 (0.24)	0.21 (0.02)	2.26 (0.23)	12.07 (0.40)	0.29 (0.03)	29.86 (0.19)	1.68 (0.12)	0.03 (0.2)	0.02 (0.1)	0.01 (0.02)	101.27 (0.37)	0.82	0.98
Las-18	1025	Gl	4	57.19 (2.08)	0.78 (0.04)	15.87 (0.44)	6.19 (0.38)	0.14 (0.09)	3.81 (0.12)	6.77 (0.20)	2.85 (0.21)	1.86 (0.16)	0.19 (0.02)	94.57 (0.70)	0.52	0.72
		Cpx	6	52.71 (0.85)	0.35 (0.06)	2.74 (0.52)	7.01 (0.20)	0.22 (0.06)	17.84 (0.53)	19.50 (0.46)	0.33 (0.05)	0.06 (0.03)	0.05 (0.02)	100.80 (0.46)	0.82	0.98
		Opx	6	55.43 (0.44)	0.17 (0.04)	1.65 (0.49)	11.07 (0.55)	0.27 (0.02)	30.95 (0.48)	1.78 (0.15)	0.03 (0.02)	0.02 (0.01)	0.02 (0.03)	101.39 (0.41)	0.83	0.98
Las-19	1025	Gl	3	66.54 (1.01)	1.42 (0.05)	13.50 (0.14)	4.36 (0.37)	b.d.	1.03 (0.04)	3.08 (0.08)	1.92 (0.27)	3.93 (0.30)	0.41 (0.02)	96.39 (0.99)	0.30	0.64
		Opx	5	52.92 (0.27)	0.37 (0.07)	1.56 (0.97)	20.03 (0.69)	0.42 (0.05)	21.14 (1.19)	4.07 (1.03)	0.17 (0.17)	0.04 (0.02)	0.06 (0.03)	100.80 (0.47)	0.65	0.96
Las-20	1025	Gl	3	67.07 (0.66)	1.27 (0.06)	13.45 (0.15)	4.41 (0.16)	0.09 (0.06)	0.97 (0.05)	2.92 (0.11)	2.95 (0.10)	4.23 (0.17)	0.33 (0.02)	97.85 (0.80)	0.28	0.52
Las-30	1000	Gl	4	55.93 (0.33)	0.69 (0.06)	15.09 (0.57)	5.93 (0.33)	0.15 (0.07)	3.69 (0.08)	6.44 (0.15)	2.60 (0.18)	1.58 (0.11)	0.19 (0.05)	92.29 (0.17)	0.53	0.73
		Ol	8	39.81 (0.17)	0.01 (0.01)	0.02 (0.2)	17.41 (0.32)	0.30 (0.05)	43.98 (0.30)	0.17 (0.03)	0.02 (0.02)	0.01 (0.01)	0.09 (0.01)	101.82 (0.23)	0.82	0.90
		Cpx	5	52.94 (0.50)	0.31 (0.03)	2.06 (0.30)	5.92 (0.16)	0.18 (0.4)	17.86 (0.43)	20.59 (0.37)	0.25 (0.03)	0.05 (0.02)	0.03 (0.01)	100.20 (0.40)	0.84	0.99
Las-31	1000	Gl	3	55.43 (0.04)	0.73 (0.05)	15.33 (0.04)	5.55 (0.51)	0.17 (0.09)	3.67 (0.08)	6.28 (0.17)	2.83 (0.09)	1.78 (0.13)	0.23 (0.01)	92.09 (0.40)	0.54	0.71
		Ol	6	39.49 (0.36)	0.01 (0.01)	0.02 (0.01)	18.83 (0.62)	0.30 (0.04)	42.48 (0.42)	0.20 (0.03)	0.00 (0.01)	0.01 (0.01)	0.20 (0.06)	101.54 (0.67)	0.80	1.00
		Cpx	6	52.68 (0.98)	0.35 (0.08)	2.37 (0.66)	6.52 (0.35)	0.20 (0.04)	16.96 (0.45)	20.86 (0.17)	0.31 (0.06)	0.07 (0.02)	0.02 (0.03)	100.35 (0.79)	0.82	0.99
Las-32	1000	Gl	3	55.54 (0.14)	0.81 (0.04)	15.40 (0.11)	5.66 (0.06)	0.15 (0.03)	3.71 (0.09)	6.21 (0.07)	2.72 (0.10)	1.85 (0.06)	0.20 (0.01)	92.18 (0.53)	0.54	0.72
		Ol	7	39.10 (0.11)	0.01 (0.01)	0.01 (0.01)	19.37 (0.50)	0.29 (0.07)	43.15 (0.32)	0.17 (0.02)	0.03 (0.01)	0.01 (0.01)	0.15 (0.03)	102.28 (0.48)	0.80	0.90
		Cpx	8	52.62 (0.68)	0.39 (0.07)	2.45 (0.49)	6.67 (0.45)	0.20 (0.05)	17.22 (0.40)	20.53 (0.39)	0.27 (0.04)	0.04 (0.01)	0.10 (0.05)	100.48 (0.37)	0.82	0.99
Las-33	1000	Gl	6	59.17 (0.23)	0.92 (0.04)	16.03 (0.20)	5.61 (0.42)	0.13 (0.05)	2.15 (0.12)	5.17 (0.12)	3.20 (0.10)	2.23 (0.13)	0.24 (0.02)	94.95 (0.52)	0.41	0.64
		Cpx	7	50.87 (0.62)	0.70 (0.06)	4.28 (0.67)	9.76 (0.50)	0.24 (0.05)	15.28 (0.56)	18.53 (0.68)	0.39 (0.07)	0.09 (0.04)	0.07 (0.05)	100.21 (0.51)	0.74	0.98
		Opx	8	53.10 (0.23)	0.32 (0.03)	2.30 (0.29)	16.87 (0.46)	0.31 (0.06)	25.46 (0.24)	1.99 (0.18)	0.02 (0.02)	0.03 (0.03)	0.04 (0.02)	100.42 (0.34)	0.73	0.99
Las-55	975	Gl	7	56.20 (0.33)	0.74 (0.05)	15.85 (0.21)	5.22 (0.21)	0.10 (0.06)	2.87 (0.10)	5.77 (0.12)	3.02 (0.17)	1.66 (0.05)	0.16 (0.11)	91.59 (0.43)	0.49	0.68
		Ol	10	38.39 (0.24)	0.01 (0.01)	0.02 (0.02)	23.74 (0.36)	0.34 (0.10)	37.44 (0.32)	0.15 (0.02)	0.01 (0.01)	0.01 (0.01)	0.07 (0.04)	100.18 (0.34)	0.74	0.94
		Cpx	10	53.18 (0.36)	0.32 (0.05)	1.70 (0.40)	7.12 (0.47)	0.21 (0.04)	17.01 (0.45)	19.92 (0.76)	0.19 (0.03)	0.04 (0.01)	0.02 (0.03)	99.70 (0.39)	0.81	0.99
Las-56	975	Gl	5	56.97 (0.16)	0.76 (0.04)	16.14 (0.14)	5.01 (0.25)	0.12 (0.08)	2.78 (0.12)	5.70 (0.05)	3.23 (0.17)	1.76 (0.08)	0.18 (0.05)	92.65 (0.22)	0.50	0.66
		Ol	10	38.38 (0.21)	0.01 (0.01)	0.01 (0.01)	24.26 (0.46)	0.34 (0.05)	37.13 (0.24)	0.18 (0.06)	0.01 (0.01)	0.05 (0.02)	0.07 (0.03)	100.37 (0.44)	0.73	0.95
		Cpx	8	51.43 (0.31)	0.49 (0.08)	3.09 (0.41)	7.59 (0.29)	0.24 (0.05)	15.86 (0.36)	20.38 (0.50)	0.27 (0.03)	0.04 (0.01)	0.03 (0.02)	99.42 (0.39)	0.79	0.99
		Opx	7	53.82 (0.60)	0.24 (0.03)	2.50 (0.36)	13.83 (0.86)	0.30 (0.05)	26.35 (0.68)	1.84 (0.35)	0.05 (0.03)	0.02 (0.01)	0.02 (0.2)	98.97 (0.46)	0.77	0.98
Las-57	975	Gl	7	57.90 (0.44)	0.75 (0.05)	16.59 (0.25)	5.06 (0.17)	0.10 (0.09)	2.15 (0.10)	5.32 (0.17)	3.42 (0.21)	1.94 (0.07)	0.20 (0.10)	93.43 (0.20)	0.43	0.63
		Cpx	9	49.77 (0.53)	0.68 (0.05)	4.86 (0.66)	8.51 (0.35)	0.20 (0.05)	14.30 (0.35)	20.46 (0.38)	0.34 (0.05)	0.04 (0.03)	0.05 (0.02)	99.20 (0.36)	0.75	0.99
		Opx	9	52.99 (0.37)	0.26 (0.03)	2.57 (0.38)	15.92 (0.24)	0.36 (0.04)	24.89 (0.22)	1.68 (0.13)	0.05 (0.03)	0.04 (0.03)	0.05 (0.02)	98.83 (0.41)	0.74	0.97
Las-58	975	Gl	9	61.33 (0.41)	0.95 (0.04)	16.20 (0.24)	4.78 (0.15)	0.10 (0.08)	1.65 (0.09)	4.46 (0.19)	3.78 (0.13)	2.35 (0.07)	0.25 (0.10)	95.86 (0.49)	0.38	0.57
		Cpx	7	50.86 (0.78)	0.71 (0.09)	3.65 (1.03)	10.22 (0.54)	0.26 (0.06)	14.19 (0.44)	18.64 (0.67)	0.29 (0.08)	0.07 (0.04)	0.06 (0.03)	98.94 (0.43)	0.71	0.99
		Opx	10	53.59 (0.33)	0.21 (0.06)	1.08 (0.22)	18.77 (0.31)	0.52 (0.03)	24.02 (0.36)	1.38 (0.21)	0.02 (0.03)	0.01 (0.01)	0.03 (0.02)	99.63 (0.53)	0.70	0.99
		Pl	5	53.81 (0.57)	0.16 (0.06)	27.68 (0.84)	1.10 (0.23)	0.03 (0.05)	0.35 (0.09)	11.82 (0.49)	3.73 (0.13)	0.49 (0.13)	0.07 (0.05)	99.28 (0.55)	0.36	0.78
Las-35	950	Gl	3	54.81 (1.55)	16.25 (0.81)	0.69 (0.01)	5.40 (0.09)	0.07 (0.04)	2.59 (0.30)	5.68 (0.15)	2.91 (0.35)	1.72 (0.04)	0.20 (0.02)	90.31 (1.61)	0.46	0.68
		Cpx	5	51.64 (0.48)	0.45 (0.08)	3.10 (0.55)	8.34 (0.34)	0.25 (0.01)	15.96 (0.69)	20.39 (0.47)	0.28 (0.03)	0.04 (0.01)	0.04 (0.03)	100.50 (0.30)	0.77	0.99
		Opx	5	55.07 (0.39)	0.15 (0.02)	1.21 (0.34)	15.28 (0.63)	0.38 (0.05)	27.68 (0.44)	1.66 (0.22)	0.02 (0.02)	0.06 (0.04)	0.06 (0.04)	101.53 (0.49)	0.76	0.99
		Hbl	8	44.44 (0.59)	1.71 (0.06)	11.05 (0.44)	9.93 (0.36)	0.14 (0.06)	16.84 (0.32)	11.26 (0.18)	2.13 (0.09)	0.47 (0.04)	0.08 (0.03)	98.04 (0.37)	0.75	0.85
Las-36	950	Gl	6	57.53 (0.36)	0.70 (0.03)	16.27 (0.22)	5.24 (0.29)	0.13 (0.06)	2.34 (0.13)	5.41 (0.25)	3.27 (0.11)	1.74 (0.06)	0.22 (0.04)	92.86 (0.32)	0.44	0.65
		Cpx	6	50.75 (0.98)	0.62 (0.12)	4.10 (0.32)	7.71 (0.32)	0.23 (0.06)	15.55 (0.57)	20.59 (0.50)	0.33 (0.04)	0.07 (0.08)	0.07 (0.02)	100.02 (0.37)	0.78	0.99
		Opx	5	53.63 (0.67)	0.24 (0.04)	2.30 (0.56)	15.85 (0.38)	0.36 (0.04)	27.13 (0.50)	1.59 (0.27)	0.03 (0.01)	0.01 (0.01)	0.00	101.15 (0.18)	0.75	0.98
		Hbl	6	43.91 (0.43)	2.04 (0.09)	10.92 (0.45)	11.11 (0.35)	0.15 (0.05)	15.70 (0.41)	10.98 (0.12)	2.07 (0.06)	0.50 (0.03)	0.04 (0.03)	97.45 (0.30)	0.72	0.85
		Pl	5	49.85 (0.50)	0.07 (0.03)	31.21 (0.63)	0.73 (0.03)	0.01 (0.02)	0.20 (0.07)	14.83 (0.55)	2.66 (0.17)	0.23 (0.05)	0.08 (0.02)	99.85 (0.72)	0.33	0.86
Las-37	950	Gl	3	58.15 (0.48)	16.72 (0.44)	0.86 (0.3)	5.21 (0.14)	0.10 (0.04)	1.76 (0.05)	5.00 (0.30)	3.34 (0.18)	2.09 (0.08)	0.29 (0.02)	93.50 (0.27)	0.38	0.62
		Cpx	9	50.63 (0.71)	0.83 (0.05)	4.66 (0.46)	9.75 (0.25)	0.25 (0.05)	14.72 (0.43)	18.99 (0.59)	0.44 (0.10)	0.11 (0.07)	0.15 (0.04)	100.52 (0.57)	0.73	0.98
		Opx	9	52.90 (0.37)	0.30 (0.07)	2.62 (0.31)	17.60 (0.63)	0.37 (0.06)	24.91 (0.45)	1.63 (0.06)	0.03 (0.01)	0.12 (0.02)	0.03 (0.02)	100.50 (0.39)	0.72	0.98
		Hbl	8	43.19 (0.31)	2.36 (0.54)	11.85 (0.19)	11.64 (0.29)	0.15 (0.03)	14.60 (0.57)	11.10 (0.16)	2.30 (0.07)	0.52 (0.06)	0.18 (0.04)	97.89 (0.43)	0.69	0.84
		Pl	7	52.57 (1.15)	0.22 (0.10)	27.64 1.49)	1.53 (0.52)	0.04 (0.03)	0.48 (0.16)	12.39 (0.97)	3.16 (0.33)	0.58 (0.20)	0.15 (0.05)	98.77 (0.61)	0.36	0.81
Las-38	950	Gl	3	61.03 (0.13)	15.96 0.20)	0.82 (0.01)	4.51 (0.03)	b.d.	1.26 (0.01)	4.07 (0.09)	3.27 (0.11)	2.60 (0.02)	0.31 (0.03)	93.92 (0.07)	0.33	0.58
		Cpx	7	51.27 (0.65)	0.79 (0.14)	3.97 (0.74)	11.18 (0.93)	0.30 (0.06)	14.35 (0.62)	18.04 (0.55)	0.45 (0.14)	0.13 (0.07)	0.06 (0.02)	100.54 (0.39)	0.70	0.98
		Opx	9	52.38 (0.42)	0.38 (0.05)	2.48 (0.40)	20.28 (0.28)	0.40 (0.05)	23.27 (0.55)	1.97 (0.24)	0.07 (0.05)	0.04 (0.05)	0.05 (0.03)	100.04 (0.61)	0.67	0.97
		Pl	6	54.36 (0.77)	0.25 (0.17)	27.13 (0.46)	1.94 (1.06)	0.02 (0.03)	0.32 (0.13)	11.04 (0.37)	4.34 (0.24)	0.53 (0.15)	0.12 (0.07)	100.04 (0.61)	0.23	0.74
		Mt	5	0.25 (0.03)	11.66 (0.09)	5.34 (0.09)	66.93 (0.48)	0.23 (0.06)	3.44 (0.08)	0.22 (0.03)	0.05 (0.05)	0.04 (0.01)	0.02 (0.02)	88.18 (0.47)	0.08	0.83
Las-65	925	Gl	7	59.27 (0.35)	0.45 (0.03)	15.84 (0.26)	4.38 (0.22)	0.10 (0.09)	1.72 (0.06)	5.27 (0.16)	2.97 (0.16)	1.90 (0.06)	0.24 (0.03)	92.14 (0.41)	0.41	0.66
		Cpx	4	49.56 (0.19)	0.51 (0.03)	3.66 (0.21)	9.33 (0.45)	0.24 (0.05)	13.58 (0.60)	20.35 (0.83)	0.28 (0.06)	0.03 (0.01)	0.03 (0.02)	97.60 (0.30)	0.72	0.99
		Opx	6	52.55 (0.21)	0.23 (0.02)	1.24 (0.39)	18.91 (0.55)	0.56 (0.04)	22.79 (0.41)	1.83 (0.46)	0.05 (0.06)	0.02 (0.2)	0.03 (0.02)	98.21 (0.57)	0.68	0.98
		Hbl	9	43.26 (0.21)	1.57 (0.08)	10.42 (0.19)	11.39 (0.27)	0.16 (0.04)	14.29 (0.22)	11.08 (0.35)	1.83 (0.06)	0.48 (0.02)	0.06 (0.04)	94.54 (0.44)	0.69	0.87
		Mt	5	0.20 (0.11)	5.11 (0.03)	4.15 (0.06)	80.13 (0.63)	0.35 (0.07)	2.65 (0.11)	0.19 (0.03)	0.02 (0.06)	0.03 (0.01)	0.02 (0.02)	92.85 (0.60)	0.06	0.91
Las-66	925	Gl	7	61.60 (0.45)	0.41 (0.03)	15.62 (0.31)	3.96 (0.11)	b.d.	1.31 (0.06)	4.19 (0.06)	3.94 (0.26)	2.21 (0.08)	0.23 (0.09)	93.50 (0.34)	0.37	0.54
		Cpx	4	52.44 (0.75)	0.35 (0.06)	6.12 (0.63)	8.83 (0.43)	0.32 (0.06)	11.20 (0.44)	17.03 (0.63)	0.74 (0.08)	0.39 (0.11)	0.07 (0.04)	97.50 (0.61)	0.69	0.96
		Hbl	10	43.39 (0.61)	1.68 (0.07)	10.68 (0.50)	11.31 (0.47)	0.16 (0.05)	14.08 (0.69)	10.71 (0.24)	1.85 (0.08)	0.47 (0.07)	0.10 (0.03)	94.44 (0.29)	0.69	0.86
		Pl	5	48.42 (0.39)	0.08 (0.01)	30.29 (0.27)	1.09 (0.11)	0.05 (0.04)	0.10 (0.04)	14.82 (0.27)	2.51 (0.15)	0.20 (0.02)	0.12 (0.02)	97.66 (0.58)	0.14	0.87
		Mt	6	0.16 (0.05)	5.87 (0.06)	4.19 (0.06)	80.15 (0.28)	0.26 (0.06)	2.35 (0.07)	0.18 (0.02)	0.04 (0.06)	0.02 (0.01)	0.02 (0.02)	93.24 (0.24)	0.05	0.83
Las-67	925	Gl	6	62.34 (0.29)	0.47 (0.04)	15.74 (0.24)	3.88 (0.07)	0.15 (0.08)	1.18 (0.9)	3.77 (0.22)	4.23 (0.27)	2.40 (0.08)	0.14 (0.4)	94.26 (0.26)	0.35	0.50
		Cpx	4	51.57 (0.84)	0.64 (0.15)	5.50 (0.57)	9.44 (0.24)	0.26 (0.04)	11.37 (0.52)	16.46 (0.48)	0.56 (0.20)	0.38 (0.08)	0.08 (0.01)	96.27 (1.30)	0.68	0.97
		Opx	4	53.02 (1.24)	0.32 (0.04)	4.41 (1.24)	17.62 (1.59)	0.43 (0.05)	18.41 (1.09)	2.28 (0.17)	0.26 (0.21)	0.28 (0.17)	0.06 (0.04)	97.08 (0.58)	0.65	0.91
		Hbl	8	42.28 (0.36)	2.33 (0.21)	11.22 (0.27)	13.03 (0.37)	0.18 (0.03)	12.72 (0.15)	11.02 (0.14)	2.00 (0.09)	0.54 (0.02)	0.08 (0.04)	95.40 (0.31)	0.64	0.86
		Pl	4	53.75 (1.22)	0.14 (0.07)	26.16 (1.71)	1.44 (0.38)	0.02 (0.02)	0.33 (0.13)	10.68 (1.29)	3.40 (0.27)	0.68 (0.28)	0.10 (0.08)	96.70 (1.10)	0.29	0.78
		Mt	6	0.13 (0.03)	7.77 (0.05)	3.98 (0.08)	77.88 0.33)	0.27 (0.04)	2.46 (0.10)	0.11 (0.02)	0.07 (0.08)	0.02 (0.01)	0.01 (0.02)	92.69 (0.48)	0.05	0.63
Las-68	925	Gl	6	64.77 (0.31)	0.58 (0.03)	15.08 (0.17)	3.43 (0.23)	b.d.	0.77 (0.16)	2.99 (0.25)	4.10 (0.32)	3.24 (0.8)	0.29 (0.12)	95.29 (0.25)	0.29	0.45
		Cpx	4	49.71 (0.96)	0.62 (0.04)	4.65 (0.47)	10.27 (0.41)	0.25 (0.04)	12.27 (0.47)	18.39 (0.76)	0.62 (0.18)	0.13 (0.12)	0.05 (0.03)	96.97 (0.46)	0.68	0.97
		Opx	8	51.08 (0.33)	0.41 (0.26)	2.48 (0.28)	19.76 (0.58)	0.49 (0.06)	20.62 (0.44)	1.74 (0.30)	0.30 (0.35)	0.04 (0.04)	0.05 (0.10)	96.97 (0.46)	0.65	0.87
		Pl	6	53.26 (0.24)	0.12 (0.08)	26.33 (1.25)	1.38 (0.59)	0.04 (0.04)	0.49 (0.49)	10.84 (0.46)	4.62 (0.33)	0.45 (0.10)	0.06 (0.01)	97.61 (0.49)	0.39	0.72
		Mt	5	0.19 (0.09)	9.92 (0.14)	3.74 (0.09)	73.98 (0.48)	0.22 (0.08)	2.45 (0.07)	0.08 (0.02)	0.08 (0.01)	0.00		90.64 (0.58)	0.06	0.64
Las-60	900	Gl	6	60.05 (0.36)	0.36 (0.03)	15.99 (0.31)	3.70 (0.17)	0.10 (0.07)	1.23 (0.13)	4.91 (0.07)	3.09 (0.24)	1.96 (0.05)	0.25 (0.05)	91.64 (0.28)	0.37	0.64
		Hbl	10	44.68 (0.68)	1.72 (0.06)	10.55 (0.80)	12.55 (0.46)	0.18 (0.03)	14.00 (0.36)	10.87 (0.25)	1.87 (0.08)	0.46 (0.05)	0.07 (0.02)	96.94 (0.40)	0.67	0.87
		Pl	9	46.93 (0.42)	0.01 (0.01)	33.47 (0.25)	0.47 (0.05)	0.00	0.02 (0.02)	17.17 (0.47)	1.67 (0.21)	0.07 (0.02)	0.04 (0.02)	99.85 (0.37)	0.01	0.92
Las-61	900	Gl	7	61.97 (0.33)	0.32 (0.03)	15.56 (0.16)	3.70 (0.16)	b.d.	1.17 (0.05)	4.11 (0.15)	3.25 (0.18)	2.12 (0.6)	0.22 (0.05)	92.49 (0.23)	0.36	0.58
		Hbl	10	44.28 (0.45)	1.81 (0.05)	10.81 (0.40)	12.99 (0.37)	0.22 (0.03)	13.85 (0.24)	10.50 (0.25)	1.82 (0.07)	0.43 (0.03)	0.07 (0.02)	96.79 (0.29)	0.66	0.86
		Pl	5	50.11 (0.67)	0.05 (0.01)	31.25 (0.39)	0.71 (0.09)	0.03 (0.04)	0.15 (0.08)	15.03 (0.56)	2.49 (0.38)	0.23 (0.04)	0.06 (0.02)	100.11 (0.36)	0.27	0.87
Las-62	900	Gl	6	65.08 (0.31)	0.49 (0.05)	15.30 (0.22)	3.41 (0.23)	b.d.	0.81 (0.07)	3.19 (0.05)	3.44 (0.15)	2.72 (0.09)	0.15 (0.04)	94.68 (0.26)	0.30	0.51
		Cpx	7	51.66 (0.27)	0.52 (0.04)	2.49 (0.17)	13.52 (0.63)	0.39 (0.06)	14.14 (0.32)	16.68 (0.91)	0.22 (0.05)	0.07 (0.02)	0.04 (0.03)	99.73 (0.38)	0.65	0.99
		Opx	10	51.82 (0.43)	0.29 (0.06)	2.30 (0.51)	22.86 (0.33)	0.50 (0.06)	20.67 (0.34)	1.81 (0.33)	0.06 (0.05)	0.01 (0.04)	0.04 (0.04)	100.36 (0.40)	0.62	0.97
		Hbl	6	44.00 (0.26)	2.39 (0.27)	11.10 (0.40)	13.74 (0.26)	0.17 (0.05)	13.16 (0.29)	10.74 (0.12)	1.95 (0.07)	0.54 (0.02)	0.07 (0.02)	97.87 (0.36)	0.63	0.86
		Pl	7	55.09 (0.58)	0.10 (0.01)	27.58 (0.61)	0.89 (0.22)	0.03 (0.03)	0.21 (0.17)	11.20 (0.49)	4.13 (0.24)	0.56 (0.08)	0.07 (0.04)	99.86 (0.31)	0.30	0.75
Las-63	900	Gl	6	66.23 (0.34)	0.45 (0.04)	15.12 (0.40)	2.97 (0.35)	b.d.	0.69 (0.12)	2.75 (0.09)	3.67 (0.28)	3.42 (0.05)	0.11 (0.05)	95.50 (0.19)	0.29	0.45
		Cpx	7	52.02 (0.47)	0.50 (0.03)	2.54 (0.36)	12.97 (0.52)	0.32 (0.04)	13.90 (0.34)	17.19 (0.68)	0.35 (0.08)	0.12 (0.07)	0.07 (0.01)	99.99 (0.51)	0.66	0.98
		Opx	6	52.08 (0.36)	0.28 (0.06)	1.55 (0.36)	23.30 (0.36)	0.49 (0.07)	20.61 (0.28)	1.72 (0.31)	0.02 (0.02)	0.01 (0.01)	0.02 (0.03)	100.09 (0.30)	0.61	0.99
		Pl	6	56.57 (0.94)	0.12 (0.02)	26.22 (0.64)	1.07 (0.11)	0.01 (0.01)	0.25 (0.05)	9.85 (0.46)	4.39 (0.28)	0.80 (0.18)	0.05 (0.03)	99.32 (0.77)	0.29	0.71

Table AT6.2: Composition of experimental phases (500 MPa; NNO+1.5).

Sample	T°C	Phase	n	SiO₂	TiO₂	Al2O3	FeO[a]	MnO	MgO	CaO	Na₂O	K₂O	P₂O₅	Total	#Mg[b]	#Ca[c]
Las-5-6	1050	Gl	12	54.23 (0.35)	0.68 (0.04)	14.50 (0.24)	6.09 (0.32)	0.12 (0.08)	4.25 (0.14)	6.26 (0.14)	2.54 (0.13)	1.42 (0.07)	0.19 (0.07)	90.28 (0.70)	0.55	0.73
Las-5-7	1050	Gl	12	55.02 (0.33)	0.71 (0.04)	14.91 (0.24)	5.92 (0.19)	0.12 (0.10)	4.31 (0.15)	6.23 (0.16)	2.97 (0.08)	1.43 (0.05)	0.21 (0.07)	91.82 (0.42)	0.56	0.70
Las-5-8	1050	Gl	12	56.84 (0.20)	0.75 (0.05)	16.17 (0.29)	6.02 (0.23)	0.09 (0.06)	3.55 (0.14)	6.29 (0.25)	3.38 (0.16)	1.57 (0.07)	0.22 (0.10)	94.90 (0.36)	0.51	0.67
		Cpx	8	52.25 (0.98)	0.42 (0.15)	3.27 (0.74)	7.47 (0.76)	0.19 (0.07)	16.86 (0.52)	19.62 (0.41)	0.35 (0.05)	0.04 (0.02)	0.03 (0.05)	100.50 (0.40)	0.80	0.98
		Opx	7	54.18 (0.80)	0.21 (0.05)	3.25 (0.89)	11.54 (0.92)	0.29 (0.05)	29.36 (0.99)	1.77 (0.17)	0.06 (0.02)	0.02 (0.01)	0.01 (0.01)	100.69 (0.37)	0.82	0.97
Las-5-9	1050	Gl	8	58.00 (0.51)	0.76 (0.04)	16.43 (0.3!)	6.09 (0.19)	0.16 (0.08)	3.23 (0.11)	6.12 (0.29)	3.51 (0.13)	1.56 (0.05)	0.22 (0.06)	96.09 (0.77)	0.49	0.66
		Cpx	7	49.84 (0.63)	0.63 (0.07)	5.60 (0.73)	9.01 (0.29)	0.22 (0.03)	15.47 (0.49)	18.68 (0.32)	0.44 (0.04)	0.06 (0.03)	0.05 (0.04)	100.00 (0.31)	0.75	0.98
		Opx	7	54.36 (0.53)	0.23 (0.03)	2.80 (0.30)	13.12 (0.34)	0.28 (0.04)	28.08 (0.80)	1.90 (0.74)	0.06 (0.03)	0.03 (0.03)	0.03 (0.03)	100.88 (0.52)	0.79	0.97
Las-5-10	1050	Gl	8	65.09 (0.76)	1.39 (0.07)	14.17 (0.34)	4.90 (0.32)	b.d.	1.31 (0.28)	3.59 (0.28)	3.39 (0.13)	3.25 (0.12)	0.41 (0.06)	97.56 (0.66)	0.32	0.54
		Cpx	4	52.68 (0.21)	0.66 (0.05)	3.50 (0.93)	17.44 (0.70)	0.42 (0.06)	16.44 (0.61)	8.50 (0.62)	0.55 (0.19)	0.22 (0.06)	0.06 (0.05)	100.46 (0.40)	0.63	0.94
Las-5-31	1025	Gl	14	55.95 (0.40)	0.71 (0.04)	15.71 (0.30)	5.81 (0.25)	0.12 (0.07)	3.65 (0.19)	6.11 (0.21)	3.11 (0.16)	1.50 (0.07)	0.24 (0.11)	92.92 (0.43)	0.53	0.68
Las-5-32	1025	Gl	7	55.52 (0.39)	0.68 (0.04)	14.80 (0.18)	5.93 (0.25)	0.11 (0.08)	4.18 (0.18)	6.24 (0.14)	2.94 (0.16)	1.42 (0.08)	0.22 (0.07)	92.04 (0.61)	0.56	0.70
		Cpx	7	52.19 (0.93)	0.38 (09.9)	3.26 (0.62)	7.38 (0.35)	0.15 (0.02)	16.93 (0.61)	19.39 (0.50)	0.36 (0.06)	0.05 (0.05)	0.05 (0.02)	100.13 (0.33)	0.80	0.98
		Opx	8	54.90 (0.18)	0.17 (0.01)	2.01 (0.05)	11.78 (0.17)	0.28 (0.03)	30.08 (0.13)	1.36 (0.07)	0.03 (0.01)	0.01 (0.01)	0.01 (0.02)	100.62 (0.28)	0.82	0.98
Las-5-33	1025	Gl	14	56.59 (0.42)	0.73 (0.04)	16.06 (0.23)	5.93 (0.31)	b.d.	3.32 (0.13)	6.02 (0.13)	3.33 (0.11)	1.59 (0.05)	0.23 (0.09)	93.89 (0.58)	0.50	0.67
		Cpx	5	51.96 (0.95)	0.41 (0.07)	3.70 (0.47)	7.25 (0.47)	0.19 (0.04)	16.02 (0.30)	20.20 (0.37)	0.43 (0.07)	0.06 (0.04)	0.06 (0.03)	100.28 (0.44)	0.80	0.98
		Opx	8	55.00 (0.74)	0.18 (0.04)	2.01 (0.63)	12.49 (0.46)	0.28 (0.02)	29.59 (0.64)	1.66 (0.16)	0.03 (0.02)	0.02 (0.01)	0.06 (0.02)	101.31 (0.47)	0.81	0.98
Las-5-34	1025	Gl	11	57.85 (0.35)	0.74 (0.03)	16.74 (0.30)	5.63 (0.25)	0.15 (0.06)	2.65 (0.08)	5.81 (0.19)	3.66 (0.18)	1.64 (0.08)	0.23 (0.09)	95.09 (0.58)	0.46	0.64
		Cpx	6	48.99 (0.97)	0.70 (0.11)	6.13 (0.87)	8.99 (0.52)	0.24 (0.03)	14.76 (0.39)	19.76 (0.58)	0.53 (0.07)	0.03 (0.03)	0.08 (0.02)	100.22 (0.25)	0.75	0.98
		Opx	7	53.08 (0.49)	0.23 (0.02)	3.55 (0.23)	15.28 (0.33)	0.28 (0.04)	26.70 (0.32)	1.51 (0.06)	0.04 (0.02)	0.02 (0.01)	0.07 (0.02)	100.76 (0.41)	0.76	0.98
Las-5-1	1000	Gl	12	54.81 (0.46)	0.68 (0.05)	15.00 (0.16)	5.73 (0.26)	b.d.	3.94 (0.20)	6.14 (0.21)	2.54 (0.18)	1.47 (0.08)	0.17 (0.05)	90.54 (0.36)	0.55	0.73
Las-5-2	1000	Gl	10	55.17 (0.28)	0.71 (0.06)	15.44 (0.12)	6.02 (0.31)	0.14 (0.07)	3.69 (0.12)	5.86 (0.21)	3.06 (0.13)	1.48 (0.05)	0.17 (0.08)	91.75 (0.42)	0.52	0.68
		Cpx	7	52.14 (0.65)	0.42 (0.10)	2.82 (0.52)	7.13 (0.41)	0.16 (0.07)	16.71 (0.50)	20.47 (0.43)	0.31 (0.03)	0.01 (0.01)	0.02 (0.02)	100.21 (0,46)	0.81	0.99
		Opx	7	55.04 (0.16)	0.21 (0.02)	2.08 (0.15)	11.89 (0.28)	0.27 (0.04)	29.61 (0.24)	2.03 (0.11)	0.03 (0.02)	0.01 (0.01)	0.02 (0.02)	101.20 (0.44)	0.82	0.98
Las-5-3	1000	Gl	9	57.86 (0.55)	0.73 (0.03)	16.71 (0.28)	5.58 (0.17)	b.d.	2.64 (0.08)	5.70 (0.21)	3.50 (0.12)	1.65 (0.07)	0.24 (0.06)	94.70 (0.27)	0.46	0.64
		Cpx	7	50.88 (0.26)	0.60 (0.05)	4.40 (0.54)	8.52 (0.26)	0.20 (0.03)	15.12 (0.46)	19.78 (0.29)	0.42 (0.04)	0.06 (0.04)	0.03 (0.03)	100.01 (0.42)	0.76	0.98
		Opx	6	53.52 (0.50)	0.22 (0.04)	2.74 (0.66)	15.00 (0.22)	0.32 (0.03)	26.94 (0.46)	1.67 (0.05)	0.03 (0.01)	0.02 (0.01)	0.00 (0.03)	100.45 (0.23)	0.76	0.98
Las-5-4	1000	Gl	11	63.09 (0.37)	1.01 (0.04)	15.57 (0.36)	4.86 (0.28)	0.10 (0.06)	1.31 (0.12)	3.94 (0.17)	3.87 (0.14)	2.64 (0.10)	0.39 (0.11)	96.78 (0.53)	0.32	0.53
		Cpx	7	49.95 (0.65)	0.92 (0.07)	4.42 (0.66)	11.77 (0.49)	0.25 (0.05)	14.08 (0.47)	18.02 (0.65)	0.42 (0.03)	0.06 (0.03)	0.07 (0.04)	99.96 (0.59)	0.68	0.98
		Opx	6	52.06 (0.17)	0.42 (0.02)	2.71 (0.08)	20.44 (0.12)	0.40 (0.04)	22.96 (0.27)	1.79 (0.12)	0.05 (0.01)	0.02 (0.01)	0.00 (0.03)	100.86 (0.44)	0.67	0.98
		Ilm	3	5.02 (1.10)	42.70 (0.72)	1.59 (0.05)	42.73 (0.80)	0.33 (0.04)	4.23 (0.16)	0.52 (0.05)	0.25 (0.10)	0.16 (0.04)	0.03 (0.03)	97.58 (0.34)	0.15	0.70
Las-5-26	975	Gl	10	54.93 (0.38)	0.70 (0.06)	15.26 (0.31)	5.45 (0.24)	0.14 (0.08)	3.56 (0.07)	5.65 (0.24)	2.60 (0.12)	1.53 (0.09)	0.20 (0.08)	90.02 (0.64)	0.54	0.71
		Cpx	5	52.76 (0.51)	0.37 (0.09)	2.43 (0.40)	7.21 (0.49)	0.23 (0.04)	17.68 (0.35)	19.96 (0.75)	0.30 (0.04)	0.04 (0.01)	0.02 (0.02)	100.98 (0.52)	0.81	0.99
		Opx	7	54.86 (0.22)	0.21 (0.02)	2.26 (0.16)	12.11 (0.19)	0.29 (0.04)	30.18 (0.28)	1.51 (0.239)	0.03 (0.01)	0.01 (0.01)	0.02 (0.02)	101.47 (0.21)	0.82	0.98
		Mt	5	0.29 (0.27)	3.74 (0.05)	4.23 (0.15)	77.80 (0.33)	0.16 (0.03)	4.63 (0.05)	0.20 (0.03)	0.03 (0.04)	0.03 (0.01)	0.01 (0.02)	91.12 (0.65)	0.10	0.88
Las-5-27	975	Gl	10	55.81 (0.46)	0.68 (0.04)	15.59 (0.23)	5.28 (0.28)	0.13 (0.07)	3.09 (0.12)	5.62 (0.23)	3.13 (0.11)	1.56 (0.09)	0.18 (0.08)	91.06 (0.52)	0.51	0.66
		Cpx	7	52.13 (0.76)	0.40 (0.09)	2.87 (0.57)	7.82 (0.25)	0.27 (0.04)	17.23 (0.63)	19.82 (0.60)	0.31 (0.03)	0.03 (0.01)	0.05 (0.04)	100.93 (0.20)	0.80	0.99
		Opx	6	54.34 (0.27)	0.21 (0.02)	2.36 (0.09)	13.51 (0.31)	0.32 (0.04)	29.39 (0.38)	1.42 (0.09)	0.03 (0.02)	0.01 (0.01)	0.04 (0.04)	101.61 (0.49)	0.79	0.98
		Mt	5	0.19 (0.04)	4.30 (0.02)	4.69 (0.12)	77.42 (0.50)	0.21 (0.03)	4.27 (0.07)	0.19 (0.02)	0.02 (0.02)	0.03 (0.01)	0.01 (0.01)	91.32 (0.44)	0.09	0.91
Las-5-28	975	Gl	10	58.22 (0.39)	0.64 (0.04)	16.85 (0.22)	5.21 (0.28)	0.13 (0.06)	2.28 (0.14)	5.31 (0.08)	3.54 (0.20)	1.76 (0.05)	0.29 (0.07)	94.22 (0.33)	0.44	0.62
		Cpx	6	51.27 (0.35)	0.51 (0.07)	4.73 (0.87)	8.88 (0.23)	0.24 (0.06)	15.19 (0.62)	19.18 (0.21)	0.51 (0.10)	0.11 (0.03)	0.07 (0.05)	100.68 (0.53)	0.75	0.98
		Opx	7	52.44 (0.38)	0.27 (0.04)	4.01 (0.36)	14.76 (0.48)	0.34 (0.06)	26.35 (0.55)	1.67 (0.38)	0.09 (0.08)	0.02 (0.02)	0.04 (0.04)	99.99 (0.59)	0.76	0.95
		Mt	4	0.43 (0.07)	5.37 (0.06)	6.10 (0.06)	76.15 (0.66)	0.24 (0.04)	3.49 (0.09)	0.21 (0.21)	0.04 (0.04)	0.04 (0.01)	0.02 (0.01)	92.09 (0.66)	0.08	0.85
Las-5-29	975	Gl	9	60.51 (0.35)	0.74 (0.04)	16.47 (0.32)	4.74 (0.13)	0.08 (0.05)	1.73 (0.14)	4.63 (0.26)	3.82 (0.12)	2.10 (0.08)	0.29 (0.05)	95.11 (0.34)	0.39	0.57
		Cpx	5	49.54 (0.76)	0.89 (0.02)	5.48 (0.28)	9.86 (0.23)	0.24 (0.04)	13.93 (0.35)	19.57 (0.22)	0.50 (0.06)	0.06 (0.02)	0.07 (0.04)	100.15 (0.44)	0.72	0.98
		Opx	4	53.81 (0.80)	0.24 (0.04)	2.31 (0.43)	16.76 (0.99)	0.39 (0.06)	25.28 (0.68)	1.66 (0.03)	0.05 (0.02)	0.03 (0.02)	0.06 (0.04)	100.60 (0.28)	0.73	0.97
		Pl	4	54.86 (0.66)	0.15 (0.06)	27.10 (0.76)	1.29 (0.32)	0.03 (0.02)	0.27 (0.14)	11.19 (0.42)	4.22 (0.08)	0.53 (0.12)	0.10 (0.03)	99.73 (0.41)	0.27	0.75
		Mt	3	0.57 (0.11)	8.24 (0.03)	5.25 (0.07)	74.86 (0.45)	0.24 (0.04)	3.12 (0.04)	0.23 (0.05)	0.03 (0.04)	0.04 (0.01)	0.02 (0.03)	92.61 (0.62)	0.07	0.89
Las-5-12	950	Gl	10	58.34 (0.28)	0.59 (0.05)	15.81 (0.12)	5.02 (0.30)	0.11 (0.07)	2.41 (0.08)	5.42 (0.22)	2.99 (0.24)	1.81 (0.07)	0.22 (0.09)	92.72 (0.24)	0.46	0.67
		Cpx	6	51.68 (0.40)	0.43 (0.05)	3.09 (0.28)	8.17 (0.24)	0.24 (0.02)	15.54 (0.46)	20.60 (0.39)	0.31 (0.03)	0.01 (0.01)	0.02 (0.02)	100.12 (0.44)	0.77	0.99
		Hbl	7	44.69 (0.60)	1.63 (0.14)	10.77 (0.29)	10.83 (0.30)	0.17 (0.04)	15.91 (0.79)	10.80 (0.67)	1.94 (0.09)	0.54 (0.06)	0.06 (0.05)	97.32 (0.36)	0.72	0.86
Las-5-13	950	Gl	13	61.35 (0.46)	0.46 (0.03)	16.65 (0.27)	4.47 (0.30)	0.09 (0.06)	1.70 (0.08)	4.91 (0.20)	3.48 (0.24)	2.00 (0.08)	0.23 (0.07)	95.33 (0.73)	0.40	0.61
		Cpx	9	44.31 (0.77)	0.34 (0.04)	3.58 (0.80)	8.79 (0.58)	0.25 (0.05)	15.35 (0.72)	18.63 (0.54)	0.39 (0.03)	0.08 (0.06)	0.04 (0.04)	91.77 (0.82)	0.76	0.98
		Opx	5	54.15 (0.71)	0.25 (0.02)	5.46 (0.46)	16.16 (0.74)	0.35 (0.09)	20.57 (1.22)	3.30 (1.58)	0.25 (0.19)	0.31 (0.04)	0.05 (0.02)	100.85 (0.57)	0.89	0.94
		Hbl	6	42.19 (0.60)	2.15 (0.27)	13.31 (0.45)	12.86 (0.22)	0.15 (0.04)	13.63 (0.20)	10.36 (0.15)	2.19 (0.08)	0.50 (0.04)	0.06 (0.03)	97.39 (0.34)	0.65	0.84
		Pl	4	50.54 (0.54)	0.01 (0.01)	31.69 (0.54)	0.64 (0.06)	0.04 (0.02)	0.04 (0.03)	14.57 (0.35)	3.27 (0.18)	0.14 (0.01)	0.02 (0.02)	100.95 (0.43)	0.83	0.83
Las-5-11	950	Gl	10	63.09 (0.40)	0.51 (0.06)	16.59 (0.31)	4.39 (0.19)	0.14 (0.06)	1.36 (0.08)	4.44 (0.18)	3.49 (0.28)	2.33 (0.08)	0.29 (0.11)	96.63 (0.58)	0.36	0.58
		Cpx	3	49.93 (0.50)	0.63 (0.03)	4.98 (0.06)	9.82 (0.21)	0.26 (0.03)	14.24 (0.09)	19.85 (0.09)	0.39 (0.05)	0.06 (0.02)	0.03 (0.02)	100.20 (0.53)	0.72	0.98
		Opx	8	51.53 (0.42)	0.29 (0.04)	3.82 (0.58)	20.03 (0.61)	0.45 (0.04)	22.05 (0.50)	1.87 (0.59)	0.07 (0.05)	0.01 (0.01)	0.02 (0.03)	100.13 (0.80)	0.66	0.97
		Hbl	9	43.24 (0.60)	1.77 (0.13)	12.42 (0.75)	12.39 (0.35)	0.15 (0.04)	14.34 (0.28)	10.53 (0.24)	2.03 (0.08)	0.50 (0.04)	0.08 (0.02)	97.44 (0.41)	0.67	0.85
		Mt	3	2.94 (1.65)	5.33 (0.12)	6.33 (0.34)	75.10 (1.37)	0.24 (0.06)	3.77 (0.45)	0.79 (0.25)	0.17 (0.09)	0.05 (0.01)	0.02 (0.01)	94.74 (1.29)	0.08	0.84
Las-5-14	950	Gl	7	63.44 (0.34)	0.74 (0.2)	16.07 (0.28)	4.63 (0.23)	0.15 (0.05)	1.27 (0.11)	4.12 (0.18)	3.85 (0.22)	2.53 (0.07)	0.27 (0.08)	97.08 (0.42)	0.33	0.54
		Cpx	5	49.11 (0.15)	0.87 (0.07)	5.30 (0.64)	10.43 (0.45)	0.26 (0.07)	13.73 (0.38)	19.14 (0.77)	0.46 (0.04)	0.05 (0.01)	0.05 (0.05)	99.40 (0.51)	0.70	0.98
		Opx	8	52.41 (0.53)	0.32 (0.02)	3.04 (0.49)	18.71 (0.52)	0.41 (0.07)	23.80 (0.45)	1.66 (0.16)	0.06 (0.03)	0.02 (0.01)	0.02 (0.02)	100.44 (0.67)	0.69	0.97
		Hbl	5	41.95 (0.63)	3.41 (0.13)	12.37 (0.57)	13.93 (0.19)	0.18 (0.04)	12.35 (0.24)	10.67 (0.13)	2.30 (0.10)	0.63 (0.04)	0.06 (0.04)	97.84 (0.41)	0.61	0.84
		Pl	6	54.93 (0.49)	0.05 (0.01)	27.82 (0.39)	0.71 (0.07)	0.01 (0.01)	0.06 (0.03)	10.88 (0.34)	5.10 (0.23)	0.32 (0.03)	0.02 (0.03)	99.93 (0.19)	0.13	0.70
Las-5-21	925	Gl	9	58.76 (0.49)	0.52 (0.03)	15.57 (0.23)	4.31 (0.20)	b.d.	1.87 (0.10)	5.36 (0.15)	2.65 (0.13)	1.71 (0.11)	0.25 (0.06)	91.08 (0.46)	0.44	0.69
		Hbl	6	44.49 (0.29)	1.40 (0.06)	10.99 (0.08)	10.87 (0.31)	0.16 (0.06)	15.31 (0.11)	11.45 (0.15)	1.91 (0.04)	0.59 (0.01)	0.05 (0.04)	97.21 (0.52)	0.72	0.87
		Mt	4	0.74 (0.28)	4.95 (0.02)	3.82 (0.11)	79.07 (0.36)	0.26 (0.06)	2.52 (0.10)	0.28 (0.02)	0.02 (0.02)	0.04 (0.01)	0.02 (0.02)	91.74 (0.47)	0.05	0.94
Las-5-22	925	Gl	9	60.50 (0.47)	0.48 (0.03)	15.98 (0.16)	4.32 (0.26)	b.d.	1.63 (0.11)	5.23 (0.18)	3.09 (0.23)	1.85 (0.09)	0.26 (0.06)	93.42 (0.29)	0.40	0.65
		Hbl	6	43.76 (0.30)	1.53 (0.14)	11.36 (0.15)	11.69 (0.28)	0.16 (0.05)	14.71 (0.24)	11.61 (0.13)	1.93 (0.07)	0.57 (0.02)	0.08 (0.05)	97.39 (0.17)	0.69	0.87
		Mt	5	0.19 (0.03)	5.16 (0.04)	4.12 (0.09)	79.47 (0.09)	0.24 (0.07)	2.32 (0.06)	0.21 (0.02)	0.02 (0.02)	0.03 (0.01)	0.01 (0.01)	91.77 (0.08)	0.05	0.92
Las-5-23	925	Gl	10	63.75 (0.40)	0.37 (0.04)	15.85 (0.20)	3.79 (0.23)	0.07 (0.05)	1.25 (0.12)	4.26 (0.26)	3.33 (0.20)	2.14 (0.12)	0.27 (0.04)	95.09 (0.48)	0.37	0.59
		Hbl	6	43.47 (0.47	1.77 (0.04)	11.66 (0.32)	13.03 (0.61)	0.20 (0.03)	13.74 (0.41)	11.11 (0.34)	1.97 (0.05)	0.52 (0.03)	0.12 (0.05)	97.59 (0.41)	0.65	0.86
		Pl	6	54.41 (0.62)	0.10 (0.03)	27.15 (0.18)	1.17 (0.26)	0.03 (0.03)	0.26 (0.07)	11.66 (0.22)	5.33 (0.43)	0.56 (0.08)	0.16 (0.01)	99.60 (0.43)	0.28	0.79
Las-5-24	925	Gl	9	66.13 (0.33)	0.48 (0.05)	15.39 (0.22)	3.50 (0.25)	b.d.	0.93 (0.11)	3.59 (0.15)	3.54 (0.19)	2.75 (0.08)	0.25 (0.02)	96.58 (0.50)	0.32	0.53
		Cpx	4	51.02 (0.63)	0.47 (0.03)	3.74 (0.43)	12.64 (0.58)	0.38 (0.04)	14.10 (0.73)	17.04 (0.43)	0.46 (0.08)	0.07 (0.06)	0.11 (0.04)	100.03 (0.55)	0.67	0.98
		Opx	4	51.89 (0.08)	0.24 (0.01)	3.12 (0.26)	20.29 (0.83)	0.53 (0.04)	22.06 (0.52)	1.76 (0.12)	0.05 (0.01)	0.02 (0.01)	0.10 (0.05)	100.07 (0.18)	0.66	0.97
		Hbl	5	43.33 (0.30)	2.31 (0.11)	11.53 (0.23)	13.22 (0.87)	0.22 (0.04)	13.69 (0.87)	10.90 (0.12)	2.13 (0.06)	0.59 (0.01)	0.19 (0.04)	98.08 (0.23)	0.65	0.85
		Pl	4	55.33 (0.25)	0.12 (0.02)	26.89 (0.45)	1.40 (0.17)	0.01 (0.01)	0.31 (0.10)	10.55 (0.38)	4.61 (0.11)	0.53 (0.10)	0.17 (0.04)	99.92 (0.41)	0.28	0.72
		Mt	4	0.42 (0.23)	9.13 (0.07)	4.25 (0.05)	75.90 (0.30)	0.24 (0.04)	2.03 (0.09)	0.23 (0.03)	0.02 (0.02)	0.03 (0.01)	0.01 (0.01)	92.26 (0.56)	0.05	0.93
Las-5-16	900	Gl	13	60.11 (0.43)	0.43 (0.04)	15.76 (0.24)	3.21 (0.15)	0.09 (0.04)	1.45 (0.10)	5.03 (0.18)	2.85 (0.19)	1.81 (0.07)	0.24 (0.07)	91.00 (0.61)	0.45	0.66
		Hbl	6	43.95 (0.67)	1.51 (0.07)	11.06 (0.77)	12.21 (0.03)	0.13 (0.03)	14.60 (0.43)	11.48 (0.28)	1.89 (0.09)	0.59 (0.07)	0.08 (0.06)	97.50 (0.42)	0.68	0.87
		Mt	4	0.14 (0.02)	3.98 (0.09)	3.72 (0.09)	81.74 (0.24)	0.26 (0.06)	2.35 (0.06)	0.11 (0.04)	0.01 (0.01)	0.02 (0.01)	0.03 (0.03)	92.35 (0.26)	0.05	0.92
Las-5-17	900	Gl	8	61.79 (0.45)	0.40 (0.03)	16.25 (0.25)	3.22 (0.34)	0.12 (0.07)	1.31 (0.10)	5.06 (0.24)	3.14 (0.15)	1.94 (0.11)	0.24 (0.06)	93.46 (0.49)	0.42	0.64
		Hbl	6	44.59 (0.74)	1.37 (0.03)	10.93 (0.71)	10.63 (0.12)	0.19 (0.05)	15.63 (0.33)	11.44 (0.09)	1.79 (0.00)	0.55 (0.03)	0.08 (0.04)	97.20 (0.30)	0.72	0.88
		Mt	4	0.24 (0.07)	4.21 (0.04)	3.97 (0.04)	81.51 (0.48)	0.33 (0.05)	2.11 (0.04)	0.13 (0.02)	0.01 (0.01)	0.04 (0.04)	92.61 (0.51)	0.04	0.78
Las-5-18	900	Gl	9	65.94 (0.48)	0.32 (0.03)	15.27 (0.26)	2.93 (0.20)	b.d.	0.97 (0.15)	3.69 (0.14)	3.46 (0.26)	2.40 (0.16)	0.26 (0.10)	95.27 (0.60)	0.37	0.54
		Hbl	5	43.03 (0.74)	1.66 (0.02)	11.87 (0.22)	13.29 (0.21)	0.23 (0.03)	13.14 (0.11)	11.22 (0.07)	1.92 (0.05)	0.54 (0.03)	0.05 (0.04)	96.95 (0.29)	0.64	0.87
		Pl	3	54.13 (0.37)	0.06 (0.02)	28.07 (0.48)	0.91 (0.07)	0.01 (0.01)	0.13 (0.02)	12.14 (0.51)	3.92 (0.40)	0.41 (0.01)	0.13 (0.17)	99.90 (0.42)	0.20	0.77
		Mt	4	0.20 (0.02)	4.62 (0.05)	4.01 (0.03)	81.14 (0.37)	0.33 (0.04)	1.83 (0.06)	0.19 (0.04)	0.01 (0.01)	0.02 (0.02)	92.37 (0.39)	0.04	0.95
Las-5-19	900	Gl	8	67.49 (0.36)	0.37 (0.04)	14.69 (0.35)	2.61 (0.23)	b.d.	0.72 (0.07)	2.93 (0.19)	3.52 (0.14)	3.00 (0.11)	0.25 (0.08)	95.69 (0.57)	0.33	0.48
		Opx	5	52.86 (0.37)	0.19 (0.02)	1.89 (0.26)	20.57 (0.20)	0.60 (0.07)	22.88 (0.25)	1.39 (0.14)	0.05 (0.02)	0.01 (0.01)	0.02 (0.02)	100.46 (0.22)	0.66	0.97
		Hbl	4	43.65 (0.38)	1.74 (0.31)	11.61 (0.47)	13.51 (0.24)	0.25 (0.05)	13.38 (0.29)	11.02 (0.18)	1.98 (0.04)	0.56 (0.04)	0.11 (0.03)	97.80 (0.40)	0.64	0.86
		Pl	4	57.17 (0.46)	0.11 (0.02)	25.43 (0.37)	1.24 (0.24)	0.02 (0.01)	0.22 (0.12)	9.34 (0.38)	4.76 (0.21)	0.75 (0.06)	0.03 (0.04)	99.07 (0.27)	0.24	0.68
		Mt	3	0.64 (0.28)	6.98 (0.05)	3.78 (0.12)	78.85 (0.37)	0.29 (0.03)	1.82 (0.09)	0.24 (0.01)	0.05 (0.04)	0.05 (0.01)	0.02 (0.02)	92.71 (0.29)	0.04	0.84

Table AT6.2: Composition of experimental phases (300 MPa; NNO+3.3).

Sample	T°C	Phase	n	SiO₂	TiO₂	Al2O3	FeOᵃ	MnO	MgO	CaO	Na₂O	K₂O	P₂O₅	Total	#Mgᵇ	#Caᶜ
Las-SH-18	1040	Gl	6	54.73 (0.50)	0.72 (0.04)	15.12 (0.24)	6.02 (0.41)	0.09 (0.09)	4.29 (0.12)	6.66 (0.23)	3.42 (0.29)	1.59 (0.06	0.13 (0.07)	92.76 (0.47)	0.56	0.68
		Opx	6	55.80 (0.44)	0.19 (0.02)	2.48 (0.14)	9.68 (0.35)	0.26 (0.02)	29.82 (0.39)	1.77 (0.20)	0.05 (0.02)	0.04 (0.04)	0.03 (0.04)	100.13 (0.67)	0.96	0.98
		Mt	2	0.17 (0.04)	2.08 (0.02)	5.98 (0.19)	69.93 (0.59)	0.00 (0.00)	6.93 (0.03)	0.17 (0.02)	0.05 (0.01)	0.02 (0.00)	0.01 (0.00)	85.34 (0.46)	0.75	0.79
Las-SH-19	1040	Gl	5	55.86 (0.24)	0.73 (0.03)	16.06 (0.27)	5.86 (0.25)	0.10 (0.08)	3.32 (0.11)	6.46 (0.20)	3.35 (0.33)	1.71 (0.08)	0.18 (0.08)	93.62 (0.33)	0.61	0.68
		Cpx	8	49.68 (0.82)	0.59 (0.07)	4.76 (0.40)	8.49 (0.36)	0.23 (0.04)	15.17 (0.63)	20.75 (0.43)	0.41 (0.04)	0.01 (0.01)	0.05 (0.03)	100.13 (0.67)	0.98	0.98
		Opx	6	54.48 (0.18)	0.22 (0.05)	3.20 (0.21)	11.49 (0.57)	0.30 (0.05)	29.10 (0.11)	1.64 (0.09)	0.03 (0.02)	0.02 (0.00)	0.03 (0.03)	100.51 (0.49)	0.98	0.98
		Mt	4	2.62 (0.95)	2.82 (0.02)	7.57 (0.22)	69.52 (0.39)	0.09 (0.03)	6.29 (0.20)	0.43 (0.09)	0.17 (0.08)	0.08 (0.02)	0.02 (0.02)	89.62 (1.01)	0.68	0.74
Las-SH-17	1040	Gl	9	57.14 (0.45)	0.77 (0.05)	16.30 (0.39)	5.95 (0.34)	0.12 (0.05)	3.03 (0.08)	6.17 (0.16)	3.49 (0.10)	1.81 (0.09)	0.22 (0.10)	95.00 (0.32)	0.59	0.66
		Cpx	6	50.45 (0.94)	0.56 (0.09)	5.01 (0.45)	8.02 (0.42)	0.21 (0.05)	15.36 (0.59)	19.69 (0.65)	0.43 (0.05)	0.10 (0.09)	0.06 (0.04)	99.89 (0.41)	0.98	0.98
		Opx	8	53.97 (0.20)	0.25 (0.02)	3.59 (0.36)	11.28 (0.86)	0.32 (0.04)	29.12 (0.69)	1.68 (0.22)	0.06 (0.04)	0.02 (0.03)	0.03 (0.04)	100.33 (0.41)	0.96	0.97
		Mt	4	0.37 (0.24)	3.50 (0.03)	6.45 (0.13)	74.12 (0.54)	0.14 (0.05)	4.97 (0.10)	0.22 (0.01)	0.03 (0.02)	0.04 (0.01)	0.01 (0.02)	89.86 (0.89)	0.81	0.89
Las-SH-20	1040	Gl	9	65.22 (0.48)	1.32 (0.05)	13.79 (0.34)	5.31 (0.21)	0.10 (0.04)	1.26 (0.07)	3.44 (0.09)	3.60 (0.27)	3.56 (0.05)	0.41 (0.10)	98.00 (0.54)	0.39	0.51
		Cpx	4	53.74 (0.81)	0.72 (0.16)	7.12 (1.52)	13.60 (0.79)	0.29 (0.06)	13.42 (0.23)	10.60 (2.92)	1.05 (0.40)	0.51 (0.13)	0.11 (0.6)	101.16 (0.24)	0.89	0.92
		Opx	4	55.81 (0.639	0.67 (0.05)	6.20 (2.38)	15.08 (2.12)	0.35 (0.04)	14.15 (2.98)	5.76 (1.08)	0.84 (0.40)	0.95 (0.26)	0.14 (0.04)	99.95 (0.74)	0.81	0.88
Las-SH-12	1000	Gl	8	60.24 (0.70)	0.73 (0.05)	16.21 (0.55)	3.76 (0.26)	0.14 (0.09)	2.22 (0.19)	4.97 (0.37)	3.71 (0.35)	2.00 (0.06)	0.21 (0.04)	94.20 (0.23)	0.52	0.60
		Cpx	5	50.52 (0.68)	0.64 (0.09)	4.81 (0.63)	7.13 (0.65)	0.20 (0.02)	15.92 (0.74)	20.75 (0.43)	0.40 (0.05)	0.07 (0.03)	0.04 (0.02)	100.50 (0.31)	0.98	0.98
		Opx	6	55.09 (0.33)	0.23 (0.01)	3.14 (0.13)	8.70 (0.26)	0.30 (0.05)	31.90 (0.25)	1.46 (0.23)	0.02 (0.02)	0.02 (0.01)	0.06 (0.02)	100.93 (0.52)	0.98	0.99
		Mt	5	0.15 (0.07)	2.66 (0.04)	6.86 (0.08)	76.35 (0.52)	0.33 (0.05)	6.28 (0.14)	0.15 (0.03)	0.00 (0.01)	0.02 (0.01)	0.00 (0.01)	92.81 (0.53)	0.93	1.00
Las-SH-11	1000	Gl	10	61.36 (0.30)	0.75 (0.03)	15.94 (0.30)	3.90 (0.27)	0.08 (0.07)	2.24 (0.12)	4.97 (0.19)	3.76 (0.15)	2.16 (0.09)	0.22 (0.11)	95.39 (0.51)	0.51	0.59
		Cpx	6	49.91 (0.51)	0.71 (0.08)	5.51 (0.64)	8.00 (0.66)	0.25 (0.05)	15.45 (0.40)	20.21 (0.61)	0.45 (0.08)	0.07 (0.03)	0.04 (0.02)	100.61 (0.73)	0.98	0.98
		Opx	8	54.52 (0.25)	0.25 (0.02)	3.27 (0.22)	10.39 (0.35)	0.39 (0.04)	30.45 (0.32)	1.30 (0.11)	0.03 (0.02)	0.01 (0.01)	0.02 (0.02)	100.63 (0.40)	0.98	0.98
		Pl	4	53.19 (0.46)	0.14 (0.02)	27.96 (0.29)	1.37 (0.06)	0.02 (0.01)	0.46 (0.04)	12.74 (0.37)	3.30 (0.21)	0.48 (0.02)	0.05 (0.03)	99.72 (0.32)	0.80	0.81
		Mt	6	0.61 (0.55)	2.96 (0.04)	4.84 (0.10)	77.55 (0.61)	0.32 (0.06)	5.66 (0.17)	0.30 (0.20)	0.03 (0.02)	0.04 (0.02)	0.01 (0.01)	92.32 (0.62)	0.85	0.92
Las-SH-13	1000	Gl	7	66.33 (0.42)	0.77 (0.05)	14.48 (0.26)	3.44 (0.14)	0.05 (0.04)	1.30 (0.11)	3.36 (0.14)	3.81 (0.24)	3.05 (0.09)	0.29 (0.10)	96.87 (0.42)	0.39	0.49
		Cpx	5	51.79 (0.45)	0.63 (0.07)	3.56 (0.70)	8.27 (0.41)	0.29 (0.04)	15.52 (0.32)	19.71 (0.40)	0.48 (0.06)	0.09 (0.03)	0.04 (0.02)	100.38 (0.60)	0.98	0.98
		Opx	6	54.11 (0.89)	0.32 (0.04)	2.40 (0.41)	13.56 (0.57)	0.48 (0.04)	27.61 (0.41)	1.59 (0.15)	0.08 (0.05)	0.04 (0.03)	0.03 (0.03)	100.21 (0.38)	0.94	0.96
		Pl	5	56.41 (0.72)	0.14 (0.07)	25.85 (0.78)	1.53 (0.16)	0.02 (0.02)	0.49 (0.35)	10.29 (0.42)	4.71 (0.33)	0.62 (0.25)	0.06 (0.05)	100.13 (0.39)	0.69	0.71
		Mt	4	0.33 (0.32)	4.55 (0.06)	3.86 (0.10)	77.66 (0.65)	0.31 (0.07)	4.14 (0.03)	0.17 (0.04)	0.02 (0.03)	0.03 (0.01)	0.02 (0.03)	91.10 (0.58)	0.83	0.90
Las-SH-07	950	Gl	6	58.06 (0.35)	053 (0.02)	16.49 (0.22)	3.97 (0.20)	0.14 (0.04)	2.28 (0.13)	5.38 (0.26)	3.20 (0.20)	1.85 (0.07)	0.21 (0.08)	92.07 (0.55)	0.51	0.65
		Cpx	5	51.84 (0.90)	0.53 (0.09)	4.61 (0.75)	6.48 (0.52)	0.21 (0.04)	15.12 (0.58)	21.40 (0.74)	0.40 (0.06)	0.16 (0.13)	0.04 (0.03)	100.80 (0.57)	0.98	0.98
		Hbl	5	44.91 (0.37)	1.61 (0.10)	10.57 (0.54)	8.63 (0.18)	0.15 (0.04)	17.36 (0.32)	11.55 (0.21)	1.95 (0.11)	0.46 (0.03)	0.08 (0.04)	97.26 (0.53)	0.85	0.87
		Mt	4	0.07 (0.02)	2.71 (0.06)	4.58 (0.11)	80.26 (0.48)	0.32 (0.04)	4.78 (0.03)	0.12 (0.01)	0.09 (0.11)	0.02 (0.00)	0.01 (0.01)	92.94 (0.52)	0.56	0.60
Las-SH-06	950	Gl	10	58.62 (0.31)	0.51 (0.02)	16.48 (0.23)	3.66 (0.28)	0.13 (0.09)	2.05 (0.11)	5.31 (0.24)	3.42 (0.30)	1.90 (0.04)	0.20 (0.08)	92.26 (0.37)	0.56	0.63
		Cpx	5	50.58 (0.64)	0.57 (0.06)	4.57 (0.59)	7.48 (0.26)	0.25 (0.04)	15.20 (0.62)	20.91 (0.66)	0.53 (0.23)	0.10 (0.03)	0.05 (0.03)	100.23 (0.38)	0.97	0.98
		Hbl	6	44.32 (0.53)	1.85 (0.09)	11.55 (0.38)	9.86 (0.29)	0.17 (0.04)	16.20 (0.35)	11.50 (0.29)	1.95 (0.11)	0.46 (0.03)	0.07 (0.03)	97.92 (0.45)	0.85	0.87
		Mt	4	0.16 (0.06)	2.69 (0.08)	4.99 (0.08)	79.51 (0.47)	0.31 (0.04)	4.57 (0.06)	0.16 (0.03)	0.09 (0.02)	0.03 (0.01)	0.01 (0.01)	92.51 (0.41)	0.62	0.66
Las-SH-08	950	Gl	6	68.70 (0.73)	0.58 (0.05)	13.64 (0.26)	2.82 (0.24)	0.08 (0.06)	0.84 (0.23)	2.32 (0.14)	3.23 (0.31)	3.60 (0.12)	0.16 (0.05)	95.98 (0.64)	0.31	0.44
		Cpx	5	51.67 (0.86)	0.68 (0.04)	4.23 (0.47)	9.19 (0.43)	0.35 (0.07)	14.53 (0.42)	18.95 (0.83)	0.57 (0.10)	0.18 (0.14)	0.03 (0.03)	100.37 (0.20)	0.97	0.97
		Opx	4	54.29 (0.77)	0.31 (0.00)	2.18 (0.29)	15.05 (0.51)	0.55 (0.08)	26.45 (0.40)	1.70 (0.18)	0.12 (0.08)	0.10 (0.06)	0.03 (0.05)	100.85 (0.56)	0.91	0.94
		Pl	5	56.22 (0.55)	0.07 (0.01)	26.97 (0.38)	1.04 (0.09)	0.01 (0.02)	0.16 (0.07)	10.31 (0.39)	5.28 (0.19)	0.47 (0.03)	0.06 (0.04)	100.60 (0.44)	0.67	0.68
		Mt	3	0.58 (0.52)	6.69 (0.10)	3.18 (0.13)	78.89 (0.48)	0.30 (0.07)	2.94 (0.07)	0.27 (0.04)	0.03 (0.03)	0.06 (0.03)	0.04 (0.05)	92.98 (0.57)	0.81	0.91
Las-SH-09	950	Gl	6	70.82 (0.45)	0.51 (0.05)	12.90 (0.40)	2.37 (0.08)	0.03 (0.04)	0.62 (0.18)	1.74 (0.12)	3.52 (0.27)	3.91 (0.19)	0.20 (0.04)	96.62 (0.37)	0.24	0.35
		Cpx	5	51.12 (0.40)	0.82 (0.10)	5.00 (0.56)	9.79 (0.41)	0.34 (0.03)	14.57 (0.48)	18.72 (0.43)	0.57 (0.09)	0.14 (0.02)	0.06 (0.03)	101.13 (0.42)	0.97	0.97
		Opx	9	54.07 (0.38)	0.28 (0.03)	3.58 (1.18)	14.74 (1.10)	0.52 (0.05)	24.89 (0.94)	2.10 (0.80)	0.25 (0.22)	0.07 (0.08)	0.03 (0.04)	100.54 (0.60)	0.89	0.90
		Pl	4	56.82 (0.47)	0.08 (0.00)	26.55 (0.52)	0.99 (0.10)	0.00 (0.00)	0.21 (0.14)	10.40 (0.25)	4.94 (0.25)	0.59 (0.08)	0.06 (0.03)	100.64 (0.14)	0.68	0.70
		Mt	5	0.16 (0.03)	7.59 (0.06)	2.78 (0.04)	78.37 (0.45)	0.28 (0.04)	2.45 (0.10)	0.17 (0.02)	0.01 (0.01)	0.03 (0.00)	0.01 (0.01)	91.86 (0.49)	0.86	0.95
Las-SH-02	900	Gl	5	62.04 (0.74)	0.43 (0.05)	15.55 (0.13)	2.60 (0.17)	0.09 (0.08)	1.30 (0.39)	4.39 (0.37)	3.73 (0.34)	2.18 (0.11)	0.15 (0.07)	92.46 (0.37)	0.47	0.57
		Hbl	6	44.92 (0.43)	1.64 (0.06)	10.32 (0.43)	9.89 (0.23)	0.19 (0.04)	16.05 (0.24)	11.88 (0.21)	1.68 (0.08)	0.48 (0.03)	0.16 (0.14)	97.22 (0.17)	0.87	0.89
		Pl	6	50.77 (0.82)	0.05 (0.02)	30.08 (0.87)	1.03 (0.08)	0.04 (0.04)	0.16 (0.08)	14.36 (0.69)	2.94 (0.50)	0.27 (0.08)	0.08 (0.04)	99.78 (0.92)	0.84	0.84
		Ap	3	4.22 (2.93)	0.08 (0.03)	1.02 (0.62)	1.08 (0.61)	0.12 (0.05)	1.01 (1.06)	50.32 (1.76)	0.07 (0-06)	0.14 (0.05)	37.03 (1.92)	95.10 (1.18)	1.00	1.00
		Mt	4	0.50 (0.36)	2.47 (0.01)	3.36 (0.03)	82.32 (0.88)	0.42 (0.06)	3.32 (0.03)	0.23 (0.09)	0.05 (0.04)	0.04 (0.00)	0.02 (0.02)	92.72 (0.43)	0.77	0.84
Las-SH-01	900	Gl	6	64.79 (0.38)	0.36 (0.04)	14.72 (0.20)	2.21 (0.17)	0.10 (0.05)	0.96 (0.04)	3.38 (0.16)	3.77 (0.15)	2.55 (0.08)	0.21 (0.12)	93.04 (0.51)	0.44	0.50
		Hbl	6	45.01 (0.44)	1.79 (0.06)	10.52 (0.58)	10.18 (0.26)	0.22 (0.06)	16.10 (0.45)	11.63 (0.48)	1.74 (0.08)	0.45 (0.01)	0.11 (0.05)	97.35 (0.53)	0.86	0.88
		Pl	5	55.26 (0.95)	0.09 (0.01)	26.44 (0.76)	0.99 (0.12)	0.03 (0.02)	0.26 (0.06)	11.13 (0.58)	3.78 (0.46)	0.60 (0.16)	0.07 (0.02)	98.64 (0.72)	0.75	0.76
		Ap	1	5.68	0.03	1.74	0.67	0.13	0.24	51.12	0.30	0.20	38.34	98.45	0.99	0.99
		Mt	3	0.14 (0.03)	2.95 (0.01)	3.32 (0.08)	82.36 (0.26)	0.45 (0.02)	3.19 (0.01)	0.17 (0.00)	0.00 (0.00)	0.03 (0.00)	0.03 (0.03)	92.63 (0.16)	0.90	1.00
Las-SH-03	900	Gl	7	65.09 (0.26)	0.35 (0.02)	14.84 (0.17)	2.32 (0.36)	0.12 (0.09)	1.01 (0.10)	3.15 (0.17)	3.95 (0.21)	2.56 (0.09)	0.16 (0.06)	93.55 (0.31)	0.38	0.47
		Cpx	2	51.06 (0.48)	0.51 (0.04)	5.71 (0.71)	7.00 (1.10)	0.33 (0.08)	11.83 (0.60)	20.41 (0.11)	0.43 (0.17)	0.36 (0.07)	2.57 (0.55)	100.22 (0.42)	0.97	0.98
		Hbl	7	45.41 (0.51)	1.83 (0.11)	10.92 (0.79)	9.94 (0.50)	0.26 (0.02)	15.58 (0.82)	11.58 (0.12)	1.75 (0.17)	0.48 (0.04)	0.07 (0.02)	97.82 (0.76)	0.88	0.88
		Pl	5	54.61 (0.66)	0.09 (0.01)	27.43 (0.94)	1.18 (0.43)	0.02 (0.02)	0.19 (0.02)	11.36 (0.86)	3.91 (0.54)	0.46 (0.08)	0.05 (0.02)	99.31 (0.25)	0.75	0.76
		Mt	5	0.24 (0.17)	2.79 (0.05)	3.31 (0.06)	82.58 (0.34)	0.43 (0.04)	3.17 (0.05)	0.15 (0.03)	0.04 (0.06)	0.03 (0.01)	0.02 (0.03)	92.76 (0.34)	0.74	0.81
Las-SH-04	900	Gl	9	67.75 (0.59)	0.40 (0.03)	14.47 (0.25)	2.00 (0.25)	0.03 (0.05)	0.73 (0.08)	2.51 (0.23)	3.50 (0.29)	3.23 (0.11)	0.15 (0.05)	94.77 (0.40)	0.33	0.44
		Cpx	4	51.39 (0.24)	0.57 (0.17)	3.78 (0.64)	7.59 (0.60)	0.29 (0.06)	14.55 (0.82)	20.66 (0.78)	0.37 (0.01)	0.14 (0.09)	0.40 (0.70)	99.74 (0.15)	0.98	0.98
		Opx	5	54.52 (0.26)	0.21 (0.02)	2.17 (0.23)	13.66 (0.23)	0.59 (0.04)	28.01 (0.49)	1.32 (0.20)	0.05 (0.06)	0.02 (0.01)	0.02 (0.02)	100.56 (0.43)	0.96	0.97
		Hbl	4	45.52 (0.29)	1.89 (0.20)	10.50 (0.35)	10.57 (0.33)	0.15 (0.04)	15.23 (0.72)	10.79 (0.30)	1.91 (0.05)	0.66 (0.08)	0.09 (0.05)	97.31 (0.75)	0.84	0.86
		Pl	3	57.16 (1.32)	0.11 (0.05)	25.02 (1.74)	1.37 (0.54)	0.04 (0.01)	1.03 (1.09)	9.33 (0.88)	4.38 (0.38)	0.71 (0.20)	0.05 (0.01)	99.19 (0.28)	0.68	0.70
		Mt	4	0.14 (0.10)	3.98 (0.09)	3.21 (0.03)	80.95 (0.27)	0.31 (0.05)	3.06 (0.08)	0.15 (0.04)	0.00 (0.00)	0.02 (0.01)	0.02 (0.02)	91.84 (0.18)	0.93	1.00

2 PART II

The data presented in Part II contain electron microprobe analysis of samples from Lastarria, which were collected by A. Stechern during a field campaign in 2010. The data was obtained using a Cameca SX-100 microprobe at the Leibniz University of Hannover. The analyses are not listed here; tables can be found in the digital Appendix.
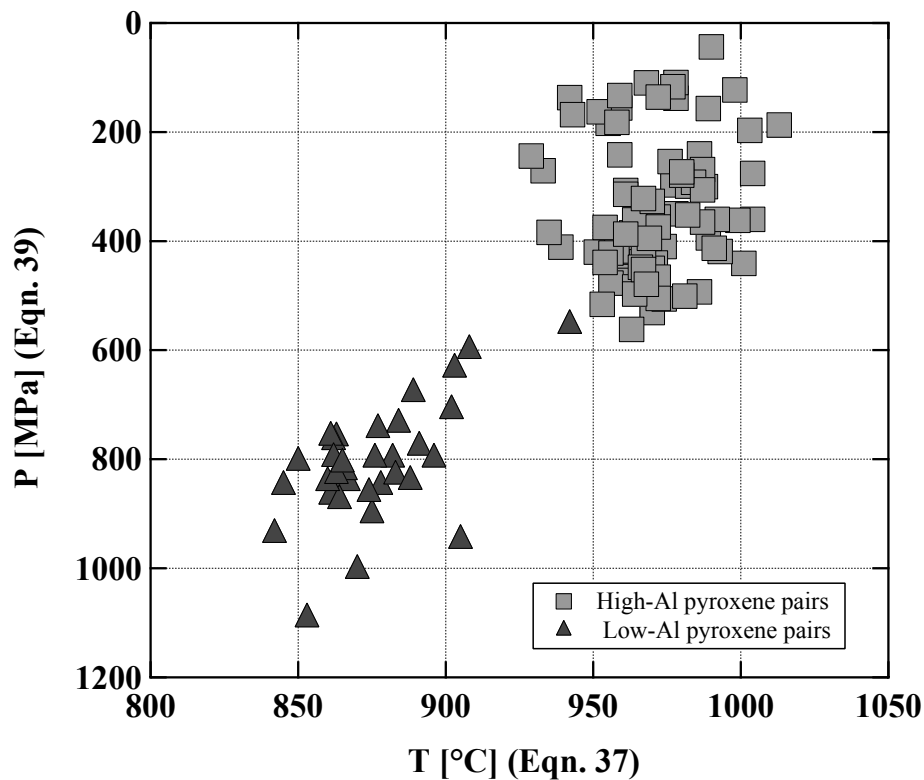

Figure AF.II.1: Results of the two-pyroxene themobarometric calculations using Putirka (2008). Symbols distinguish between high-Al and low-Al pyroxenes independent of the samples.

Curriculum Vitae

■ Personal details

André Stechern
Contacts: a.stechern@mineralogie.uni-hannover.de

■ Education

10.2009 – present	**Ph.D. Petrology/Volcanology** Dissertation: "Decoding Magma Plumbing and Geochemical Evolution of Active Volcanoes of the Central Andes (North Chile) with Petrological Methods" Leibniz Universität Hannover (Germany), in cooperation with the Georg-August-Universität Göttingen (Germany)
10.2004 – 03.2008	**M.Sc. equivalent Earth Sciences (German: "Diplom Geowissenschaftler")** Thesis: "Speziesgebundene (Sulfat[SO_4]$^{2-}$) Schwefeldiffusion on einer andesitischen Schmelze" Leibniz Universität Hannover (Germany), *final grade: 1.5, very good*
10.2002 – 10.2004	**Undergraduate Studies Earth Sciences (German: "Vordiplom")** Leibniz Universität Hannover (Germany)

■ Work Experience

01.2015 – present	**Scientific Coordinator FI:GEO** Leibniz Universität Hannover (Germany)
12.2011 – present	**Scientific Coordinator Graduate School *GeoFluxes*** Leibniz Universität Hannover (Germany)
10.2009 – present	**Research Assistant** Leibniz Universität Hannover (Germany) ▪ Experimental work with high pressure vessels ▪ Analytics: EPMA, IR, KFT, CS ▪ Supervision of Bachelor theses
03.2008 – 09.2009	**Research Assistant** Helmholtz-Zentrum Potsdam Deutsche Geoforschungszentrum GFZ (Germany) ▪ Experimental work with high pressure vessels ▪ Analytics: XANES, EPMA, IR, Raman
10.2003 – 03.2008	**Student Research Assistant – Petrology** Leibniz Universität Hannover (Germany)

■ List of publications

2014

Robert, G., Knipping, J.L., Scherbarth, S., Robertson, T.E., **Stechern, A.**, Behrens, H., Whittington, A.G. (2014) Heat capacity and viscosity of basaltic melts with $H_2O \pm F \pm CO_2$. *Chemical Geology* - online first.

Robert G., Whittington A.G., **Stechern, A.**, Behrens, H. (2014) Heat capacity of hydrous basaltic glasses and liquids. *Journal of Non-Crystalline Solids* 390, 19–30.

2013

Robert, G., Whittington, A.G., **Stechern, A.**, Behrens, H. (2013) The effect of water on the viscosity of a synthetic calc-alkaline basaltic andesite. *Chemical Geology* 346, 135–148.

2009

Stechern, A., Wilke, M., Schmidt, C., Rickers, K., Pascarelli, S., Manning, C.E. (2009) XAFS measurements on Zr in aqueous fluids at high pressures and temperatures using a modified hydrothermal diamond-anvil cell. *Journal of Physics Conference Series* 190.

Whittington, A.G., Hellwig, B.M., Behrens, H., Joachim, B., **Stechern, A.**, Vetere, F., 2009. The viscosity of hydrous dacitic liquids: implications for the rheology of evolving silicic magmas. *Bulletin of Volcanology*. 71, 185–199.

■ Conference Abstracts

2015

Charlier, B., Hövelmann, S., Namur O., **Stechern A.**, F. Holtz (2015): Rhyolite tapping of the Bushveld magma chamber: Experiments on the parent magma to the Upper Zone, AGU 2015, Vienna, Austria.

2014

Hövelmann, S., Charlier, B., Namur, O., **Stechern, A.**, Fischer, L., Holtz, F. (2014): The late-stage evolution of basalts in the Bushveld Complex, DMG Jahrestagung 2014, Jena, Germany.

2012

Stechern, A., Botcharnikov, R. E., Holtz, F., Banaszak, M., Wörner, G. (2012): Tracing magma chambers beneath Lascar volcano with petrological, geochemical and geophysical methods. EMC, Franfurt a.M., Germany.

Stechern, A., Botcharnikov, R. E., Holtz, F., Banaszak, M., Wörner, G. (2012): Experimental constraints on the role of magma mixing vs. differentiation in magma chambers beneath Lascar Volcano, Chile, EMPG XIV, Kiel, Germany

2011

Robert, G., Whittington, A., **Stechern, A.**, Behrens, H. (2011): Viscosity of natural and synthetic analogue hydrous basaltic and basaltic andesite melts from Fuego and Pacaya volcanoes, Guatemala, Guatemala. 9th Silicate Melts Workshop, La Petite Pierre, Alsace, France

Stechern, A., Banaszak, M., Botcharnikov, R. E., Holtz, F., Wörner, G. (2011): Tracing magma chambers in the lab: A case study on Lascar volcano, Goldschmidt 2011, Prag, Czech Republic

2010

Stechern, A., Botcharnikov, R. E., Holtz, F., Banaszak, M. , Wörner, G. (2010): Compositional variations of Parinacota and Taapaca volcanic rocks, Central Andes: Experimental constraints on the role of differentiation vs. magma mixing, DMG Jahrestagung 2010, Münster, Germany

Stechern, A., Botcharnikov, R. E., Holtz, F., Banaszak, M., Wörner, G. (2010): Compositional variation of Parinacota volcanic rocks, Central Andes: Experimental constraints on the role of differentiation vs. magma mixing, EMPG XIII, Toulouse, France

2009

Stechern, A., Wilke, M., Schmidt, C., Pascarelli, S., Manning, C.E. (2009): XAFS measurements on Zr in aqueous fluids at high pressures and temperatures using a modified hydrothermal diamond-anvil cell, XAFS XIV Meeting, Camerino, Italy

Stechern, A., Wilke, M., Schmidt, C., Rickers, K., Pascarelli, S., Manning, C.E. (2009): Zircon solubility and complexation of Zr in subduction zone fluids, DMG Jahrestagung 2009, Halle, Germany

2008

Stechern, A., Wilke, M., Schmidt, C., Pascarelli, S., Manning, C.E. (2008): Zircon solubility and speciation of Zr in subduction zone fluids: First results of a SR-μXRF and XAFS study, EMPG XII Abstract, Innsbruck, Austria

Whittington, A.G., Hellwig, B.M., Behrens, H., Joachim, B., **Stechern, A.** (2008): The Viscosity of Hydrous Dacitic Liquids: Implications for the Rheology of Evolving Silicic Magmas, GSA North Central section meeting, Evansville, USA

Wilke, M., **Stechern, A.**, Schmidt, C., Manning, C.E., Rickers, K., Pascarelli, S. (2008): Mobility of HFSE - insights to the complexation in aqueous fluids at hight P-T conditions, DMG Jahrestagung 2008, Berlin, Germany

2006

Hellwig, B.M., Behrens, H., Joachim, B., **Stechern, A.**, Whittington, A. (2006): Rheological Effects of Dissolved Water on Silicic Melts: The Viscosity of Hydrous Dacites and Rhyodacites from 800 to 400°C, 2006 Joint Assembly, Baltimore, USA

Joachim, B., **Stechern, A.**, Behrens, H. (2006): Quantification of water contents of aluminosilicate glasses by infrared spectroscopy, Berichte der Deutschen Mineralogischen Gesellschaft, Beih. z. Euro. J. Mineral. Vol. 18, 2006, S. 63, No. 1, 2006

Stechern, A., Joachim, B., Behrens, H. (2006): Influence of water on the viscosity of dacitic and andesitic melts, Berichte der Deutschen Mineralogischen Gesellschaft, Beih. z. Euro. J. Mineral. Vol. 18, 2006, S. 143, No. 1, 2006.